The role of Mep2 in yeast pseudohyphal growth

Anupama Chembath

Thesis submitted for the degree of Doctor of Philosophy

Institute for Cell and Molecular Biosciences

September 2017

Abstract

In response to limiting levels of nitrogen in the environment, the diploid yeast *Saccharomyces cerevisiae* undergoes a dimorphic switch from yeast like growth to filamentous pseudohyphal growth. During this morphological change yeast cells grow as elongated chains of cells attached to each other away from the colony to forage for nutrients. Earlier studies have established the two major signalling pathways that regulate pseudohyphal growth include the MAP Kinase and cAMP-PKA pathways. The Mep2 ammonium transporter is an indispensable but poorly understood element of the pseudohyphal pathway. Although the role of Mep2 in this dimorphic switch has been recognized, the precise molecular mechanisms that link ammonium transport to this dimorphic switch is still unclear. Two distinct models of Mep2 function have been proposed. In the first, pH model, import of substrate during ammonium transport (either ammonium ion, ammonia gas or ammonia gas plus proton) would result in localised cytosolic pH changes which is sensed by an appropriate signal transduction pathway. In the second, transceptor model, Mep2 behaves like a transceptor by undergoing a conformational change during ammonium transport allowing it to physically engage a downstream signalling partner to initiate pseudohyphal growth. The pH model was tested which demonstrates that Mep2 signalling is independent of intracellular pH changes. The genetic screen to identify potential interaction partners of Mep2 identified an interaction between Mep2 and the 14-3-3 protein Bmh1. This interaction has been confirmed using western analysis of membrane fractions and demonstrated that this interaction is lost in signalling deficient Mep2 mutants. The 14-3-3 protein binding site in Mep2 has been identified which is required for the Mep2 dependent activation of the MAP Kinase pathway during pseudohyphal growth. A model for Mep2 sensing is proposed where Mep2 recruits signalling components to the membrane enabling cells to establish polarity where Mep2 is most active.

Declaration

I certify that this thesis contains my own work, except where acknowledged, and that no part of this material has previously been submitted for a qualification at this or any other University.

Dedication

This thesis is dedicated to my parents and grandmother

for their unconditional love, support and encouragement.

I couldn't have done it without you.

Acknowledgements

Table of contents

List of Tables

List of Figures

List of Abbreviations

AAP – Amino Acid Permease

AI – Auto-inhibitory Region

AMP – Adenosine Monophosphate

AMT – Ammonium Transporter

ATP – Adenosine Triphosphate

AUC – Area Under Curve

CEN – Centromere

CTR – C-terminal Region

DIC – Differential Interference Contrast

DNA – Deoxyribonucleic Acid

DSP – Dithiobis[SuccinimidylPropionate]

ECL – Extracellular Loop

EDTA – Ethylene Diamine Tetraacetic Acid

FC – Flow Cytometry

FGM – Fermentable Growth Medium

GFP – Green Fluorescent Protein

GO – Gene Ontology

GPCR – G-protein coupled receptor

GTP – Guanosine Triphosphate

HEPES – 4-(2-HydroxyEthyl)-1-PiperazineEthaneSulfonic acid

HXT – Hexose Transporter

IgG – Immunoglobin G

IL – Intracellular loops

IP – Immunoprecipitation

LB – Luria-Bertani

MAPK – Mitogen Activated Protein Kinase

MD – Molecular Dynamics

mDHFR – Murine DiHydroFolate Reductase

MEP – Methylammonium Permease

MM – Molecular Mechanics

NCR – Nitrogen Catabolite Repression

NPR1 – Nitrogen Permease Reactivator 1

OD – Optical Density

ONPG – O-NitroPhenyl ß-D-Galactopyranoside

PAGE – Polyacrylamide Gel Electrophoresis

PCA – Protein-fragment Complementation Assay

PCR – Polymerase Chain Reaction

PHE – Phenyl Alanine

PKA – Protein-Kinase A

QFA – Quantitative Fitness Analysis

RFP – Red Fluorescent Protein

RGS – Regulator of G-protein signalling

SCAM – Substituted Cysteine Accessibility Method

SDS – Sodium Dodecyl Sulphate

SEP – Superecliptic pHluorin

SLAD – Synthetic Low Ammonia Dextrose

SPS – Ssy1-Ptr3-Ssy5 complex

SURE – Stop Unwanted Rearrangement Events

TBE – Tris-Borate-EDTA

TCA – Trichloroaectic Acid

TM – Transmembrane Helix

TOR – Target of Rapamycin

WT – Wildtype

YNB – Yeast Nitrogen Base

1. Introduction

1.1. Ammonium transport in yeast

In its natural environment the yeast *Saccharomyces cerevisiae* is able to utilize a wide range of nitrogen containing sources allowing it to uptake preferred sources of nitrogen over poor/non-preferred sources (Hofman-Bang, 1999). Ammonia (NH_3) and ammonium (NH_4^+) are preferred nitrogen sources for most fungi, bacteria and plants as they are readily available for utilisation in biosynthetic pathways for synthesizing glutamine and glutamate, precursors for the synthesis of all other nitrogen containing cellular components (Magasanik & Kaiser, 2002). Asparagine, glutamine and glutamate are other preferred sources of nitrogen supporting optimal rate of growth in yeast. Intermediate nitrogen sources include leucine and phenylalanine while proline, urea and methionine are classed as poor sources of nitrogen (Cooper, 1982). Depending on the pH of the solution, ammonia exists as either gas (NH_3) which is uncharged and membrane permeable, or as ammonium ion (NH_4^+) in aqueous solution. However, in biological systems, it exists mainly in the NH_4^+ form due to the high pKa value (9.24) of ammonium ion (Lande *et al*, 1995). Membrane permeable NH_3 gas can readily pass through the cytoplasmic cell membrane as it is permeable to small uncharged molecules. It was initially believed that specific membrane transporters were not necessary for the transport of ammonia across membranes. Nonetheless, passage of ions is not supported across biological membranes due to their cationic membrane-impermeable nature except when specific transporters or pores are present on the membrane surface (Ritchie and Gibson, 1987). Thus, transport of ammonium across cell membranes in yeast is dependent on dedicated transmembrane ammonium transport proteins.

A family of ammonium transporters in *S. cerevisiae* comprising of Mep1, Mep2 and Mep3 proteins were characterised (Marini *et al*, 1997) belonging to the evolutionarily conserved Mep (methylammonium permease)/Amt (ammonium transporter)/Rh (rhesus) protein superfamily. Among the three Mep transporters in *S. cerevisiae*, Mep2 shows highest affinity for ammonium followed by Mep1, whereas Mep3 has much lower affinity. All the three proteins have high levels of sequence similarity between them with 79% sequence identity between Mep1 and Mep3, 41% identity between Mep1 and Mep2, and 39% identity between Mep2 and Mep3 sequences. Thus, among the three Meps, Mep1 and Mep3 are more closely related. Mep ammonium permeases are under the control of Nitrogen Catabolite Repression (NCR), a

regulation mechanism that allows yeast cells to prevent uptake of poor/non-preferred sources of nitrogen if preferred nitrogen sources are available (Magasanik & Kaiser, 2002). NCR allows yeast cells to select for sources of nitrogen that supports optimal growth by repressing expression of NCR-sensitive genes in the presence of preferred nitrogen sources and derepressing their expression during nitrogen limiting conditions (Georis *et al*, 2009) making uptake of ammonium a tightly regulated process. Nitrogen limitation induces expression of all three *MEP* genes via NCR and nitrogen availability at higher concentrations acts as a repressor (Marini *et al* 1997; Neuhauser *et al*, 2011). Notably, expression of *MEP2* transcripts are 20 and 50 times higher than *MEP1* and *MEP3* transcripts respectively on a poor nitrogen source (Marini *et al*, 2006).

In addition to its role as transporter, Mep2 fulfils another vital function whereby it acts as an ammonium sensor to induce pseudohyphal growth during ammonium starvation. During nitrogen limitation, diploid strains of *S. cerevisiae* undergo pseudohyphal differentiation characterized by a dimorphic switch from a normal yeast-like growth form to a filamentous, pseudohyphal growth form. Mutation of the high affinity ammonium permease, Mep2, did not have any effect on ammonium uptake or metabolism, but impaired pseudohyphal growth (Lorenz & Heitman, 1998a). Among the three Mep proteins in *S. cerevisiae,* only Mep2 is essential for the induction of pseudohyphal growth. Mutations of the other two ammonium permeases, Mep1 and Mep3, did not lead to any defects in pseudohyphal differentiation. When grown on poor nitrogen sources, such as proline or low levels of ammonium, the rate of pseudohyphal differentiation is Mep2-dependent and relies on the ability of Mep2 to transport ammonium (Lorenz & Heitman, 1998b). However, the mechanism of ammonium sensing by Mep2 for the induction of signal transduction pathways mediating pseudohyphal growth is still not resolved.

Ammonium transporters in bacteria and plants, designated as Amt, have high levels of sequence similarity with yeast Mep transporters. Furthermore, human Rh blood group antigens involved in the regulation of blood pH and ammonium uptake and excretion are also related to Amt/Mep ammonium transporters (Marini *et al*, 1997). A number of different homologues of ammonium transporters have been identified across a range of organisms. These ammonium transporters represent a distinct family of transmembrane transporters with high degrees of conservation (Fig.1) (Andrade & Einsle, 2007). The human fungal pathogen, *Candida albicans,* encodes two ammonium transporters Mep1p and Mep2p which facilitate ammonium uptake under nitrogen limiting conditions. They have high levels of sequence similarity to *S. cerevisiae* Mep proteins and are 52% similar to each other. CaMep2p was able to rescue pseudohyphal growth defects
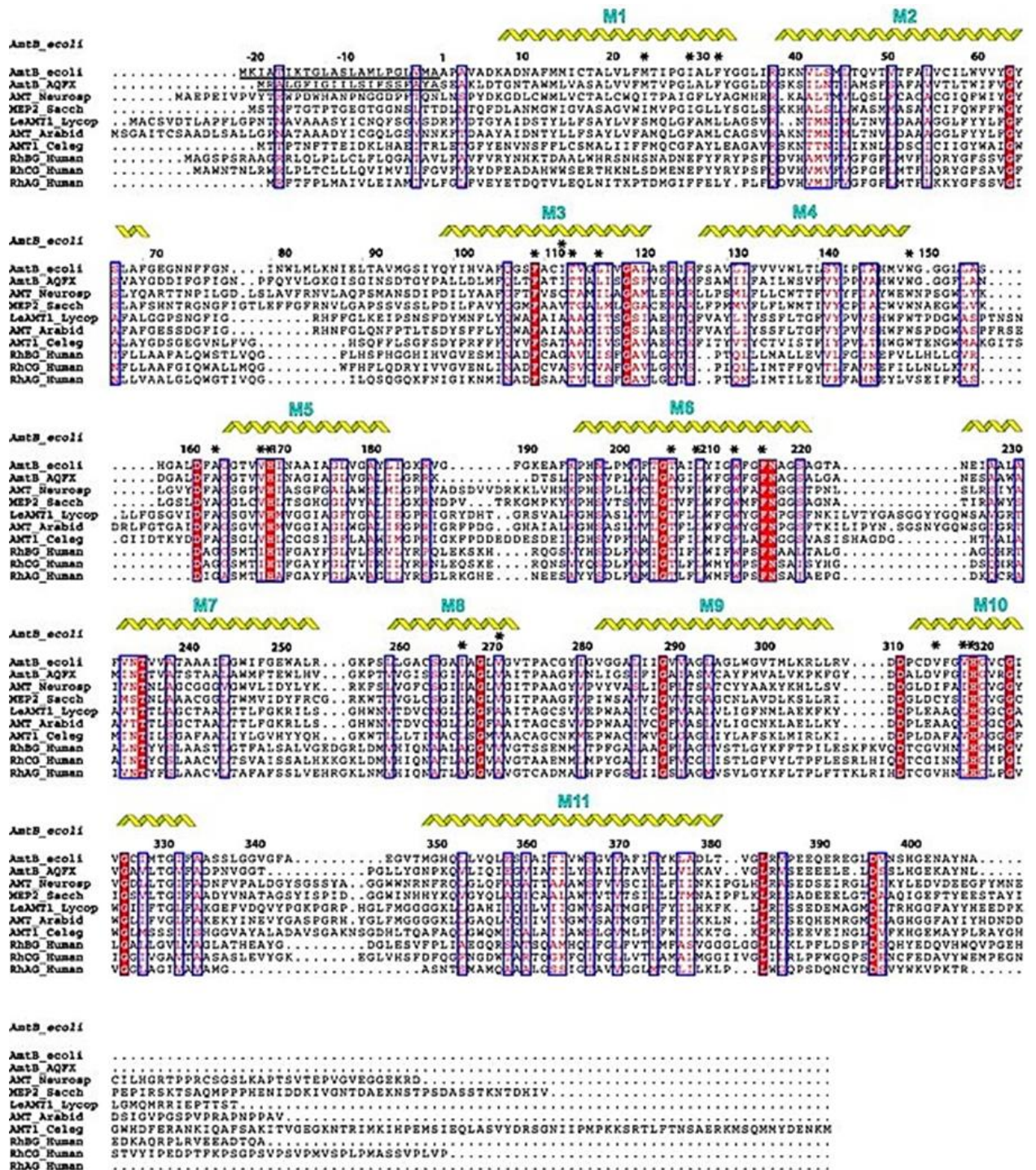
Figure 1: Multiple sequence alignments of homologues from the Amt/Mep/Rh ammonium transporter family highlighting conserved sequences in red, identical residues in blue boxes and 11 transmembrane helices M1 to M11. Residues lining the lumen of the pore are indicated by the asterisks above their respective positions within the sequence. Figure taken from Khamedi *et al*, 2004.

in a *mep2/mep2Δ* strain in *S. cerevisiae* lacking endogenous Mep2 (Biswas & Morschhauser, 2005). The plant pathogenic fungus *Ustilago maydis* has two Mep homologues Ump1p and Ump2p. Both Ump1p and Ump2p are closely related to the *S. cerevisiae* Mep2 protein and Ump2p is thought to be a homologue of Mep2 as it was able to rescue pseudohyphal growth defects when expressed in a *mep2/mep2Δ* background strain. Moreover, these proteins were able to rescue growth defects in a *S. cerevisiae mep123Δ* strain when grown under limiting ammonium conditions suggesting that these proteins are part of a large family of Amt/Mep proteins conserved across a range of organisms including microbes, plants and mammals (Smith *et al*, 2003). The rice pathogenic fungus, *Fusarium fujikuroi*, has *mepA, mepB* and *mepC* which encodes for three ammonium permease genes. MepB is the major ammonium permease followed by MepC. All three proteins showed high degrees of similarity to other ammonium transporters in the Mep/Amt/Rh family and clustered along with the ammonium permease MeaA from *Aspergillus nidulans* in the phylogenetic tree of Mep/Amt family protein sequences from known plant, mammalian, bacterial, and fungal permeases. Protein expression levels were highest for MepA and the expression of all three genes were strictly monitored by a nitrogen regulator. All three Meps fully rescued growth defects in *S. cerevisiae mep123Δ* strains when grown under ammonium limiting conditions despite their evolutionary distances from *S. cerevisiae*. However, only MepA and MepC were able to rescue pseudohyphal growth in a *mep2/mep2Δ* strain. This suggests that even though MepB functions as the major transporter and acts as a regulatory element during nitrogen sensing in *F. fujikuroi*, it does not have a signalling role identical to *S. cerevisiae* Mep2 (Teichert *et al*, 2008).

The most important biological function of Mep proteins is to scavenge for ammonium from the growth medium to use as a nitrogen source when grown under ammonium limiting conditions. All three Mep proteins functioning on their own are capable of supporting growth on low ammonia media. They have an additional role in the retention of ammonium inside the cell when grown on a nitrogen source other than ammonium. To compensate for the leak-out of ammonium from the cells, Mep1 and Mep2 efficiently take up excreted ammonium as they are high affinity transporters (Marini *et al*, 1997). The consequence of ammonium leakage on the rate of growth varies according to the availability of nitrogen source in the growth media. The activity of Mep proteins is essential when grown on a non-preferred source of nitrogen sustaining slow rate of growth. A portion of the ammonium generated in the cell during catabolism gets excreted into extracellular space, and is retrieved by the Mep proteins to support optimal growth. Regulated retrieval of excreted ammonium by Mep proteins keeps intracellular ammonium levels under control as excess ammonium causes toxicity in plants and animals

(Marini *et al*, 1997; Boeckstaens *et al*, 2007). Structural information on these ammonium transporters would help to advance our understanding of the mechanisms regulating their function.

1.2. Structural insights into AmtB, Amt-1 and RhCG

Advancement in our understanding of ammonium transporter function has been made possible through the availability of crystal structures of AmtB from *Escherichia coli* (Khamedi *et al*, 2004; Zheng *et al*, 2004), Amt1 from *Archaeoglobus fulgidus* (Andrade *et al*, 2005) and human RhCG (Gruswitz *et al*, 2010). Structural data from these transporters display similar structures with the transporter as a stable trimer of three channels with each monomer containing 11 transmembrane (TM) α-helices with the N-terminus positioned on the periplasmic side and the C-terminus on the cytoplasmic side of the membrane. RhCG contains an additional transmembrane α-helix, which is conserved in higher eukaryotes.

A well-conserved central hydrophobic pore connecting the periplasmic and cytoplasmic vestibules is present in the centre of AmtB crystal structure for each monomer (Fig. 2). This pore is proposed to be the passage through which the substrate is imported. The hydrophobic nature of the pore would only allow poor conductance of water and seems to be more suitable for the conductance of NH_3 or CH_3NH_2 (methylamine) substrates (Khamedi *et al*, 2004; Zheng *et al*, 2004). This led to the proposition that Amts are gas channels that conduct uncharged NH_3 and have highly-conserved pore lining residues that are non-polar in nature (Khamedi et al, 2004). Many of the most conserved residues of the Amt/Mep transporter family are seen within the pore. At the entrance to the pore on the periplasmic side, a putative ammonium binding site (W148 in AmtB) has been identified whose primary function is to recruit NH_4^+ ions via pi-cation attraction. This residue is suggested to have important roles in improving net substrate transport by scavenging ammonium when faced with low external concentrations of ammonium, and to distinguish between water and substrate. This tryptophan residue is found to be widely conserved across Amt/Mep protein family, and is crucial for AmtB function (Javelle *et al*, 2004; Zheng *et al*, 2004). However, structural studies have identified that the site is not conserved in Rh proteins consistent with their lower affinity for ammonium ion as they saturate at millimolar concentrations of ammonium. Nonetheless, the ammonium binding site for *A. fulgidus* homologue Amt1 was found to be crucial for discrimination of the substrate (Andrade *et al*, 2005).
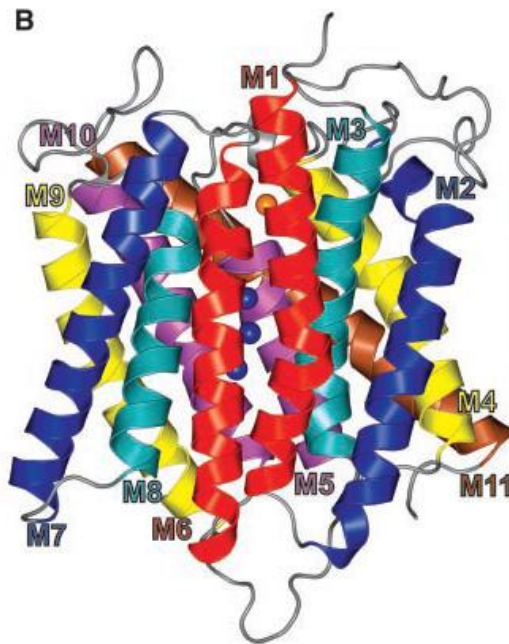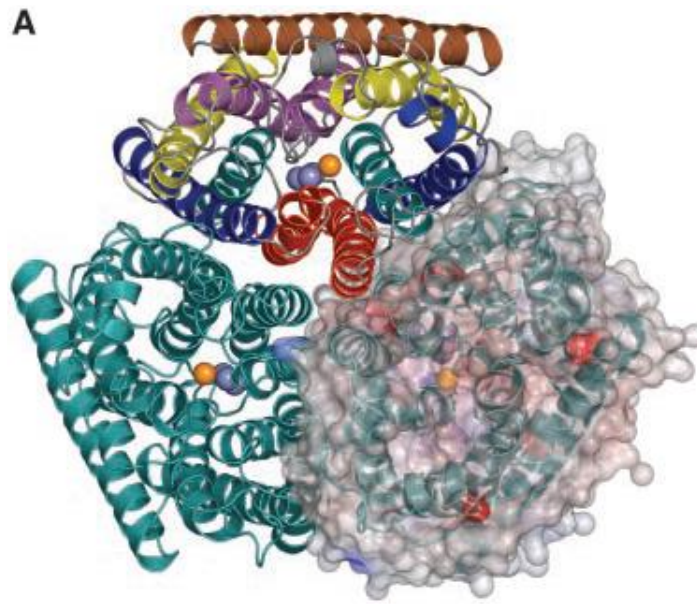
Figure 2A: Ribbon representation of AmtB trimer in its three dimensional fold as viewed from the extracellular side. The blue and orange spheres in the pore of each monomer represent potential ammonia and ammonium ions respectively. 2B: Side-view representation of AmtB monomer as positioned in the membrane identifying transmembrane (TM) helices. Figure taken from Khamedi *et al*, 2004.

Adjoining the binding site are two highly conserved phenylalanine residues which forms a putative 'phe gate' at the periplasmic site making the pore very constricted. These phenyl alanine residues (F107 and F215 in AmtB) seem to be partly stacked on top of each other and block the entrance to the pore making the phe gate closed in Amts. They are extremely conserved across the whole Amt/Mep/Rh protein family even though they adopt different conformations between AmtB and RhCG crystals (Zidi-Yahiaoui *et al*, 2009). Structural alteration of the phe gate is thought to open the channel and allow passage of small molecules through the pore. In RhCG, the outer phenylalanine residue (F130) does not obstruct the substrate-conducting pore as seen in AmtB (Fig. 3). Small spaces on either sides of the F235 side chain permits the necessary motion essential to open the phe gate (Gruswitz *et al*, 2010).

A notable feature specific to RhCG structure is the presence of a pocket termed as the 'shunt' lined with hydrophobic residues conserved among members of the Rh protein family. The equivalent version in Amts is a large void which does not open into the cytosol. The presence of hydrophobic residues in the shunt without the presence of water suggests that it could be an alternative path for NH_4^+/NH_3 entry (Gruswitz *et al*, 2010).
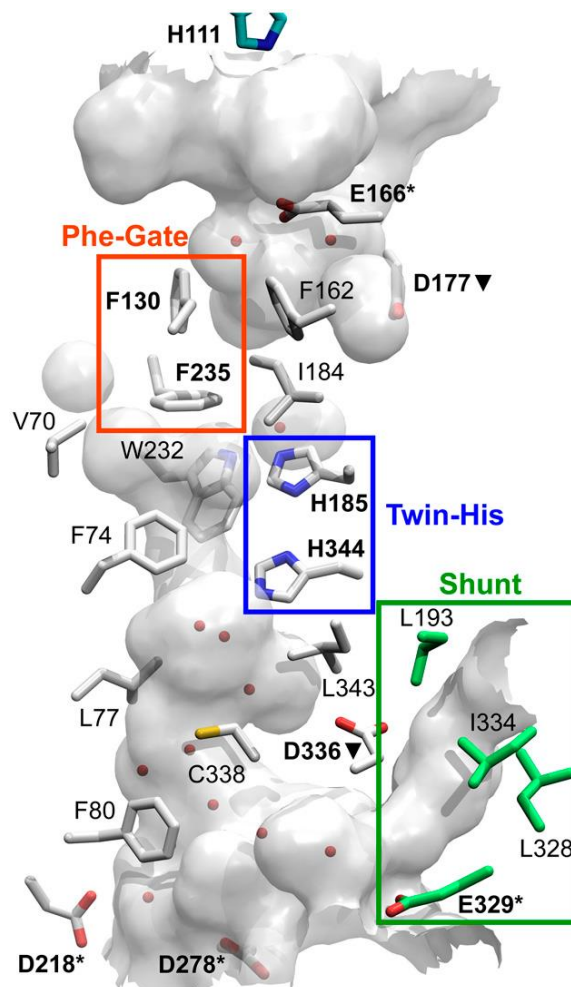
Figure 3: RhCH gas channel revealing the phe gate (red box), highly conserved twin-Histidine residues (blue box), the shunt (green box) and the red spheres representing water molecules within the channel. Figure taken from Gruswitz *et al*, 2010.

In AmtB, the pathway then leads to a continuous channel lined by hydrophobic side chains essentially non-polar. Two highly conserved Histidine residues (H168 and H318 in AmtB) are present adjacent to each other in the centre of the pore. The side chains of the two His residues project into the channel and form an unusual hydrogen bond between their δ-nitrogen atoms. The exact role of these residues in ammonium transport is still unclear. Earlier studies have suggested that these His residues might have roles in the deprotonation of ammonium ions before they pass through the channel as NH_3 (Khamedi *et al*, 2004; Zheng *et al*, 2004; Winkler, 2006). On the contrary, it has been shown that deprotonation occurs at the ammonium binding site in the periplasm (Thomas *et al*, 2000). Later mutagenesis studies have suggested that these twin-His residues are essential for optimal conductance of substrate and for mediating ammonium transport in AmtB (Javelle *et al*, 2006). Although these Histidine residues are highly conserved across most Amt/Mep proteins, a number of fungal Amt proteins have a glutamate residue replacing the first conserved Histidine residue (Glu-His instead of His-His). These Amt proteins are still capable of ammonium transport as the replaced residue is thought to behave similar to the corresponding Histidine residue during transport, and take part in the same hydrogen bond interactions if present in its neutral form (Marini *et al*, 1997; Smith *et al*, 2003). Most fungal species encode multiple Amt/Mep proteins, at least one of which contains the twin His residues and the others containing a minimum of one glutamate substitution (Soupene *et al*, 2001; Li *et al*, 2006). In *S. cerevisiae* the twin His residues are conserved in Mep2 whereas the first residue is replaced by a glutamate in both Mep1 and Mep3. Boeckstaens *et al* (2008) showed that replacement of the first conserved residue with glutamate in Mep2 renders Mep1-like properties to the transporter in terms of its rate of substrate transport, substrate affinity, and optimal pH for transport. Mep2 has an additional signalling function where it acts as an ammonium sensor, and sensing and transport functions seem to be strongly linked in Mep2. This substitution uncouples transport from the signalling functions of Mep2 suggesting that the mechanism of transport might be distinct in the homologues of the Mep2 ammonium transporter.

The C-terminal region (CTR) is located on the cytoplasmic side downstream of the eleventh transmembrane helix (TMH 11) and has residues conserved across bacteria, fungi, archae and plants. The length of the C-terminal tail however varies across prokaryotes and eukaryotes, and in members of the eukaryotic family this region is found to be further extended by up to an additional 80 residues (Thomas *et al*, 2000). The structure of AmtB CTR was not fully resolved in *E. coli*. However, it was later determined in Amt1. The ammonium transporter Amt1 from *A. fulgidus* shares a similar protein structure and assembly model to AmtB and shares a modest

41.6% sequence similarity to AmtB sequences. The differences between the two proteins are more evident in the intra and extracellular loop regions. Moreover, the highly conserved Histidine residues (H157 and H305) in the channel pore of Amt1 are almost co-planar, increasing the stability of their hydrogen bond, which is in contrast to that of AmtB. The CTR of Amt1 appears as two short helices that forms a substantial part of the cytoplasmic region of the protein (Andrade *et al*, 2005). The exact role of the C-terminal tail in AmtB includes complex formation with GlnK, a cytosolic signal transduction protein that regulates the channel, blocking the pore and controlling influx of ammonium (Conroy *et al*, 2007). Amts are paired with GlnKs in most prokaryotes and evidence for its direct interaction and complex formation has been revealed (Coutts *et al*, 2002; Strosser *et al*, 2004). The binding of the regulatory protein, GlnK, is thus thought to confer a closed state to the channel inactivating substrate conduction by AmtB. A docking model for interaction between Amt1 and its interaction partner GlnB-1 to form a tight complex was proposed (Fig. 4) (Andrade *et al*, 2005). In the model, the T loops of GlnB-1 were inserted deeply into the cytoplasmic exit channels of Amt1 creating an inactive but stable transporter blocking the transport pathway through the substrate channels. The more open structural state might correspond to a non-conducting state of the channel, making the AmtB pore unobstructed or open on the intracellular side (Coutts *et al*, 2002; Javelle *et al*, 2004). In *C. albicans,* the cytoplasmic C-terminal tail is essential for signalling functions but dispensable for ammonium transport. This suggests the presence of a signalling domain in the C-terminal tail which is crucial for signalling functions but not inevitable for its functions in the transport of ammonium (Biswas & Morschhauser, 2005).

In the plant ammonium transporters Amt1 and Amt2 in *Arabidopsis thaliana*, the C-terminal tail is thought to have roles in the mediation of cross talk between the monomeric units in the protein trimer for the regulation of ammonium transport. Here, phosphorylation of the C-terminal tail prevents uptake of ammonium in an ammonium rich environment (Neuhauser *et al*, 2007). Deletion of the CTR from AmtB diminishes the activity of the protein to almost 30% when compared to wild-type protein, and dissociates complex formation with GlnK (Coutts *et al*, 2002). It has thus been inferred that the C-terminal tail has an important role in signalling and regulation of ammonium transport. However, GlnKs are only conserved across prokaryotes and in some plants, which makes alternative mechanisms for regulation of ammonium transport in fungi essential. The precise purpose of the extended C-terminal tail in eukaryotes is mostly undefined. The C-terminal tail in *S. cerevisiae* Mep2 contains distinct regulatory domains and plays a significant role in optimal substrate transport. A Mep2 strain lacking the entire C-terminal region displayed significant reduction in the transport activity of the protein suggesting
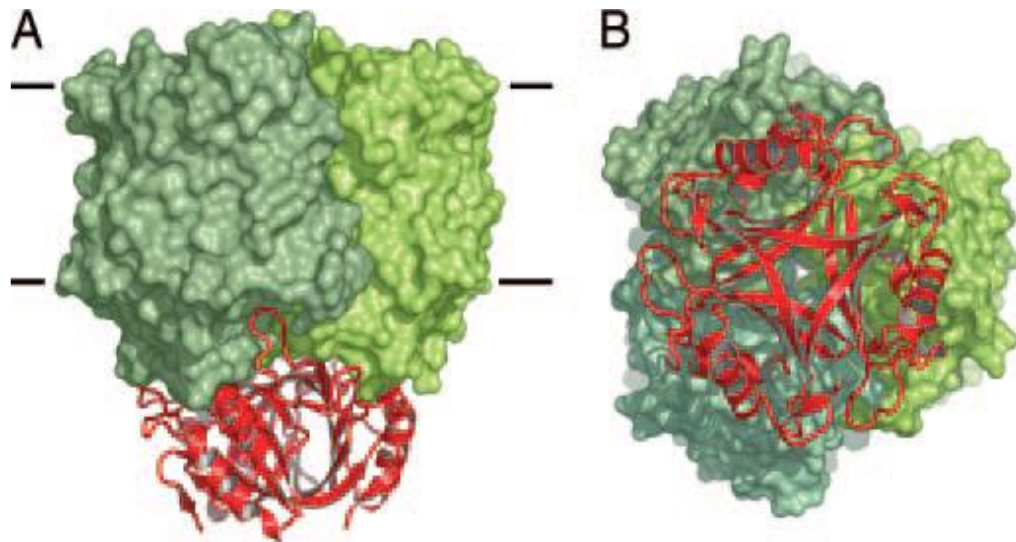
Figure 4: Docking model for interaction between Amt1 and its interaction partner GlnB-1. A) Side-view of the interaction between the T loops of GlnB-1 inserted into the cytoplasmic exit channels of Amt1 forming a tight complex B) Cytoplasmic side view of the trimers in their stable docked state. Figure taken from Andrade *et al*, 2005.

that the C-terminus has an important role in modulating the activity of the protein (Boeckstaens *et al*, 2014).

The availability of structural information would help to advance our understanding of the mechanisms regulating the signalling and transport functions of Mep2. Furthermore, the exact mechanism of ammonium transport or the nature of species that gets transported across still remains a matter of debate.

1.3. Proposed mechanisms of ammonium transport

The precise mechanism of ammonium transport and the chemical nature of substrate that is transported through these transporters still remains controversial. It is unclear whether NH_3 gas or NH_4^+ ion or both NH_3/ H^+ are co-transported across the membrane, and the transport mechanism represented by these transporters resemble that of a channel or a transporter (Khamedi *et al*, 2004; Conroy *et al*, 2007). Experimental studies so far in this field have put forward three different mechanisms of ammonium transport: NH_3 transport which is electroneutral (Javelle *et al*, 2008; Khamedi *et al*, 2004; Zheng *et al*, 2004; Ishikita *et al*, 2007), co-transport of NH_3/ H^+ (Ludewig, 2006; Boeckstaens *et al*, 2008) and NH_4^+ transport (Marini *et al*, 1997; Ludewig *et al*, 2002; Fong *et al*, 2007) both of which are electrogenic.

Earlier studies have favoured the proposition that ammonium transporters are gas channels transporting NH_3 gas (Soupene *et al*, 2001; Khamedi *et al*, 2004). In *E. coli* AmtB, the hydrophobic nature of the central conducting pore would only allow poor conductance of water and seems to be more suitable for the conductance of NH_3 or CH_3NH_2 (methylamine) substrates. Moreover, Amt/Mep proteins are impermeable to any other ions and conductance of uncharged NH_3 gas and not charged NH_4^+ ion could possibly ensure this selectivity against other ions (Ludewig, 2006). This led to the proposition that AmtBs are gas channels that conduct uncharged NH_3 and have highly conserved pore lining residues that are non-polar in nature (Khamedi *et al*, 2004). Since the hydrophobic pore of these transporters prevent translocation of charged NH_4^+ ion, NH_4^+ should be deprotonated in the periplasmic vestibule and uncharged NH_3 would get transported across the membrane resulting in an electroneutral transport, leaving the charge on the periplasmic site. The immediate reprotonation of NH_3 inside the cell would result in a net electroneutral NH_4^+/ H^+ antiport (Wang *et al*, 2012; Wacker *et al*, 2014). With the help of molecular dynamics (MD) simulation data Lin *et al* (2006) showed that charged NH_4^+ cannot make its way through the pore because of its very hydrophobic nature and

the species that gets conducted through the pore should be neutral ammonia gas. Ripoche *et al* (2004) argued that a similar mechanism exists in human Rhesus protein RhAG where transport of NH_3 gas is facilitated across the erythrocyte membrane. The fact that the gradient across the membrane is opposite for both species i.e. for uncharged NH_3 and charged NH_4^+, it is of substantial significance the chemical nature of the substrate that gets transported across the membrane. Free energy calculations imply insignificant probability of finding NH_3 molecules in the pore of AmtB compared to that of finding water, and the presence of water in the pore favours proton transport (Baday *et al*, 2013). Electrophysiological studies support the model that Amt/Mep proteins transport either NH_4^+ or co-transport NH_3/ H^+ with a net charge being transported across the membrane (Mayer *et al*, 2006; Fong *et al*, 2007). Electrophysiological experiments on *Lycopersicon esculentum* Amt protein LeAMT1, when expressed in Xenopus oocytes, supported NH_4^+ as the substrate (Ludewig *et al*, 2002). Similar studies on human RhBG proposed that the mechanism of transport could either be NH_4^+/ H^+ antiport or NH_4^+ import (Ludewig, 2004; Nakhoul *et al*, 2005). Earlier studies on plant Amts proposed the idea that they were uniporters for NH_4^+ (Ludewig *et al*, 2002) but later studies pointed towards the involvement of an H^+ coupled mechanism (Neuhauser *et al*, 2014). However, it is possible that not all plant Amts support similar mechanisms of transport. PvAmt1, ammonium transporter from bean, was shown to exhibit electrogenic transport which was dependent on pH (Ortiz Ramirez *et al*, 2011).

Considering the high degrees of sequence identity and conservation among members of the Amt/Mep/Rh protein family it is entirely possible that they share a similar mechanism of substrate transport. Regardless of electrogenic or electroneutral mode of transport found in these ammonium transporters, it could very well be that NH_4^+ binds to the deprotonation site in the substrate-conducting pore and that NH_3 gets transported through the pore into the cytoplasm. The fate of the H^+ ion, whether it gets transferred into the cytoplasm or gets shuttled back into the periplasmic space, would determine the mode of transport.

Two highly conserved Histidine residues (H194 and H348 in Mep2) line the pore of AmtB such that their side chains protrude into the channel (Khamedi *et al*, 2004; Zheng *et al*, 2004). Earlier studies have shown that the twin-His motifs in Mep2 are essential for optimum substrate conductance and are important in the initiation of pseudohyphal growth (Javelle *et al*, 2006; Rutherford *et al*, 2008a). It has been speculated that the two conserved His residues at the centre of the hydrophobic pore could be involved in the deprotonation/reprotonation of the substrate (Javelle *et al*, 2006; Khamedi and Stroud, 2006). These twin-Histidine residues might have a central role in the deprotonation of NH_4^+ ions, to serve as proton acceptors for uncharged NH_3

gas to travel through the channel (Winkler, 2006; Khamedi *et al*, 2004; Zheng *et al*, 2004). Using computational methods and molecular simulation data, Wang *et al* (2012) proposed a pathway in AmtB where the twin-His motifs act as a proton relay system whilst NH_3 gas traverses down the pore resulting in electrogenic NH_3/ H^+ co-transport (Fig. 5). They call the site where NH_4^+ gets recruited at the entrance to the pore as S1 and show that the site is selective to NH_4^+ over naturally abundant cations like Na^+ or K^+. They suggested that the highly conserved twin His dyad is central for ammonium binding and deprotonation, and named the site where the substrate forms a hydrogen bond with the first Histidine residue as S2 and the site where it forms a second hydrogen bond with the second Histidine residue as S4. Once NH_4^+ reaches the S2 site de-protonation occurs and the proton gets transferred to the H168 residue which illustrates the role of H168 residue as a transient proton acceptor (Javelle *et al*, 2008). The re-protonation event takes place at the S4 site where the substrate accepts a proton from H318 residue and diffuses into the cytoplasm as NH_4^+ ion. The proton would most likely be on the H318 residue when NH_3 reaches the S4 site, ready to be re-protonated and diffuses down into the cytoplasm as NH_4^+. Their mutagenesis studies have revealed that the residues surrounding the S2 site is central to its activity.

Using electrophysiological techniques Wacker *et al* (2014) investigated the mechanism of ammonium transport in *Af*-Amt1 and observed that Amt1 sustains electrogenic NH_4^+ transport. They established that Amt proteins were able to discriminate between NH_4^+ and other cations, and absence of interactions between Na^+ or K^+ and the transporter. Moreover, they showed that transport in Amt1 is pH dependent displaying a reduction in the rate of transport with a shift towards alkaline pH.

a)
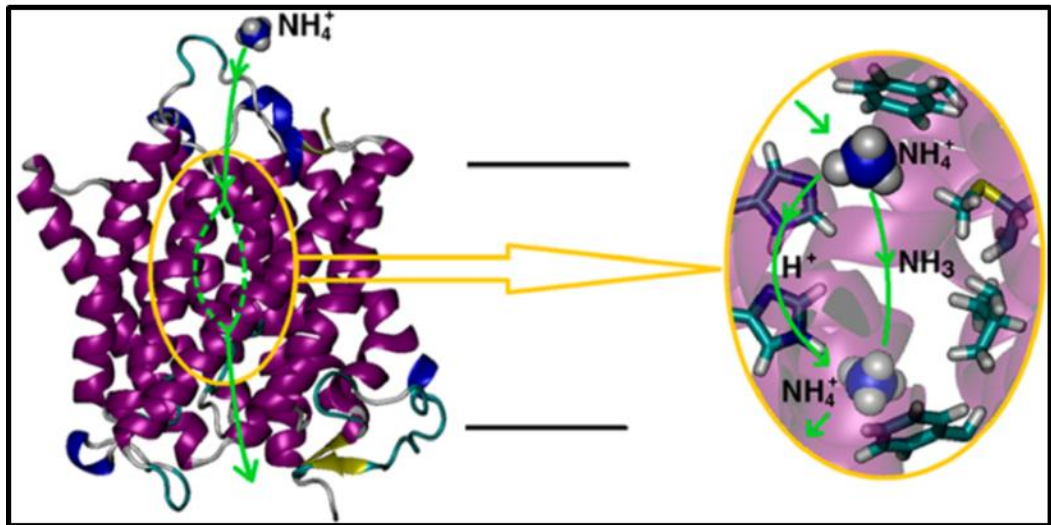
b)
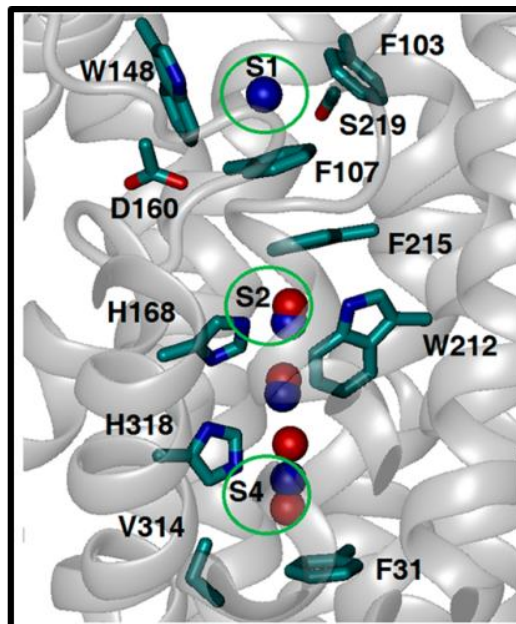
Figure 5: Electrogenic transport in AmtB. a) NH_4^+ in the AmtB pore transfers a proton to the conserved Histidine residue (H168) and diffuses down the pore as NH_3 gas. The proton gets co-transported through hydrogen bond between the highly conserved H168-H318 pair and is reprotonated at the second conserved Histidine residue (H318). b) AmtB conducting pore with ammonium recruitment site marked as S1, deprotonation site as S2 and re-protonation site as S4. Figure taken from Wang *et al* (2012).

With the help of quantum mechanic and molecular simulations Baday *et al* (2015) proposed a mechanism for NH_4^+ recruitment and NH_3 transport in RhCG (Fig. 6). Their calculations suggest that NH_4^+ recruitment takes place at the first twin-Histidine residue (H185) and proton gets transferred from NH_4^+ to H185 residue after deprotonation at that site. This proton then gets shuttled back to the extracellular bulk comprising a network of hydrogen bonds involving H185, D177 and S181 residues. Their molecular simulation studies propose that the proton on H185 residue initially gets transferred to a water molecule which in turn gets transferred to D177 residue. The involvement of S181 residue is indirect and is more structural as it helps to keep D177 residue in position and stabilises the water chain between H185 and D177 residues. Both D177 and S181 residues are crucial for ammonium transport in RhCG as mutation to either would affect its ability to transport ammonia. As a result of the hydrogen bond formation between the H185-D177 network involving S181, the proton gets shuttled back into the periplasmic space while NH_3 diffuses down the pore resulting in electroneutral transport. Thus the main role for D177 residue in RhCG proteins might have to do with the release of proton form the Histidine dyad during substrate transport, and the signature Histidine residues as the acceptor of protons.

The major mechanistic differences between the mode of substrate transport amongst AmtB and RhCG could thus be determined by the status of the proton after deprotonation of NH_4^+ during ammonium transport. The fate of the proton, whether it gets co-transported along with the substrate through the pore during ammonium transport or gets shuttled through the periplasmic space determines the mode of transport to be either electrogenic (as seen in AmtB) or electroneutral (as in RhCG) across these transporters.

It is highly plausible that proteins with distinctive mechanisms of substrate transport are able to co-exist within the Amt/Mep/Rh protein family. Many mechanistic questions still remain unanswered regarding the biological functions of these transporters. In addition to its role as ammonium transporter, since *S. cerevisiae* Mep2 functions as an ammonium sensor during pseudohyphal growth, Mep2 combines the functions of an active ammonium transporter and a nutrient sensor or receptor making it a 'transceptor'. However, the mechanism of ammonium sensing by Mep2 for the induction of signal transduction pathways mediating pseudohyphal growth has still not been resolved.
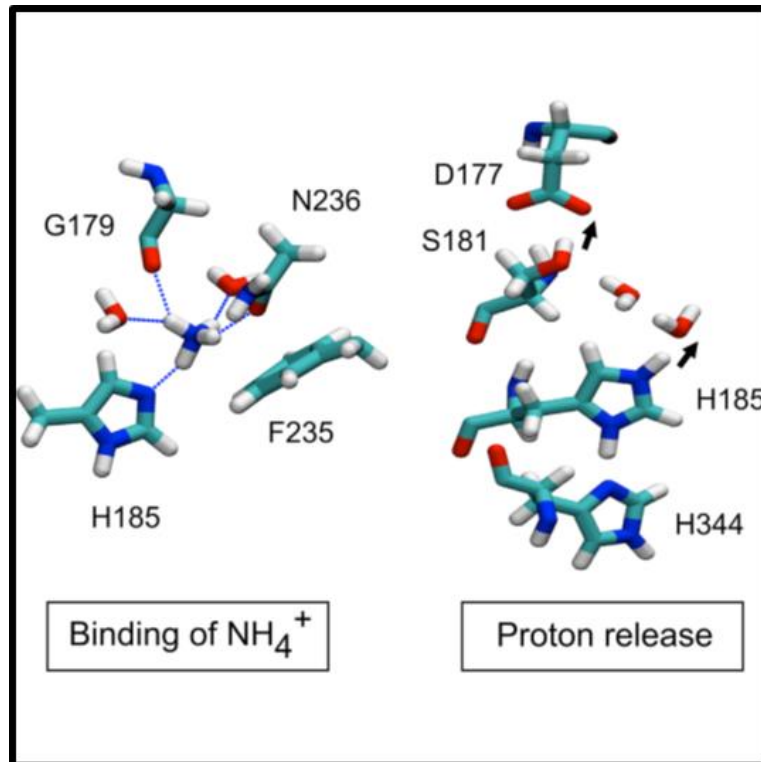
Figure 6: Mechanism of NH_4^+ recruitment and NH_3 transport in RhCG. NH_4^+ recruitment and proton transfer at H185 residue followed by proton release to the periplasmic space through hydrogen bond network involving H185, D177 and S181 residues whilst the substrate diffuses down the pore as NH_3 resulting in electroneutral transport. Figure taken from Baday *et al*, 2015.

1.4. Nutrient sensing in yeast

A fundamental question in biology is how organisms are able to sense their environment, and co-ordinate growth with nutrient availability. The ability to sense and respond to changing environmental conditions allows an organism to adapt to adverse circumstances in order to maximise chances of growth and survival. This adaptation is facilitated by a range of signalling pathways including those that promote nutrient sensing at the plasma membrane. Nutrient sensing mechanisms enable organisms like yeast to respond to fluctuating nutrient supply in its natural environment in order to regulate levels of growth, development and metabolism (Conrad *et al*, 2014). When starved for an essential nutrient, yeast cells induce specific transporters, simultaneously downregulate growth, gene expression and accumulate trehalose, the stress protection sugar. The pathway involved in this stress response as a result of nutrient starvation is the protein-kinase A pathway (PKA). Low levels of PKA activity result in cell characteristics similar to that of starvation and an over-active pathway prevents entry into stationary phase (Thevelein & de Winde, 1999). However, the exact molecular link between availability of nutrients, rate of growth and activation of the PKA pathway is not clear. Nonetheless, evidence exists for the rapid activation of the PKA pathway by various nutrient sensors upon re-addition of the starved substrate (Donaton *et al*, 2003, Giots *et al*, 2003; Van Nuland *et al*, 2006; Schepers *et al*, 2012; Kankipati *et al*, 2015; Schothorst *et al*, 2017). This pathway, although not directly associated with transport or metabolism of the substrate involved, plays a major role in a wide range of biological and developmental functions in yeast. Nutrient sensing in *S. cerevisiae* is mediated by plasma membrane proteins belonging to three different classes: G-protein coupled receptors (GPCRs), transporting transceptors and non-transporting transceptors (Fig. 7).
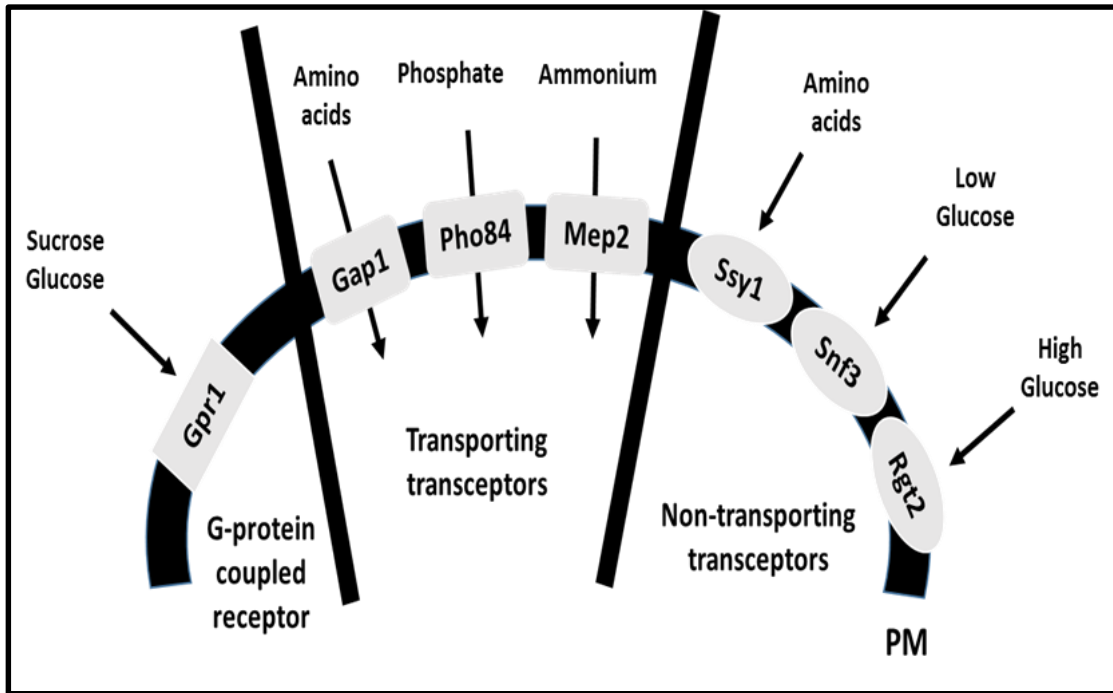
Figure 7: Summary of the different types of plasma membrane nutrient sensors in yeast. Nutrient sensing in *S. cerevisiae* mediated by membrane proteins belonging to three different classes: G-protein coupled receptors (Gpr1), transporting transceptors (Gap1, Pho84, Mep2) and non-transporting transceptors (Ssy1, Snf3, Rgt2). Figure adapted from Rubio-Texeira *et al*, 2009.

1.4.1. G-protein coupled receptors (GPCRs)

G-protein coupled receptors (GPCRs) form the largest family of transmembrane receptors having crucial roles in nutrient and pheromone sensing in yeast. GPCRs are plasma membrane sensors comprising of seven transmembrane-spanning domains. The extracellular sugar sensing GPCR system comprises of Gpr1 (receptor), Gpa2 (Gα protein) and regulator of Rgs2, a G-protein signalling (RGS) protein (Versele *et al*, 1999) in fungi. In yeast, the pheromone sensing GPCRs comprises of three types of receptors: Ste2p, Ste3p and Gpr1p. Gpr1 acts as a sugar receptor, and Ste2p and Ste3p are pheromone binding receptors. Changes to extracellular environment are communicated to G-proteins by GPCRs which in turn activates signalling pathways to co-ordinate suitable responses. When carbon sources such as glucose or sucrose is added to glucose-starved cells, a rapid activation of the cAMP-PKA signalling pathway due to activation of adenylate cyclase (Cyr1) is observed. Detection of extracellular sugars for sugar-induced PKA activity occurs through the GPCR system (Thevelein & de Winde, 1999; Xue *et al*, 1998). Gpr1 was shown to have a higher binding affinity towards sucrose compared to glucose. The sugar receptor Gpr1 senses extracellular glucose and sucrose sources and upon ligand binding, interacts with the Gα protein Gpa2. The function of the membrane associated signalling protein Rgs2 is to negatively regulate Gpr1-Gpa2 signalling alongside its additional function as a GTPase-activating protein (Versele *et al*, 1999). Both Gpr1 and Gpa2 act as part of the same G-protein coupled signalling system which senses and activates cAMP regulated signalling pathways in response to extracellular glucose concentrations (Yun *et al*, 1998). Upon ligand binding, the glucose receptor Gpr1 activates Gpa2 whose GTPase activity is stimulated by Rgs2. Gpa2 in turn activates adenylate cyclase resulting in activation of the PKA by cAMP resulting in the induction of pseudohyphal differentiation and growth during nitrogen limiting conditions (Versele *et al*, 2001).

Intriguingly, both Gpr1 and Gpa2 are required for the induction of pseudohyphal growth in yeast during conditions of nitrogen starvation. The presence of a fermentable source of carbon is a prerequisite for pseudohyphal growth induction in diploid cells under nitrogen limitation (Lorenz *et al*, 2000). Although the components of the Gβγ complex for Gpa2 have not been identified, the kelch repeat proteins Krh1/Gpb2 and Krh2/Gpb1 have been proposed to be involved in the Gβγ complex formation with Gpa2 (Harashima & Heitman, 2002). However, later studies have proposed that the binding between Gpa2 and Krh1 does not correspond to the binding as observed between the Gα and Gβ subunits (Niranjan *et al*, 2007). Rolland *et al* (2000) suggested that the role of glucose transporters was limited to uptake of sugars, and the actual mechanism of sensing glucose was carried out using two dissimilar mechanisms: levels

of extracellular glucose were sensed by Gpr1 and their intracellular levels via a phosphorylation dependent mechanism. A later model put forward the notion that addition of glucose to carbon starved cells activated the PKA pathway via two diverse mechanisms: initially via stimulation of the Gpa2-Gpr1 complex, resulting in a direct activation of the PKA pathway by increasing the levels of cAMP, and, the second mechanism via inhibition of the Krh proteins as a result of Gpa2-Gpr1 complex stimulation resulting in a lower requirement of cAMP levels for the activation of the PKA pathway (Peeters *et al*, 2006).

1.4.2. Non-transporting transceptors

Non-transporting nutrient sensors are identical to transport proteins and share similar structure and sequence identity. They are thought to be evolved from transporters but have lost their ability to transport substrate whilst acquiring a receptor function (Ozcan & Johnston, 1999). Ssy1 is an amino acid sensor, and, Snf3 and Rgt2 are glucose sensors that have lost their ability for substrate transport and function to regulate the expression of their transporter homologues encoding amino acid or glucose transporters respectively. Ssy1 is a receptor of the SPS complex (Ssy1-Ptr3-Ssy5) and a member of the conserved amino acid permease (AAP) family of plasma membrane amino acid sensors. Ssy1 is involved in a complex formation with Ptr3 and Ssy5 and detects the presence of extracellular amino acids followed by activation of signalling pathways to initiate amino acid transport and metabolism (Didion *et al*, 1998). Although Ssy1 resembles an amino acid permease, it functions as an amino acid sensor activating transcription factors to induce expression of genes encoding permeases and enzymes metabolizing amino acids. The members of the SPS complex are involved in the de-repression of genes encoding specific amino acid permeases in response to extracellular amino acids (Andre, 1995; Forsberg & Ljungdahl, 2001). Mutagenesis studies demonstrated that certain mutations to Ssy1 were capable of altering the amino acid sensitivity of the SPS complex. Conversely, mutations to Ptr3 or Ssy5 leads to an increase in the amino acid availability in the vacuole. This suggests that the SPS complex is critical for appropriate amino acid compartmentalisation in the vacuole (Poulsen *et al*, 2008; Klasson *et al*, 1999). According to a model proposed to explain the signalling mechanism of Ssy1, amino acid binding enables Ssy1 to undergo a conformational change enabling it to lock itself in a signalling conformation (Wu *et al*, 2006). The long N-terminal extension of Ssy1 which makes it different from other AAPs enables it to transmit nutrient availability to downstream signalling partners. The N-terminal region of Ssy1 is highly

conserved in the homologues found in other species and is thought to be indispensable for its sensor function (Klasson *et al*, 1999).

Extracellular glucose sensors Snf3 and Rgt2 are plasma membrane proteins and are members of the hexose transporter (HXT) family responsible for the induction of transporters in response to extracellular glucose or hexose. They regulate the expression of HXT genes with the help of Rgt1, a transcriptional repressor (Zaman *et al*, 2008). Snf3 acts as a low-glucose level sensor promoting the transcription of high-affinity HTX transporters whereas Rgt2 acts as a high-glucose level sensor promoting the expression of low affinity HTX transporters (Ozcan *et al*, 1996). Rgt1 binds to the HTX promoters blocking its transcription in the absence of glucose. When glucose is present, a PKA dependent hyperphosphorylation of Rgt1 results in its dissociation from HTX promoters and successive transcription. The unusually long C-terminal tails of both Snf3 and Rgt2 plays a vital role in their sensing function. The unique C-terminal domains are central to their role as glucose sensors (Ozcan *et al*, 1998). Both Snf3 and Rgt2 were found to be essential for the proper expression of other HXT transporter family members. Mutational studies have indicated that dominant mutations to Snf3 and Rgt2 results in constitutively expressed HXT transporters which were active even in the absence of glucose (Ozcan *et al*, 1996).

Cross-talk between the two types of glucose sensors, Gpr1-Gpa2 and Snf3-Rgt2 through Rgt1 regulation have been demonstrated (Kim & Johnston, 2006). They showed that activation of Gpr1-Gpa2 resulted in the direct phosphorylation of Rgt1 via cAMP-PKA activation. Furthermore, it is interesting that the two classes of non-transporting transceptors (Ssy1; Snf3 and Rgt2) share downstream signalling components regulating phosphorylation and ubiquitination. This puts forward the notion that these non-transporting transceptors in yeast might have evolved from a common ancestor as their transporting counterparts, and the non-transporters lost their ability to transport substrate owing to the mutations acquired during the course of evolution.

1.4.3. Transporting transceptors

Transporting transceptors combine the functions of an active nutrient transporter and a receptor. When the depleted substrate is added back to nutrient starved cells, the rapid activation of the PKA pathway is initiated through the functions of these transceptors (Durnez *et al*, 1994). Gap1 amino acid permease (Donaton *et al*, 2003), Mep2 ammonium permease (Van Nuland *et al*,

2006) and Pho84, the phosphate carrier (Giots *et al*, 2003), Sul1 and Sul2 sulphate transceptors (Kankipati *et al*, 2015) and Ftr1 and Zrt1, iron and zinc micronutrient transceptors (Schothorst *et al*, 2017) are examples of such nutrient transporters which act like receptors for rapid activation of the PKA pathway. Starvation for essential substrate even in the presence of a fermentable sugar source results in a G1 arrest and demonstrates characteristics of low PKA activity such as trehalose accumulation, induction of stress responsive elements and stress resistance. Rapid addition of the starved substrate results in a swift switch to a high PKA phenotype. In order to maintain this high PKA phenotype, the presence of a rapidly fermentable sugar source such as glucose and a complete growth medium is indispensable. For this reason, the signalling pathways involved in this process have been termed the Fermentable Growth Medium (FGM) induced pathway, which does not use cAMP as a second messenger (Thevelin, 1994). Other than PKA, the activity of the protein kinase, Sch9, is also essential for the FGM-induced pathway activation, and they most likely act in parallel owing to the high sequence similarity within their catalytic subunits (Roosen *et al*, 2005). The activation of the FGM pathway, however, does not require phosphorylation of the fermentable sugars by the hexokinases. This is a major feature that distinguishes the FGM pathway form the glucose-induced activation of Ras-adenylate cyclase pathway (Pernambuco *et al*, 1996). The notion of PKA pathway and the nutrient responsive TORC1 pathway operating via two parallel pathways in response to nutrient signals was put forward by Zurita-Martinez & Cardenas (2005). They argued that these parallel pathways converge at a later point to co-ordinate nutrient sensing of both nitrogen and carbon sources in order to coordinate appropriate growth responses.

The amino acid transceptor Gap1 belongs to the AAP family of integral membrane proteins comprising of 12 predicted transmembrane domains with N and C terminal regions (Gilstring & Ljungdahl, 2000). The general AAP Gap1 shares homology with other members of the AAP family, and is considered to be a low affinity, high capacity permease capable of transporting amino acids. Growth on poor nitrogen sources and nitrogen starvation conditions strongly induces *GAP1* expression and localisation of the protein at the plasma membrane surface in an active, stable form. Nitrogen replete conditions leads to rapid ubiquitination, internalisation and vacuolar sorting for degradation of the protein. The presence of extracellular amino acids determines the fate of neosynthesized Gap1 as it gets rerouted and sorted to the vacuole for degradation even before it reaches the plasma membrane (Rubio-Texeira & Kaiser, 2006). Gap1 transcription is positively regulated by nitrogen catabolite repression (NCR) pathway and the transcriptional activators Gln3 and Gat1 regulate *GAP1* expression during nitrogen limiting conditions (Stanbrough *et al*, 1995). Alongside its role as an amino acid transporter, Gap1 has

an additional receptor role whereby it acts as an amino acid sensor, involved in the rapid activation of the PKA pathway upon re-addition of amino acids to nitrogen starved cells. It is interesting to note that Gap1 signalling does not cause an increase in cAMP levels, rather result in cAMP-independent activation of the PKA pathway (Durnez *et al*, 1994). Truncation of the C-terminal region resulted in a constitutively active transporter causing hyperactivation of the PKA pathway. This was due to a specific mutation in the background strain which resulted in the erroneous sorting of the truncated mutants to the plasma membrane (Donaton *et al*, 2003). They demonstrated that amino acid metabolism was not a prerequisite for signalling, as the non-metabolizable D-amino acids were still able to trigger signalling. In other words, amino acid transporter function of Gap1 appeared to be independent from its PKA signalling function as transport does not always lead to signalling (Van Zeebroeck *et al*, 2014). With the help of substituted cysteine accessibility method (SCAM) analysis and identification of non-transporting signalling analogues Van Zeebroeck *et al* (2009) proposed that Gap1 engages the same amino acid binding site for both its transport and receptor functions, and, the transport cycle does not have to be completed in order to achieve its signalling function. They show that mere binding of a molecule to the substrate binding site of Gap1 is not adequate to initiate signalling by the transporter. The ability of Gap1 to function as a receptor must be the consequence of the transporter undergoing a conformational change upon substrate or ligand binding. The downstream signalling partners might include components of the PKA complex or the protein kinase, Sch9. However, the exact mechanisms by which Gap1 induces downstream signalling to fulfils its receptor function is still unclear.

The phosphate carrier Pho84 is one of the five phosphate transporters and part of the major phosphate transport system in yeast (Wykoff & O'Shea, 2001). Pho84 is a plasma membrane localised high affinity phosphate transporter whose expression is controlled by the PHO regulatory pathway and is strongly induced during conditions of phosphate starvation. The PHO pathway co-ordinates intracellular responses and aids in the adaptation to variations in extracellular phosphate levels. Addition of phosphate to cells starved for the substrate resulted in a rapid activation of PKA pathway targets, and a reduction in the activity of PKA was shown to abolish phosphate activation (Giots *et al*, 2003). Addition of phosphate back into the medium resulted in ubiquitination and phosphorylation of Pho84 leading to internalisation and targeting to the vacuole for degradation (Lundh *et al*, 2009). This rapid activation of the PKA pathway requires Pho84, and this activation does not result in an increase in the cAMP levels suggesting that cAMP is not a second messenger in the activation of the PKA pathway involving phosphate (Hirimburegama *et al*, 1992). However, the presence of a rapidly fermentable source of carbon

is essential for this signalling. The presence of this carbon source is sensed by one of the two carbon-sensing pathways, either the Gpr1 or the sugar phosphorylation-based system as deletion of both results in loss of signalling. Nonetheless, the protein kinase Sch9 found to be essential for nitrogen signalling was not critical for phosphate signalling as deletion of Sch9 did not prevent its signalling function. This proposes that nitrogen and phosphate signalling follow independent pathways for activating PKA. It was also shown that non-metabolizable analogue of phosphate was able to trigger PKA signalling suggesting that metabolism of the substrate was not essential to initiate rapid signalling. Nevertheless, Pho84 was indispensable to act as a specific phosphate sensor to rapidly activate phosphate signalling (Giots *et al*, 2003). With the help of non-signalling agonists Popavo *et al* (2010) demonstrated that signalling in Pho84 does not necessitate a complete cycle of substrate transport. They show that Pho84 can behave similar to that of a nontransporting transceptor as a complete transport cycle is not essential for its signalling function and points to their unique role in sensing phosphate at the plasma membrane. Their study also reveals that a conformational change is vital for the signalling function of Pho84 although mere binding of the substrate is not sufficient to elicit signalling. The binding of the substrate should bring about a conformational change in the transporter in order to trigger downstream signalling. Using SCAM analysis, they revealed that the transceptor uses the same substrate binding site for its transport and signalling functions.

The *S. cerevisiae* genome encodes three Mep proteins – Mep1, Mep2 and Mep3, belonging to the conserved Amt/Mep/Rh superfamily of ammonium transporters, which facilitate transmembrane ammonium transport (Marini *et al*, 1997). Mep1 and Mep3 are highly homologous transporters with similar predicted structures of 11 membrane spanning domains. Mep2, the most diverse member of the family is the only transceptor among the three which has evolved a sensing function, and shows the highest affinity for ammonia (Marini *et al*, 1994). *MEP2* is transcriptionally activated by Gln3 and Gat1, and the activity of Mep2 protein is controlled by the TORC1 effector kinase, Npr1 (Boeckstaens *et al*, 2007). During higher levels of the substrate, Mep2 is internalised and targeted to the vacuole for degradation (Zurita-Martinez *et al*, 2007). Alongside ammonium transport, Mep2 initiates pseudohyphal growth during nitrogen limiting conditions. The activity of Mep1 or Mep3 is not necessary, only Mep2 is required for the induction of pseudohyphal growth, where it is expressed on the membrane surface (Lorenz & Heitman, 1998; Rutherford *et al*, 2008). A rapid activation of the PKA pathway was observed when ammonia was added to cells starved for the substrate. Mep2 acts as a transceptor regulating both pseudohyphal growth and PKA activation, although its role in the activation of the PKA pathway is different from its ammonium sensing role during initiation

of pseudohyphal growth. Proof for this comes from certain Mep2 mutants that are able to activate PKA targets but unable to undergo pseudohyphal differentiation during nitrogen limitation. Prevention of ammonia incorporation into metabolism did not abolish signalling (Van Nuland et al, 2006). This suggests that the mechanism of ammonium sensing by Mep2 does not seem to respond to changes in the internal nitrogen metabolism levels, but rather to the physical act of ammonium transport through the transporter. Transport is necessary but insufficient to initiate signalling, which suggests that a sensing mechanism comparable to that of GPCRs might be essential to induce signalling. The cAMP-PKA and MAPK pathways have been proposed to be involved in the induction of pseudohyphal growth (Lorenz & Heitman, 1998). The association between Mep2 and the two signalling pathways however remains unclear. Mep2 being a transceptor might cause a conformational change of the protein during ammonium import, allowing it to engage downstream signalling partners to initiate pseudohyphal growth (Rutherford *et al*, 2008). Ammonium import through Mep2 could have an influence on intracellular pH, which could be sensed and signalling could be initiated, although signalling and non-signalling transporters might influence intracellular pH differently depending on the mode of ammonium transport (Boeckstaens *et al*, 2008). Nonetheless, the exact mechanism of ammonium sensing by Mep2 for the induction of signal transduction pathways mediating pseudohyphal growth is still unresolved.

1.5. Pseudohyphal growth in yeast

Pseudohyphal growth is a fungal-specific developmental switch between two diverse differentiation stages in response to extracellular stimuli. In this dimorphic switch to initiate filamentous growth, the cells assume a distinctive morphological form allowing them to explore new environments. One stimulus that triggers pseudohyphal growth is nutrient limitation, precisely, low nitrogen and high glucose conditions. This dimorphic switch is considered to be an adaptive response for non-motile yeast to forage for nutrients. The filaments that branch out during pseudohyphal growth induction allows extensive exploration of the nearby environment at lower energy costs (Gimenzo *et al*, 1992). The major changes associated with pseudohyphal growth are increased cell-cell adhesion, increased cell length and elongated cell morphology, re-organisation of cell polarity resulting in unipolar budding and invasion of the growth substrate (Kron *et al*, 1994). *S. cerevisiae* does not undergo true hyphal growth, instead a pseudohyphal growth is observed, where cells fully separate from each other following cytokinesis and are not multinucleate, but remain attached to each other forming a chain of cells

(Kron & Gow, 1995). Haploid and diploid yeast cells undergo an altered version of this switch although the extracellular stimuli triggering the response and the subsequent morphological alterations vary between both (Fig. 8). Invasive growth is often used to describe the filamentation response in haploid cells which is subtler when compared to the pseudohyphal growth response seen in diploid cells. Invasive growth in haploid cells takes place in response to limiting carbon and is characterised by the formation of shorter filaments adopting an invasive growth phenotype enabling them to invade agar substrates (Roberts & Fink, 1994; Cullen & Sprague, 2000). Additional environmental stimuli triggering pseudohyphal growth include mating pheromones and alcohols (Lorenz *et al*, 2000).

The ability of fungi to alternate between their yeast and filamentous growth forms is thought to be essential for tissue invasion and colonisation, and crucial for virulence in pathogenic fungi such as *Candida albicans*, *Magnaporthe grisea* (rice blast) and *Ustilago maydis* (corn smut) (Sanchez-Martinez & Perez-Martin, 2001; Palacek *et al*, 2002). Information acquired on the regulation of filamentous growth in budding yeast would enhance our understanding towards the genetic basis of virulence in fungal pathogens. Lessons learnt from budding yeast could be applicable in pathogenic fungi, which could lead to the development of specifically-targeted anti-fungal agents to treat fungal infections in plants and animals.

In *S. cerevisiae* under ammonium limiting conditions, the high affinity ammonium permease Mep2 is indispensable for the induction of pseudohyphal growth whereby it functions as an ammonium sensor and transmits signals to initiate pseudohyphal growth. During pseudohyphal growth, Mep2 monomers interact to form a trimeric complex that is localised throughout the membrane surface. Strains lacking Mep2 are able to obtain ammonium and grow at normal rate but are unable to undergo pseudohyphal differentiation. This implies that Mep2 functions as an ammonium sensor mediating the signal transduction pathways to initiate filamentous growth (Lorenz & Heitman, 1998). Overexpression of Mep2 resulted in an increase in the rate of pseudohyphal differentiation and even a modest increase in the expression level of the protein was able to trigger pseudohyphal growth even when grown under nitrogen replete conditions (Rutherford *et al*, 2008).
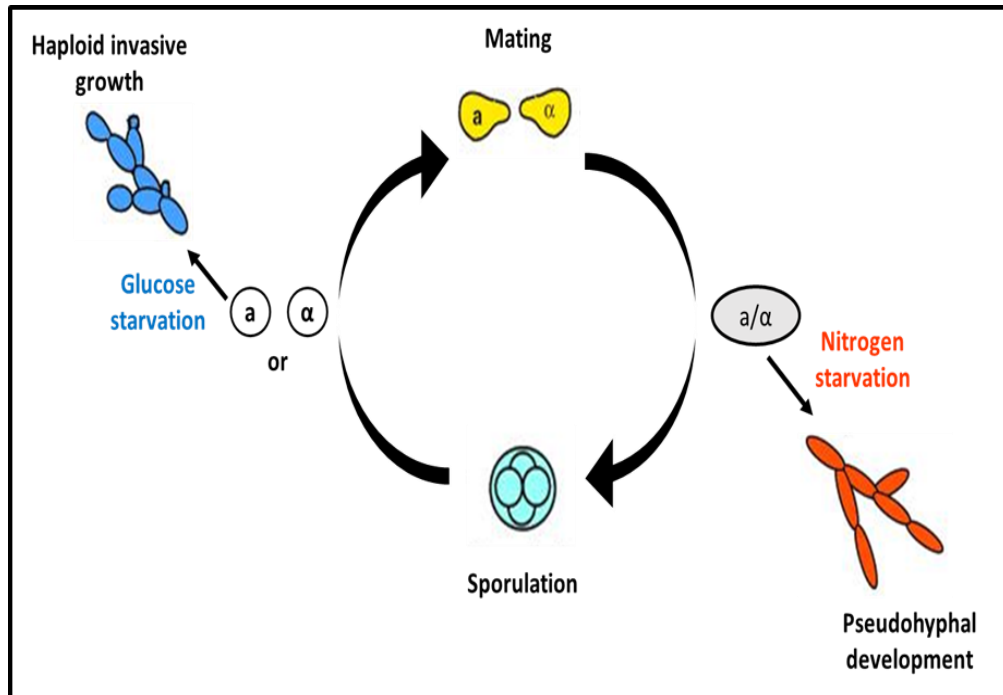
Figure 8: Developmental choices of *S. cerevisiae* cells under nutrient limiting conditions. In response to glucose starvation, haploid a or α cells undergo an invasive growth form. In response to nitrogen starvation and in the presence of abundant glucose diploid a/α cells switch to filamentous pseudohyphal growth. When starved for nitrogen and glucose concomitantly, diploid cells undergo sporulation to produce haploid gametes. Figure adapted from Madhani, 2000.

The transport and sensing functions seem to be strongly linked in Mep2 and transport is essential for signalling. The connection between the transport and sensing functions of Mep2 have been scrutinized using mutational studies. Site-directed mutagenesis was used to assess transport and signalling functions of Mep2 mutants (Van Nuland *et al*, 2006). The overall conclusion from the study revealed a close correlation between transport and signalling functions indicating that the conformational changes that happen during substrate transport through the channel might trigger a signalling pathway. However, the study identified mutants that uncoupled transport from signalling functions of Mep2. Single amino acid substitution of asparagine 246 into alanine (N246A) rendered the mutant transport-proficient but signalling defective. Mutation of a residue (G349C) adjacent to the second conserved twin-His residue made the mutant hyperactive for both transport and signalling functions in an Npr1-independent fashion (Boeckstaens *et al*, 2007). This mutation does not affect substrate recognition although the substrate flux through the pore gets markedly increased. Mutational analysis of the conserved Histidine residues lining the pore of Mep2 revealed that the transport and signalling functions of Mep2 could be separated. Transport is essential to initiate signalling pathway activating pseudohyphal growth, and mutation of the conserved Histidine residues inhibits Mep2 signalling (Rutherford *et al*, 2008). Short deletions in the N-terminal tail on the periplasmic region made the protein Npr1-independent. A few mutations around the vicinity of important conserved residues was found to influence substrate translocation of the transporter (Boeckstaens *et al*, 2014).

Moreover, the abundance of the protein seems to be vital for the signalling function of Mep2. Thus, massive substrate uptake by the transporter during substrate transport might be crucial for its sensing function (Boeckstaens *et al*, 2007). The molecular mechanisms connecting Mep2 to pseudohyphal growth appears to be strongly conserved and could be studied across various evolutionarily distant homologues using *S. cerevisiae* as a model. Mep2 homologues from other fungal species such as *U. maydis*, *F. fujikuroi*, *C. albicans* were able to restore pseudohyphal growth when introduced into *S. cerevisiae* strains lacking endogenous Mep2. This suggests that the signalling roles of these high affinity ammonium permeases might be evolutionarily conserved across homologues in various fungi (Smith *et al*, 2003).

Although nitrogen starvation initiates pseudohyphal differentiation in yeast, the precise mechanisms leading to pseudohyphal induction or the components of the pathway involved in the dimorphic switch is still unclear. In *S. cerevisiae,* the signalling pathways that are involved in the regulation of pseudohyphal growth are complex pathways working in parallel that crosstalk, feedback and interact with each other to orchestrate this morphogenetic switch. Two

signalling pathways that are key players in the induction of pseudohyphal growth and invasiveness are the pheromone responsive MAP-Kinase (MAPK) pathway and the cAMP-PKA pathway (PKA) pathway (Liu et al, 1993; Robertson & Fink, 1998). However, a physical interaction between Mep2 and these signalling pathways to regulate filamentous growth in yeast has not been proven yet. Two distinct models have been proposed to explain the sensing and signalling mechanisms of Mep2 and how Mep2 regulates this dimorphic switch.

1.5.1. pH model of ammonium sensing

The first model, the pH model (Fig. 9) (Boeckstaens *et al*, 2008) proposes pH to be a key governing factor in the sensing function of Mep2. They show that Mep2 signalling relies on the pH gradient across the membrane enabled by an inwardly directed proton gradient. During ammonium import, deprotonation of ammonium at the entrance to the pore would result in ammonia gas being transported into the cell which would then be reprotonated inside the cell and gets trapped in the cytosol. It is uncertain whether the free proton makes its way out to the periplasmic space or gets co-transported through the pore into the cell. Alterations in the net import of protons subsequent to uptake of ammonium could have an impact on the internal pH. If the proton gets co-transported alongside NH_3 gas, that would result in the acidification of the yeast cytosol. On the other hand, if the proton makes its way out to the periplasmic space, then that would result in alkalization within the cell. The pH model argues that these localised pH changes could trigger an internal pH sensor which could then rely this information to activate a signalling pathway leading to pseudohyphal growth. Thus, signalling could be an indirect consequence of ammonium ion import resulting in localised pH changes within the cytosol modulating Mep2 signalling. Boeckstaens *et al* (2008) suggest that alkaline extracellular pH might be unfavourable for Mep2 activity as pH values above 6 might result in an inversion in the proton gradient across the membrane.
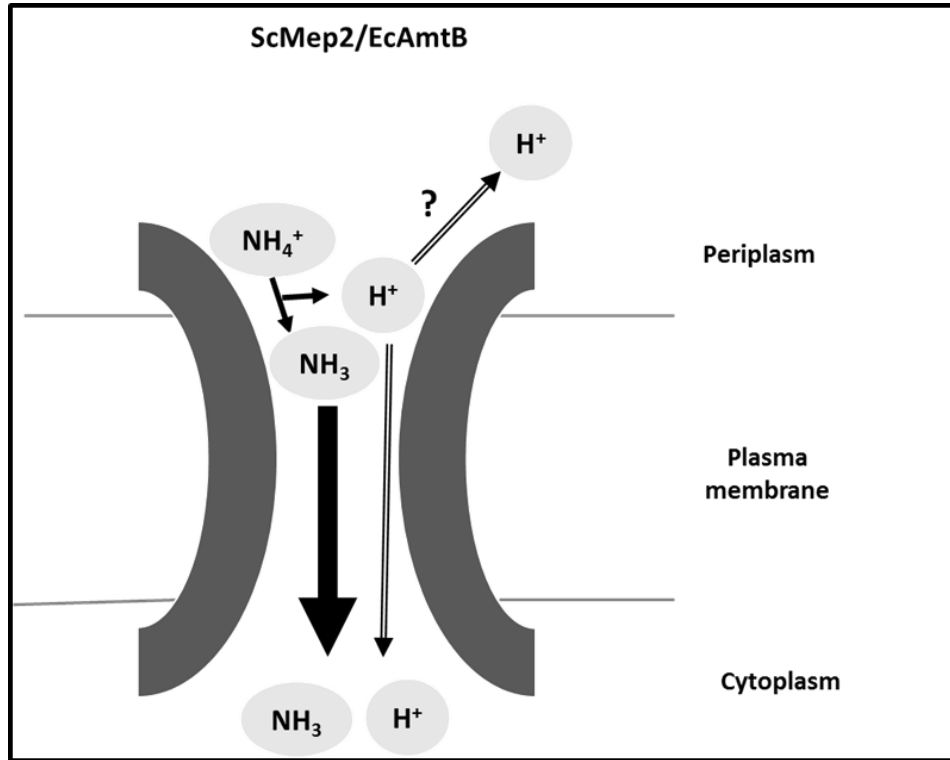
Figure 9: pH model of ammonium sensing – During ammonium import, deprotonation of ammonium could result in ammonia gas alone or both ammonia gas and the proton being co-transported into the cell. This could result in localised acidic or alkaline pH changes within the cytosol which could trigger a signalling pathway to initiate pseudohyphal growth. Thus, Mep2 signalling could thus be an indirect consequence of ammonium import resulting in localised changes in intracellular pH. Figure adapted from Boeckstaens *et al*, 2008.

1.5.2. Transceptor model of ammonium sensing

The second model proposes the transceptor model of Mep2 sensing (Fig. 10) (Rutherford *et al*, 2008). The transceptor model suggests that downstream signalling is dependent on the conformational changes of Mep2 during substrate transport allowing it to physically interact with downstream signalling partners to initiate pseudohyphal growth. Under low ammonium conditions, Mep2 is expressed and is localised to the plasma membrane. If no ammonium is present in the environment, Mep2 does not transport ammonium and its signalling function is repressed. During limiting ammonium conditions, transport of ammonium through the transporter triggers a conformational change of the protein, presumably involving the C-terminal tail, which then allows Mep2 to engage downstream signalling partners, thereby initiating pseudohyphal growth. When ammonium levels are high in the environment, transcription of *MEP2* is repressed, and Mep2 is internalised and degraded. This results in a loss of pseudohyphal growth induction signal from Mep2 leading to pseudohyphal growth being repressed. Rutherford *et al* (2008) proposed that the physical act of transport through the transporter allows Mep2 to engage downstream signalling partners resulting in the generation of a transcriptional profile that is consistent with the activation of the MAP Kinase pathway for the initiation of pseudohyphal growth.
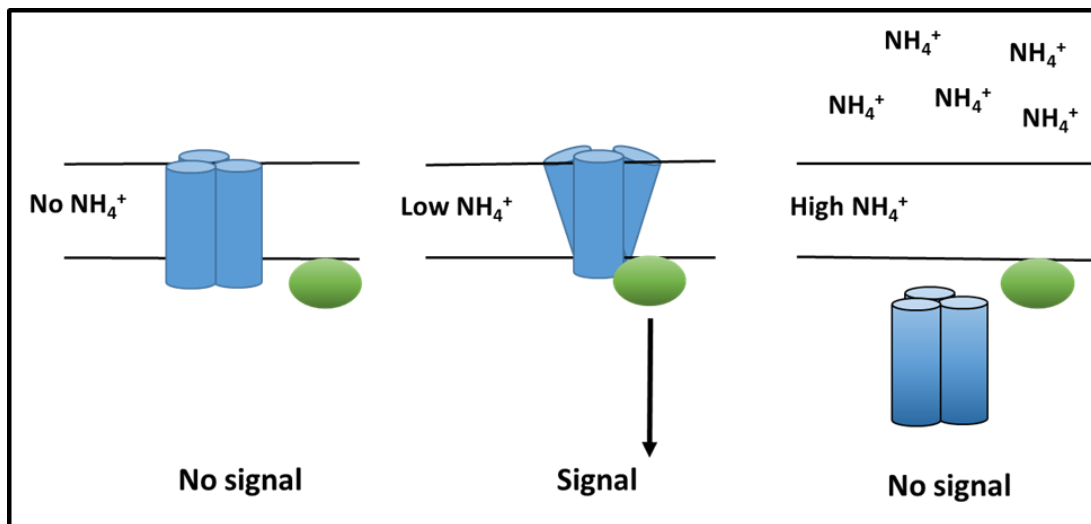
Figure 10: Transceptor model of Mep2 function – During nitrogen starvation conditions Mep2 gets localised to the plasma membrane. Ammonium transport through Mep2 leads to a conformational change in the transporter which allows it to interact with a signalling partner to initiate signalling. The presence of ammonia in the growth media leads to internalisation and sorting of Mep2, transcription of *MEP2* gene gets repressed resulting in a loss of pseudohyphal signalling. Figure adapted from Rutherford *et al*, 2008.

1.5.3. Signalling pathways involved in the induction of pseudohyphal growth

In *S. cerevisiae* induction of pseudohyphal growth under nitrogen limitation appears to be much more complex than just a simple morphogenetic switch. Filamentous growth regulation assimilates signals from various events including nutrient signal integration, alteration of cell physiology, cell cycle, morphology, re-organisation of polarity and regulation of physiological responses for individual cells. The regulation of this dimorphic switch is complex, involving multiple interconnected signalling pathways that elicit a number of distinct adaptive responses. The major signalling pathways involved in the regulation of pseudohyphal growth in yeast include Mitogen Activated Protein Kinase (MAPK) cascades (Posas *et al*, 1998; Madhani & Fink, 1998), cyclic AMP dependent Protein Kinase A (PKA) pathway (Robertson & Fink, 1998; D'souza & Heitman, 2001), Sucrose Non-Fermentable (SNF1) (Cullen & Sprague, 2000) and Target of Rapamycin (TOR) (Cutler *et al*, 2001) signalling pathways. A central component in the signalling pathway shared between the MAPK and cAMP pathways appears to be the GTP binding protein Ras2 (Mosch *et al*, 1999).

The four different MAP Kinase cascades in *S. cerevisiae* include the pheromone response pathway, the pseudohyphal growth pathway, the Protein Kinase C (PKC) pathway and the osmoregulatory pathway (Posas *et al*, 1998). The mating pheromone pathway and the pseudohyphal growth pathway have components in common even though they are activated in response to different environmental cues. The MAP Kinase cascade involved in filamentous growth (Fig. 11) includes Ras2, Cdc42, protein kinases Ste20, Bmh1/2, Ste11, Ste7, Kss1 and transcription factors Ste12 and Tec1 (Liu *et al*, 1993; Madhani *et al*, 1997). An external signal activates Ras2 which in turn activates Ste20 through Cdc42, a Rho-type GTP binding protein in its GTP bound form binds and activates Ste20. The 14-3-3 proteins Bmh1 and Bmh2 associate with Ste20 *in vivo* and are essential for initiation of pseudohyphal growth. 14-3-3-Ste20 complexes play a central role in cell elongation which is independent of their MAP Kinase cascade function (Roberts *et al*, 1997). Protein kinases Ste20 and Ste11 seem to integrate multiple aspects of signalling to co-ordinate filamentous growth through MAP Kinase pathway, and act in sequence along with Ste7. Depending on the phosphorylation state of Kss1 it can either activate or inhibit pseudohyphal growth by preventing Ste12 activation (Cook *et al*, 1997). Kss1 plays a role in the mating pathway too, and acts as a shared component between the two pathways similar to Ste12. Transcription factors Ste12 and Tec1 bind to filamentous response elements (FREs) to activate gene transcription (Madhani *et al*, 1997).
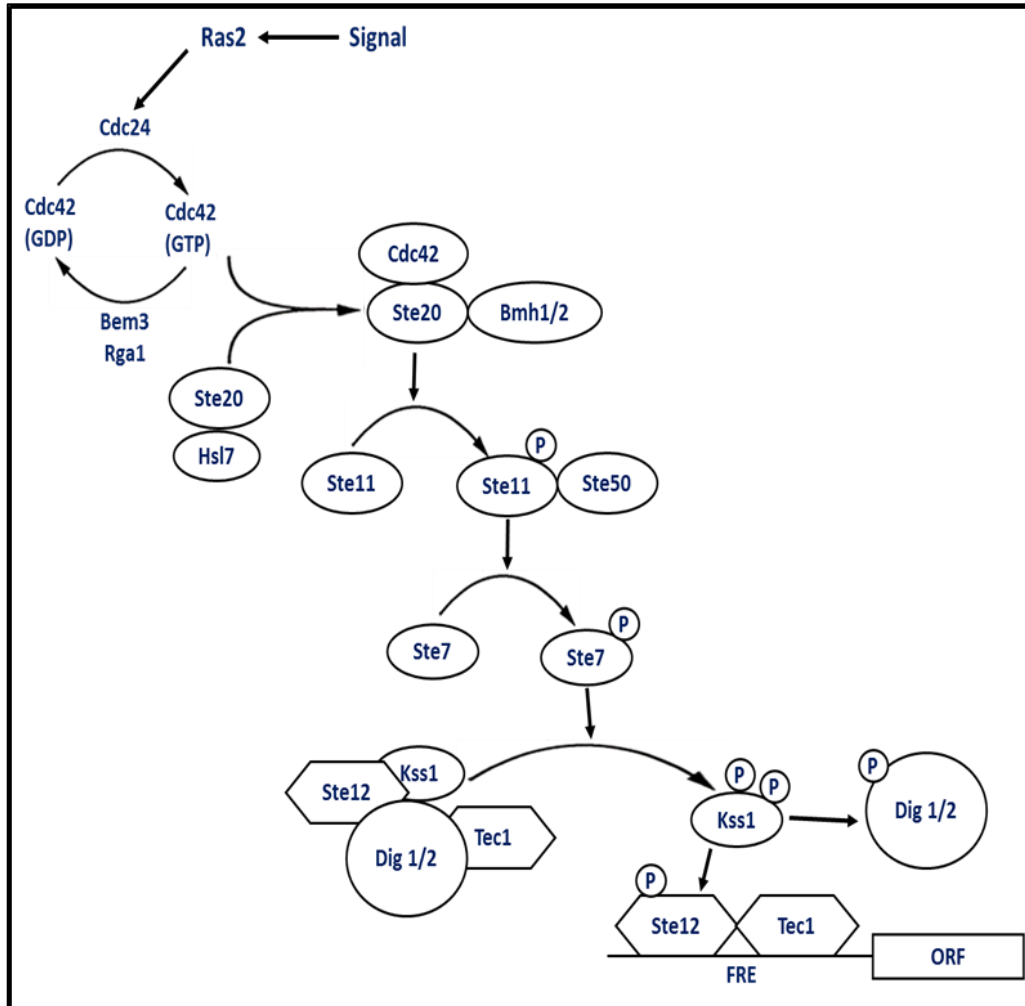
Figure 11: MAP Kinase cascade regulates pseudohyphal growth in *S. cerevisiae*. External signal activates Ras2 which activates the MAP Kinase cascade through a series of events including phosphorylation of components and transcriptional activation of FREs. Figure adapted from Gancedo, 2000.

The nutrient sensing cAMP-PKA pathway functions in parallel to the MAP Kinase pathway to regulate filamentous growth. In this pathway (Fig. 12) the cyclic AMP dependent PKA plays a vital role in the regulation of pseudohyphal growth. Activation of Ras2 stimulates adenylate cyclase Cyr1 raising the intracellular concentration of cAMP. Increased levels of cAMP activate cAMP-dependent protein kinases. Elevated cAMP levels activate the regulatory subunit of the PKA pathway which includes Bcy1 and three catalytic subunits Tpk1-3 which forms a complex with Bcy1 (Pan & Heitman, 1999). Tpk2 subunit has a role in the regulation of the transcription factor FLO8 and thereby regulating the expression of the cell surface flocculin FLO11 which is vital for pseudohyphal growth (Robertson & Fink, 1998). Earlier studies have demonstrated that both MAP Kinase and cAMP signalling pathways work in parallel to regulate pseudohyphal growth and they converge on the *FLO11* promoter, a cell surface glycoprotein required for cell-cell adhesion and flocculation (Rupp *et al*, 1999). The GPCR Gpr1 is considered to act upstream of the PKA pathway. The Gα protein Gpa2 might be involved in the regulation of the Ras dependent activation of PKA pathway to regulate pseudohyphal growth (Lorenz & Heitman, 1997).

The depletion of a fermentable carbon source acts as a trigger to initiate pseudohyphal growth. SNF1 pathway senses glucose levels and feeds the information into regulation of the pseudohyphal growth pathway. SNF1 functions using a different signalling pathway compared to the other sugar sensor Gpr1. This suggests that two independent glucose sensing pathways exist to regulate filamentous growth in yeast (Cullen & Sprague, 2000).

The TOR pathway, a serine/threonine protein kinase involved in the maintenance of cellular homeostasis by regulating the levels of cellular nutrients plays a role in the regulation of filamentous growth in yeast (Sengupta *et al*, 2010). The TOR pathway achieves this by regulating the transcription factor Gcn4 which regulates *FLO11* expression (Braus *et al*, 2003). The regulation of filamentous growth by the TOR pathway appears to be independent of the existing signalling mechanisms regulating pseudohyphal growth, namely cAMP-PKA and MAP Kinase pathways.
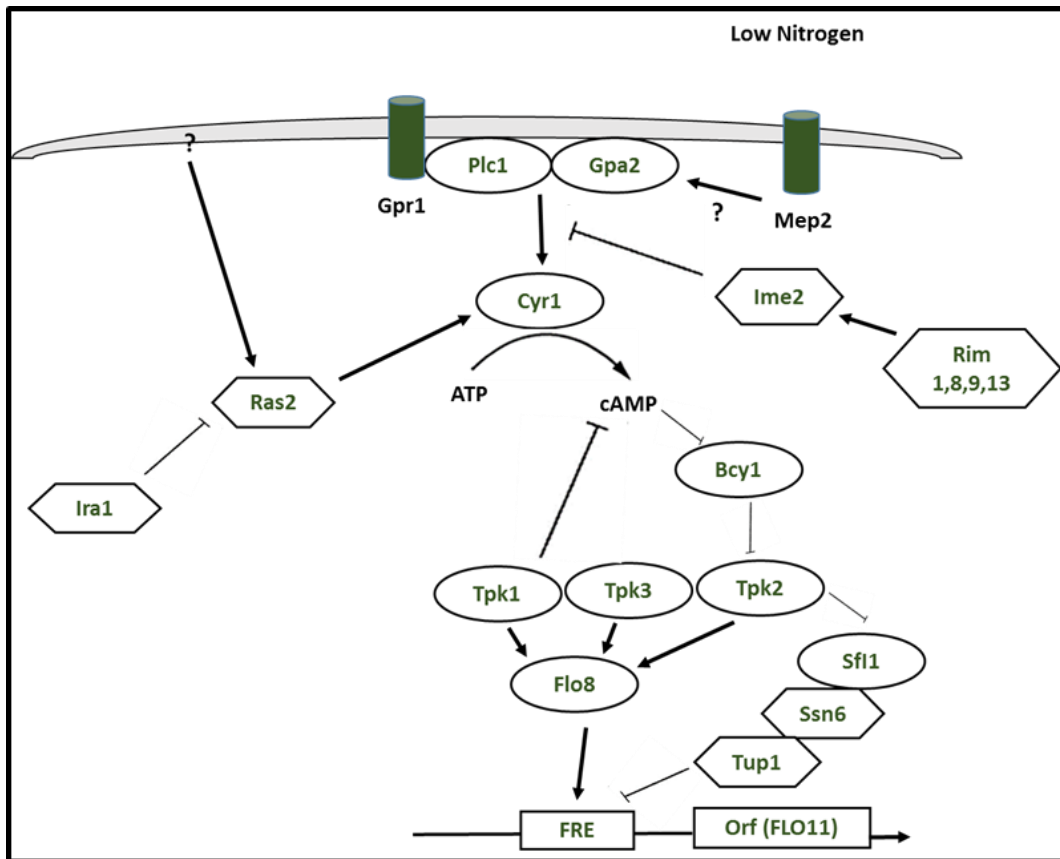
Figure 12: cAMP-PKA pathway regulates pseudohyphal growth in *S. cerevisiae*. External glucose and nitrogen signals activate Ras2 which stimulates cAMP production and activates the Tpks resulting in the activation of PKA signalling. Figure adapted from Palecek *et al*, 2002.

1.5.4. Cross-talk between cAMP-PKA and MAP Kinase pathways

Several lines of evidence from earlier studies suggest that these signalling pathways cross talk. The small G protein Ras2 is shared between the two pathways and it plays a dual signalling role activating both pathways. The first line of evidence was obtained by showing that dominant mutations in *RAS2* or *GPA2* were able to rescue the pseudohyphal growth defects in MAP Kinase mutant strains (Lorenz & Heitman, 1997). The second line of evidence was obtained from experiments showing that a dominant *GPA2-2* mutant was able to fully rescue the pseudohyphal growth defect in a *ste12Δ/ste12Δ* mutant strain, but was able to only partially rescue in a *tec1Δ/tec1Δ* mutant strain. The final line of evidence comes from Lorenz & Heitman (1998) using their constitutively active MAP Kinase alleles (*STE11*) where they show that these alleles were able to supress the pseudohyphal growth defects in *mep2Δ/mep2Δ* or *gpa2Δ/gpa2Δ* mutant strains. The expression of *FLO11*, the cell wall protein essential for invasive and filamentous growth in yeast is controlled by both cAMP-PKA and MAP Kinase pathways. cAMP and Kss1 control *FLO11* transcription, and *FLO11* contains multiple segments which independently respond to each signalling pathway. Both the signalling pathways converge at the point of *FLO11*, an essential step during pseudohyphal growth induction to regulate *FLO11* promoter (Rupp *et al*, 1999). The presence of putative PKA phosphorylation sites on the transcription factor Ste12 suggests that it could be a potential PKA target and this acts as another line of evidence (Lorenz & Heitman, 1998).

These findings suggest that the functions of one pathway can be bypassed by hyperactivating the other and these two pathways are able to function independently and parallel to each other for the induction of pseudohyphal growth. Moreover, the pathways have a shared role in regulating the transcription of the cell surface flocculin FLO11 (Pan & Heitman, 1999). The MAP Kinase and PKA pathways co-ordinate regulation of pseudohyphal growth and transmits signals to initiate filamentation in *C. albicans*. When effectors of the MAPK and PKA signalling pathways were deleted, filamentation defects were observed and significant reduction in virulence was detected suggesting that non-filamentous mutants were avirulent (Lo *et al*, 1997). Pseudohyphal differentiation in the plant pathogen *U. maydis* requires synchronisation between MAPK and cAMP-PKA pathways for the formation of filaments for colonisation and virulence. Nevertheless, cAMP pathway helps the pathogen to switch from the filamentous form to a normal yeast form as opposed to *S. cerevisiae*, and activation of PKA pathway represses formation of filaments suggesting that pseudohyphal growth in *U. maydis* is regulated by the MAP Kinase pathway (Kronstad *et al*, 1998; Durrenberger *et al*, 1998; Andrews *et al*, 2000).

1.6. Mep2 regulation by the TORC1 effector kinase Npr1

The Npr1 (nitrogen permease reactivator 1) kinase is a serine/threonine protein kinase under the regulation of TORC1 complex which responds to the availability of nutrients. Earlier studies have suggested that Npr1 kinase is a regulator of ammonium transporters required for optimum uptake of nitrogen when grown on non-preferred nitrogen sources, and regulates the stability of these transporters (Schmidt *et al*, 1998). The Npr1 kinase has further roles in the regulation of sorting and localisation of Gap1, the general amino acid permease (De Craene *et al*, 2001). When poor sources of nitrogen are available, TORC1 is downregulated which results in the activation of Npr1 kinase as it is only weakly phosphorylated, and in the presence of rich sources of nitrogen increased phosphorylation renders the kinase inactive (Gander *et al*, 2008). Cells lacking Npr1 kinase and all three Meps displayed comparable growth defects when grown on low ammonium medium suggesting a role for Npr1 in the regulation of Mep proteins (Feller *et al*, 2006). Growth defects of cells lacking Npr1 kinase might thus be due to the absence of Mep activity in those cells as Npr1 kinase is a positive regulator of the Mep protein function, and is essential for the stable expression of the transporter. For optimal transport of ammonium, Mep proteins need Npr1 kinase and growth defects of cells lacking Npr1 kinase could be partly due to the inefficient re-uptake of ammonium from the surroundings lost during leakage of ammonium from the cells, and also due to the inability of the transporter to transport ammonium from the available surrounding sources, both due to an inactive Npr1 kinase (Boeckstaens et al, 2007). Constitutively active Mep2 showed hyperactivity both in the presence and absence of Npr1 kinase, and restored growth defects even in ammonium rich conditions suggesting that transport and sensing function of Mep2 are strongly coupled. It was later shown that Npr1 kinase plays central roles in ammonium induced pseudohyphal growth and Mep2-mediated ammonium transport (Boeckstaens et al, 2007). The localisation of Mep2 in mutants lacking Npr1 kinase revealed that Mep2 gets localised correctly to the plasma membrane under both high and low ammonium conditions. Therefore, the pseudohyphal growth defect observed in these mutants could not be corroborated to the lack of localisation of Mep2 to the membrane surface. This suggests that Npr1 kinase is dispensible for the synthesis, membrane targeting ability or the stability of Mep2 ammonium transporter. Furthermore, although expression levels of Mep2 were found to be high in Npr1 mutants, they were unable to transport ammonium in the absence of kinase function. The inability of these mutants for ammonium transport in the absence of Npr1 kinase might account for the failure of the mutants to undergo pseudohyphal differentiation (Rutherford *et al*, 2008).

An earlier study (Boeckstaens *et al*, 2014) revealed that Npr1 kinase fine tunes the activity of Mep2 ammonium transporter. This was achieved by regulating the phosphorylation of a conserved regulatory domain in the C-terminal tail. Although protein stability or membrane targeting functions of Mep2 were not affected in cells lacking Npr1 kinase, phosphorylation event of Mep2 occured in an Npr1-dependent manner. Npr1 mutants were unable to grow on low ammonium concentrations and were unable to undergo pseudohyphal differentiation. Inherent activity of Mep2 relied on the preservation of kinase function and Npr1 inactivation resulted in an instant disappearance of the phosphorylated form of Mep2 revealing a direct link between Npr1 activation and Mep2 phosphorylation. Phosphorylation site prediction combined with site-directed mutagenesis identified a serine at the C-terminal tail of the transporter at position 457 as the site of Npr1 phosphorylation on Mep2. The kinase action on the transporter was found to be direct and phosphorylation at the S457 residue was critical for Mep2 function. The activity of the ammonium permease was controlled by Npr1 kinase via this phosphorylation event. Analysis of suppressor mutations revealed the involvement of C-terminal tail, cytoplasmic facing domains and intracellular loops (ILs) in regulating the transport efficacy and activity of the transporter. The activity of the transporter was found to be dependent on the ability of Npr1 kinase to control Mep2 conformation to keep the protein in its active form. Thus, Npr1 tunes Mep2 activity by mediating S457 phosphorylation, and thereby hindering the auto-inhibitory domain of the C-terminal tail showing that Mep2 activity is dependent on the exact phosphorylation of this regulatory C-terminal domain.

Boeckstaens *et al* (2014) propose a model for regulation of Mep2 by Npr1 kinase (Fig. 13). During nitrogen starvation conditions, Npr1 phosphorylates Mep2 at position S457 of the C-terminal tail activating the transporter. This phosphorylation silences the C-terminal autoinhibitory domain which results in the enhancer domain of the CTR to activate the transporter for substrate import. This activation of the permease results in the import of ammonium into the cell. Upon supplementation of a rich or preferred source of nitrogen rapid dephosphorylation of Mep2 by the plasma membrane phosphatases Psr1 and Psr2 results in the inactivation of the transporter. The autoinhibitory domain which is no longer phosphorylated prevents the enhancer domain from activating the transporter. Therefore, transporter activity is maintained and regulated through an active equilibrium between Npr1-dependent phosphorylation and Psr-dependent dephosphorylation events where the TORC1 effector Npr1 kinase occupies a central role (Boeckstaens *et al*, 2014).
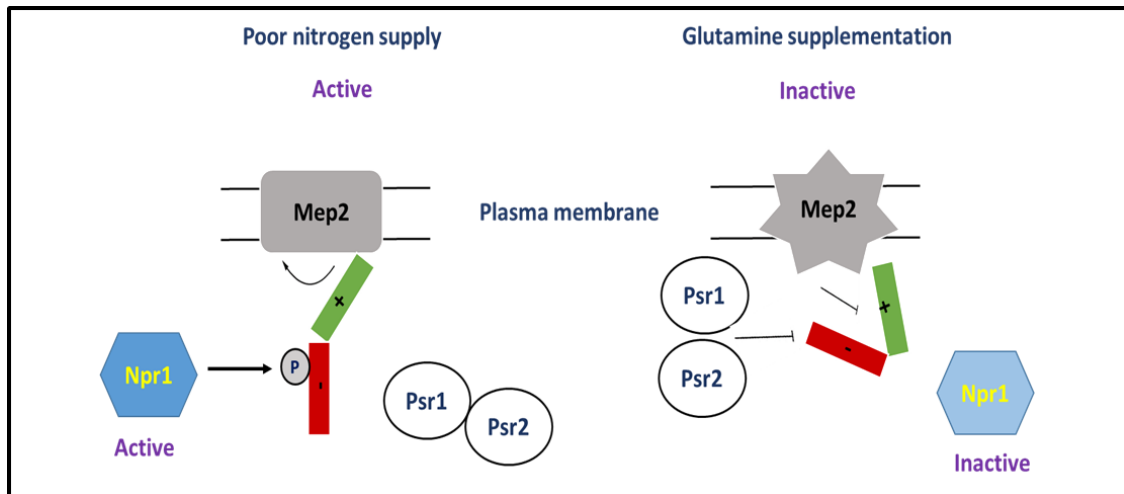
Figure 13: Model of Mep2 regulation by Npr1 kinase. In the presence of a poor source of nitrogen, TORC1 is downregulated which activates Npr1 kinase to phosphorylate Mep2 at position S457 and silence the autoinhibitory domain of the C-terminal tail. The enhancer domain consequently activates Mep2 ammonium transport. The presence of a rich nitrogen source inactivates Npr1 kinase and the plasma membrane phosphatases Psr1 and Psr2 de-phosphorylate Mep2 and inactivates the transporter. Figure adapted from Boeckstaens *et al*, 2014.

TORC1 controls the transport activity of the other Mep proteins, Mep1 and Mep3. Boeckstaens *et al* (2015) demonstrated that the activity of the Mep1 and Mep3 ammonium transporters were stable in Npr1 mutant strains. However, Npr1 activity was essential for the inherent transport ability of these transporters, and inactivation of Npr1 was associated with the inactivation of Mep1 transporter protein function. Inherent activity of Mep1 was largely dependent on the integrity of kinase function. They showed that overexpression of *MEP1* and *MEP3* genes were able to compensate for the lack of kinase function and relieved the prerequisite for Npr1 kinase function in those transporters. They identified an inhibitory partner for kinase function to be Amu1/Par32 and it functioned as a negative regulator of ammonium transport. Amu1/Par32 is characterized by four-fold repeat motifs and is of unknown biological function (Bah *et al*, 2015). Loss of *AMU1* activity allowed restoration of Mep1 and Mep3 transporter function in Npr1 mutant strains. Immunoprecipitation studies revealed a physical interaction between Amu1, and Mep1 and Mep3 ammonium transporters. They proposed a model for the regulation of Mep1 and Mep3 ammonium transporters by TORC1-Npr1 kinase during nitrogen limitation. During nitrogen limitation, Npr1 kinase is active and mediates Amu1/Par32 phosphorylation, which remains cytosolic. In the mean time, Mep1 and Mep3 are active and transport ammonia. Upon supplementation of a preferred nitrogen source in the growth media, TORC1 is upregulated which results in the inhibition of Npr1 kinase function. This results in the dephosphorylation of Amu1/Par32 which is then localised to the membrane surface to interact with Mep1 and Mep3 transporters to inhibit their function and prevent ammonium import.

1.7. Aims and Context

This study thus aims to enhance our understanding towards the role of ammonium transporter Mep2 in regulating pseudohyphal growth, and the molecular mechanisms governing ammonium sensing and signalling in yeast. Structural studies including elucidation of X-ray crystal structure of Mep2 and comparison with existing structures of homologues would help to gain new insights into the functions of this ammonium transporter. By undertaking structure based mutational analysis and characterisation of Mep2 mutants, their ability to transport ammonium, initiate pseudohyphal growth and protein expression levels could be tested. This would allow us to identify key residues having potential roles in ammonium transport and signalling. Once these conserved residues are identified that have crucial roles in Mep2 ammonium transport and pseudohyphal growth, the next step would be to identify non-signalling Mep2 variants which are able to uncouple ammonium transport and signalling

functions of Mep2. With the help of these non-signalling mutants that are able to uncouple the transport and signalling functions of Mep2, the two distinct models of ammonium sensing by Mep2 could be tested. The first model, the pH model of ammonium sensing could be tested to see whether Mep2-mediated intracellular pH changes are essential to activate a signalling pathway to initiate pseudohyphal growth. Intracellular pH changes within the cytosol during ammonium transport could be measured to test whether localised pH changes if any is Mep2 dependent. In order to test the second model of Mep2 function which is the transceptor model of ammonium sensing, a global analysis of protein interactions could be undertaken to identify potential interaction partners of Mep2. By testing these potential interaction partners, a downstream signalling partner capable of physically interacting with Mep2 to initiate downstream signalling during pseudohyphal growth could be identified. Further mutants could be generated to identify residues essential for this interaction and thereby identify the signalling pathway involved in the regulation of this dimorphic switch. This would then allow us to propose a model for ammonium sensing and signalling by Mep2.

The molecular mechanisms that link ammonium transport and signalling are robustly coupled. Understanding the precise mechanisms behind ammonium sensing in fungi and the regulation of these ammonium transporters could help us to devise strategies to develop specific and effective anti-fungal agents to manage fungal infections in plants and animals.

2. Methods

2.1. Strains and growth conditions

The *S. cerevisiae* strains used in this study are listed in Table 1. All of the strains are isogenic with the wild type Σ1278b strain except for BY4741 which is isogenic with S288C strain. For yeast transformation, YP media (1% yeast extract and 2% peptone) with 2% glucose as carbon source was used. For western analysis the cells were grown in amino acid deficient synthetic minimal medium containing 2% glucose. 2% galactose was used instead of glucose for induction under a Gal promoter. Nitrogen sources were included depending on the requirement of each experiment which included 0.1% proline, 0.1% glutamate and 1mM ammonium sulphate. For *E. coli* transformation, LB media was used (1% tryptone, 0.5% yeast extract and 1% sodium chloride). PCR mediated gene deletions were performed in haploid strain by replacing the gene of interest with a Nat cassette or G418 via homologous recombination conferring resistance to the antibiotics Nourseothricin (nat) or Kanamycin (Kan). Pseudohyphal growth assays were performed by growing the strains in synthetic low ammonia dextrose (SLAD) medium containing 50 µM ammonium sulphate, 0.17% yeast nitrogen base (YNB) lacking amino acids and ammonium sulphate, 2% agar and 2% glucose, or 2% galactose along with 0.4% glucose for induction under a Gal promoter.

Table 1: Strains used in this study

Strains	Genotype	Reference
BY4741	*MAT**a** his3Δ leu2Δ met15Δ ura3Δ*	Brachmann *et al* (1998)
Mep2-KanMX-BY4741	*MAT**a** his3Δ leu2Δ met15Δ ura3Δ mep2Δ::G418*	Brachmann *et al* (1998)
MLY54	*MAT**a**/α ura3-52/ura3-52 npr1::LEU2/npr1::LEU2 leu2::hisG/leu2::hisG*	Lorenz & Heitman (1998a)
MLY40	*MATα ura3-52*	Lorenz & Heitman (1997)

MLY108	*MAT**a**/α ura3-52/ura3-52 Δmep2::LEU2/Δmep2::LEU2 Δleu2::hisG/Δleu2::hisG*	Lorenz & Heitman (1998a)
MLY225	*MAT**a**/ α mep2::G418/mep2::G418 leu2::hisG/leu2::hisG ura3-52/ura3-52*	Lorenz & Heitman (1998a)
NMY32	*MAT**a** his3delta200 trp1-901 leu2-3, 112 LYS2::(lexAop)$_4$-HIS3 URA3::(lexAop)$_8$-lacZ (lexAop)$_8$-ADE2 GAL4*	Dualsystems Biotech, Switzerland
mep123Δ	*MATα ura3-52 mep1Δ mep2Δ::LEU2 mep3Δ::G418*	This study
mep123-npr1Δ	*MATα ura3-52 mep1Δ mep2Δ::LEU2 mep3Δ::G418 npr1Δ::nat*	This study
GPA2-13Myc KanMX-MLY108	GPA2-13Myc KanMX *MAT**a**/α ura3-52/ura3-52 Δmep2::LEU2/Δmep2::LEU2 Δleu2::hisG/Δleu2::hisG*	This study
Bmh1-13Myc KanMX-MLY108	Bmh1-13Myc KanMX *MAT**a**/α ura3-52/ura3-52 Δmep2::LEU2/Δmep2::LEU2 Δleu2::hisG/Δleu2::hisG*	This study
MLY108 pJRJH7	*MAT**a**/α ura3-52/ura3-52 Δmep2::LEU2/Δmep2::LEU2 Δleu2::hisG/Δleu2::hisG* + respective plasmid	This study
MLY108 pRS316		This study
MLY108 T288E		This study
MLY108 Y53A		This study
MLY108 N2-27 delta		This study
MLY108 T229D		This study
MLY108 N246A		This study
MLY108 E441A		This study
MLY108 G349C		This study
MLY108 H226A		This study
MLY108 Δ434		This study
MLY108 Δ454		This study
MLY108 Δ430 FLAG		This study
MLY108 Y444A		This study
MLY108 Δ439G		This study

mep123Δ pJRJH7	*MATα ura3-52 mep1Δ mep2Δ::LEU2 mep3Δ::G418*	This study
mep123Δ pRS316	*+ respective plasmid*	This study
mep123Δ T288E		This study
mep123Δ Y53A		This study
mep123Δ N246A		This study
mep123Δ E441A		This study
mep123Δ Y444A		This study
mep123Δ N2-27 delta		This study
mep123Δ H226A		This study
mep123Δ G349C		This study
mep123Δ T229D		This study
mep123Δ Δ430		This study
mep123Δ Δ434		This study
mep123Δ Δ439G		This study
mep123Δ Δ454		This study
MLY108 Mep2 WT	*MAT**a**/α ura3-52/ura3-52 Δmep2::LEU2/Δmep2::LEU2 Δleu2::hisG/Δleu2::hisG*	This study
MLY108 pRS316	*+ respective plasmid*	This study
MLY108 K/R		This study
MLY108 D/Y/F		This study
MLY108 N246A		This study
MLY108 H194E		This study
MLY108 H348A		This study
MLY108 G349C		This study
MLY108 T459A		This study
MLY108 T459D		This study
mep123Δ Mep2 WT	*MATα ura3-52 mep1Δ mep2Δ::LEU2 mep3Δ::G418*	This study
mep123Δ pRS316	*+ respective plasmid*	This study
mep123Δ K/R		This study
mep123Δ D/Y/F		This study
mep123Δ N246A		This study
mep123Δ H194E		This study

mep123Δ H348A		This study
mep123Δ G349C		This study
Bmh1-13Myc pRS316	Bmh1-13Myc KanMX *MAT**a**/α ura3-52/ura3-52* *Δmep2::LEU2/Δmep2::LEU2* *Δleu2::hisG/Δleu2::hisG* + respective plasmid	This study
Bmh1-13Myc pJRJH7		This study
Bmh1-13Myc N246A		This study
Bmh1-13Myc H194E		This study
Bmh1-13Myc H348A		This study
Bmh1-13Myc G349C		This study
Bmh1-13Myc T459A		This study
Bmh1-13Myc T459D		This study
mep123Δ pRS316	*MATα ura3-52 mep1Δ mep2Δ::LEU2 mep3Δ::G418* + respective plasmid	This study
mep123Δ pJRJH7		This study
mep123Δ N246A		This study
mep123Δ H194E		This study
mep123Δ H348A		This study
mep123Δ G349C		This study
mep123Δ T459A		This study
mep123Δ T459D		This study
*mep123-npr1Δ*WT His	*MATα ura3-52 mep1Δ mep2Δ::LEU2 mep3Δ::G418 npr1Δ::nat* + respective plasmid	This study
mep123-npr1Δ pRS316		This study
mep123-npr1Δ 2-27Δ		This study
mep123-npr1Δ Y53A		This study
mep123-npr1Δ Δ446		This study
mep123-npr1Δ Δ457		This study
mep123-npr1Δ RD/SD		This study
mep123-npr1Δ S457D		This study
GPA2-13Myc pRS316	GPA2-13Myc KanMX *MAT**a**/α ura3-52/ura3-52* *Δmep2::LEU2/Δmep2::LEU2* *Δleu2::hisG/Δleu2::hisG* + respective plasmid	This study
GPA2-13Myc pJRJH7		This study
GPA2-13Myc S457D		This study
GPA2-13Myc R/D		This study

2.2. Genomic DNA extraction, PCR and agarose gel electrophoresis

Genomic DNA was isolated from *S. cerevisiae* strains using Gentra Puregene Yeast/Bact Kit (QIAGEN) following manufacturer's protocol. Routine PCRs for cloning and sequencing were performed using Vent DNA polymerase (New England Biolabs) and colony PCRs using GoTaq DNA polymerase (Promega). Oligonucleotide primers used in this study are listed in Table 2. The following would be a typical PCR reaction mix.

10X PCR reaction buffer	-	5µl
dNTP mix (10mM)	-	1 µl
Primers F&R (10µM)	-	0.75µl
Template DNA (~1µg)	-	1µl
DNA polymerase (5U/µl)	-	0.5µl
dH₂O	-	up to 50µl

The following cycling program was generally used for PCR.

Initial denaturation	1 cycle	95ºC 10min
Denaturation	35 cycles	95ºC 1min
Annealing		55ºC 1min
Extension		72ºC 1min/kb
Final extension	1 cycle	72ºC 10min

5µl of PCR product was run on 1% agarose gel to check for amplified products. DNA gel electrophoresis was performed using 1 X TBE buffer and imaged using ChemiDoc XRS gel documentation system (Bio-Rad).

Table 2: Oligonucleotide primers used in this study

Primer name	Sequence (5'→3')
M13F	GTAAAACGACGGCCAGTG
M13R	CAGGAAACAGCTATGACC
Mep2 S1	GCGGCGTGAAGACCCTGTG

Mep2 S2	GTAGCTTGGACTATGCAGG
Mep2-1	CTTTCAAAGCTCTGTGCAGAC
Mep2-2	CATTCGTGCTTTCACGTCC
Mep2-3	CTAGGCCAGCGATGATACCTG
Mep2-4	CAGATGCGGAAGAAAGTGGAC
GPA2-13Myc F	AATTTTGGAAAATACATTGAAAGACTCTGGAGTGTTA CAA CGGATCCCCGGGTTAATTAA
GPA2-13Myc R	AGAAGAGGCATGCAGTTTTGTCTCTGTTTTAGCTGTG CAT GAATTCGAGCTCGTTTAAAC
BMH1-13Myc F	ACAGCAGCCACCTGCTGCCGCCGAAGGTGAAGCACC AAAG CGGATCCCCGGGTTAATTAA
BMH1-13Myc R	TCTTTTTTTTAGTAATTTCTCTTTAGATTTATCAGAAT AC GAATTCGAGCTCGTTTAAAC
GPA2-13Myc D F	CTAAGCATATATCCTCACGTG
BMH1-13Myc D F	GTCCGAGTCCGGTCAAGCTG
Y53A F	GGTCCCAGGTATCGGTTTATTAGCTTCTGGTTTATCCA GGAAAAAGCATGC
Y53A R	GCATGCTTTTTCCTGGATAAACCAGAAGCTAATAAAC CGATACCTGGGACC
2-27Δ F	CTTAATATATTACAATACAATATCAACAATGGACTTG GCCAACATGGGATGGATCGG
2-27Δ R	CCGATCCATCCCATGTTGGCCAAGTCCATTGTTGATA TTGTATTGTAATATATTAAG
Δ446no tag F	GGTGAATTTACATACGAGGAATAATGATATACTCAAG CAGACTATG
Δ446no tag R	CATAGTCTGCTTGAGTATATCATTATTCCTCGTATGTA AATTCACC
Δ446 F	GTGAATTTACATACGAGGAACATCACCATCACCATCA CTAAC
Δ446 R	GTTAGTGATGGTGATGGTGATGTTCCTCGTATGTAAA TTCAC
Δ457no tag F	CATCCCAGAACCAATCAGATCTTAAGATATACTCAAG CAGACTATG

Δ457no tag R	CATAGTCTGCTTGAGTATATCTTAAGATCTGATTGGTT CTGGGATG
Δ457 F	CATCCCAGAACCAATCAGATCTCATCACCATCACCAT CACTAAC
Δ457 R	GTTAGTGATGGTGATGGTGATGAGATCTGATTGGTTC TGGGATG
R456D/S457D F	CTTACATCCCAGAACCAATCGACGATAAAACATCGGC ACAAATGCC
R456D/S457D R	GGCATTTGTGCCGATGTTTTATCGTCGATTGGTTCTGG GATGTAAG
S457D F	CATCCCAGAACCAATCAGAGATAAAACATCGGCACA AATGCC
S457D R	GGCATTTGTGCCGATGTTTTATCTCTGATTGGTTCTGG GATG
K210A/R211G F	CTAGTTTACGCTTTGATACTGGGTGCGGGTAATGACC CTGTTACACGTAAAGGG
K210A/R211G R	CCCTTTACGTGTAACAGGGTCATTACCCGCACCCAGT ATCAAAGCGTAAACTAG
D279A/Y280G/F281A F	GGCTTGACATGGATGGTTATCGCTGGTGCCAGATGCG GAAGAAAGTGGACT
D279A/Y280G/F281A R	AGTCCACTTTCTTCCGCATCTGGCACCAGCGATAACC ATCCATGTCAAGCC
H194E F	GACTATGCAGGTGGTTTATGTGTCGAGTTAACATCTG GACATGGTGGTCTA
H194E R	TAGACCACCATGTCCAGATGTTAACTCGACACATAAA CCACCTGCATAGTC
H348A F	GATGGTCTAGATTGTTACTCTATCGCTGGTGTGGGTG GTTGTATTGGTTCT
H348A R	AGAACCAATACAACCACCCACACCAGCGATAGAGTA ACAATCTAGACCATC
T459A F	CATCCCAGAACCAATCAGATCTAAAGCATCGGCACA AATGCCACCTCCTC
T459A R	GAGGAGGTGGCATTTGTGCCGATGCTTTAGATCTGAT TGGTTCTGGGATG

T459D F	CATCCCAGAACCAATCAGATCTAAAGACTCGGCACAAATGCCACCTCCTC
T459D R	GAGGAGGTGGCATTTGTGCCGAGTCTTTAGATCTGATTGGTTCTGGGATG
G349C F	GTCTAGATTGTTACTCTATCCATTGTGTGGGTGGTTGTATTGGTTCTG
G349C R	CAGAACCAATACAACCACCCACACAATGGATAGAGTAACAATCTAGAC
N246A F	CTTATGGTTTGGTTGGATGTTCTTTGCCGGAGGCTCTGCAGGTAATGCAAC
N246A R	GTTGCATTACCTGCAGAGCCTCCGGCAAAGAACATCCAACCAAACCATAAG
pYES2.1 – Mep2 F	AATATACCTCTATACTTTAACGTC
pYES2.1 – Mep2 R	CTAAGAACACTGACCATATAGTACATCACCATCACCATCACTAATAGAGGGCCGCATCATGTAATTAGTTATGTCACGCTTACA
pYES2.1 – Mep2 Termi	GTGAGCTGATACCGCTCGCCGC
Mep2 Gal P	GGTAATTAATCAGCGAAGCGATG
pCCW-Mep2 F	TCTGCAGGAATTCGATATCAATGTCTTACAATTTTACAGGTACGC
pCCW-Mep2 R	CATGGTCGACGGTATCGATATACTATATGGTCAGTGTTCTTAGTAGAAG
pDL2-xN-Mep2 F	CAGAGTGGCCATTACGGCCCATGTCTTACAATTTTACAGGTACGC
pDL2-xN-Mep2 R	CGGCCGACATGTTTTTTCCCTACTATATGGTCAGTGTTCTTAGTAGAAG
pDL2-xN-Bmh1 F	CAGAGTGGCCATTACGGCCCATGTCAACCAGTCGTGAAGATTCTGTGTACC
pDL2-xN-Bmh1 R	CGGCCGACATGTTTTTTCCCCTTTGGTGCTTCACCTTCGGCGGCAGCAGG

2.3. Plasmids and mutagenesis

The plasmids used in this study are listed in Table 3. Site directed mutagenesis of *MEP2* was performed by PCR amplifying *MEP2* from the plasmid pJRH7 (Rutherford *et al*, 2008) containing endogenous promoter (1kb) and terminator, and N4Q mutation to prevent glycosylation of Mep2. All *MEP2* mutants included in this study were generated from this plasmid replacing FLAG tag with a His6 tag where appropriate. Desired single or double amino acid changes or truncations were introduced using 45-55mer oligonucleotides. The plasmids were generated by homologously recombining HindIII linearised pRS316 vector (URA3) and PCR products for generating mutants into Mep2-KanMX strain. C-terminal 13-Myc tags of full length proteins were introduced by PCR based gene tagging using pFA6a-13Myc-kanMX6 plasmid as PCR template. This was achieved by designing the gene specific sequences of the forward primer to end just upstream of the stop codon and those of the reverse primer to end just downstream of the stop codon for PCR based gene modification.

2.4. Plasmid recovery

Recovery of recombined plasmids were carried out following the protocol of Robzyk and Kassir (1992) to rescue autonomous plasmids from yeast. 2ml of overnight culture was grown in selective media. Cells were pelleted by spinning at 3000g for 5 minutes and resuspended in 200µl of STET buffer. Equal volumes of glass beads were added followed by two 30 second pulses with samples on ice for 2 minutes in between pulses. The cell lysates were then incubated at 100ºC for 3 minutes before cooling on ice for 2 minutes. Cell lysates were then centrifuged at 13,000rpm for 10 minutes and the top layer was transferred to 100µl 7.5M ammonium acetate. The tubes were vortexed briefly and freeze precipitate at -20ºC for 2 hours (3 hours ideal). This was followed by high speed centrifugation at 13,000rpm for 10 minutes. The top layer was transferred to 500µl ice cold ethanol, vortexed and centrifuged at 13,000rpm for 10 minutes. The small white pellet was washed with 500µl 70% ice cold ethanol, gently vortexed and centrifuged at 13,000rpm for 10 minutes. The pellet was dried at 65ºC for 3 to 4 minutes and re-suspended in 30µl dH$_2$O.

2.5. Preparation of competent *E. coli*

To a flask containing 200ml of 2XLB medium, 2ml of overnight *E. coli* SURE competent cells (Stratagene) were inoculated and shaken at 30°C for 2 hours. At OD$_{595}$ 0.2ml sterile magnesium

chloride (20mM) was added and left to grow at 30°C until OD_{595} 0.5 when the culture was incubated for 2 hours in an ice water bath. The cells were then pelleted by centrifugation at 4°C for 5 minutes at 900g. The cell pellet was resuspended in 100ml of ice cold calcium/manganese medium (100mM $CaCl_2$, 70mM $MnCl_2$, 40mM $C_2H_3O_2Na$, pH 5.5) and incubated in the cold room overnight. The cells were pelleted next morning by centrifugation at 4°C for 5 minutes at 900g. The supernatant was discarded and the cell pellet was resuspended in 20ml of ice cold calcium/manganese medium with glycerol (15% v/v). 200µl aliquots of competent cells were transferred to pre-cooled eppendorf tubes, snap frozen in liquid nitrogen and stored at -80°C.

2.6. *E. coli* transformation and plasmid mini-prep

Bacterial transformation was carried out using *Escherichia coli* SURE competent cells (Stratagene). Cells stored at -80°C were thawed on ice and to 50 µl of competent cells 1µl of plasmid DNA was added and incubated on ice for 30 minutes. The cells were then heat-shocked at 42°C for 45 seconds before adding 800µl of LB and incubated at 37°C for 60 minutes. The cells were pelleted by spinning at 7000rpm for 1 minute and resuspended in 200µl of LB before plating on LB plates with appropriate antibiotic selection and incubated overnight at 37°C. Isolation of plasmid DNA from *E. coli* was carried out using plasmid mini-prep kit (Sigma Aldrich) following manufacturer's protocol. Accuracy of mutagenesis for all plasmids were verified by sequencing.

Table 3: Plasmids used in this study

Construct	Description	Reference
pRS316	URA3-CEN	Siroski and Hieter (1989)
pJRH7	Mep2-N4Q-FLAG-CEN	Rutherford *et al* (2008)
pJRH8	Mep2-N4Q-H194A-FLAG-CEN	Rutherford *et al* (2008)
pJRH9	Mep2-N4Q-H348A-FLAG-CEN	Rutherford *et al* (2008)
pMep2[H348A]	Mep2-N4Q-H348A-HIS-CEN	Rutherford *et al* (2008)
pYES2.1-Mep2	GAL-Mep2 2µ	Smith *et al* (2003)
pMep2[H194E]	Mep2-N4Q-H194E-FLAG-CEN	Boeckstaens *et al* (2008)

pMep2^{H194E}	Mep2-N4Q-H194E-HIS-CEN	Boeckstaens *et al* (2008)
pMep2$^{K210A/R211G}$	Mep2-N4Q-K210A/R211G-HIS-CEN	Van Nuland *et al* (2006)
pMep2$^{D279A/Y280G/F281A}$	Mep2-N4Q-D279A/Y280G/F281A-HIS-CEN	Van Nuland *et al* (2006)
pMep2^{N246A}	Mep2-N4Q-N246A-HIS-CEN	Van Nuland *et al* (2006)
pMep2^{N246A}	Mep2-N4Q-N246A-FLAG-CEN	Van Nuland *et al* (2006)
pMep2^{G349C}	Mep2-N4Q-G349C-FLAG-CEN	Boeckstaens *et al* (2007)
pMep2^{G349C}	Mep2-N4Q-G349C-HIS-CEN	Boeckstaens *et al* (2007)
pAS1NB Rosella	Rosella-RFP-GFP-LEU2 2µ	Rosado *et al* (2008)
pCCW	Cub-LexA-VP16- LEU2	Dualsystems Biotech, Switzerland
pDL2-xN	Nub-TRP1-2µ	Dualsystems Biotech, Switzerland
pFA6a	pFA6a-13Myc-kanMX6	Longtine *et al* (1998)
pIL30-LEU2	FG(TyA)::lacZ LEU2 CEN	Mösch *et al* (1996)
pMep2^{WT}	Mep2-N4Q-HIS-CEN	This study
pMep2^{Y53A}	Mep2-N4Q-Y53A-HIS-CEN	This study
pMep2^{S457D}	Mep2-N4Q-S457D-HIS-CEN	This study
pMep2$^{R456D/S457D}$	Mep2-N4Q-R456D/S457D-HIS-CEN	This study
pMep2$^{2-27\Delta}$	Mep2-N4Q-2-27Δ-HIS-CEN	This study
pMep2$^{\Delta446}$	Mep2-N4Q-Δ446-HIS-CEN	This study
pMep2$^{\Delta457}$	Mep2-N4Q-Δ457-HIS-CEN	This study
pMep2$^{\Delta457notag}$	Mep2-N4Q-Δ457-CEN	This study
pMep2^{S457A}	Mep2-N4Q-S457A-FLAG-CEN	This study
pMep2^{T459A}	Mep2-N4Q-T459A-FLAG-CEN	This study

pMep2^{T459D}	Mep2-N4Q-T459D-FLAG-CEN	This study
pYES2.1-Mep2^{H194E}	GAL-Mep2-H194E 2µ	This study
pYES2.1-Mep2^{H348A}	GAL-Mep2-H348A 2µ	This study
pCCW-Mep2	Mep2-Cub-LexA-VP16- LEU2	This study
pDL2-xN-Mep2	Mep2-Nub-TRP1-2µ	This study
pDL2-xN-Bmh1	Bmh1-Nub-TRP1-2µ	This study

2.7. Yeast transformation

S. cerevisiae strains were transformed alongside positive and negative controls using lithium acetate method (Schiestl & Gietz, 1989). Overnight cultures were inoculated in 5 ml liquid YPD and were diluted to a starting OD of 0.2 in 50ml YPD the following morning and grown until OD 0.7. Cells were pelleted by spinning at 3,000 rpm for 3 min at room temperature and washed in 1ml sterile distilled water twice by spinning at 7000 rpm for 30 seconds. The pellet was resuspended in 300µl of 100mM LiAc and to make the cells competent.

In a separate tube added

50% PEG	-	240 µl
Competent Cells (from above)	-	50 µl
Plasmid	-	3 µl

(Epitope Tagging - PCR product 50 µl, homologous recombination - 10 µl of PCR products and 10 µl of linearised plasmid)

Single stranded DNA	-	10ul

(Salmon sperm carrier DNA)

Briefly vortex the contents of the tube, then add

1M LiAc	-	32 µl

Briefly vortexed the contents of the tube again, and incubated for 20 min at 30°C followed by heat shocking for 15 min at 42°C. The tubes were centrifuged in a microfuge for 7000 rpm for 30sec followed by two washes with 1 ml sterile distilled water thoroughly resuspending the pellet each time. Selection of transformants were carried out by plating on selective media plates for 2 to 3 days at 30°C, and later re-streaked for single colony.

71

2.8. Pseudohyphal growth and photo microscopy

Transformants along with controls were streaked on Synthetic Low Ammonia Dextrose (SLAD) plates for single colonies and grown for 6 days at 30°C to initiate pseudohyphal growth. The colonies were screened microscopically to evaluate filamentation and colony morphology. Single colonies were directly photographed from petri plates using a Euromex Oxion microscope with a 40X objective lens and CMEX 5000 camera attached to it. Images were captured through Image focus v 3.0 software.

2.9. Transport assay

Transport assay was performed robotically as previously described (Addinall *et al*, 2008). Quantitative fitness analysis (QFA) was performed by growing liquid cultures to comparable OD, diluted and spotted onto solid agar plates. Growth was measured following a time course and photographed. Image analysis provided a logistic growth model to correlate growth with other parameters such as transport of ammonium.

Overnight cultures of *mep123Δ* and *mep123-npr1Δ* transformants and controls grown in selective media were OD checked, pelleted and washed twice with sterile water before resuspending in 1ml sterile water. 200µl of the diluted cultures were inoculated into 96 well plates with 5 sets of repeats in each plate. Cultures were then spotted onto solid agar plates containing 0.17% YNB and varying sources of nitrogen namely 1mM ammonium sulphate, control (no ammonium sulphate), 0.1% glutamate and incubated at 30°C. These were grown for three days to saturation at 30°C without shaking. They were then photographed on a splmager robotically (S&P Robotics Inc, Canada) for 72 hours following a time course. The dilution and spotting of cultures onto solid agar plates was achieved using a Biomek FX robot (Beckman Coulter Limited, UK) equipped with a 96-pintool (2mm diameter). The quantification of cell density from captured images was accomplished using image analysis tool Colonyzer (Lawless *et al*, 2010) which is capable of detecting very low cell densities even after dilution. Data analysis was carried out by calculating the average of area under curve (AUC) for 3 colonies each. Mean values and standard deviation for each mutant strain was calculated which was then used to plot a growth curve and compare growth, and thereby ammonium transport in these mutant strains, and across genotypes.

2.10. Protein extraction

Trichloroacetic acid (TCA) precipitation was used to prepare protein extracts for western blot (Delaunay *et al*, 2000). Overnight cultures of transformants were grown in SD media without amino acids containing 0.1% proline as nitrogen source. They were then diluted to a starting OD_{595} of 0.1 and grown until OD_{595} 0.5 before pelleting. Cell lysates were prepared by ribolysing the pellets with an equal volume of glass beads in the presence of 10% TCA to precipitate proteins. The cell lysates were further diluted in 10% TCA and centrifuged at 3000rpm for 3 minutes to remove unbroken cells and debris. This was followed by high speed centrifugation of the supernatant at 13,000 rpm for 10 minutes. The pellet was neutralised with 1M Tris and resuspended in 1X SDS loading buffer (2X SDS PAGE buffer, 0.5M EDTA, ß-mercaptoethanol, 200X bromophenol blue dye) and boiled for 3 minutes or gently heated at 37°C for 15 minutes. The supernatant was saved for Western analysis after a quick spin at 13,000 rpm for 30 seconds.

2.11. Co-immunoprecipitation

Co-immunoprecipitation was carried out following the protocol modified from P.J.Hansen lab protocol. The cultures were grown in minimal synthetic medium containing 0.1% proline as nitrogen source to an OD_{595} 0.5 before pelleting. The pellets were dissolved in 250μl of TNE lysis buffer containing protease inhibitor cocktail (50mM Tris-HCl pH 7.4, 150 mM NaCl, 5mM EDTA). An equal volume of glass beads was added to the pellets before vigorous cell lysis by bead beating the mixture for 1 minute each with 30 second intervals on ice in between each cycle for 3 cycles. Centrifuged the mixture at 500g for 5 minutes and the supernatant was aspirated to a fresh tube. This was followed by the addition of 10% Triton X-100 to a final concentration of 1% and incubation on ice for 30 minutes. Centrifuged again at 500g for 5 minutes to collect the cell lysate and a portion of it was saved as control ahead of immunoprecipitation. Protein G Sepharose fast flow beads (Sigma Aldrich) were washed thrice with ice cold buffer at 12,000g for 30 seconds and were divided across tubes (30μl per tube). The cell lysates were added to the beads and incubated at 4°C for 30 minutes to pre-clear the lysate. This was followed by addition of the pre-cleared cell lysate to 6μl of primary antibody at appropriate dilution and incubated overnight at 4°C by gently mixing them on a suitable shaker. Next morning Protein G Sepharose fast flow beads were washed with ice cold buffer and divided across tubes (30μl per tube). This was followed by incubation at 4°C for 60 minutes. The immunoprecipitated complexes were collected by centrifugation at 3000g for 30

seconds and the supernatant was discarded. The pellet containing the beads were washed with ice cold buffer at 12,000g for 30 seconds and re-suspended in 2X protein loading buffer (100 mM Tris-HCl pH 6.8, 4 mM EDTA, 4% SDS, 20% glycerol, 0.02% bromphenol blue, 2% ß-mercaptoethanol) and gently heated at 37°C for 15 min or boiled at 100°C for 3 min. The supernatants were collected by centrifugation at 12,000g for 30 seconds and SDS PAGE was performed with the supernatant.

2.12. Preparation of Membrane proteins and Immunoprecipitation

The preparation of membrane proteins and Immunoprecipitation was carried out following previously published protocol (Rutherford *et al*, 2008) with slight modifications. The cultures were grown in minimal synthetic medium containing 0.1% proline as nitrogen source to an OD_{595} 0.5 before pelleting. The cell pellets were re-suspended in 200µl of lysis buffer (100mM Tris-HCl pH 7.5, 150mM NaCl, 5mM EDTA, 0.5mM phenylmethylsulfonyl fluoride) and 10µl of proteinase inhibitor cocktail (Sigma Aldrich). Equal volumes of glass beads were added before vigorous cell lysis by vortexing the mixture for 5 minutes. Cell lysates were further diluted by adding 500µl of lysis buffer and centrifuged at 3000rpm for 3 minutes at 4°C and the supernatant was transferred to a fresh tube. Membrane proteins were pelleted by high speed centrifugation at 13,000 rpm for 45 minutes at 4°C. The pellet was re-suspended in 900µl of lysis buffer and 100µl of 10% TCA and incubated on ice for 5 minutes before pelleting at 13,000 rpm for 10 minutes at 4°C. For immunoprecipitation, the pellet was re-suspended in 600µl of TNET buffer (50mM Tris-HCl pH 7.4, 150mM NaCl, 5mM EDTA, 1% Triton X-100) and 10µl of proteinase inhibitor cocktail (Sigma Aldrich). This was followed by addition of washed anti-FLAG beads (Sigma Aldrich) to the cell lysate (30 µl per tube) and incubate at 4°C for 90 minutes. The pellet containing the beads and immunoprecipitated complexes were washed thrice with buffer to which 5µl FLAG peptide (5mg/ml) (Sigma Aldrich) was added and incubated at room temperature for 30 minutes. The immunoprecipitated complex was heated at 37°C for 15 min and the supernatants were collected by a quick spin at 12,000 rpm for 30 seconds and Western analysis was carried out using the supernatant.

2.13. Cross linking and Preparation of Membrane proteins

Cultures were grown in minimal synthetic medium containing 0.1% proline as nitrogen source to an OD_{595} 0.5 before pelleting. Crosslinking was carried out following the protocol of

Boeckstaens *et al* (2015) with modifications. The cell pellets were washed at 12,000rpm for 1 minute and re-suspended in 600µl of cross linking buffer (20mM HEPES pH 7.4, 0.8M sorbitol, 100mM potassium acetate) and 10µl of proteinase inhibitor cocktail (Sigma Aldrich). Crosslinking was conducted with 4mM dithiobis[succinimidylpropionate] (DSP) (ThermoScientific) for 30 minutes at 4°C and the reaction was quenched by adding 100mM Tris pH 7.4 for 15 minutes at 4°C. The cells were pelleted by spinning at 13,000rpm for 1 minute and membrane enriched cell extracts were prepared. The preparation of membrane proteins was carried out following previously published protocol (Rutherford *et al*, 2008). The cell pellets were re-suspended in 200µl of lysis buffer (100mM Tris-HCl pH 7.5, 150mM NaCl, 5mM EDTA, 0.5mM phenylmethylsulfonyl fluoride) and 10µl of proteinase inhibitor cocktail (Sigma Aldrich). Equal volumes of glass beads were added before vigorous cell lysis by vortexing the mixture for 5 minutes. Cell lysates were further diluted by adding 500µl of lysis buffer and centrifuged at 3000rpm for 3 minutes at 4°C to remove unbroken cells and debris. The supernatant was transferred to a fresh tube and membrane proteins were pelleted by high speed centrifugation at 13,000 rpm for 45 minutes at 4°C. The tiny pellet was re-suspended in 900µl of lysis buffer and 100µl of 10% TCA and incubated on ice for 5 minutes before pelleting at 13,000 rpm for 10 minutes at 4°C. The pellet was neutralized in 20µl of 1M Tris base followed by resuspension in 80µl of sample loading buffer (100 mM Tris-HCl pH 6.8, 4 mM EDTA, 4% SDS, 20% glycerol, 0.02% bromphenol blue, 2% ß-mercaptoethanol) and heated at 37°C for 15 min or boiled at 100°C for 3 min. The supernatants were collected by a quick spin at 13,000 rpm for 30 seconds.

2.14. Western immunoblotting

SDS-PAGE was performed with the supernatant by loading the samples on appropriate percentage gels and separated proteins were blotted onto the surface of a nitrocellulose membrane. Western analysis was carried out by probing the proteins with monoclonal Anti-His6-peroxidase (2) antibody conjugated to horseradish peroxidase (Roche) (1:5000), monoclonal Anti-FLAG (Sigma Aldrich) (1:2000), monoclonal Anti-Myc (Sigma Aldrich) (1:2500) or monoclonal Anti-Pma1 (Thermoscientific) (1:2000) and the relevant horseradish-peroxidase conjugated IgG antibody (1:5000) followed by chemiluminescent detection (Konica Minolta). Ponceau S staining was carried out to confirm equal loading among samples where necessary.

2.15. Split-ubiquitin based Yeast Two Hybrid (Y2H) screen for membrane proteins

In the membrane based Y2H system the C-terminal half of ubiquitin conjugated to a reporter transcription factor is fused to the bait of interest (Mep2) and the N-terminal half to the prey of interest (Bmh1). To screen for potential interactions between Mep2 and Bmh1, Cub-LexA-VP16- LEU2 based vector pCCW (Dualsystems Biotech) was used as the bait vector and Nub-TRP1-2μ vector pDL2-xN (Dualsystems Biotech) was used as the prey vector. PCR products corresponding to *MEP2* and *BMH1* were amplified and homologously recombined into HindIII linearised pCCW and SmaI linearised pDL2-xN plasmids respectively resulting in pCCW-Mep2 (Mep2-Cub-LexA-VP16- LEU2) and pDL2-xN-Bmh1 (Bmh1-Nub-TRP1-2μ). *MEP2* PCR products were introduced into pDL2-xN plasmid to act as a positive control to generate pDL2-xN-Mep2 (Mep2-Nub-TRP1-2μ). Accuracy of all the plasmids were verified by sequencing. The yeast reporter strain NMY32 (Dualsystems Biotech) was transformed using the bait and prey constructs. Empty prey or bait constructs were included in the transformation to control for false positive interactions and transformants were selected on synthetic media lacking leucine and tryptophan (SD-Leu-Trp) and grown at 30°C for 2 to 3 days. A single colony from the transformants was selected and grown overnight in synthetic media lacking leucine and tryptophan. The following morning the cultures were OD checked to confirm uniform growth and 1ml of the overnight culture was pelleted and washed twice in sterile water before resuspending in 1ml sterile water. They were then serially diluted before spotting on solid synthetic media lacking leucine and tryptophan (SD-Leu-Trp), synthetic media lacking Leucine, Tryptophan and Histidine (SD-Leu-Trp-His) and synthetic media without amino acids except Adenine containing 0.1% proline as nitrogen source (SD+0.1%P+Ade-aā) and grown at 30°C for 3 days.

2.16. Fluorescence microscopy

For fluorescence imaging of live yeast strains carrying the Rosella biosensor, the cells were grown to mid-log phase in synthetic media without amino acids containing 0.1% proline as nitrogen source before harvesting. 200μl of the culture was pelleted and resuspended in 40μl of growth medium after discarding the top 160μl of supernatant. 5μl of the resuspended culture was pipetted onto the surface of a glass plate before adding a cover slip on top and sealing the edges with nail varnish to view under the microscope. A drop of oil was added on top of the coverslip before viewing and inverted to place under a Zeiss Axiovert 200M fluorescence/live cell imaging microscope (Zeiss, Germany) connected to a Zeiss Axiocam HRm camera at 100X

magnification. Green fluorescence emission (508 nm) and red fluorescence emission (587 nm) images were documented successively upon excitation with 488 nm and 568 nm lasers respectively. High resolution images were taken and processed using Adobe Photoshop CS3 (Adobe systems, USA).

2.17. ß-Galactosidase assays

For ß-Galactosidase assays, the transcriptional reporter *FG(TyA)::lacZ* (Mösch *et al*, 1996) was used where the *lacZ* gene is under the transcriptional control of the filamentation response element from Ty1 containing a Ste12 binding site. The reporter plasmid was co-transformed with plasmids expressing *MEP2* mutants and controls, and the transformants were grown in synthetic minimal media without amino acids containing 0.1% proline as nitrogen source. The cells were grown upto OD_{595} 0.6 before pelleting and 15ml of cell pellets were used for the assay. The cell pellets were washed in 1.5ml of Z buffer pH 7.0 (40mM $Na_2HPO_4.7H_2O$, 60mM $NaH_2PO_4.H_2O$, 10mM KCl, 1mM $MgSO_4.7H_2O$) and re-suspended in 300µl of Z buffer from which 100 µl of the cell suspension was transferred to a fresh tube. The tubes were then freeze-thawed by placing in liquid nitrogen for 1 min and immediately transferring the tubes to thaw in a water bath at 37°C for 1 min. The freeze-thaw cycles were repeated thrice to make sure the cells have broken open. A blank tube was set up alongside with 100 µl of Z buffer after the freeze-thaw cycle. 700µl of Z buffer containing ß-mercaptoethanol (50mM) was added to the reaction and blank tubes followed by immediate addition of 160µl of ONPG (o-nitrophenyl ß-D-galactopyranoside) in Z buffer pH 7.0 (4 mg/ml) to all the tubes. Start recording the time elapsed in minutes and the samples were incubated at 30°C until yellow colour develops. The reaction was stopped by the addition of 400µl of Na_2CO_3 (1M) to the reaction and blank tubes and were centrifuged at 13,000 rpm for 10 minutes to get rid of the cellular debris. The clear supernatants were transferred to cuvettes and absorbance was measured at OD_{420}. Units of ß-Galactosidase activity was calculated from the following equation.

ß-Galactosidase units = 1000x OD_{420}/ (t x V x OD_{595})

where t = incubation time in minutes, V = 0.1ml x concentration factor, concentration factor is 15/0.3= 50-fold)

2.18. Flow Cytometry

For flow cytometry analysis, Rosella biosensor comprising of a pH stable variant of red fluorescent protein (RFP) DsRed fused to a pH sensitive variant of green fluorescent protein (GFP) pHluorin described elsewhere (Rosado *et al*, 2008) was used. The biosensor plasmid was co-transformed with plasmids expressing Mep2 mutants and controls and plated on appropriate selective media plates. The transformants were grown in synthetic minimal media without amino acids containing 0.1% proline as nitrogen source to OD_{595} 0.5 before analysing the samples by flow cytometry. Yeast cells expressing a control non-fluorescent plasmid was used to set the background fluorescence levels for the instrument. Flow cytometry analysis was accomplished using LSR Fortessa X20 cell analyser (Becton Dickinson, USA). The fluorescence emission for GFP (530 ± 30 nm) and RFP (586 ± 15nm) were measured after subsequent excitation at 488 and 561 nm lasers respectively. Threshold settings were adjusted to include only single yeast cells and to exclude cell debris from data acquisition. 30,000 live cells were measured for each sample under a low flow rate. Cells expressing the rosella biosensor fluorescent for both green and red channels were used to create a gate for double positive fluorescent cells. Fluorescence emission ratio for all the samples were calculated by dividing the emission rate at 530nm by the emission rate at 586nm. All the experiments were carried out in triplicates, and standard deviation and error bars were calculated from triplicate datasets.

2.19. Protein-fragment Complementation Assay (PCA)

Protein-fragment Complementation Assay (PCA) was employed to study protein – protein interactions using high throughput screening based on the murine dihydrofolate reductase (mDHFR) assay adapted for yeast (Tarassov *et al*, 2008; Remy *et al*, 2007). Methotrexate-insensitive complementary fragments of the reporter protein mDHFR were fused to proteins of interest X (bait) and Y (prey) to create X (bait) + N-terminal DHFR [1,2] and Y (prey) + C-terminal DHFR[3]. Complementation of the reporter protein upon protein interaction allows reconstituted enzyme activity and survival on media containing methotrexate. The haploid bait strain (Mep2-DHFR) was initially grown in liquid culture and robotically spotted onto solid agar plates whereas the library containing the haploid prey strains were spotted straight onto solid media plates. Mating assay was carried out where the haploid bait and prey stains were spotted together on non-selection YPD agar plates and grown for 24 hours at 30°C. Diploid strains were selected by spotting the strains on YPD agar + hygromycin B + nourseothricin

selection plates and grown for 24 hours at 30°C. The resulting diploid strains were spotted on the surface of PCA selection plates comprising of synthetic agar media containing methotrexate (200mg/ml) and control media without methotrexate. The selection plates and controls were left to grow at 30°C for 2 days before imaging to record the colony size. The images were analysed using the image analysis tool Colonyzer (Lawless *et al*, 2010) for automated quantification of culture density analyses on solid agar.

3. Structural basis for Mep2 ammonium transceptor activation by phosphorylation

3.1. Introduction

Ammonium serves as a principal source of nitrogen for many organisms including plants, bacteria and fungi. The transport of ammonium across cell membrane is mediated by members of the evolutionarily conserved Mep/Amt/Rh protein superfamily (von Wiren & Merrick, 2004). In the budding yeast *Saccharomyces cerevisiae* Mep1, Mep2 and Mep3 facilitate transmembrane ammonium transport (Marini *et al*, 1997) and they differ from each other in their kinetic properties and levels of protein expression. In *S. cerevisiae*, under nitrogen limiting conditions, the high affinity ammonium permease Mep2 fulfils its additional signalling function where it acts as an ammonium sensor by transmitting signals to initiate pseudohyphal growth (Lorenz & Heitman, 1998b). The ammonium sensing and transport functions seems to be strongly linked in Mep2. The levels of protein expression of the Mep2 transporter is crucial for its role as a sensor (Marini & Andre, 2000). The transport function of Mep2 is linked to its ability to initiate pseudohyphal growth and Mep2 expression levels are proportional to the extent of pseudohyphal differentiation. Even though nitrogen starvation initiates pseudohyphal differentiation, the exact mechanisms leading to the induction of this dimorphic switch is still unclear.

The elucidation of X-ray crystal structures of AmtB from *E coli* (Khamedi *et al*, 2004; Zheng *et al*, 2004), Amt1 from *A. fulgidus* (Andrade et al, 2005), human RhCG (Gruswitz et al, 2010) and Mep2 from *S. cerevisiae* and *C. albicans* (van den Berg *et al*, 2016) have helped to gain new insights and advance our understanding towards the functions of these ammonium transporters. Nonetheless, the exact mechanism of ammonium transport or the nature of species that gets transported across still remains a matter of debate. It is unclear whether NH_3 gas or NH_4^+ ion or both NH_3/H^+ are transported across the membrane, and if the mechanism of transport resembles that of a channel or a transporter (Khamedi *et al*, 2004; Conroy *et al*, 2007).

A recent study (Boeckstaens *et al*, 2014) has shown that Npr1 kinase fine tunes the activity of Mep2 ammonium transporter by regulating phosphorylation of a conserved regulatory domain

in the C-terminal tail. Prediction of putative phosphorylation sites in Mep2 followed by site-directed mutagenesis identified a serine at position 457 as the site of Npr1-dependent phosphorylation of Mep2. S457 phosphorylation is critical for Mep2 function as Npr1 controls the activity of the ammonium permease via this phosphorylation event, and the kinase action on Mep2 is direct. Transporter activity is dependent on the ability of Npr1 kinase to control Mep2 conformation to keep the protein in its active form and activation of the ammonium permease leads to transport of ammonium into the cell. Availability of rich or preferred sources of nitrogen leads to a rapid dephosphorylation by plasma membrane phosphatases Psr1 and Psr2 leading to inactivation of Mep2. Thus, activity of the high affinity transporter is regulated through an active equilibrium involving Npr1-dependent phosphorylation and Psr-dependent dephosphorylation events wherein Npr1 kinase occupies a central role (Boeckstaens *et al*, 2014).

There are several other important mechanistic questions that still remains unanswered including the regulation of ammonium transport in eukaryotes. This chapter aims to elucidate the mechanism of Mep2 ammonium transporter regulation with the help of structural data. Structurally significant epitope tagged Mep2 mutants were generated using site directed mutagenesis. N-terminal truncation mutants were generated to understand the significance of this vestibule and to determine whether the N-terminal region is essential to increase the overall stability of the trimer. In order to comprehend the role of the moderately conserved tyrosine residue which forms the hydrogen bond essential for the first tier channel block within Mep2 pore, that residue was mutated by replacing it with an Alanine. A truncated version of Mep2 lacking the autoinhibitory (AI) region was generated in order to assess the effect of loss of this region on the activity of the protein, as it was shown to be essential for Npr1 kinase activation of Mep2. Δ457 truncation mutants were generated in order to examine whether deletion of this region would have an impact on the activity and phosphorylation state of Mep2, as Npr1 modulates Mep2 activity via S457 phosphorylation of the CTR. In order to test whether phosphorylation of the S457 residue by Npr1 kinase would result in steric clashes and electrostatic repulsion bringing about conformational changes within the C-terminal tail of the protein, phosphorylation-mimicking S457D and R456D/S457D mutants were generated. The ability of these mutants to transport ammonium, initiate filamentous growth and protein expression levels were determined. These data together with the structural evidence allows us to propose a model for phosphorylation-based regulation of Mep2 ammonium transporters.

3.2. Expression studies for elucidation of Mep2 structure

In order to enable structure determination of Mep2 using X-ray crystallography, Mep2 protein was overexpressed in *S. cerevisiae*. The *MEP2* gene was amplified from genomic DNA and homologously recombined into W303 *pep4Δ* strain using SmaI linearised 83 nu vector. N4Q substitution was present in Mep2 to prevent glycosylation. The expression vector 83 nu is based on pRS423-Gal1 shuttle vector with an LIC cloning cassette and has 2-micron origin of replication, ampicillin antibiotic resistance, HIS3 selection marker and a strong Gal1 promoter and a Cyc terminator. For overexpression of Mep2, the transformants were grown in 2L culture flasks in synthetic minimal medium lacking Histidine for 24 hours at 30°C in a shaking incubator at 220rpm. This was done to scale up the culture growth to OD_{595} 6 to 9. The cells were spun down the following day at 4000rpm for 15 minutes at 4°C and inoculated into YP medium containing 2% galactose for induction of the expression vector. The cultures were incubated for a further 16-18 hours at 30°C in a shaking incubator at 220rpm before harvesting the cell pellet by centrifugation. The final OD_{595} values would typically be around 18 to 24. Further structural biology work including purification, crystallization and structure determination of Mep2 was carried out by the van den Berg lab following the protocol in van den Berg *et al*, 2016.

3.3. General architecture of Mep2 ammonium transceptors

The X-ray crystal structures of the Mep2 orthologues from *S. cerevisiae* and *C. albicans* were solved to 3.2 Å resolution by collaborating with the van den Berg lab. These structures were comparable except for differences confined to the N and C terminal regions (Fig 14). These structures are similar to existing structures of ammonium transporters showing a trimeric assembly with each monomer consisting of 11 transmembrane helices (TM) and a central narrow hydrophobic pore for substrate conductance. Central functional features such as the extracellular substrate binding site, putative Phe gate formed by phenylalanine residues and the twin-His motif within the hydrophobic channel are all very similar to those present in the bacterial and human transporters.
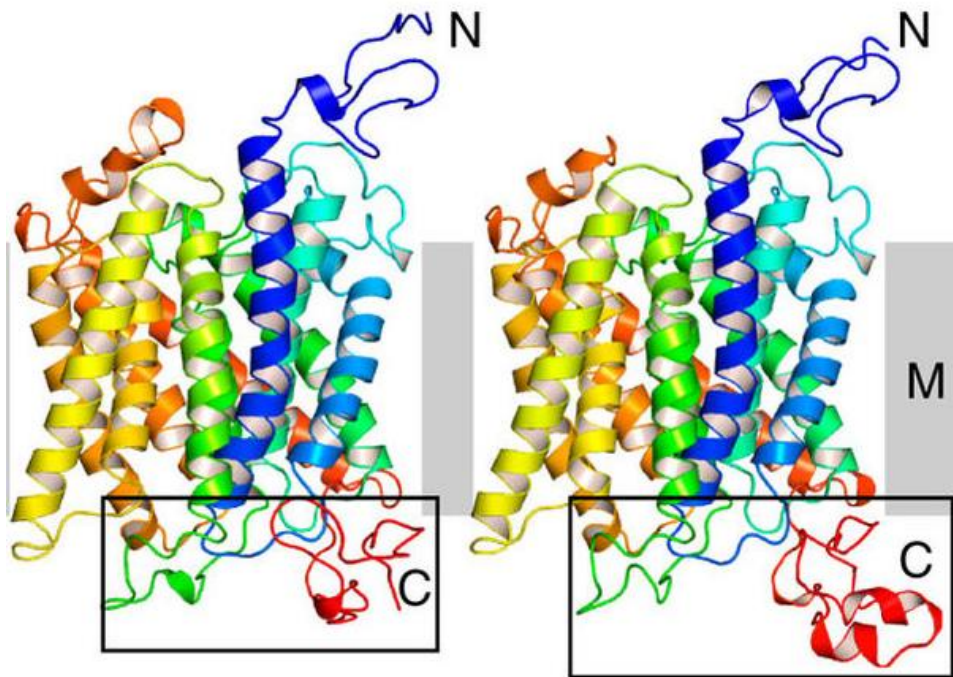
Figure 14: Monomeric cartoon representation of Mep2 orthologues from *S. cerevisiae* (left) and *C. albicans* (right) demonstrating 11 transmembrane helices, Membrane (M), N and C terminal tails and the pore for substrate conductance. Figure taken from van den Berg *et al*, 2016.

The major differences between Mep2 and the existing crystal structures are confined to the N and C terminus and Intracellular loops (ICL). The N-terminus of *S. cerevisiae* Mep2 is 20-25 residues longer making the extracellular domain considerably bigger in size compared to the existing structures of homologues. Extended extracellular loop (ECL) of one monomer interacts with the N-terminus of the neighbouring monomer creating a distinctive vestibule leading to the ammonium binding site which is much more evident than in bacterial transporters. Although this might result in an increased stability of the Mep2 trimer, the significance of the N-terminal region for Mep2 transporter function is not clear.

3.3.1. Mep2-channels are closed by a two-tier block

The most remarkable difference between Mep2 and other known transporter structures is Mep2 is closed on the intracellular side. Intracellular loop ICL1 is longer in Mep2 and has moved inwards when compared to bacterial transporters. This inward movement of ICL1 has a significant functional consequence where a moderately conserved residue of TM1 (Tyr 53) forms a strong hydrogen bond with one of the highly conserved twin-Histidine residues (His348), thereby closing the channel (Fig. 15). ICL2 shows backbone conformational changes even though smaller when compared to ICL1. Lastly, ICL3 which links the two pseudo-symmetrical halves together is shifted upwards and has undergone a major conformational change in fungal transporters. This conformational shift in ICL3 helps to form an additional barrier closing the channel on the cytoplasmic side. This two-tier channel block ensures that ammonium transport only occurs under nitrogen starvation conditions.

The C-terminal tail of Mep2 is not compactly packed as found in bacterial Amts, conversely it moves away considerably from the protein main body creating an elongated protein structure. The autoinhibitory (AI) region comprising of residues 450-457 is folded back onto the C-terminal tail physically connecting the CTR to the main body of the protein through main and side chain interactions of conserved residues.
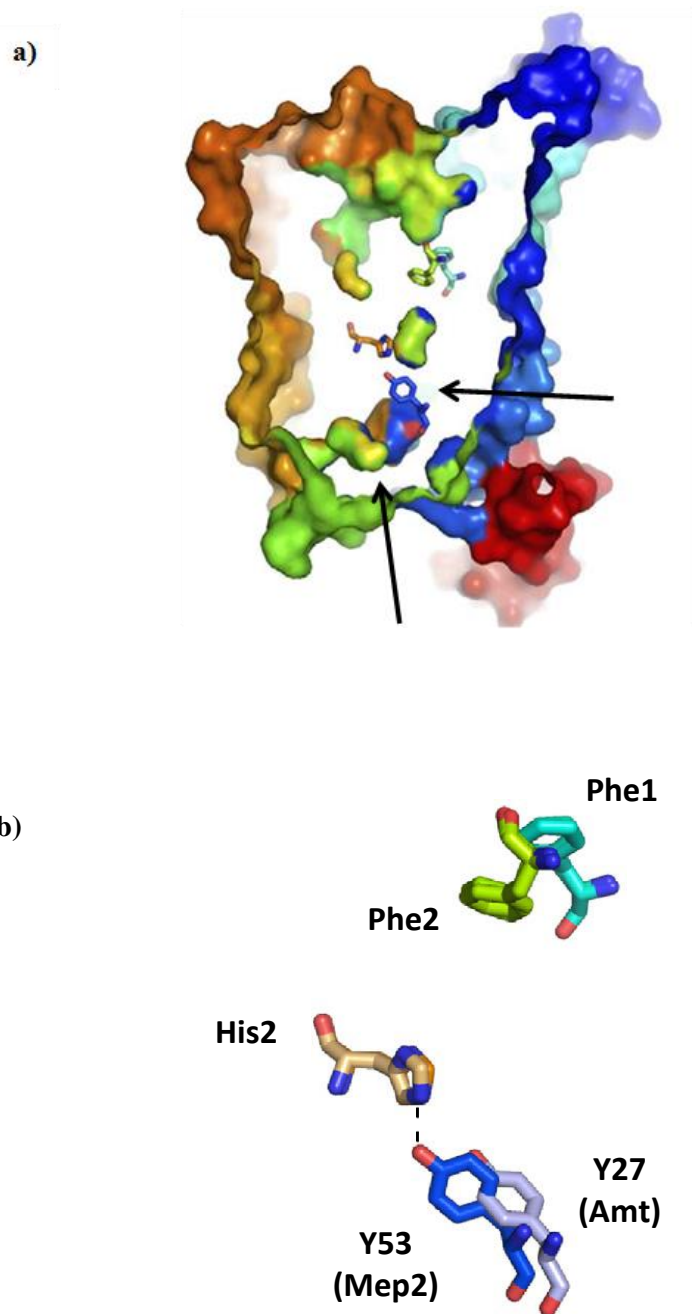
Figure 15: a) Surface views of the Mep2 conducting pore showing the two-tier channel block indicated by arrow marks. b) Stereo superposition of conserved residues from Amt-1 and Mep2 displaying the Phe gate, His2 of the twin-His motif and the tyrosine residue Y53 of TM1 that forms a hydrogen bond with His2. Figure taken from van den Berg *et al*, 2016.

3.3.2. Phosphorylation causes a conformational change in the CTR

Since the Npr1 kinase target residue Ser457 is located in a solvent-accessible electronegative pocket in *S. cerevisiae* Mep2, the prediction was that phosphorylation of Ser457 residue might result in steric clashes and electrostatic repulsion, which consecutively could cause significant conformational changes within the C-terminal tail. In order to test this hypothesis, the structures of the phosphorylation-mimicking R456D/S457D (DD) and S457D (D) mutants were solved. The structural data shows that phosphorylation causes a large conformational change to the conserved part of the CTR (Fig: 16) confirming the hypothesis. The conformational changes result in a disorder of almost 20 residues around the conserved motifs of CTR.

3.4. Sequence conservation within the family of ammonium transporters

To gain a better understanding of the structure-function relationships and to illustrate the degree of sequence conservation among the members of the ammonium transporter family, multiple sequence alignment of sequences highlighting the conserved residues and domains was undertaken (Fig. 17).

a)

b)

S457
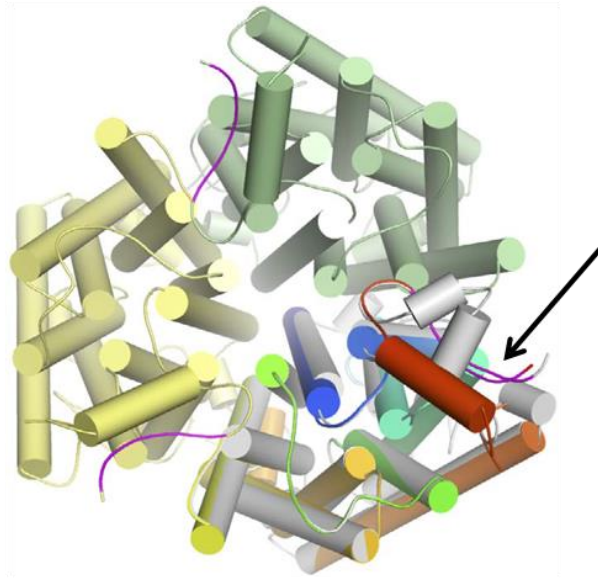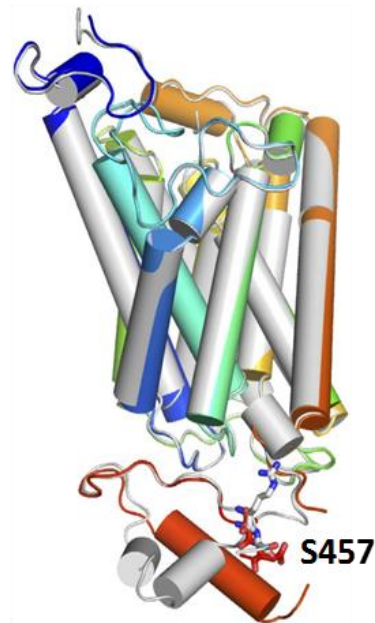
Figure 16: a) Cytoplasmic view of the DD mutant trimer with WT Mep2 superposed in grey for one of the monomer units. The phosphorylation site is revealed by the arrow mark and AI region is represented in magenta. b) Monomer side-view of WT Mep2 superposed with the DD mutant, displaying the conformational change and disorder around the motif regions. Figure taken from van den Berg *et al*, 2016.

```
                                    N terminus                              1
Calbicans    MSGNFTGT----GTGGDVFKVDLNEQFDRADMVWIG----------TASVLVWIM-IPGV 45
Scerevisiae  MSYNFTGTPTGEGTGGNSLTTDLNTQFDLANMGWIG----------VASAGVWIM-VPGI 49
AfAmt-1      MSD------------------------GNVAWIL----------ASTALVMLM-VPGV 23
EcAmtB       MKIATIKTGLASLAMLPGLVMAAPAVADKADNAFMM----------ICTALVLFMTIPGI 28
AtAmt1-1     MSCSATDLAVLLGPNATAAANYICGQLGDVNNKFIDTAFAIDNTYLLFSAYLVFSMQLGF 60
                *.                        :    ::          :. : :       *.

                     IL1                    2                        EL1
Calbicans    GLLYSGISRKKHALSLMWAALMAACVAAFQWFWWGYSLVFAHN--GSVFLGTLQNFCLKD 103
Scerevisiae  GLLYSGLSRKKHALSLLWASMMASAVCIFQWFFWGYSLAFSHNTRGNGFIGTLEFFGFRN 109
AfAmt-1      GFFYAGMVRRKNAVNMIALSFISLIITVLLWIFYGYSVSFGND--ISGIIGGLNYALLSG 81
EcAmtB       ALFYGGLIRGKNVLSMLTQVTVTFALVCILWVVYGYSLAFGEG--NNFFGNINWLMLKN 85
AtAmt1-1     AMLCAGSVRAKNTMNIMLTNVLDAAAGGLFYYLFGYAFAFGSP--SNGFIG-KHYFGLKD 117
              .::  .*   * *:.::    :          : : **:.* *.    . ::*    : .

              EL1                   3                 IL2              4
Calbicans    VLGAPSIVKTVPDILFCLYQGMFAAVTAILMAGAGCERARLGPMMVFLFIWLTVVYCPIA 163
Scerevisiae  VLGAPSSVSSLPDILFAVYQGMFAAVTGALMLGGACERARLFPMMVFLFLWMTIVYCPIA 169
AfAmt-1      VKGE--------DLLFMMYQMMFAAVTIAILTSAIAERAKVSSFILLSALWLTFVYAPFA 133
EcAmtB       IELTAVMG-SIYQYIHVAFQGSFACITVGLIVGALAERIRFSAVLIFVVVWLTLSYIPIA 144
AtAmt1-1     IPTAS------ADYSNFLYQWAFAIAAAGITSGSIAERTQFVAYLIYSSFLTGFVYPVVS 171
              :         :*  ** **  :   **  :. ::    .   :      *

                                        5                         IL3
Calbicans    YWTWGGNGWLVSL----------GALDFAGGGPVHENSGFAALAYSLWLGKRHDPV-AKG 212
Scerevisiae  CWVWNAEGWLVKL----------GSLDYAGGLCVHLTSGHGGLVYALILGKRNDPV-TRK 218
AfAmt-1      HWLWGG-GWLAKL----------GALDFAGGMVVHISSGFAALAVAMTIGKR-----AGF 177
EcAmtB       HMVWGG-GLLASH----------GALDFAGGTVVHINAAIAGLVGAYLIGKR-----VGF 188
AtAmt1-1     HWFWSVDGWASPFRTDGDLLFSTGAIDFAGSGVVHMVGGIAGLWGALIEGPRLGRFDNGG 231
              *.  *              *::*:**. **   .. ..*  :    * *

                               6                                7
Calbicans    KVPKYKPHSVSSIVMGTIFLWFGWYGFN------------GGSTGNSSMRSWYACVNTNL 260
Scerevisiae  GMPKYKPHSVTSVVLGTVFLWFGWMFFN------------GGSAGNATIRAWYSIMSTNL 266
AfAmt-1      EEYSIEPHSIPLTLIGAALLWFGWFGFN------------GGSALAANDVAINAVVVTNT 225
EcAmtB       GKEAFKPHNLPMVFTGTAILYIGWFGFN------------AGSAGTANEIAALAFVNTVV 236
AtAmt1-1     RAIALRGHSASLVVLGTFLLWFGWYGFNPGSFNKILVTYETGTYNGQWSAVGRTAVTTTL 291
              .*. .   . *:  *:  :*::** **        *:        :  *

                          7                  8                   9
Calbicans    AAATGGLTWMLVDWFRTGGKWSTVGLCMGAIAGLVGITPAAGYVPVYTSVIFGIVPAIIC 320
Scerevisiae  AAACGGLTWMVIDYFRCGRKWTTVGLCSGIIAGLVGITPAAGFVPIWSAVVIGVVTGAGC 326
AfAmt-1      SAAVAGFVWMVIGWIK--GKPGSLGIVSGAIAGLAAITPAAGFVDVKGAIVIGLVAGIVC 283
EcAmtB       ATAAAILGWIFGEWALR-GKPSLLGACSGAIAGLVGVTPACGYIGVGGALIIGVVAGLAG 295
AtAmt1-1     AGCTAALTTLFGKRLLS-GHWNVTDVCNGLLGGFAAITGGCSVVEPWAAIICGFVAALVL 350
              : . . :        *    *  *  :.*:..:* ... :   ::: *.*..

                             10                         EL5        11
Calbicans    NFAVDLKD-LLQIDDGMDVWALHGVGGFVGNFMTGLFAAD-YVAMIDG---TEIDGGWMN 375
Scerevisiae  NLAVDLKS-LLRIDDGLDCYSIHGVGSVLTGIFAAD-YVNATAGSYISPIDGGWIN 384
AfAmt-1      YLAMDFRI-KKKIDESLDAWAIHGIGGLWGSVAVGILANP-EVNGYAG--------LLF 332
EcAmtB       LWGVTMLKRLLRVDDPCDVFGVHGVCGIVGCIMTGIFAAS-SLGGVGF--------AEGV 346
AtAmt1-1     LGCNKLAE-KLKYDDPLEAAQLHGGCGAWGLIFTALFAQEKYLNQIYGNKPGRPHGLFMG 409
              :       :   * *:  :   :**   *   * .  ..::*       :

                                 11                CTR
Calbicans    HHWKQLGYQLAGSCAVAAWSFTVTSIILLAMDRIPFLRIRLHEDEEMLGTDLAQIGEYAY 435
Scerevisiae  HHYKQVGYQLAGICAALAWTVTVTSILLLTMNAIPFLKLRLSADEEELGTDAAQIGEFTY 444
AfAmt-1      GNPQLLVSQLIAVASTTAYAFLVTLILAKAVDAA--VGLRVSSQEEYVGLDLSQHEEVAY 390
EcAmtB       TMGHQLLVQLESIAITIVWSGVVAFIGYKLADLT--VGLRVPEEQEREGLDVNSHGENAY 404
AtAmt1-1     GGGKLLGAQLIQIIVITGWVSATMGTLFFILKKMK--LLRISSELEMAGMDMTRHGGFAY 467
              :: **     :.    .   :          :*:  ::* * * *:

              11
Calbicans    YADDDPETNPYVLEPIRSITISQPLPHIDGVAD----------GSSNNDSGEAKN----- 480
Scerevisiae  -----EESTAYIPEPIRSKTSAQMPPPHENIDDKIVGNTDAEKNSTPSDASSTKNTDHIV 499
AfAmt-1      T---------------------------------------------------------- 391
EcAmtB       NA--------------------------------------------------------- 406
AtAmt1-1     MYFDDDESHKAIQLRRVEPRSPSPSGANTTPTPV------------------------- 501
```

Figure 17: Clustal W alignment of sequences within the ammonium transporter family. Conserved motifs are boxed for ICL1 in blue, ICL2 in green, CTR in red and AI domain in yellow. Conserved residues are highlighted displaying Phe gate in blue, substrate binding site in magenta, twin-His residues in red and Npr1 kinase phosphorylation site for Mep2 in pink. Figure taken from van den Berg *et al*, 2016.

Multiple sequence alignment of Mep2 from *C. albicans* and *S. cerevisiae*, Amt1 from *A. fulgidus,* AmtB from *E. coli* and Amt1-1 from *A. thaliana* shows high degrees of sequence identity among the conserved residues, domains and motifs including the intracellular loops, C-terminal domain, Phe gate, substrate binding site, twin-His motifs etc. The grey sequences at the C-terminal tail beyond the serine phosphorylation site of Mep2 orthologues from *S. cerevisiae* and *C. albicans* suggests that the region beyond that is disordered and might not be conserved among members of the ammonium transporter family.

3.5. Specific amino acid substitutions alter growth and provides Npr1 kinase independent ammonium transport

Site-directed mutagenesis was performed to identify residues or domains having specific roles in ammonium transport and signalling. Mep2 mutants were expressed in *mep123Δ* and *mep123-npr1Δ* strains and their ability to transport ammonium was tested by growing them on minimal media with 1mM ammonium sulphate. Growth was documented robotically for 72 hours following a time course photography (Fig. 18). Growth of Mep2 mutants were also assayed by serially diluting the cultures and spotting them on solid agar plates containing glutamate (0.1%) which was the positive control being a preferred source of nitrogen or ammonium sulphate (1mM) as nitrogen source, a poor and non-preferred source of nitrogen (Fig. 19) and growing them for 3 days at 30°C.
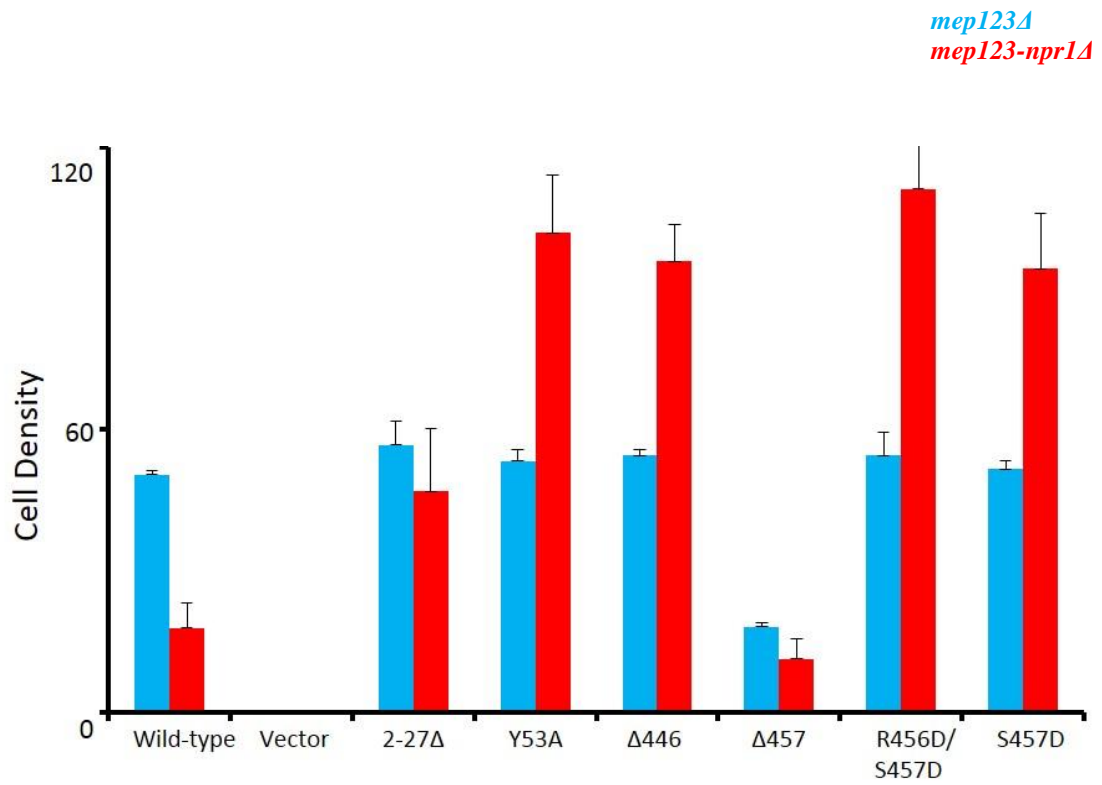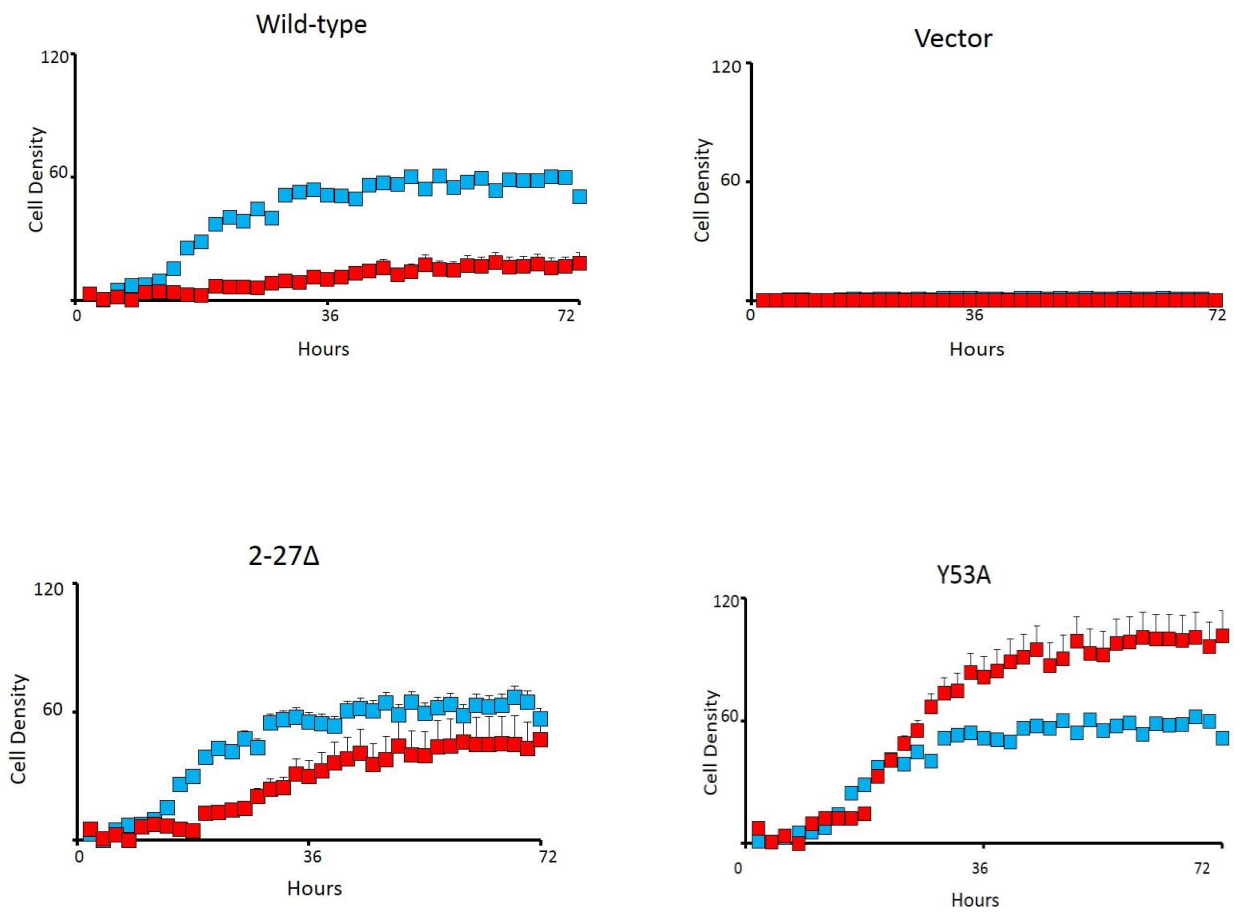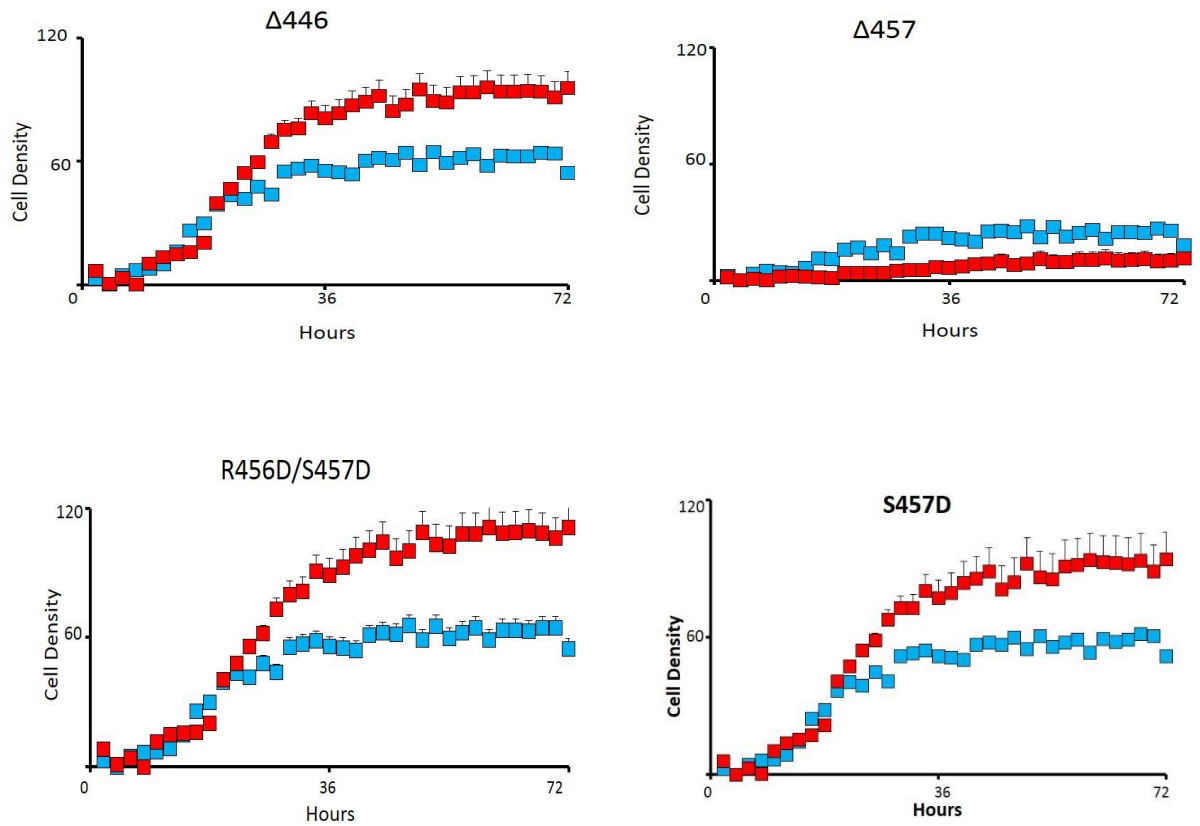
Figure 18: a) & b) Growth of Mep2 mutants and controls generated via site-directed mutagenesis expressed in *mep123Δ* (blue) and *mep123-npr1Δ* (red) strains on low ammonium medium. Cell density was quantified by photographing time-points across 72 hours of growth at 30°C from the robotic growth assay. Error bars were calculated from standard deviations for triplicate repeats of each strain. a) represents comparison of growth across all the mutants and controls whereas b) represents growth plotted for each individual strain across 72 hours. Figure taken from van den Berg *et al*, 2016.

Results from the transport and growth assays (Fig. 19a) demonstrate that specific amino acid substitutions and truncations affect ammonium transport ability widely across mutants. In *mep123Δ* strains the mutations does not seem to have a significant impact on ammonium transport as they grow similar to that of Mep2^{WT} strain. However, Mep2$^{\Delta457}$ truncation shows a major drop in its ability to grow and transport ammonium. In *mep123-npr1Δ* strains wild-type Mep2 strain shows a marked reduction in its ability to grow due to Npr1 kinase deletion. Single and double amino acid substitutions, namely Mep2^{Y53A}, Mep2^{S457D}, Mep2$^{R456D/S457D}$ and Mep2$^{\Delta446}$ truncation, caused significant increase in growth across these mutants suggesting that ammonium transport across these mutants is Npr1 kinase independent. Mep2$^{2-27\Delta}$ truncation demonstrated lower rates of ammonium transport compared to other mutants although the rate of growth was higher than that of Mep2^{WT} strain. Mep2$^{\Delta457}$ truncation, and elimination of S457 site showed very low rates of transport, even lower than that of wild-type. In order to test whether the presence of the His tag interferes with Npr1 phosphorylation for this mutant, a non-tagged version Mep2$^{\Delta457\ no\ tag}$ was made and tested for growth and ammonium transport (Fig. 19b). The Mep2$^{\Delta457\ no\ tag}$ mutant showed almost Mep2^{WT} levels of ammonium transport. These results are in agreement with the earlier finding (Boeckstaens *et al*, 2014) that Npr1 kinase integrity is essential for activation and inherent transport activity of Mep2.

a)

| | 0.1% Glu | 1mM AS | 0.1% Glu | 1mM AS |

WT Mep2
Vector
Mep2$^{2\text{-}27\Delta}$
Mep2^{Y53A}
Mep2$^{\Delta446}$
Mep2$^{\Delta457}$
Mep2$^{R456D/S457D}$
Mep2^{S457D}

mep123Δ   *mep123-npr1Δ*

b)

| | 0.1% Glu | 1mM AS |

WT
Vector
WT Mep2
Mep2$^{\Delta457}$
Mep2$^{\Delta457\,no\,tag}$
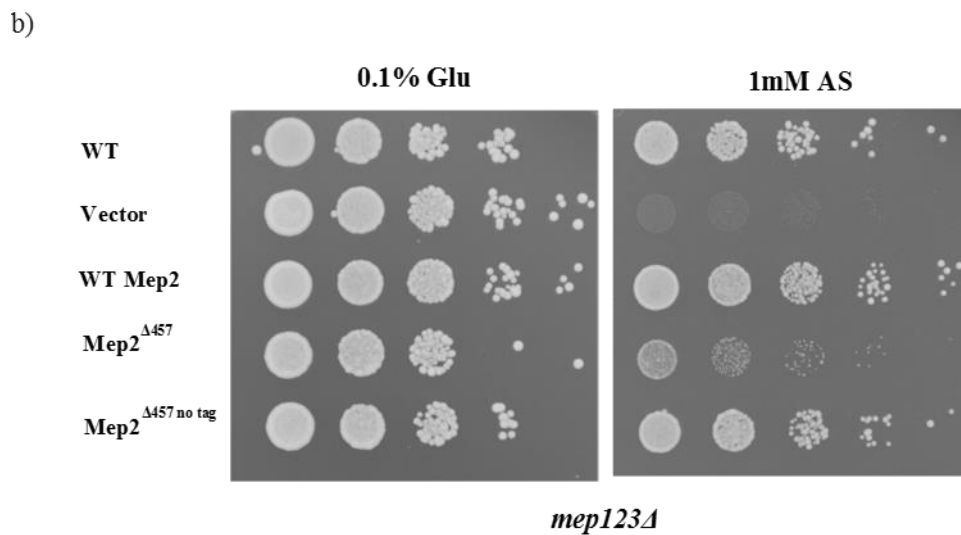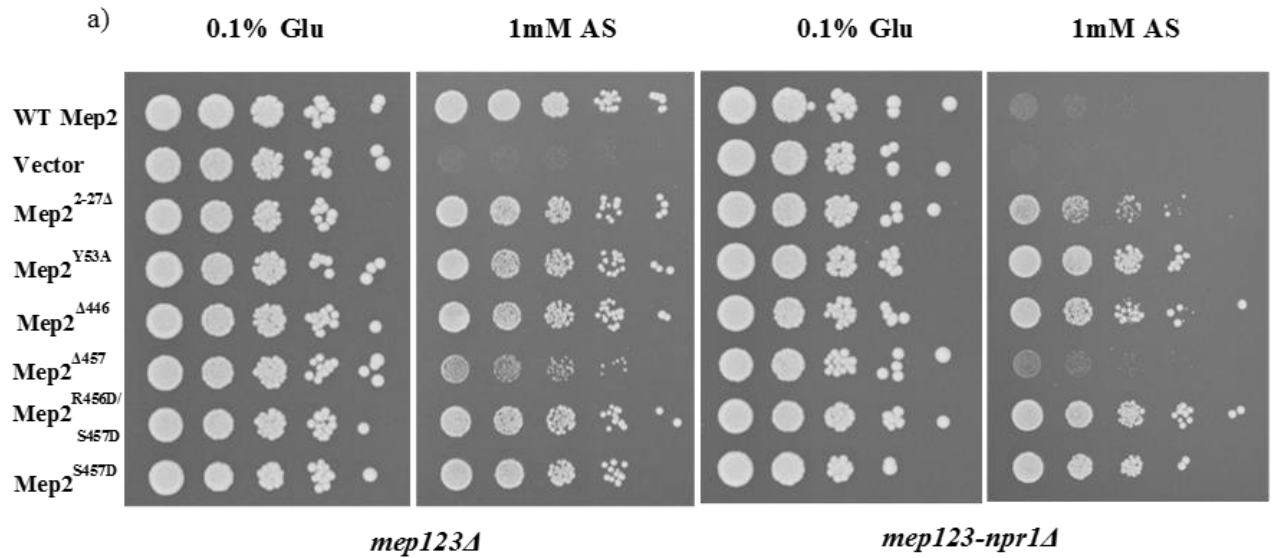
mep123Δ

Figure 19: a) & b) Growth of Mep2 mutants and controls in *mep123Δ* and *mep123-npr1Δ* strains serially diluted on solid agar medium containing 0.1% glutamate or 1mM ammonium sulphate as the sole nitrogen source at 30°C for 3 days.

93

3.6. Transport is essential for signalling and specific mutations provide Npr1 kinase independent signalling function

In order to evaluate the role of Npr1 kinase in the induction of filamentous growth all the mutants and controls were expressed in an *npr1/npr1Δ* background strain and grown on solid SLAD medium. Results from the pseudohyphal assay (Fig. 20) demonstrates that Mep2^{WT} strain fails to undergo pseudohyphal differentiation in the absence of Npr1 kinase. Mep2^{Y53A}, Mep2^{S457D}, Mep2$^{R456D/S457D}$ and Mep2^{Δ446} truncation mutants exhibited enhanced filamentation suggesting that signalling function in these mutants is Nrp1 kinase independent. Reduced rates of filamentation was observed for Mep2$^{2-27Δ}$ mutant and pseudohyphal growth was extremely reduced for the Mep2^{Δ457} truncation mutant. The results from the pseudohyphal assay correlates with that of the transport assay suggesting that signalling and transport functions are linked. The extent of pseudohyphal growth is linked to the rate of ammonium transport and transport is necessary for signalling.

a) WT – Mep2

b) Vector

c) Mep2$^{2-27\Delta}$

d) Mep2^{Y53A}

e) Mep2$^{\Delta446}$

f) Mep2$^{\Delta457}$

g) Mep2$^{R456D/S457D}$

h) Mep2^{S457D}
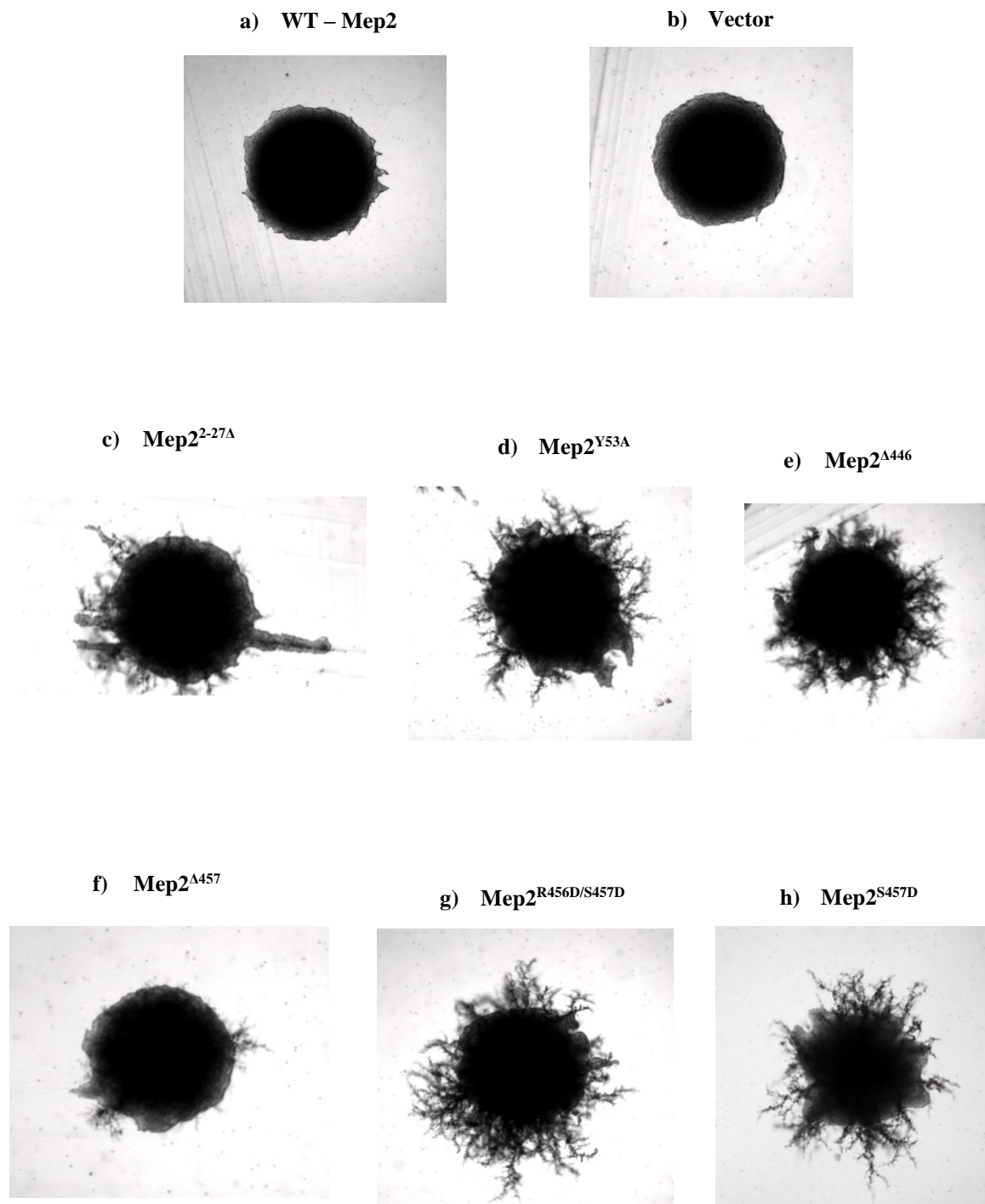
Figure 20: Pseudohyphal growth of Mep2 mutants and controls in an *npr1/npr1Δ* background strain illustrated at 40X magnification. Cells were grown at 30°C for 6 days on SLAD plates containing 50µM ammonium sulphate as nitrogen source.

3.7. Mep2 function does not correlate with protein expression levels

It has been known that Mep2 expressions levels are crucial for its regulatory function. In order to test whether expression levels of Mep2 equates with its transport and signalling abilities and to understand the impact of specific mutations on protein expression levels, western immunoblotting was carried out.

For *mep123Δ* strains Mep2^{Y53A}, Mep2$^{R456D/S457D}$ and Mep2^{S457D} mutant strains showed Mep2^{WT} protein expression levels (Fig. 21). Mep2$^{2-27Δ}$ showed a significant reduction in protein expression levels where the protein appeared as a low intensity band. The protein expression levels for Mep2^{Δ446} was however very low compared to the rest of the mutants and the protein appeared as a very faint band. Therefore, levels of protein expression do not correlate with Mep2 function for this mutant as Mep2^{Δ446} is transport and signalling proficient. For Mep2^{Δ457} the expression levels were very high in spite of the fact that transport and signalling rates were significantly lower than wild-type in this mutant. This illustrates that protein expression levels and Mep2 function does not equate.

For *mep123-npr1Δ* strains Mep2$^{R456D/S457D}$ and Mep2^{S457D} mutant strains showed Mep2^{WT} protein expression levels (Fig. 22). Mep2^{Y53A} mutant showed lower expression levels than Mep2^{WT} although it is hyperactive for transport and signalling. The expression levels for Mep2$^{2-27Δ}$ were so low that the faint band faded away after the initial exposure even though the mutant showed higher levels of transport and signalling when compared to wild-type strain. Mep2^{Δ446} showed very low levels of the protein with a very faint band which did not correlate with its transport and signalling levels. It was the reverse for Mep2^{Δ457} where protein expression levels were similar to Mep2^{WT} expression levels although there was a reduction in transport and signalling levels for this mutant. The results thus point to the fact that Mep2 function does not correlate with protein expression levels in these mutants.
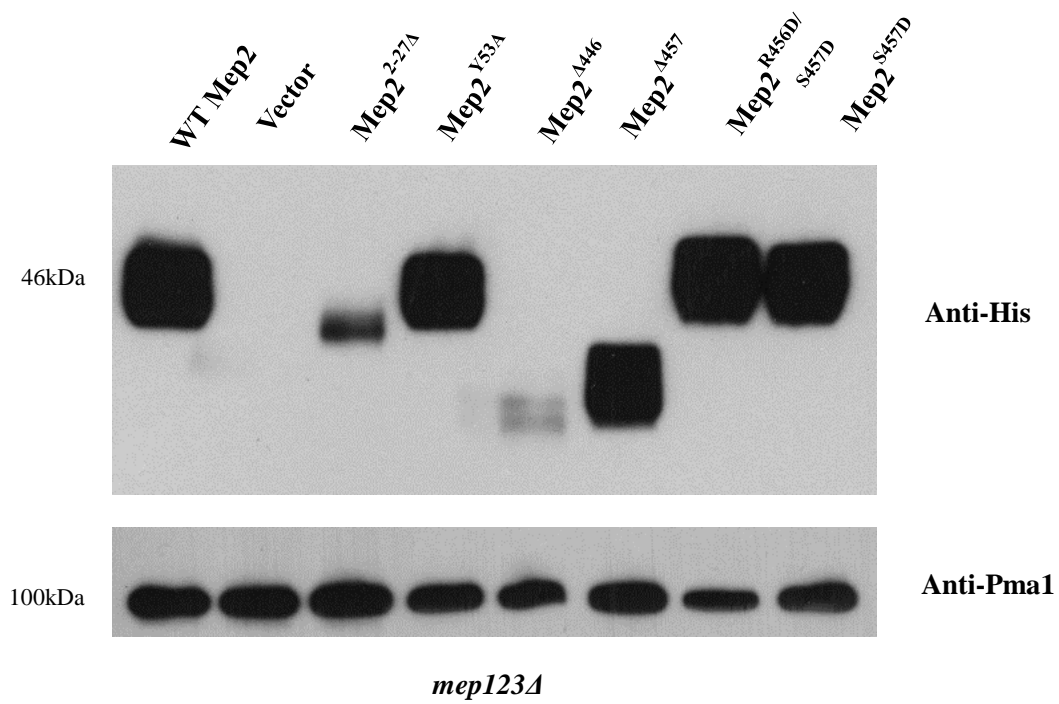
Figure 21: Immunodetection of Mep2 mutants and controls in *mep123Δ* background from membrane-enriched extracts of cells grown in 0.1% proline media. Levels of Pma1 was used as loading control.
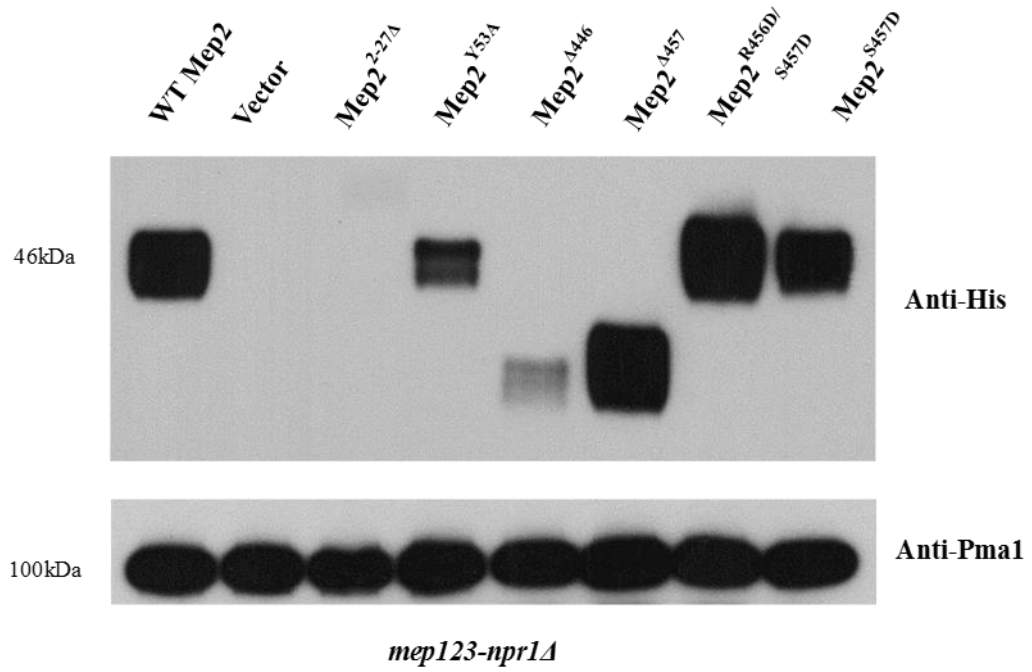
Figure 22: Immunodetection of Mep2 mutants and controls in *mep123-npr1Δ* background from membrane-enriched extracts of cells grown in 0.1% proline media. Levels of Pma1 was used as loading control.

3.8. Model for phosphorylation-based regulation of Mep2 ammonium transporter

Under nitrogen rich conditions Mep2 is in a closed, non-phosphorylated state and the CTR and ICL3 are far-off from each other with the ICL3 blocking the channel pore (Fig. 23). Upon nitrogen limitation, Mep2 is phosphorylated by Npr1 kinase as mimicked by the DD and D mutants. The region around the conserved motif of the C terminal tail undergoes a conformational change leading to the CTR and ICL3 interacting by moving towards each other, thereby opening the channel for substrate import. The open state of the channel corresponds to phosphorylated state of Mep2 and upon de-phosphorylation ICL3 and CTR move away from each other and ICL3 blocks the channel pore to prevent any further substrate import. The conformational changes in the CTR might interfere with its interactions with the ICL3 of the neighbouring monomer unit which could result in its channel opening due to the internal movement of the ICL3. Thus, if the monomers crosstalk then a single phosphorylation event could lead to the opening of the entire trimer, although this theory hasn't been verified yet.
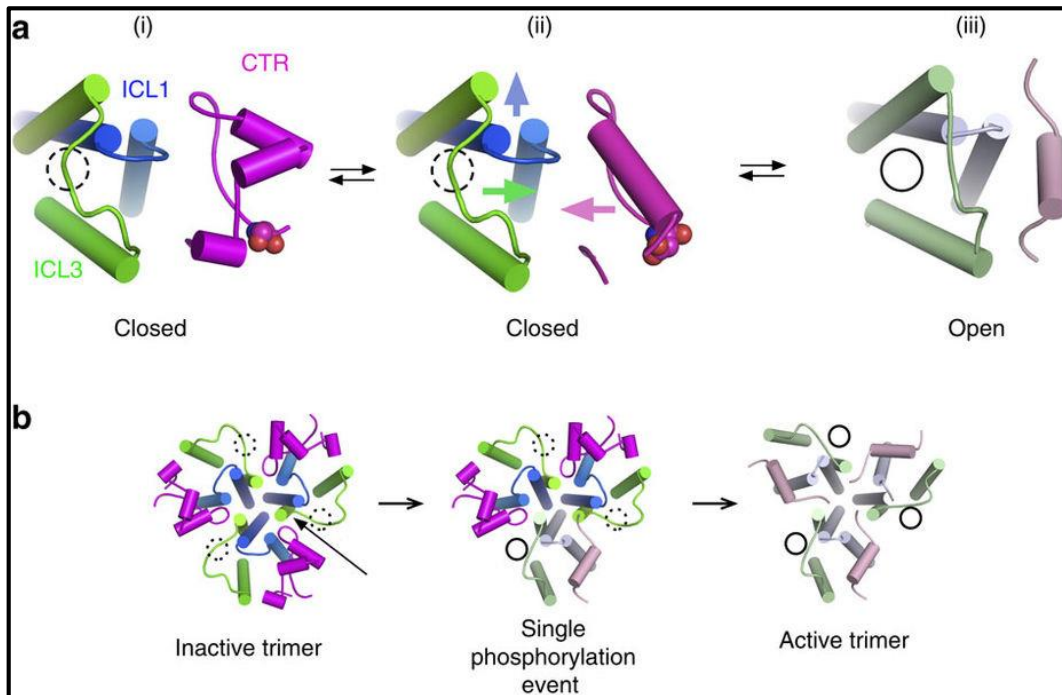
Figure 23: a) Schematic model for phosphorylation regulating channel opening and activation of the Mep2 ammonium transporter. Upon phosphorylation by Npr1 kinase during nitrogen limitation, the conserved part of the CTR undergoes a conformational change that opens the channel. b) Phosphorylation of a single Mep2 monomer could result in the activation of the entire trimer provided the monomers crosstalk. Figure taken from van den Berg *et al*, 2016.

3.9. Discussion

Transport of ammonium across biological membranes is facilitated by members of the evolutionarily conserved Amt/Mep/Rh family of ammonium permeases. Based on the structural data of Mep2 orthologues from *S. cerevisiae* and *C. albicans,* we provide mutational analysis of conserved residues and domains having crucial roles in ammonium transport and signalling. We show that single/double amino acid substitutions and truncations alter ammonium transport and signalling in Mep2, and the two functions are tightly coupled. Moreover, specific mutations can provide Npr1 kinase independent transport and signalling in Mep2, possibly by generating a constitutively open channel.

In the recently solved structure of yeast Mep2 (van den Berg *et al*, 2016) the N-terminus is almost 20 to 25 residues longer than that of its bacterial counterparts and has resulted in a significant increase in the size of the extracellular domain. Furthermore, the N-terminus of a monomer in the structure interacts with the extended extracellular loop ECL5 of the neighbouring monomer. These minor changes in the N-terminus thus gives rise to a discrete vestibule whose significance is still not clear in comparison with the bacterial transporters. One of the roles of this vestibule might be to capture ammonium ions and act as an ammonium binding site. The interactions between the extracellular loops of the monomers might help to increase the overall stability of the trimer similar to that found in the plant Amt transporters (Graff *et al*, 2011). In order to explore this further, N-terminal deletion mutant 2-27Δ was generated and expressed in two different background lines. Even though protein expression levels were lower than that of wild-type for this mutant, these mutants were able to transport ammonium and initiate signal for pseudohyphal growth more efficiently than the wild-type strain. Given that 2-27Δ mutant grew better than wild-type under ammonium limiting conditions and was able to undergo limited pseudohyphal differentiation in the absence of Npr1 kinase, the relevance of the N-terminus in Mep2 is still not clear. Earlier studies have shown that truncation of residues 20-24 in the N-terminus severely affected intracellular accumulation of ammonium when compared to the wild-type strain. Truncation of a larger part of the N-terminus involving residues 15-29 unexpectedly caused a reversal in this effect whereby considerable increase in intracellular ammonium concentration was observed (Van Nuland *et al*, 2006). These residues might be more important for sensing than the transport functions of Mep2, as truncation of this region might affect the conformation of the transporter preventing it from interacting with downstream signalling partners to initiate pseudohyphal growth. In a separate study, N-terminal deletion mutation 25-29Δ repressed the Npr1 kinase requirement for

ammonium transport or signalling in Mep2 (Boeckstaens *et al*, 2014). Then again, the fact that the N-termini of members of the Amt/Mep superfamily differ in sequence, length and hydrophilic nature (Marini *et al*, 2000) might explain for these divergent outcomes.

The biggest difference between Mep2 and existing bacterial structures resides in the intracellular side of the protein. Mep2 structure shows a longer intracellular loop 1 (IL1) due to the unwinding of the cytoplasmic end of TM2 and has a relative inward movement when compared to bacterial transporters with a key functional significance. Inside the transmembrane region the relatively conserved Tyr53 residue makes a strong hydrogen bond with the absolutely conserved His348 residue of the twin-His motif, thereby closing the channel. This interaction forms the first tier of the channel block within the pore. In order to ascertain the role of this residue in Mep2 transport and signalling, single amino acid substitution was carried out by replacing Tyr53 residue to Alanine (Y53A). Mep2^{Y53A} mutant was able to grow and transport ammonium under limited ammonium conditions, and signal in Npr1 lacking strains at rates higher than that of the wild-type strain. These findings suggest that this amino acid substitution has bypassed the need for Npr1kinase dependent activation of Mep2 resulting in a constitutively active transporter. This underscores the fact that the Tyr53- His348 bond is vital for channel closure to prevent ammonium entry during nitrogen rich conditions to alleviate ammonium toxicity. This interaction is highly conserved in fungal orthologues of Mep2 and might be the general system of channel closure in Mep2 proteins. This is a novel mutant identified in this study in which a gain of function mutation has been observed. However, alongside phosphorylation, the prerequisite for the disruption of Tyr53- His348 interaction by the incoming substrate for channel opening in Mep2 is still unclear. Similar outcomes were observed in an earlier study where substitution of Gly349 which is a conserved residue located next to the well conserved His348 residue makes the protein hyperactive and Npr1 kinase-independent. G349C substitution does not affect the stability of the protein and filamentation is more prominent in the absence of Npr1 kinase. Mep2^{G349C} mutant is thus hyperactive both in the presence and absence of Npr1 Kinase. Thus, ammonium associated pseudohyphal growth seems to be independent of Npr1 kinase activity and dependent on the transport activity of Mep2 in these mutants (Boeckstaens *et al*, 2007).

An earlier study (Boeckstaens *et al,* 2014) showed that Npr1 kinase fine-tunes Mep2 activity by phospho-silencing a carboxy-terminal autoinhibitory (AI) domain. Npr1 kinase positively controls Mep2 by mediating phosphorylation of the S457 residue which sequentially silences an AI domain in the CTR of the protein. This domain extending from residues 450 to 485 is essential for the auto-inhibition of Mep2 when Npr1 kinase loses its activity. In order to assess

the effect of loss of this autoinhibitory domain on Mep2 function, a truncated version of Mep2, Δ446 was generated. Mep2$^{\Delta446}$ lacking the autoinhibitory domain was transport active and signalling proficient at levels higher than that of wild-type even in the absence of Npr1 kinase. This shows that this domain is dispensable for activation of Mep2 both in the presence and absence of Npr1 kinase, and is essential for the autoinhibition of Mep2 in the absence of Npr1 kinase function, as suggested by Boeckstaens *et al* (2014). These data highlight the fact that Npr1 kinase integrity is thus essential to keep Mep2 in its active conformation. Truncation of amino acids from 450 till 486 in the C-terminus of Mep2 displayed ammonium transport and signalling defects and abolished intracellular accumulation and consumption of ammonium from the medium (Boeckstaens *et al*, 2014). A significant increase in intracellular ammonium levels were seen when four negative amino acids from the C-terminal 428-431 were deleted (Van Nuland *et al*, 2006). Thus, the C-terminus contains distinct regulatory domains and plays a major role in the optimal transport function of the Mep2 transporter. The AI function of yeast Mep2 CTR shows distinction to that of *Arabidopsis thaliana* ammonium transporter AtAmt1. In AtAmt1, phosphorylation of a conserved domain results in the inactivation of the transporter (Lanquar *et al*, 2009). A similar system of regulation where the activity of the transporter is fine-tuned by the conserved domains in the CTR was seen in mammalian Rh factors. The C-terminal extension of RhCG despite being divergent could be involved in a conserved gating mechanism forming a network with intracellular loops with its own as well as neighbouring monomers (Deschuyteneer *et al*, 2013). Protein expression levels were however very low for Mep2$^{\Delta446}$ mutant for both background lines. This might very well be due to the hyperactivity of this mutant and a reduction in its protein expression levels might be a mechanism to regulate the transporter activity. Another reason might be due to an unusual conformation undergone by the protein due to Δ446 truncation. Or else, the aggregation of the protein might make the His tag inaccessible during Western blot resulting in such poor levels of detection.

It has been shown that Npr1 modulates Mep2 activity via phosphorylation of residue Ser457 at the CTR. The integrity of Npr1 kinase seems to be necessary to conserve the phosphorylated form of the transporter to keep it in its active form. The Npr1 phosphorylation site is located at the periphery of CTR and the region beyond Ser457 is probably disordered in Mep2. This disordered region of the CTR is not conserved across ammonium transporters. In order to test whether deletion of this region would have an impact on the activity and phosphorylation state of Mep2, Δ457 truncation mutants were generated. Mep2$^{\Delta457}$ mutant showed lower levels of ammonium transport and significant loss of signalling compared to that of the wild-type strain. Protein expression levels were however similar to wild-type levels or higher for this mutant. In

Mep2$^{\Delta457}$ mutant Ser457 residue is immediately followed by a His tag which has higher levels of protein expression but lower levels of transporter function. This could be due to the fact that the His tag interferes with the phosphorylation function of Npr1 kinase. This was tested by generating a Mep2$^{\Delta457\,no\,tag}$ mutant which showed wild-type levels of transporter function. This endorses the notion that the region following the phosphorylation site Ser457 of Mep2 is dispensable for function. Former studies have shown that all the 22 residues of the core region of the CTR are not absolutely essential for *E. coli* AmtB activity. Alterations to the residues of the CTR might have marked effects including an impact on the interaction of AmtB with GlnK (Severi *et al*, 2007). Deletion of the C-terminus of bacterial and fungal ammonium permeases has shown to significantly reduce, but not switch off, transport. However, for *Arabidopsis thaliana* ammonium transporter AtAmt1, deletion of the CTR results in the inactivation of the protein (Coutts *et al*, 2002). A truncated version Mep2$^{\Delta426}$ mutant lacking the entire C-terminal tail demonstrated a significant reduction in transport and could only partially rescue the growth defect of a triple-*mep*Δ strain grown under nitrogen limiting conditions both in the presence and absence of Npr1 kinase (Boeckstaens *et al*, 2014). Van Nuland *et al* (2006) illustrated that residues 428-421 and 469-486 in the C-terminal tail were central regions for signalling in Mep2. The reason for abolishment of transport and signalling in certain C-terminal truncation mutants might be due to the lack of appropriate conformation of the protein to promote interactions between the C-terminal tail and intracellular loops in these mutants.

The Npr1 kinase target Ser457 is located in an electronegative pocket in the periphery of the C-terminal tail. This solvent-accessible location of this residue led to the hypothesis that phosphorylation of the Ser457 residue by Npr1 kinase would result in steric clashes and electrostatic repulsion bringing about conformational changes within the C-terminal tail. In order to test this hypothesis, phosphorylation-mimicking S457D and R456D/S457D mutants were generated. Mutation to the arginine residue prior to the phosphorylation site was introduced to increase the negative charge of the residue to make it more compatible to a phosphate group and to destabilise any interactions of the AI domain with the main body of the protein. Mep2^{S457D}, Mep2$^{R456D/S457D}$ mutants were transport and signalling proficient both in the presence and absence of Npr1 kinase and had higher levels of activity compared to the wild-type strain. Protein expression levels for both Mep2^{S457D} and Mep2$^{R456D/S457D}$ mutants were similar to or even higher than wild-type expression levels. This suggests that single /double amino acid substitutions to a negative group allows these mutants to mimic phosphorylation, and these phosphomimmetic mutants do not require Npr1 kinase for their activity. Structural data (van den Berg *et al*, 2016) from these mutants revealed that upon phosphorylation by Npr1

kinase during nitrogen limitation, the conserved motifs of the C-terminal tail undergoes a conformational change probably leading to the opening of the channel for ammonium import. The channel opening and closures in Mep2 might be due to the movements of the CTR, ICL1 and ICL3 away or towards each other. Given that the residues within CTR-ICL1/ICL3 are highly conserved the fundamental aspects of fungal ammonium transporter activation might be conserved. In *Arabidopsis thaliana* ammonium transporter AtAmt1, phosphorylation at the conserved residue T460 generates a conformational change leading to closure of the pore. This could be due to disruptions of interactions between the CTR and ICL1/ICL3 (Loque *et al*, 2007). Thus, phosphorylation could result in either opening of the channel similar to that of Mep2 or channel closure as seen in AtAmt1 depending on the location of the phosphorylation site in the CTR.

Regulation of ammonium transport in *E. coli* AmtB via complex formation with GlnK, a cytosolic signal transduction protein blocks the pore and controls influx of ammonium (Conroy *et al*, 2007). The binding of the regulatory protein GlnK confers a closed state to the channel inactivating substrate conduction by AmtB. The more open structural state might correspond to a non-conducting state of the channel making the AmtB pore unobstructed or open on the intracellular side (Coutts *et al*, 2002; Javelle *et al*, 2004). GlnKs are only conserved across prokaryotes and in some plants which makes alternate mechanisms for regulation of ammonium transport in fungi essential. Phosphorylation based regulation of ammonium transporters have been demonstrated so far for Mep2 orthologues from *S. cerevisiae*, *C. albicans* and *Arabidopsis thaliana* ammonium transporter AtAmt1 although this mechanism could be wide-spread in other eukaryotes (Lanquar *et al*, 2010; Boeckstaens *et al*, 2014; van den Berg *et al*, 2016).

Earlier studies have proposed two distinct models to explain how Mep2 regulates the dimorphic switch during pseudohyphal growth in yeast. The pH model describes Mep2 signalling in response to localised intracellular pH changes as an indirect consequence of ammonium import (Boeckstaens *et al*, 2008). The transceptor model of Mep2 function proposes that signalling is dependent on the conformational changes of the transporter during ammonium transport enabling it to engage downstream signalling partners to initiate pseudohyphal growth (Rutherford *et al*, 2008). Whilst these results do not tackle the precise mechanism of ammonium sensing and signalling during pseudohyphal growth, structural data from the phosphomimmetic Mep2 mutants reveal that the transporter undergoes a conformational change during ammonium import which might allow it to physically engage downstream signalling partners to initiate signal transduction pathways during pseudohyphal growth. Therefore, data from the structural

studies support the transceptor model of Mep2 function although no interaction partners that physically interact with Mep2 have been identified till date.

The molecular mechanisms that link ammonium transport and signalling are strongly coupled. The signalling pathways that regulate pseudohyphal growth are complex parallel pathways that feedback, crosstalk and interact with each other to co-ordinate the morphogenetic switch. Structural data reveals that Mep2 can undergo different conformations which could allow the protein to potentially engage downstream signalling partners to initiate pseudohyphal growth. The next step would be to identify proteins/interaction partners in the downstream signalling cascade to initiate pseudohyphal growth and their regulatory roles in modulating the morphological changes under low ammonium conditions. Understanding the precise mechanism behind ammonium sensing in fungi and the regulation of these ammonium transporters could help to devise strategies to control signalling pathways central to virulence in pathogenic fungi.

4. Structure based mutational analysis and characterisation of Mep2 mutants to identify residues essential for signalling

4.1. Introduction

Ammonium transport across cell membranes in *S. cerevisiae* is facilitated by a family of dedicated transmembrane ammonium transporters encompassing of Mep proteins which differ from each other in their kinetic properties and levels of protein expression. An evident biological role of these Mep proteins is to forage for ammonium from the environment for use as a nitrogen source during limiting ammonium conditions. The Mep proteins have been found to be essential for the retention of NH_4^+ inside the cell when grown on a nitrogen source other than ammonium (Marini *et al*, 1997).

The precise mechanism of ammonium transport and the chemical nature of substrate that gets transported through these transporters still remains controversial. It is unclear whether NH_3 gas or NH_4^+ ion or both NH_3/ H^+ gets co-transported across the membrane, and the transport mechanism is similar to that of a gas channel or a transporter (Khamedi *et al*, 2004; Conroy *et al*, 2007). Earlier studies have favoured the proposition that ammonium transporters are gas channels transporting NH_3 gas (Soupene *et al*, 2001). Using Molecular Mechanics (MM) simulations Wang *et al* (2012) presented that AmtB sustains electrogenic transport where NH_3/ H^+ gets co-transported through the pore. They show that during ammonium transport in AmtB, NH_4^+ gets deprotonated and transfers a proton to the first signature His residue and diffuses down the pore as NH_3 gas. The proton gets relayed to the second Histidine residue and gets reprotonated at that site proving that the signature Histidines are central for proton transport. Their simulation studies revealed that human Rh protein RhCG sustains an electroneutral transport of NH_3 gas which was in agreement with free energy calculations. With the help of molecular and quantum mechanic simulation data Baday *et al* (2015) showed that although RhCG protein recruits NH_4^+, it is NH_3 gas that gets transported and diffused down the pore. NH_4^+ gets deprotonated by transferring the proton to the first signature His residue, and the proton then gets carried back to the periplasmic space via hydrogen bonds between conserved polar residues.

These findings have led to the assumption that NH_3 has to be the species that gets transported through the pore during substrate transport in these family of ammonium transporters. After deprotonation, the proton could either get shuttled back to the extracellular space as shown in RhCG protein (Baday *et al*, 2015) resulting in an electroneutral transport or the proton could get relayed through the pore and get reprotonated in the cytosol (Wang *et al*, 2012) leading to an electrogenic transport.

The status of the proton whether it goes in through the pore or out to the periplasmic space during ammonium transport could be of great significance for the signalling function of Mep2. The deprotonation event in itself could be important to initiate conformational changes of the transporter to induce downstream signalling. This chapter aims to identify key residues involved in the ammonium sensing function of Mep2 through structure based mutational analysis and characterisation of Mep2 mutants. To gain a better understanding of the roles of these conserved residues in ammonium recruitment, transport and signalling, previously published transport efficient but at the same time signalling deficient Mep2 mutants to date which are unable to undergo pseudohyphal growth were characterized further in order to ascertain the roles of these residues in the sensing and signalling functions of Mep2. Residues K210 and R211 is part of ICL3; D279, Y280 and F281 is part of ICL4 and N246 has been shown to be part of TMD6 of Mep2, and have been shown to be essential for the initiation of pseudohyphal differentiation. Moreover, N246 of TMD6 is a well conserved residue located right next to the highly conserved F245 residue of the Phe gate. The two highly conserved Histidine residues H194 and H348 that line the pore of Mep2 have been shown to be essential for the initiation of pseudohyphal growth. Furthermore, these twin Histidine residues are thought to have central roles in the deprotonation of NH_4^+ ions and to serve as proton acceptors for uncharged NH_3 gas to travel through the channel. In order to confirm that these mutants are genuine signalling deficient mutants, the ability of these Mep2 mutants to transport ammonium, initiate filamentous growth and levels of protein expression were tested.

4.2. Mutagenesis of conserved residues of Mep2 affects optimal substrate conductance

In order to test whether the previously published signalling deficient mutants Mep2$^{K201A/R211G}$, Mep2$^{D279A/Y280G/F281A}$, Mep2^{N246A} (Van Nuland *et al*, 2006), Mep2^{H194E} (Boeckstaens *et al*, 2008) and Mep2^{H348A} (Rutherford *et al*, 2008) were transport proficient, they were transformed into *mep123Δ* background strains alongside controls and tested for their ability to grow and transport ammonium. They were grown on solid agar media containing 1mM ammonium sulphate as nitrogen source and assayed for growth robotically following a time course photography for 72 hours at 30°C.

The results from the transport assay (Fig. 24) demonstrate that mutagenesis of conserved residues of Mep2 affects optimal growth and transport rates. Mep2$^{K210A/R211G}$ mutant showed growth rates slightly less than the wild-type strain. Mep2$^{D279A/Y280G/F281A}$ mutant was unable to grow on low ammonium medium. Mep2^{N246A} mutant showed growth rates slightly higher than that of wild-type strain. Mep2^{H194E} and Mep2^{H348A} mutants were able to grow and transport ammonium at rates considerably higher than that of wild-type with Mep2^{H194E} mutant being the most transport proficient strain. Alterations in the rates of growth of Mep2 mutants and controls in *mep123Δ* background strains on low ammonium agar medium highlights the essential role of these conserved residues in maintaining optimum substrate transport. Since Mep2$^{K201A/R211G}$ and Mep2$^{D279A/Y280G/F281A}$ mutants showed growth rates less than that of the wild-type strain, they were not included in further growth tests.

The following strains - Mep2^{N246A}, Mep2^{H194E} and Mep2^{H348A} mutants were serially diluted and spotted on solid agar plates containing glutamate (0.1%) or ammonium sulphate (1mM) as nitrogen source and grown for 3 days at 30°C. A previously published positive control Mep2^{G349C} mutant (Boeckstaens *et al*, 2007) was included in the study which is transport proficient and is able to transport ammonium at rates higher than the wild-type strain. Results from the growth assay (Fig. 25) show that all the mutant strains are transport proficient and are able to grow and transport ammonium in limiting ammonium media similar to or more than the wild-type strain.
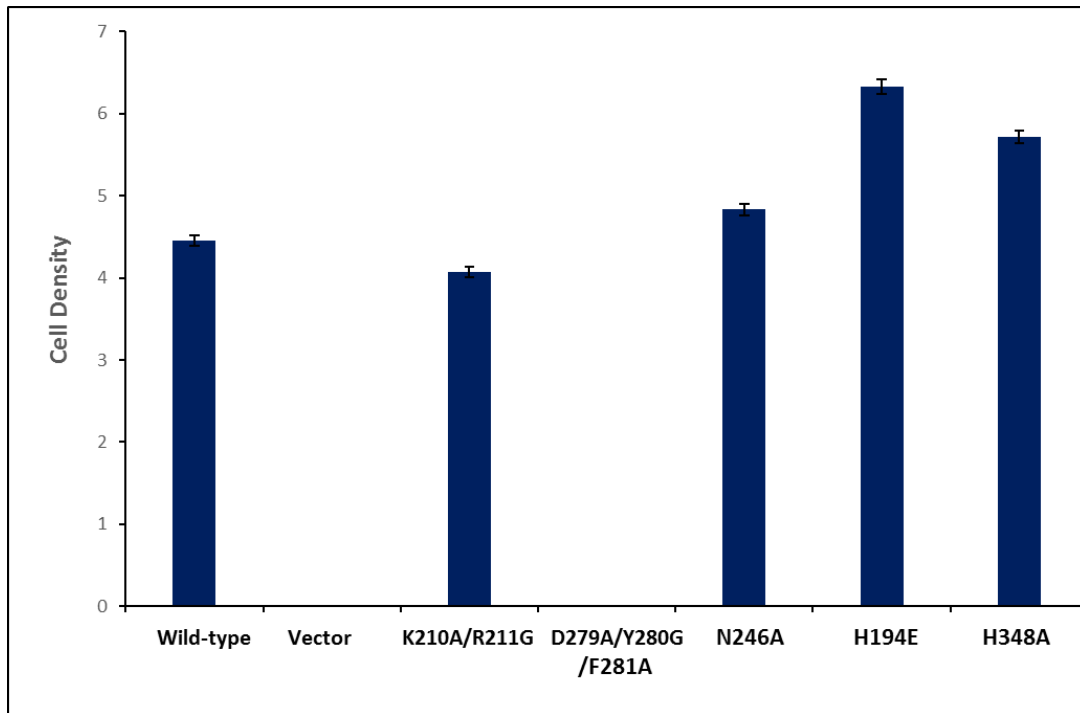
Figure 24: Growth of Mep2 mutants and controls generated via site-directed mutagenesis expressed in *mep123Δ* background strains grown on low ammonium agar medium. Cell density was quantified by photographing time-points across 72 hours of growth at 30°C. Error bars were calculated from standard deviations for triplicate repeats of each strain.
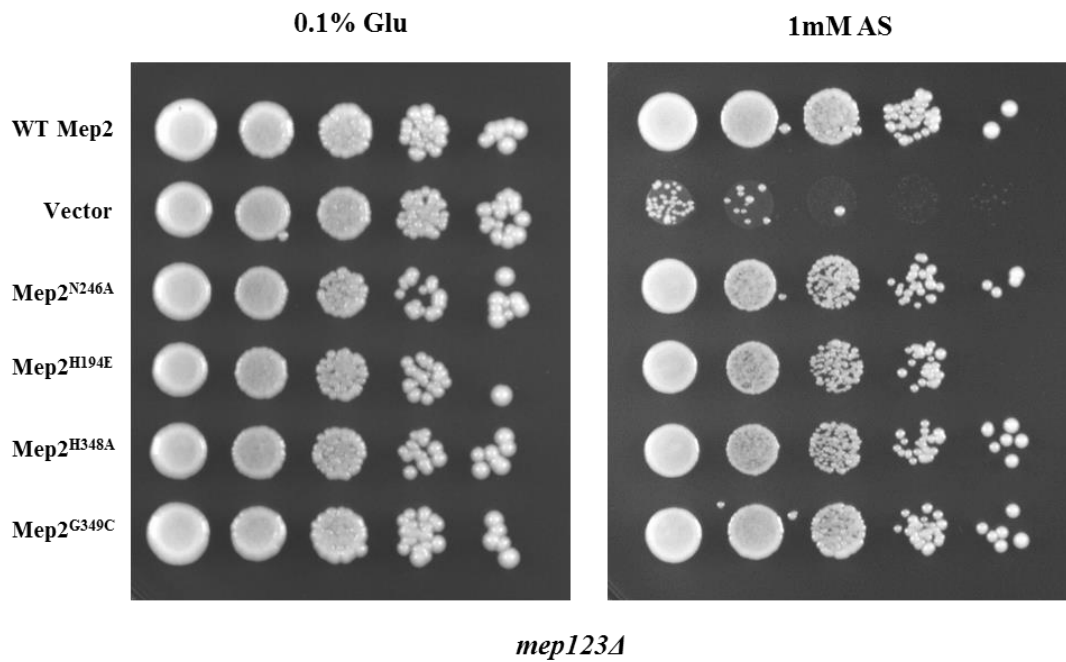
Figure 25: Growth of Mep2^{N246A}, Mep2^{H194E}, Mep2^{H348A} and Mep2^{G349C} mutant strains and controls in *mep123Δ* background strain serially diluted on solid agar medium containing 0.1% glutamate or 1mM ammonium sulphate as the sole nitrogen source and grown at 30°C for 3 days.

4.3. Specific mutations uncouple transport and signalling functions of Mep2

In order to confirm that the previously published signalling deficient mutants were unable to undergo pseudohyphal growth when grown under nitrogen limiting conditions, they were transformed alongside controls into a *mep2/mep2Δ* strain and plated on solid SLAD medium.

The results from the pseudohyphal growth test (Fig. 26) agrees with the published data as all of the mutants did not undergo pseudohyphal growth except for one. Mep2$^{K210A/R211G}$ mutant was able to initiate signalling under limiting ammonium conditions making it a signalling mutant which invalidates published data. Hence this mutant could not be used for further analysis and had to be excluded from the study. A previously published positive control Mep2^{G349C} mutant was included in the study which has hyperfilamentous phenotype. Enhanced filamentation patterns were obtained for this mutant compared to the wild-type strain.

a) **WT – Mep2**

b) **Vector**

c) **Mep2**^{K/R}

d) **Mep2**^{D/Y/F}

e) **Mep2**^{N246A}

f) **Mep2**^{H194E}

g) **Mep2**^{H348A}

h) **Mep2**^{G349C}
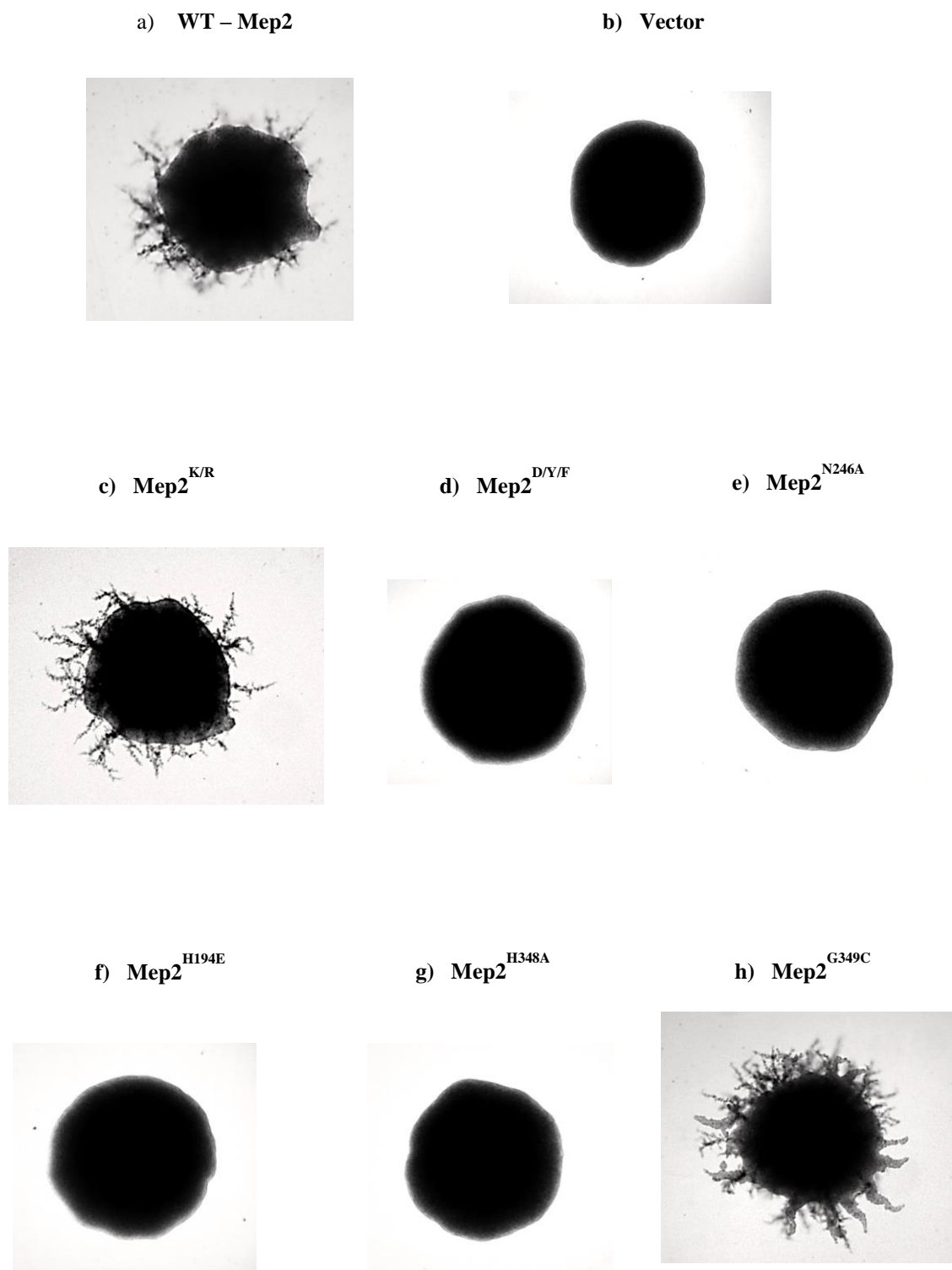
Figure 26: Pseudohyphal growth tests of Mep2 mutants and controls transformed into *mep2/mep2Δ* strain at 40X magnification. They were grown for 6 days on SLAD plates at 30°C containing 50µM ammonium sulphate as nitrogen source.

4.4. Expression levels of Mep2 does not correlate with its signalling function

It is well known that a reduction in the levels of expression of Mep2 can result in loss of signalling. Therefore, in order to confirm that the loss of signalling in these Mep2 mutants were not due to a drop in their protein expression levels, western immunoblotting was carried out. All the mutants alongside controls were expressed in *mep123Δ* and *mep2/mep2Δ* background strains.

For *mep123Δ* background strains Mep2$^{D279A/Y280G/F281A}$ mutant showed a sharp drop in its protein expression levels compared to that of wild-type (Fig. 27). Levels of protein expression for Mep2$^{K210A/R211G}$, Mep2^{H194E} and Mep2^{H348A} mutants were slightly lower than that of wild-type strain. Mep2^{N246A} mutant showed wild-type protein expression levels.

The results from the *mep2/mep2Δ* background strains were comparable to those from the *mep123Δ* background strains (Fig. 28). The Mep2$^{D279A/Y280G/F281A}$ mutant showed a severe drop in its protein expression levels as seen earlier compared to that of wild-type. Levels of protein expression for Mep2$^{K210A/R211G}$, Mep2^{H194E} and Mep2^{H348A} mutants were slightly lower than that of wild-type as shown previously. Mep2^{N246A} mutant showed wild-type protein expression levels. The hyperactive Mep2^{G349C} mutant showed slightly lower levels of protein expression levels compared to wild-type and their expression levels were similar to that of Mep2^{H194E} and Mep2^{H348A} mutants.

Given the fact that Mep2$^{K210A/R211G}$ mutant initiated pseudohyphal growth and the rate of ammonium transport and levels of protein expression for Mep2$^{D279A/Y280G/F281A}$ mutant was extremely lower than that of wild-type strain contrary to published data, these two mutants could not be further included in the study as they were not genuine signalling deficient mutants.
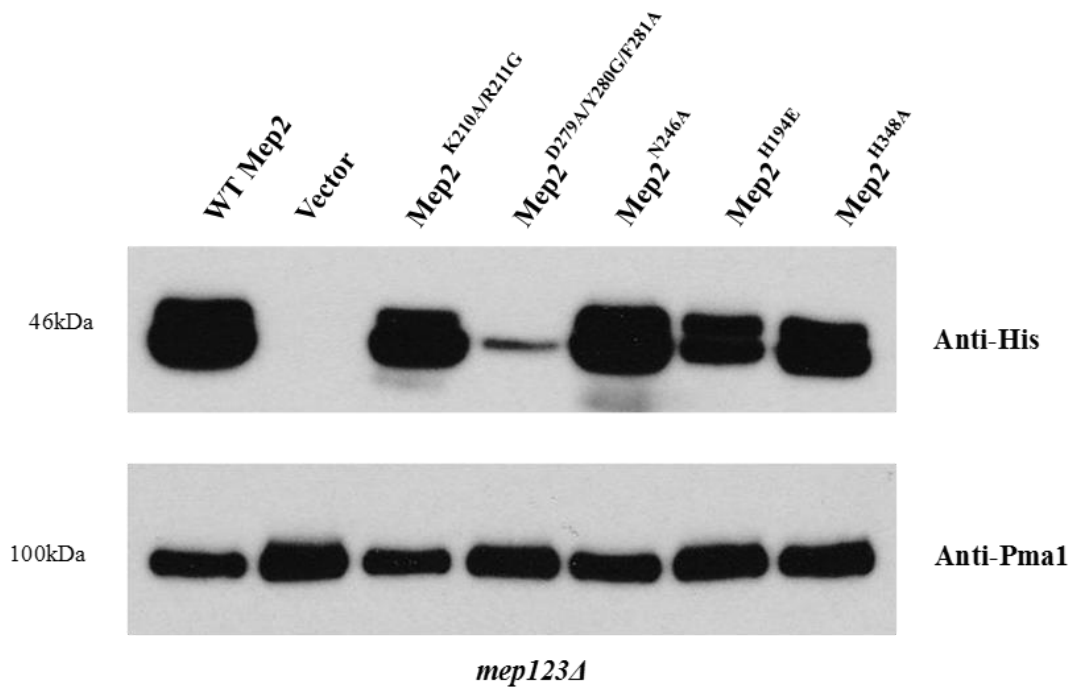
Figure 27: Immunodetection of Mep2 mutants and controls in *mep123Δ* background from membrane-enriched extracts of cells grown in 0.1% proline media. Levels of Pma1 was used as loading control.
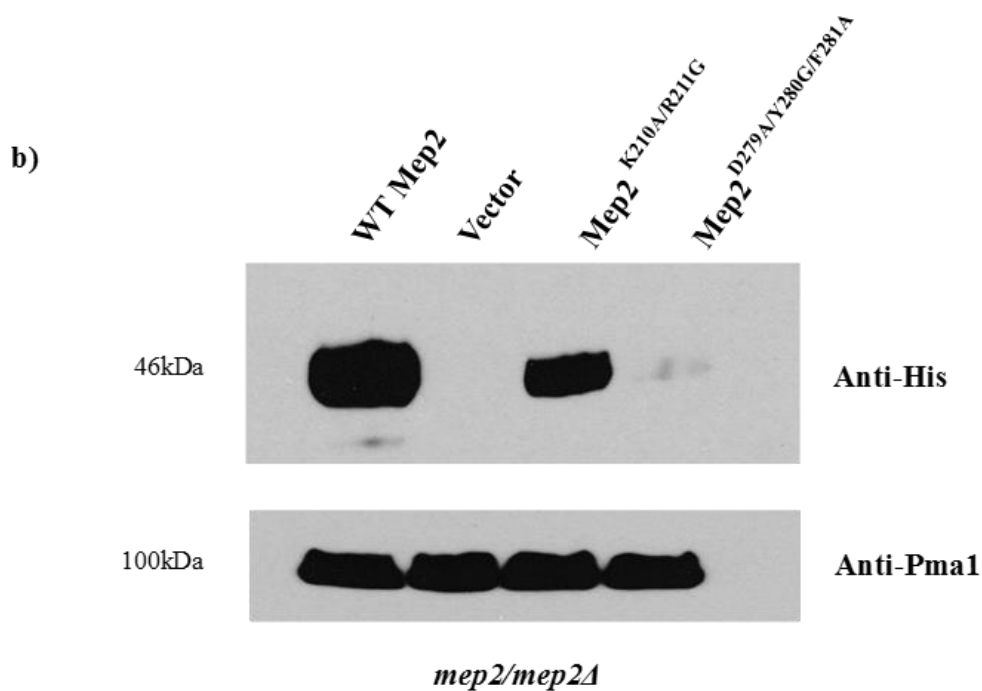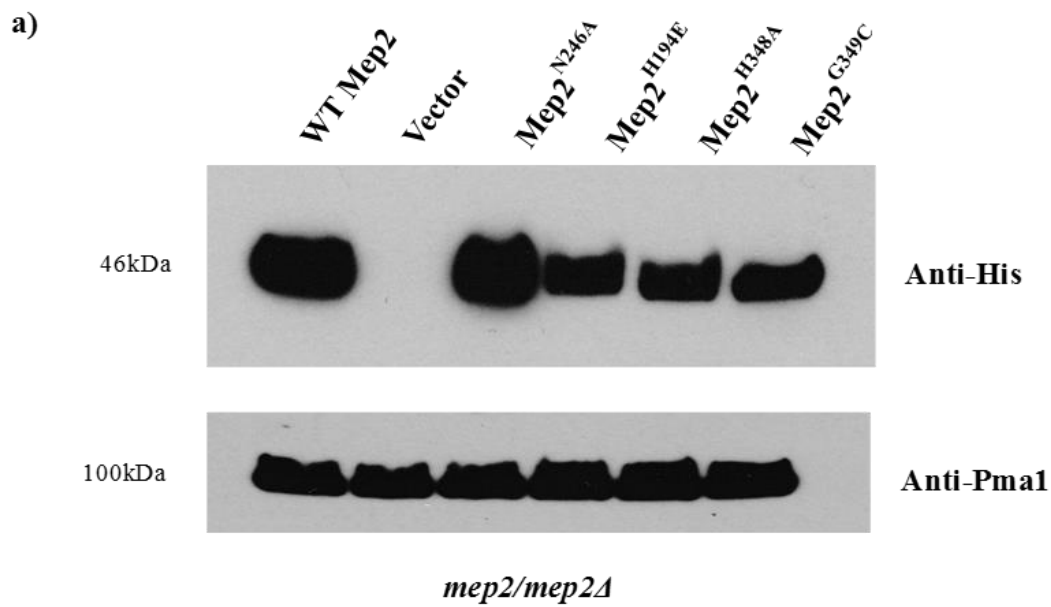
Figure 28 a) & b): Immunodetection of Mep2 mutants and controls in *mep2/mep2Δ* background from membrane-enriched extracts of cells grown in 0.1% proline media. Levels of Pma1 was used as loading control.

4.5. Overexpression of a twin-Histidine mutant does not rescue signalling in Mep2

Whilst both Mep2^{H194E} and Mep2^{H348A} mutants were able to transport ammonium and failed to undergo pseudohyphal growth, their expression levels were slightly lower than that of wild-type strain. It is well known that high levels of protein expression is necessary for the sensing function of Mep2 (Marini *et al*, 1997). In order to confirm that the twin-Histidine mutants were genuine signalling deficient mutants, they should be overexpressed to have wild-type protein expression levels to test whether that would rescue the signalling defect in these mutants. Mep2^{H194E} and Mep2^{H348A} mutants were overexpressed under the influence of a Gal promoter and transformed alongside controls into *mep123Δ* and *mep2/mep2Δ* background strains.

Western immunoblotting was carried out to check for levels of protein expression for the overexpressed Mep2^{H194E} and Mep2^{H348A} mutants alongside controls in *mep123Δ* background strain (Fig. 29). Immunodetection results reveal that Mep2^{H348A} mutant showed protein expression levels higher than that of wild-type. However, the Mep2^{H194E} mutant could not be overexpressed and it showed expression levels lower than that of wild-type.
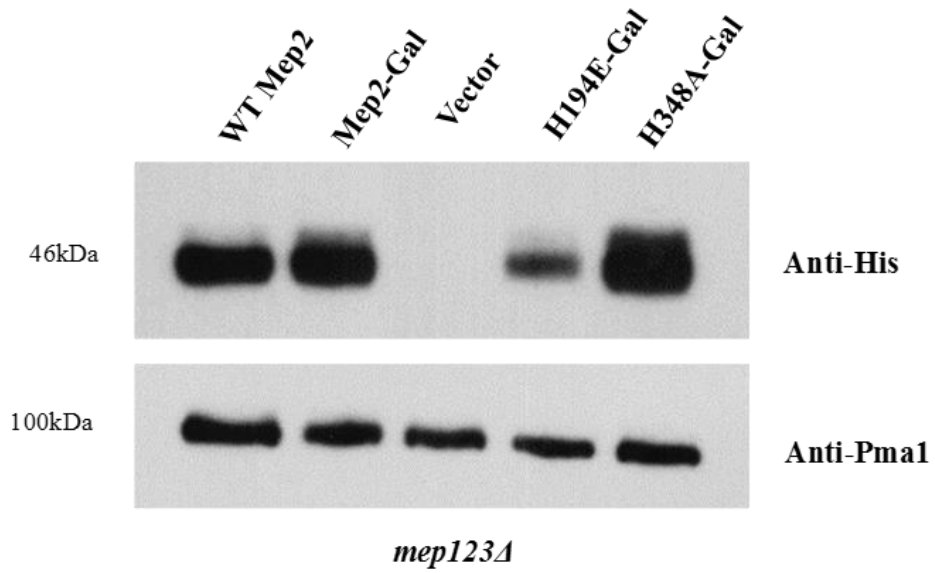
Figure 29: Immunodetection of overexpressed Mep2 mutants and controls in *mep123Δ* background from membrane-enriched extracts of cells grown in 0.1% proline media. Levels of Pma1 was used as loading control.

a) Mep2-Gal
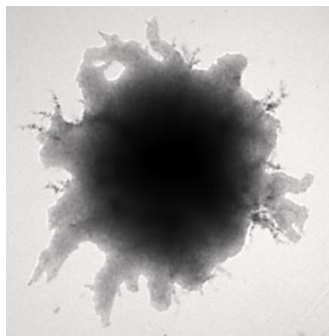
b) Vector
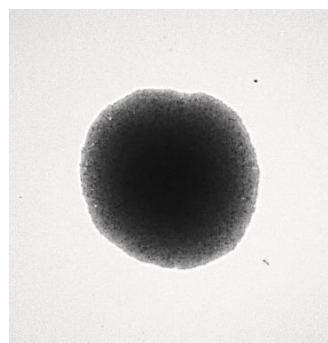
c) Mep2^{H194E-Gal}
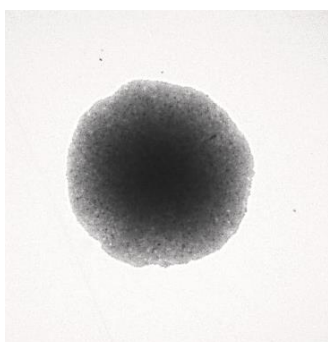
d) Mep2^{H348A-Gal}
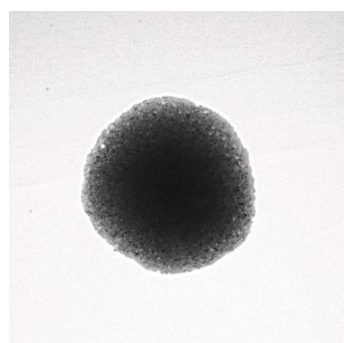
Figure 30: Pseudohyphal growth of overexpressed Mep2 mutants and controls in *mep2/mep2Δ* background strains illustrated at 40X magnification. Cells were grown at 30°C for 6 days on SLAD plates containing 50μM ammonium sulphate as nitrogen source.

In order to test whether overexpression of these twin-Histidine mutants would rescue signalling, pseudohyphal growth tests were carried out for these mutants alongside controls (Fig. 30). Overexpression of Mep2^{H194E} and Mep2^{H348A} mutants were unable to rescue signalling defects in these mutants as they failed to undergo pseudohyphal growth.

Mep2^{N246A}, Mep2^{H194E} and Mep2^{H348A} mutants were able to rescue growth defects in *mep123Δ* background strain and had protein expression levels similar to that of the hyperactive Mep2^{G349C} mutant. Moreover, these mutants failed to undergo pseudohyphal growth when grown under nitrogen limiting conditions which classifies them as genuine signalling deficient mutants.

4.6. Mapping of conserved residues essential for signalling in the Mep2 conducting pore

Using computational methods and molecular simulation data, Wang *et al* (2012) proposed a pathway for proton relay in AmtB where the twin-Histidine motifs act as a proton relay system whilst NH$_3$ gas traverses down the pore resulting in an electrogenic NH$_3$/ H$^+$ co-transport. They suggest that the highly conserved twin-His dyad is central for ammonium binding and deprotonation, and named the site where the substrate forms a hydrogen bond with the first Histidine residue as S2 and the site where it forms a second hydrogen bond with the second Histidine residue as S4. Stereo superposition of conserved residues from Mep2 and AmtB conducting pore (Fig. 31) illustrates the positions of non-signalling mutants identified through the course of this study to be part of the S2/deprotonation site (N246A, H194E) and S4/reprotonation site (H348A). The residues in the conducting pore for Mep2 and AmtB are highly conserved and identical to each other except for the Y53 residue due to its involvement in the two-tier pore closure in Mep2. This has allowed us to infer that the mechanism of ammonium transport proposed for AmtB could be extended to Mep2 where the signature Histidine residues have an essential mechanistic role.

Free energy calculations verify that NH$_4^+$ is stable in the AmtB conducting pore. During ammonium transport, once NH$_4^+$ enters the substrate conducting pore and reaches the S2 site, de-protonation occurs and the proton gets transferred to the H194 residue via a hydrogen bond which acts as a transient proton acceptor. The residues surrounding the S2 site seems to be important for its activity, and the proton then gets relayed to the second conserved Histidine residue. The re-protonation event takes place at the S4 site where the substrate accepts a proton from the conserved H348 residue through a hydrogen bond and diffuses into the cytoplasm as NH$_4^+$. (Wang *et al* 2012; Javelle *et al*, 2008).
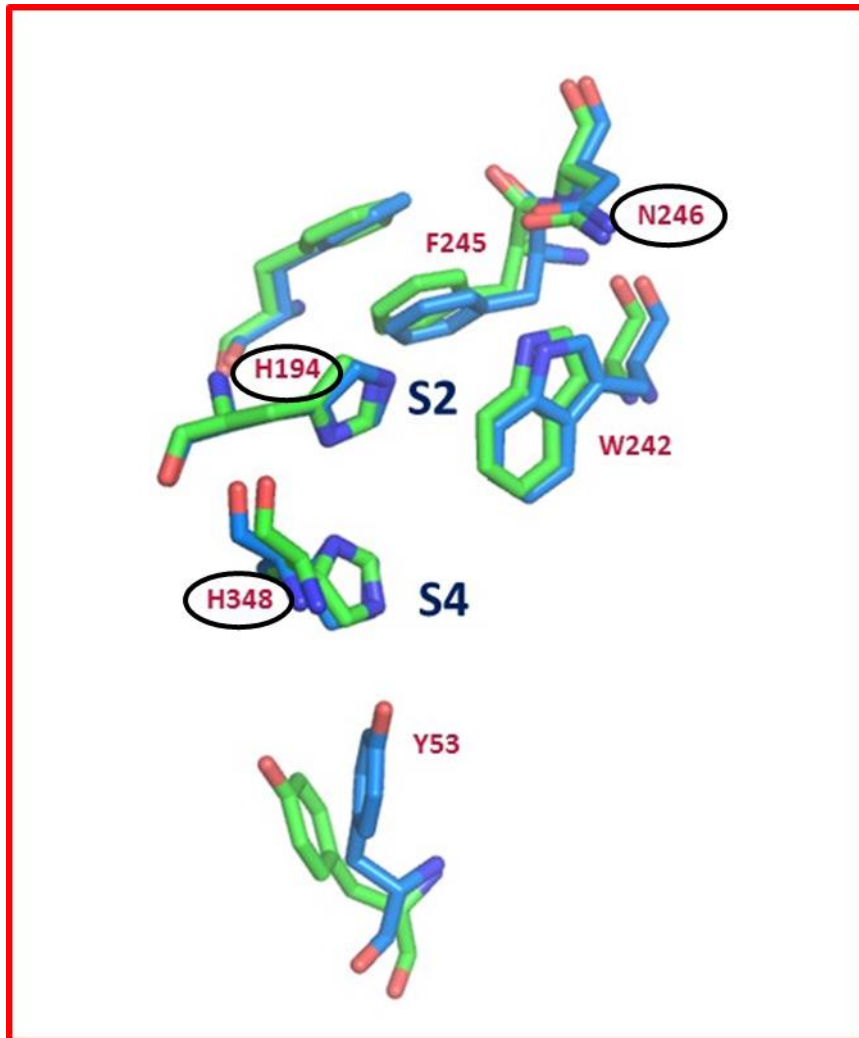
Figure 31: Stereo superposition of conserved residues from *S. cerevisiae* Mep2 and *E. coli* AmtB highlighting the separation of function mutants in the Mep2 ammonium conducting pore. Figure adapted from Chembath *et al* (in preparation).

4.7. Discussion

Mutational analysis of structurally significant residues was carried out in order to identify conserved residues critical for the sensing and signalling functions of Mep2. To gain a better understanding of the roles of these conserved residues and to identify genuine signalling deficient mutants, previously published transport-efficient, signalling-deficient Mep2 mutants to date which are unable to undergo pseudohyphal growth were characterized further. This was achieved by testing the ability of Mep2$^{K210A/R211G}$, Mep2$^{D279A/Y280G/F281A}$, Mep2^{N246A} (Van Nuland *et al*, 2006), Mep2^{H194E} (Boeckstaens *et al*, 2008) and Mep2^{H348A} (Rutherford *et al*, 2008) to transport ammonium, initiate pseudohyphal growth and levels of protein expression. A previously published hyperactive mutant for ammonium transport and pseudohyphal growth, Mep2^{G349C} mutant (Boeckstaens *et al*, 2007) was included as a positive control in the study.

When the non-signalling mutants Mep2$^{K201A/R211G}$ and Mep2$^{D279A/Y280G/F281A}$ were tested, Mep2$^{D279A/Y280G/F281A}$ was unable to support growth under low ammonium conditions and was expressed at very low levels. Mep2$^{K201A/R211G}$ on the other hand was able to undergo pseudohyphal growth under nitrogen limiting conditions making it signalling proficient mutant contradicting published data, and thus these mutants had to be excluded from the study. Western immunoblotting confirmed that Mep2^{N246A}, Mep2^{H194E} and Mep2^{H348A} mutants were expressed to the same levels as the hyperactive Mep2^{G349C} variant. These mutants were transport proficient and were able to grow considerably better than the wild-type strain on limiting ammonia media. These mutants are very active transporters and that might be the reason why their protein expression levels were slightly lower than that of wild-type. Furthermore, overexpression of these very active transporters might result in an even reduced level of protein expression as seen for the Mep2$^{H194E-Gal}$ mutant. Besides, these non-signalling variants failed to induce pseudohyphal growth, but were able to support the growth of mutants lacking the three endogenous yeast ammonium transporters under limiting ammonia conditions. Together, these experiments have demonstrated the significance of further investigating Mep2^{N246A}, Mep2^{H194E} and Mep2^{H348A} mutants as amino acid substitutions to these residues have a direct impact on the signalling function of Mep2.

Van Nuland *et al* (2006) showed that distinct regions of Mep2 are essential for its signalling function. Residues K210, R211 in IL3; and D279, Y280 and F281 in IL4 along with N246 of TMD6 were essential for the initiation of pseudohyphal differentiation. When these mutants were tested as part of this study, Mep2$^{K210A/R211G}$ and Mep2$^{D279A/Y280G/F281A}$ mutants were not genuine signalling deficient mutants. N246 of TMD6 is a conserved residue located next to the highly conserved F245 residue of the Phe gate. Single nucleotide substitution of N246 to alanine

uncoupled transport from signalling functions of Mep2 (Van Nuland *et al*, 2006). This mutation however had no effect on either ammonium transport or expression levels of the protein, yet abolished pseudohyphal growth, making it a true signalling deficient mutant. Contrasting results were observed for single nucleotide substitution of Glycine at position 349 located on transmembrane helix 10. It is a well conserved residue which lies next to the signature Histidine residue H348 in the Mep2 conducting pore. Mep2[G349C] mutant is hyperactive and hyperfilamentous (Boeckstaens *et al*, 2007). It has been shown in AmtB that deletion or obstruction of the Phe gate (F132 and F245 in Mep2) residues results in an inactive transporter (Javelle *et al*, 2008). Molecular mechanics calculations suggest that the gate might favour permeability of NH_4^+ compared to NH_3 gas probably to prevent the diffusion of NH_3 back towards the cytoplasmic side (Lamoureux *et al*, 2010).

Two highly conserved Histidine residues (H194 and H348 in Mep2) line the pore of Mep2 such that their side chains protrude into the channel (Khamedi *et al*, 2004; Zheng *et al*, 2004). Earlier studies have shown that the twin-His motifs are essential for optimum substrate conductance and are important in the initiation of pseudohyphal growth (Javelle *et al*, 2006; Rutherford *et al*, 2008; Boeckstaens *et al*, 2008). It has been proposed that these twin Histidine residues might have a central role in the deprotonation of NH_4^+ ions, to serve as proton acceptors for uncharged NH_3 gas to travel through the channel (Winkler, 2006; Khamedi *et al*, 2004; Zheng *et al*, 2004).

Using molecular mechanics (MM) simulation data Wang *et al* (2012) illustrated the mechanism by which AmtB favours electrogenic transport conferring a central role for the Histidine dyad in ammonium binding and deprotonation. They show that NH_4^+ is stable in the pore in the deprotonation S2 site, and after deprotonation the proton gets transferred to the first Histidine residue. NH_3 gas diffuses down the pore without any free energy barrier and the proton gets relayed to the second Histidine residue. Once the substrate reaches the re-protonation S4 site it accepts the proton from the second Histidine residue diffusing down the pore as NH_4^+. This deprotonation-diffusion-reprotonation cycle of ammonium leaves the Histidine dyad in an inactive protonation state for the next co-transport to happen. In order to return to their initial protonation state, a Histidine re-set mechanism involving hydrogen bond networks between the twin Histidine residues and water molecules between the S2 and S4 sites was observed.

By replacing the H194 residue with a glutamate residue Mep2 acquires Mep1 like properties uncoupling transport from signalling (Boeckstaens *et al*, 2008). The inability of Mep2[H194E] mutant to initiate signalling for pseudohyphal growth could be due to the absence or alteration of molecular events required for NH_4^+ deprotonation at the S2 site. This could mean that the proton might be directed to the wrong place or the protein might be in a different conformation

unable to initiate downstream signalling for pseudohyphal growth. Javelle *et al* (2006) argued that the partial activity of Mep2[H194E] mutant could be explained by either their inability to act as a proton acceptor for the incoming ammonium ions or due to the absence of a precise orientation for hydrogen bond formation to stabilise interactions with ammonia or water molecules. This might also explain the inability of N246A mutant to initiate filamentous growth. Residue N246 is also part of the S2 site and the mutation might alter the deprotonation event which could result in the proton either moving out to the periplasm or following an incorrect path into the cytoplasm. Another possibility would be the ability of these mutants to bypass the deprotonation event conferred by the mutation, which could account for their improved ammonium transport rates. The mutation could thus result in a conformational change within the transporter unfavourable for interaction with downstream signalling partners. These mutants thus highlight the significance of the deprotonation event at S2 site as a key event during ammonium import, and the importance of this deprotonation event in the sensing function of Mep2.

MM simulation data (Wang *et al*, 2012) suggests that the protonated state of H348 residue becomes progressively stable when NH_3 diffuses down the pore from S2 to S4. As a result, the proton would most likely be on the H348 residue when NH_3 reaches the S4 site, ready to be re-protonated. Alteration of H348 to alanine could have an effect on the landing of the proton on the Histidine residue. The hydrogen bond between the substrate and H348 residue could be affected which could in turn could lead to an inactive conformation of the transporter unable to initiate signalling. Double mutants of these conserved Histidine residues (H194A/H348A) failed to transport ammonium or methylamine in Mep2 and AmtB (Wang *et al*, 2013). The failure of these double mutants to transport ammonium could be attributed to the fact that the mutation could lower the energy barrier for the substrate to return to the periplasmic site. The dynamic state of Phe gate could be changed leading to an increased opening frequency of the gate. This could result in a loss in the unidirectional property of substrate transport. This demonstrates that both Histidine residues have been extremely conserved during evolution. Taken together, this illustrates the positions of mutants included in this study to be part of the S2/deprotonation site (N246A, H194E) and S4/reprotonation site (H348A) within the Mep2 conducting pore.

The sensing role of Mep2 thus seems to be principally dependent on the specific deprotonation/re-protonation events involving the S2 and S4 sites of the transporter as identified through the course of this study. The activity of these twin Histidine residues thus depends on a combination of precise spatial and chemical adaptations of the conducting pore.

The study thus clearly demonstrates the exact molecular events essential during ammonium transport, the deprotonation event at S2 site and the reprotonation event at S4 site to be indispensable for the signalling function of Mep2. These results illustrate the role of the S2 and S4 sites in the ammonium sensing function of Mep2.

Although these Histidine residues are highly conserved across most ammonium transporter proteins, a number of fungal Amt proteins have a glutamate residue replacing the first conserved Histidine residue. These Amt proteins are still capable of ammonium transport as the replaced residue is thought to behave similar to the Histidine residue during transport, and take part in the same hydrogen bond interactions if present in its neutral form (Marini *et al*, 1997; Smith *et al* 2003). Most fungal species encode multiple Amt/Mep proteins at least one of which contains the twin His residues and the others contain a minimum of one glutamate substitution (Soupene *et al*, 2001; Li *et al*, 2006). In *S. cerevisiae* the twin His residues are conserved in Mep2 whereas the first residue is replaced by glutamate residue in both Mep1 and Mep3. Mep2 has an additional signalling function where it acts as an ammonium sensor. The sensing and transport functions seem to be strongly connected in Mep2, and this conserved first His residue appears to be central for the signalling function of Mep2.

All the solved structures of ammonium transporters illustrate similar basic architecture with the transporter as a stable trimer with each monomer consisting of 11/12 transmembrane (TM) helices and a central hydrophobic pore for substrate conductance. Studies so far on the mechanism of substrate transport for the members of the ammonium transporter family have resulted in the proposal of three major mechanisms – transport of NH_3 gas which is electroneutral (Javelle *et al*, 2008; Khamedi *et al*, 2004; Zheng *et al*, 2004), co-transport of NH_3/ H^+ (Ludewig *et al*, 2006; Boeckstaens *et al*, 2008) or NH_4^+ transport (Marini *et al*, 1997; Fong *et al*, 2007) both of which results in electrogenic transport. The nature of the transported species or the mechanism involved have not been confirmed yet mostly because of the difficulty in distinguishing water, NH_3 and NH_4^+ in the crystal structure as they all are isoelectric molecules. Amongst other debatable issues is the possibility of the presence of water molecules in the pore lumen of ammonium transporters. The occurrence of water in the pore lumen is important for determining the electrostatic barrier for ammonium permeation through the pore (Ullmann *et al*, 2012). Using computational methods, Wang *et al* (2012) proposed that AmtB pore is occupied by water molecules in the crystal structure. The presence of water molecules can increase the stability of charged NH_4^+ molecules and proton conductance within the pore lumen thereby favouring NH_3/ H^+ co-transport (Baday *et al*, 2013).

The thermodynamics of likely mechanisms involved in the substrate transport for *Archaeoglobus fulgidus* AfAmt-1 was studied (Ullmann *et al*, 2012). They concluded that both electrogenic and electroneutral transport mechanisms were found to be feasible following thermodynamic calculations and one mechanism of transport could not be preferred over the other based on free energy profiles. Wacker *et al* (2014) later with the help of electrophysiological studies showed that AfAmt-1 sustains electrogenic NH_4^+ transport. They demonstrated that transport in AfAmt-1 is selective for its preferred substrate ammonium and the transport is pH dependent.

Although AmtB and human RhCG have various structural features in common including the conducting pore, there are important variations in the vestibule which could be determinant of the mechanism of transport (Zidi-Yahiaoui *et al*, 2009). RhCG lacks an ammonium binding site in the vestibule which, in AmtB, is situated above the Phe gate. With the help of molecular and quantum mechanic calculations Baday *et al* (2015) showed that RhCG sustains electroneutral NH_3 transport even though they recruit NH_4^+. Deprotonation takes place at the first signature Histidine (H185) residue after it accepts a proton from the bound substrate and diffuses down the pore as NH_3 gas without any free energy barrier. The proton then gets shuttled back to periplasmic space via a network of hydrogen bonds linking H185 residue and highly conserved aspartic acid (D177) and serine (S181) residues. Mutational analysis of these conserved residues D177 and S181 (Zidi-Yahiaoui *et al*, 2009) revealed that ammonium transport was impaired in these mutants presenting a crucial role for these residues in substrate transport in RhCG.

The two classes of proteins, AmtB and RhCG could be differentiated by the path followed by the proton during substrate import resulting in electrogenic NH_3/ H^+ co-transport in AmtB (Wang *et al*, 2012) or electroneutral NH_3 diffusion in RhCG (Baday *et al*, 2015). The fate of the proton during ammonium import could play an important role in determining the sensing function of Mep2. Electrogenic transport could result in localised pH changes within the cytosol resulting in Mep2 signalling. On the other hand, the molecular events during deprotonation/re-protonation of the substrate could be essential for the conformation of Mep2 to initiate signalling for pseudohyphal growth. Thus, identifying residues involved in ammonium recruitment and signalling is of vital importance in the sensing function of Mep2.

The conserved Mep2 residues identified as part of this study are central to the ammonium sensing and signalling function of Mep2, includes the N246 and H194 residues which form part of the deprotonation site of the ammonium ion during substrate transport, H194 and H348 residues which are part of the proton relay pathway and H348 residue which forms part of the

reprotonation site of ammonia gas and proton within the pore. These results highlight the fact that deprotonation, proton relay and reprotonation of the substrate during transport are essential for the signalling function of Mep2.

The central question after the identification of these residues essential for Mep2 signalling would be to elucidate which proposed model of ammonium sensing is followed by Mep2. These results could however support both the pH model or transceptor model of Mep2 function. Amino acid substitutions to the conserved residues within the Mep2 conducting pore could result in an unusual conformation of the transporter which would still allow ammonium transport but these unusual conformations could be unfavourable for a physical interaction with a downstream signalling partner to initiate pseudohyphal growth. Mutations to the conserved residues involved in the deprotonation, proton relay or re-protonation could result in the proton being directed to an incorrect path or bypassing the deprotonation event supporting increased rates of growth but resulting in alterations in the intracellular pH unfavourable for signalling. These separation of function mutants could be used to test both the transceptor and pH models of Mep2 function to gain a better understanding of the precise mechanisms behind ammonium sensing functions of Mep2.

5. Examining the pH model of ammonium sensing

5.1. Introduction

The capability of organisms to rapidly respond to changing environmental conditions including variations in temperature, nutrient availability, pH, osmolarity, oxidation etc. is critical for survival and competitive fitness. Extracellular pH changes can have a significant effect on survival, and could influence growth and differentiation strategies (Causton *et al*, 2001). Owing to their ability to affect electrostatic interactions, pH changes can also influence the structure and functions of many proteins alongside their interactions and stability. Intracellular pH (pHi) is usually defined as the proton (H^+) concentration in the cell and has a massive influence over a variety of cellular functions and must be under careful regulation (Martinez-Munoz & Kane, 2008). Changes in extracellular pH could have an effect on the intracellular pH of cells. Data from genetic and growth experiments on cytosolic pH demonstrates that high cytosolic pH is important to promote and maintain cell growth and survival (Dechant *et al*, 2014).

Membrane potential can be defined as the totality of all the ionic gradients over the plasma membrane with the main contributors being H^+ and K^+ gradients (Grossmann *et al*, 2007). H^+ gradients have roles in nutrient transport via symport or antiport mechanisms and are responsible for generating and controlling membrane potential in yeast (Seto-Young & Perlin, 1991). Membrane potential is considered to be the key driving force for ion and nutrient translocation and the gradients are created by exporting protons out of the cell at the cost of ATP hydrolysis (Orij *et al*, 2011).

One of the major contributors towards the regulation of intracellular pH includes nutrient availability. The availability of nutrients is a major determinant for cell growth and development in eukaryotes. They are essential not only to generate building blocks for biomass generation, but also as cellular signals for the regulation of numerous highly conserved signalling pathways regulating cell growth and survival (Saad *et al*, 2013). Metabolic signals could thus act as a second-messenger to orchestrate downstream signalling events. Organisms like yeast respond to extracellular changes in the environment like nutrient availability by modifying intracellular pH thereby altering cell physiology and make-up. Although tightly controlled, pH values in living cells are often highly dynamic and are unable to maintain

intracellular pH homeostasis when faced with nutrient starvation and growth arrest (Orij *et al*, 2009).

Fungi have more acidophilic pH values compared to bacteria and have the vital need to adapt to neutral or alkaline pH. A shift from neutral to alkaline pH promotes a morphogenetic switch from the normal yeast to filamentous pseudohyphal form, central for virulence in pathogenic fungi (Saville *et al*, 2013). Among the key cellular processes affected by diverging pH values are cellular transport of molecules across membranes affecting the pH gradient over the plasma membrane (Nishimura *et al*, 1998). The uptake of nutrients across the plasma membrane is dependent on the maintenance of plasma membrane proton gradient which in turn influences cytosolic pH (Orij *et al*, 2011). Rapid changes in intracellular pH could serve a signalling function coupling energy status to downstream signalling events. Cytosolic pH might act as a second messenger to report on the availability of preferred sources of carbon (Dechant *et al*, 2010). If internal pH changes can act as a cellular signal capable of triggering a physiological response, then the levels of imported substrate can be significant.

Among the two distinct hypotheses proposed to elucidate the sensing and signalling functions of Mep2 during nitrogen starvation, the first model describes Mep2 signalling in response to localised changes in intracellular pH as an indirect consequence following ammonium import (Boeckstaens *et al*, 2008). Alterations in the net import of protons subsequent to uptake of ammonium could have an impact on the internal pH. In other words, ammonium import by Mep2 might influence intracellular pH and this localised change in pH could initiate downstream signalling leading to filamentous growth.

In yeast, the vacuoles tend to have an acidic pH while the mitochondrial matrix has an alkaline pH (Brett *et al*, 2005; Llopis *et al*, 1998). Maintenance of organelle-specific pH in the cell is a critical factor when it comes to defining and maintaining cell physiology associated processes. Most organelles differ in their pH values depending on the specific functions associated with those compartments. Nutrient availability seems to be a major factor in the maintenance of organelle-specific pH gradient (Martinez-Munoz & Kane, 2008). Therefore, a tool capable of reporting pH changes within live cells is essential to accurately monitor the pH changes in different organelles. Various techniques previously used to measure pH includes the use of pH sensitive fluorescent dyes (Lanz *et al*, 1999), radio-labelled membrane-permeable acids or bases (Siegumfeldt *et al*, 2000) etc. Since none of these techniques could accurately report organelle-specific pH measurements, and manipulation of cells itself could affect intracellular pH, a more reliable technique to precisely monitor intracellular pH was required.

The use of pH sensitive fluorescent proteins has facilitated measurement of intracellular pH changes from live and unperturbed cells in a reliable and organelle-specific fashion (Bizzarri *et al*, 2009). A promising method to measure intracellular pH changes would be to express a fluorescent pH biosensor (Rosado *et al*, 2008) comprising of a pH stable red fluorescent protein fused to a pH sensitive green fluorescent protein *in situ* to measure changes in pH based on nutrient availability and on the presence or absence of the transporter. This single reporter molecule allows both qualitative and quantitative analysis, allowing monitoring of pH changes during nitrogen starvation dependent on the presence or absence of Mep2 function. In order to comprehend the pH model for ammonium sensing by Mep2, changes in intracellular pH were measured with the help of the pH biosensor during low ammonium conditions to learn if localised pH changes during ammonium import are Mep2 dependent. The key question would be regarding Mep2 dependent pH changes, if any, due to ammonium import, and if these localised pH changes are capable of acting as a signal to trigger physiological changes leading to a dimorphic change in yeast. The pH model of ammonium sensing was investigated in detail in this chapter.

5.2. Optical properties of the pH biosensor *in vivo*

A dual colour emission biosensor, Rosella, was developed and characterised by Rosado *et al* (2008) following the fusion of a pH-insensitive fast-maturing variant of the red fluorescent protein, DsRed, with a pH-sensitive variant of the green fluorescent protein SEP (supereclipstic pHluorin). Their mode of action is dependent on the pH variations between various organelles and cellular compartments in yeast. The fluorescence emission for DsRed is stable over a wide range of pH (~ 4-9) and is almost insignificant for SEP at lower pH values as it displays a pH-based loss of green fluorescence intensity. A balanced relative expression of the green and red fluorescent proteins is crucial for determining an emission ratio of the fluorescence rates that are linked to pH values. DsRed can be excited at 543 or 568nm and has an emission intensity at 587nm. SEP has an emission intensity at 508nm when excited at 488nm. The dual fluorescence emission from the biosensor provided information on the pH changes within the cellular environment.

5.3. Expression of the fluorescent pH biosensor in *S. cerevisiae* under nitrogen limitation

The pH biosensor Rosella was expressed in wild-type and *mep2/mep2Δ* background strains alongside controls. The optical properties of the biosensor were tested by growing the wild-type strain expressing the biosensor to mid-log phase under low ammonium conditions in 0.1% proline media and the cells were viewed under a fluorescence microscope (Fig. 32). Green fluorescence emission (508 nm) and red fluorescence emission (587 nm) images were obtained upon sequential excitation with 488 nm and 568 nm lasers, respectively. Red and green fluorescent images were documented at their respective emission and excitation values confirming that the biosensor is behaving as expected.

5.4. Flow cytometry analysis of Mep2 mutants expressing the pH biosensor

Rosella pH biosensor was co-transformed with plasmids expressing wild-type *MEP2* and controls in wild-type and *mep2/mep2Δ* background strains. In order to test whether the biosensor efficiently responds to and is capable of reporting pH changes, the wild-type strain expressing the pH biosensor was grown under a range of pH varying from pH 4-7 in synthetic rich media. The samples were then analysed using flow cytometry. Yeast cells expressing a non-fluorescent plasmid was used as control to set the background levels of fluorescence.

Results from the flow cytometry analysis (Fig. 33) show that the fluorescence ratio was lowest for pH 4 compared to higher pH values and the ratio increased steadily as the pH values increased from 4 to 7 in the wild-type cells. A significant reduction in the fluorescence ratio was detected in cultures grown at pH 4 compared to those grown at pH 7. The biosensor is thus capable of reporting pH changes ranging from pH 4-7 in the growth media.

In order to test whether changes in cytosolic pH are observed under low ammonium conditions using the Rosella biosensor, wild-type strain expressing the pH biosensor in BY4741 and Σ1278b background strains were grown in synthetic rich media and low nitrogen 0.1% proline media. Results from the flow cytometry assay (Fig. 34) illustrate that the fluorescence values for both BY4741 and Σ1278b background strains were significantly lower for cells grown in 0.1% proline media compared to growth under synthetic rich media. This confirms the proposition that the cytosol of cells grown in this low nitrogen 0.1% proline media which promotes pseudohyphal growth is more acidic than that of the cells grown in ammonium replete synthetic media. The acidic cytosolic pH in those cells results in a drop in the fluorescence ratio for cells grown in 0.1% proline media.

	DIC	**Red**	**Green**
Wild-type			
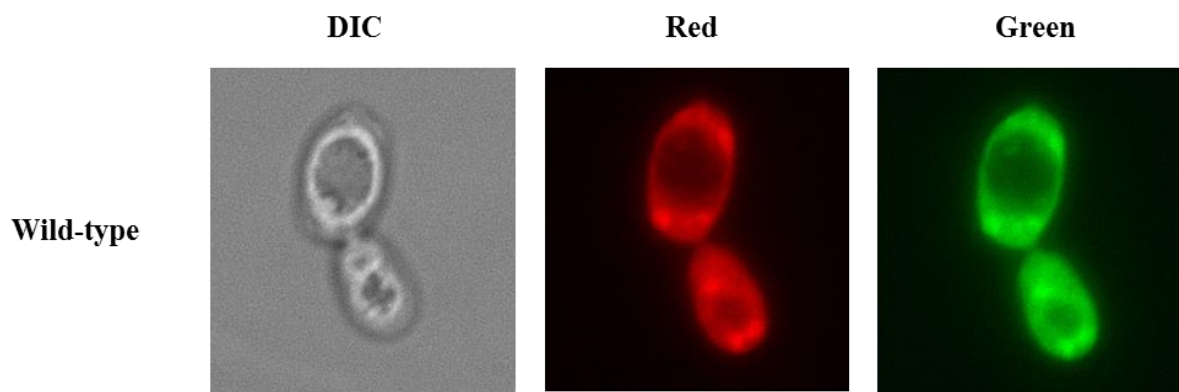
Figure 32: Rosella expressed in *S. cerevisiae* wild-type strain under nitrogen limitation. DIC (Differential Interference Contrast) and red and green fluorescent images were obtained by growing mid-log phase cells in 0.1% proline medium followed by sequential excitation and emission of the fluorophores.
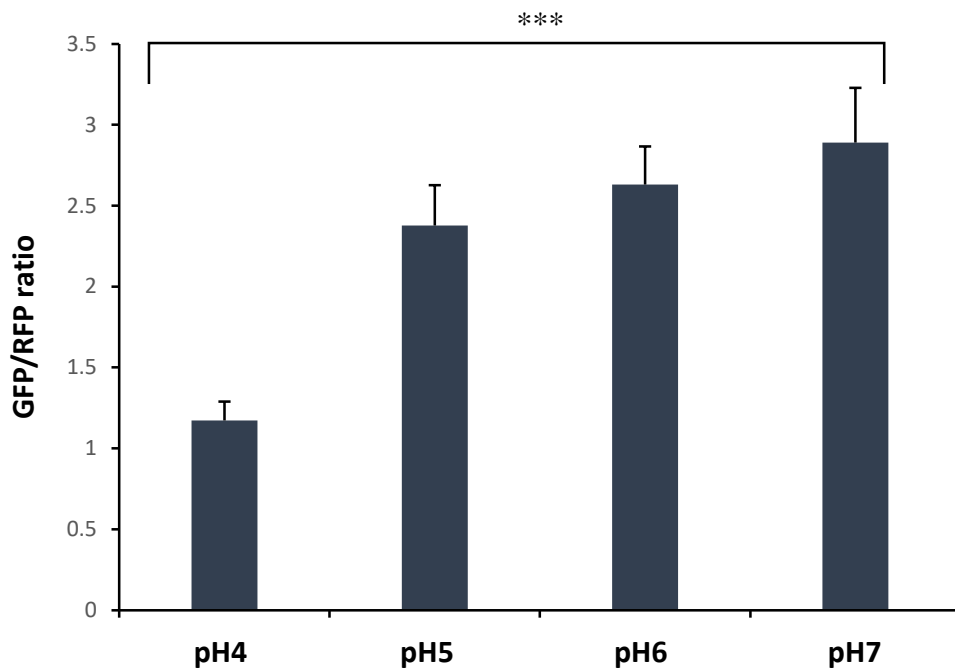
Figure 33: Flow Cytometry analysis of the wild-type strain expressing the pH biosensor grown in synthetic rich media (SD-Leu) at pH values buffered from 4 to 7. Yeast cells were grown to mid-log phase and harvested for Flow Cytometry analysis. Error bars were calculated from standard deviations for triplicate repeats of each strain and the results were statistically examined using Student's t-test. Symbol *** denotes statistical differences at the p values of 0.001.

a)
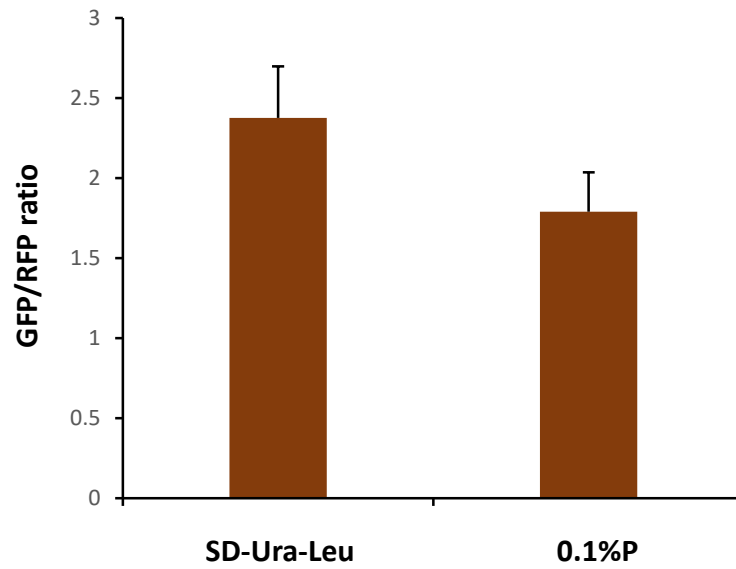
b)
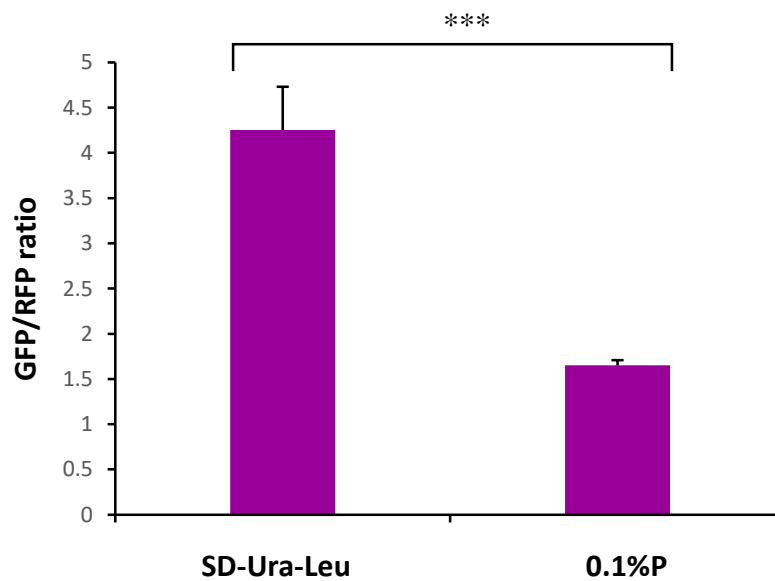
Figure 34: Flow Cytometry analysis of wild-type strain expressing the pH biosensor in a) BY4741 background and b) Σ1278b background strains grown in synthetic rich media (SD-Ura-Leu) and low nitrogen 0.1% proline media. Yeast cells were grown to mid-log phase and harvested for Flow Cytometry analysis. Error bars were calculated from standard deviations for triplicate repeats of each strain and the results were statistically examined using Student's t-test. Symbol *** denotes statistical differences at the p values of 0.001.

5.5. Ammonium sensing function of Mep2 is independent of intracellular pH changes

In order to investigate the pH model of ammonium sensing, the strain containing the Rosella pH biosensor was co-transformed with plasmids expressing Mep2 mutants and controls in BY4741 and Σ1278b wild-type and *mep2/mep2Δ* background strains. They were grown in synthetic minimal media without amino acids, containing 0.1% proline as nitrogen source to OD_{595} 0.5 before analysing the samples by flow cytometry. Flow cytometry data (Fig. 35) illustrates that the Rosella biosensor shows a range of fluorescence ratios across the mutants indicating that the intracellular pH across the mutants vary. The variations in the fluorescence ratios across mutants were much more pronounced for the Σ1278b background strains. Irrespective of the pH variations across the Mep2 mutants, they were unable to initiate signals for pseudohyphal growth (as shown earlier in chapter 4). These data thus reveal that Mep2-dependent pH changes do not act as a signal to trigger filamentous growth during nitrogen starvation, contradicting the pH model of ammonium sensing.

a)
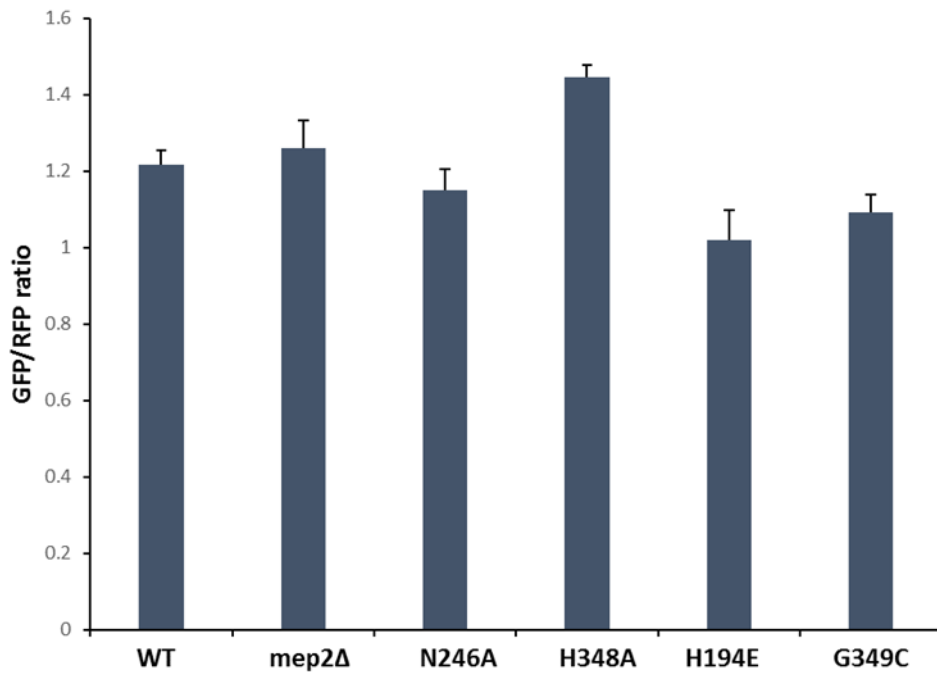
b)
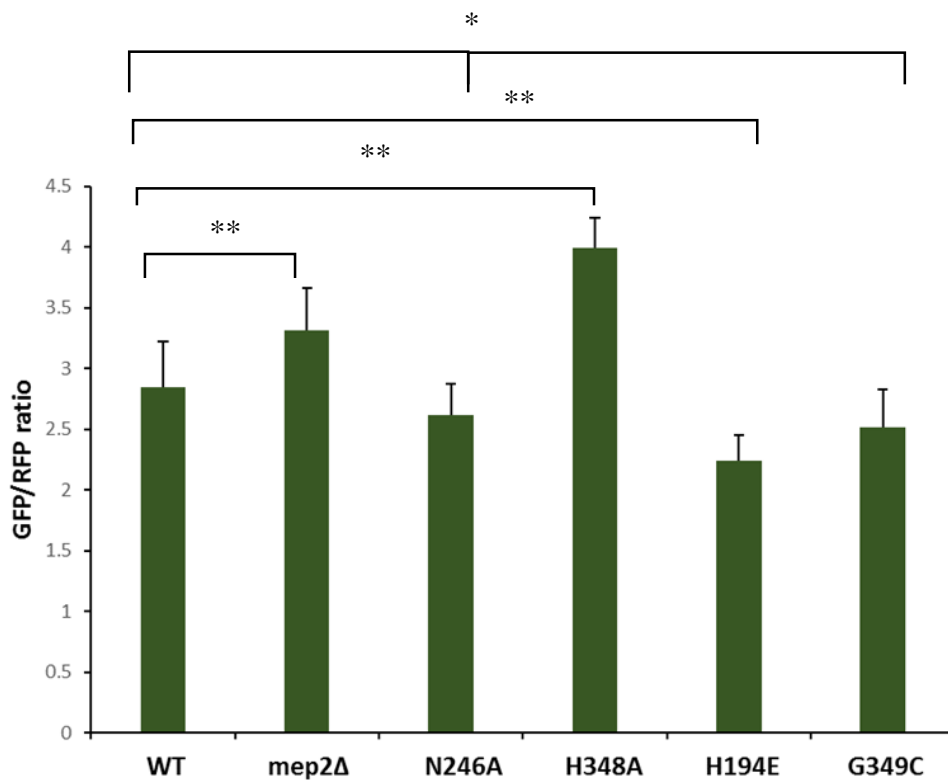
Figure 35: Flow Cytometry analysis of Mep2 mutants and controls co-transformed with the pH biosensor expressed in a) BY4741 background and b) Σ1278b background strains grown in low nitrogen 0.1% proline media. Yeast cells were grown to mid-log phase and harvested for Flow Cytometry analysis. Error bars were calculated from standard deviations for triplicate repeats of each strain and the results were statistically examined using Student's t-test. Symbols *, ** denotes statistical differences at the p values of 0.05 and 0.01 respectively.

5.5.1. Absence of Mep2 results in a minor shift towards alkaline pH

Flow cytometry data indicates that Mep2 influences intracellular pH. The absence of the transporter leads to a significant increase in the fluorescence ratio pointing to a shift towards alkaline pH in those strains compared to the wild-type strain. The results are more distinct for the Σ1278b background strain as it shows a significant variation between the fluorescence ratios for the wild-type and *mep2/mep2Δ* strain. Mep2 is activated under nitrogen limitation and deletion of the transporter results in a reduction in the influx of NH_4^+. This would result in an alkaline pH in those cells causing an increase in the fluorescence ratio levels for the *mep2/mep2Δ* strain. Thus, Mep2 appears to cause acidification of the cytosol when grown under nitrogen limiting conditions.

5.5.2. Mutations to the conserved deprotonation S2 site residues in the pore results in an acidic pH shift

The non-sensing mutants Mep2^{N246A} and Mep2^{H194E} are part of the S2/deprotonation site in the Mep2 conducting pore. Mep2^{H194E} mutant is also part of the proton relay pathway. These residues are highly conserved and are essential for signalling in Mep2. Mutations to these conserved residues leads to a significant drop in the fluorescence ratios of the pH biosensor compared to the wild-type strain under low ammonium conditions pointing towards a shift towards acidic pH. This suggests that there is ample increase in the influx of NH_4^+ into the cells leading to higher rates of substrate import and growth rates than the wild-type strain as evident from the previous growth data. The hyperactive Mep2^{G349C} mutant displayed similar behaviour and a significant drop in the fluorescence ratio resulting in a shift towards acidic pH supporting the proposition.

5.5.3. The conserved reprotonation S4 site mutation reports an alkaline pH shift

The non-signalling Mep2^{H348A} mutant is part of the proton relay and S4/reprotonation site in the Mep2 conducting pore and is a highly conserved residue essential for sensing. Mutation to this conserved residue has been found to have a significant increase in the fluorescence ratio of the pH plasmid under nitrogen limitation. Evidence from this analysis suggests that mutation to this conserved residue leads to a significant increase in intracellular pH compared to the wild-

type strain. This data proposes that a reduction in the NH_4^+ influx into the cells would result in a rise in intracellular pH resulting in an alkaline environment in those cells.

5.6. Discussion

Amongst the two models proposed to explain the sensing and signalling functions of Mep2, the first model illustrates Mep2 transport and signalling which relies on the pH gradient across the plasma membrane enabled by an inwardly directed proton gradient. During ammonium import, deprotonation of ammonium at the entrance to the pore would result in ammonia gas being transported into the cell which would then be reprotonated inside the cell. It is uncertain whether the free proton makes its way out into the periplasm or through the pore into the cytoplasm. Alterations in the net import of protons subsequent to uptake of ammonium could have an impact on the internal pH. Thus signalling could be an indirect consequence of ammonium ion import resulting in localised pH changes within the cytosol (Boeckstaens *et al*, 2008).

In order to test the pH model of ammonium sensing in ScMep2, changes in intracellular pH were examined using a dual fluorescent biosensor. The ability of this biosensor to report changes in intracellular pH in response to changes in the growth media was tested by growing the stains carrying the fluorescent biosensor in synthetic rich media under pH ranges 4 to 7. Results from the Flow Cytometry (FC) analysis (Fig. 33) to test the reportability of the biosensor shows that it responds to variations in intracellular pH and could be reliably used to report pH changes brought about by pH differences in the growth media. The next step was to test whether cytosolic pH changes were observed using the biosensor under nitrogen limitation. In order to test this, wild type strains carrying the pH biosensor were grown in synthetic rich media and low nitrogen media and compared for relative fluorescence ratios. FC analysis data (Fig 34) reveals that the fluorescence ratios for the strains grown in low nitrogen media were significantly lower compared to that of synthetic rich media indicating an acidic cytosolic pH in those strains grown in proline. This is in agreement with the notion that the cytosolic pH of cells grown in low nitrogen media is more acidic than that of the cells grown in ammonium replete synthetic media. These pH changes observed using the biosensor might be Mep dependent. Mep proteins are not activated when grown in synthetic rich media. Activation of Mep proteins occur under nitrogen limiting conditions to transport ammonium into the cell. Import of NH_4^+ would result in an influx of H^+ ions into the cell lowering the intracellular pH making it acidic. Since the optical properties of the biosensor were confirmed, the reported pH ranges were reliable and that cytosolic pH changes were observed under nitrogen limiting

conditions using the biosensor, the next step was to measure the changes in intracellular pH changes during nitrogen limiting conditions using the previously identified Mep2 separation of function mutants.

Non-signalling Mep2 mutant strains and controls carrying the fluorescent biosensor plasmid were grown in low nitrogen media. Data from FC analysis (Fig. 35) illustrated significant variations in the fluorescence ratios between the wild-type and *mep2/mep2Δ* strain where the mutants strain showed higher fluorescence intensity ratios compared to wild-type. In other words, a Mep2-dependent acidification of the cytosol was observed when cells were grown under nitrogen limiting conditions. These results make perfect sense as Mep2 is active in the wild-type strain during low nitrogen conditions bringing in H^+ ions, lowering the intracellular pH making the cytosol acidic. However, in the *mep2/mep2Δ* strain, absence of Mep2 would lead to an increase in the intracellular pH values resulting in a slightly more alkaline pH in the cytosol compared to the wild-type strain. The fluorescence ratios for the separation of function mutants Mep2[N246A], Mep2[H194E] and Mep2[H348A] were highly variable. Fluorescence intensity ratios for Mep2[N246A] and Mep2[H194E] mutants were significantly lower than that of the wild-type strain indicating an acidic pH range in those mutants. N246 and H194 residues are part of the substrate deprotonation site in the Mep2 conducting pore. Mutations to these conserved residues would cause a disruption in the substrate deprotonation during ammonium transport which could possibly result in the proton following an incorrect path hindering the relay of the proton. Another possibility would be that the mutation might result in a specific conformation of the transporter allowing transport of NH_4^+ through the pore bypassing the deprotonation event resulting in an acidic intracellular pH. Comparable evidence is provided by the hyperactive positive control Mep2[G349C] mutant which shows a significant drop in the fluorescence ratios indicating an acidic intracellular pH. G349 residue is located adjacent to the highly conserved second Histidine residue lining the Mep2 conducting pore. Substitution of a Glycine residue with a Cysteine makes it hyperactive (Boeckstaens *et al*, 2007). This mutants being hyperactive might bring in a lot more ammonium compared to the wild-type resulting in a drop in its intracellular pH values making it acidic. Although this mutant shows acidic intracellular pH values similar to the two separation of function mutants, it is able to undergo pseudohyphal growth under nitrogen limitation and is hyper-filamentous.

Fluorescence intensity ratios for Mep2[H348A] mutant was the highest amongst all the mutants tested and was significantly higher than the wild-type strain indicating an alkaline intracellular pH in this mutant. H348 residue is part of the proton relay pathway and substrate re-protonation site within the Mep2 conducting pore. As shown earlier in chapter 4, mutation to this conserved

residue does not affect substrate transport as the rate of transport for this mutant is comparable to wild-type levels. However, this mutant is unable to undergo pseudohyphal growth. The mutation might disrupt the proton relay pathway or alter the molecular events during re-protonation which might result in the H^+ ion following an incorrect route or getting re-directed to the extracellular space resulting in an alkaline intracellular pH. The conformation of the transporter following the mutation might only allow NH_3 to traverse down the pore due to the absence of the re-protonation event. Even though the separation function mutants displayed a wide range of fluorescent intensity ratios pointing to acidic and alkaline pH shifts, none of those mutants were able to rescue pseudohyphal growth defect when grown under nitrogen limiting conditions. Thus, results from the FC data analysis demonstrate that ammonium sensing functions of Mep2 is independent of intracellular pH changes. In spite of the fact that the fluorescent intensity ratios of the hyperactive mutant were similar to that of the substrate deprotonation site mutants, the difference in their ability to initiate pseudohyphal growth highlights the fact that Mep2 dependent pH changes are not responsible for ammonium sensing and signalling in *S. cerevisiae.*

Boeckstaens *et al* (2008) determined the optimum pH for transport for *S. cerevisiae* ammonium transporters Mep1, Mep2 and Mep3 by measuring the uptake of radiolabelled ammonium analogue at pH ranges from 2.4 to 7.3. Mep1 and Mep3 showed optimum pH for transport at 6 and Mep2 showed optimum transport at pH 4. The optimal pH for transport for plant AtAmt1 was observed at 7 (Ninnemann *et al*, 1994) and that for *E coli* AmtB at 4.

Substitution of the first conserved Histidine residue in the Mep2 conducting pore to a Glutamate resulted in a shift in the optimum pH for transport from 4 to 6 consequentially leading to ScMep2^{H194E} mutant behaving like ScMep1 (Boeckstaens *et al*, 2008). However, Mep2 activity dropped sharply when the extracellular pH was raised from 6 to 7 showing that ammonium transport mechanism facilitated by Mep2 is enabled by an inwardly directed proton gradient. H194E substitution in Mep2 has an effect on ammonium transport which favours the proposition that ammonium transport in Mep2 is dependent on a pH gradient via a molecular event involving the conserved H194 residue in the conducting pore. Moreover, this substitution uncouples the transport and signalling functions of Mep2. Although Mep2^{H194E} mutant is able to transport ammonium more efficiently than the wild-type strain, it is unable to undergo pseudohyphal differentiation under nitrogen limitation. Therefore, Boeckstaens *et al* (2008) suggested that the molecular mechanisms governing ammonium transport for Mep1 and Mep2 might be different and this might influence their effect on intracellular pH, in favour of the pH model of ammonium sensing. They argue that the His to Glu substitution might alter the extent

of proton import between Mep2 and Mep1, and therefore could account for the differences in their ability to initiate signalling during pseudohyphal growth. Thus, the mechanism of ammonium transport and their influence on intracellular pH changes might be different across these two transporters. However, our results point out that this is not the case as all the non-sensing Mep2 mutants except for Mep2^{H348A} resulted in the acidification of the cytosol disproving the pH model of Mep2 function.

Rutherford *et al* (2008) demonstrated that the ability to transport substrate through the transporter is essential but not enough to induce signalling. Induction of pseudohyphal growth requires additional functions as revealed by the inability of the ScMep2^{H348A} mutant to induce signalling. H348 is the second conserved Histidine residue lining the Mep2 conducting pore. Substitution of the second conserved twin Histidine residue to Alanine resulted in an increased ability to transport ammonium but unable to undergo pseudohyphal growth under nitrogen limitation. This mutation uncouples the transport and signalling functions of ScMep2 suggesting that translocation of ammonium through the conducting pore of the transporter is essential to induce filamentous growth. Mutation of this conserved Histidine residue might block the proton relay pathway following deprotonation of the substrate in the pore during ammonium import resulting in a loss in the sensing function in Mep2.

The results so far from this study support electrogenic mode of substrate transport for Mep2 ammonium transporters. Import of protons alongside substrate results in the acidification of the cytosol during substrate transport. Similar mode of electrogenic substrate transport were observed in ammonium transporters across *E. coli* AmtB (Wang et al, 2012), *A. fulgidus* AfAmt-1 (Wacker *et al*, 2014) and *A. thaliana* AtAmt1 (Rawat *et al*, 1999). Human RhCG protein however sustains electroneutral substrate transport (Baday *et al*, 2015) owing to alterations in their structure compared to these plant and fungal ammonium transporters.

Microorganisms can sense and respond to a wide range of environmental factors enabling them to adapt to changes and if needed to initiate survival strategies. Changes in cellular pH is one of the major factors microbes respond to. Maintenance of pH homeostasis is vital for all organisms and it has been shown to be a critical virulence factor in several pathogens (Merrell & Camilli, 2002). Fungi tend to adapt to neutral-to-alkaline pH as this pH range is found to promote a dimorphic switch in *Candida albicans* from a yeast like form to a filamentous hyphal form. This morphological shift is vital for infection in pathogenic fungi and, non-filamentous *C. albicans* strains were avirulent (Lo *et al*, 1997; Saville *et al*, 2003). Yeast prefers an acidic extracellular pH as the uptake of nutrients is governed by the proton gradient over the

membrane. *S. cerevisiae* is tolerant to acidic growth environments and are able to grow within pH ranges as low as 2.5. Alterations in intracellular pH was found be linked to variations in the extracellular pH, as pH changes in the growth medium would influence the plasma membrane proton gradient which in turn would affect ATPase activity (Carmelo *et al*, 1996). Thus intracellular pH changes were dependent on changes to external proton concentration. The changes in intracellular pH as a result of variations in the availability of nutrients is thought to have significant signalling functions and cytosolic pH itself could function as a signal or messenger (Srivastava *et al*, 2007).

Cytosolic pH was found to act as a second messenger regulated by levels of glucose metabolism facilitating the activation of the PKA pathway in yeast. V-ATPase functioned as the sensor of cytosolic pH and is essential for the activation of the PKA pathway in response to glucose. Activation of the PKA pathway is thus pH dependent as an alkaline pH would lead to V-ATPase assembly and activation of the PKA pathway (Dechant *et al*, 2010). The activity of the plasma membrane ATP-ases which contribute towards pH homeostasis in yeast are greatly associated with ATP levels. Thus, signalling of glucose in yeast is dependent on the maintenance of a proton gradient across the membrane involving the activity of an ATP-sensitive proton pump. An increase in ATP concentrations was shown to facilitate glucose signalling in pancreatic β-cells. The regulation of membrane potential was achieved via closure of the ATP-dependent K^+ channels in the plasma membrane for glucose sensing (MacDonald *et al*, 2005).

Dechant *et al* (2014) showed that cytosolic pH could act as a cellular signal accountable for rate of growth, cell size and proliferation and is dependent on the quality of the carbon source in the growth media. They illustrated that cytosolic pH is capable of regulating Ras activity and activation of the TORC1 pathway in response to glucose availability. The ability of yeast cells to metabolise various carbon sources regulates the changes in cytosolic pH in response to various carbon sources. The study thus provides molecular evidence for the mechanism by which cytosolic pH connects available carbon sources to signalling pathways governing cell growth and proliferation.

The model of ammonium transport in TaAMT1, the Amt/Rh homologue from wheat exhibits pH dependence during ammonium transport. During substrate transport, after deprotonation of the incoming NH_4^+, acidic extracellular pH would favour the transport of the proton through the pore and would increase the overall rate of substrate transport. On the contrary, high extracellular alkaline pH would facilitate the return of the proton to the periplasmic space

hindering NH_4^+ transport through the pore. Ammonium ion transport through TaAMT1 is thus stimulated by acidic pH (Sogaard *et al*, 2009).

Orij *et al* (2009) demonstrated that organelle-specific pH is differentially regulated by carbon source, and the pH of cytosol and mitochondria varies in response to nutrient availability. They show that glucose-starved cells exhibited a drop in their intracellular pH values displaying rapid acidification eliminating organelle-specific pH variations. Upon re-supplementation of glucose, the cells displayed immediate alkalinization thereby raising their intracellular pH values resuming growth. Acidification of glucose-starved cells might be due to the entry of protons into the cytosol as a result of nutrient uptake. The pH regulators V-ATPase would pump protons into the vacuole or plasma membrane ATPase Pma1 would pump protons out into the growth medium at the cost of ATP to counteract the acidification and to maintain cytosolic pH. Plasma membrane ATPases couple cation transport to ATP hydrolysis at a ratio of 1 H^+ per ATP hydrolysed (Morsomme *et al*, 2000). Carbon starvation would lead to a shortage of energy leading to inactivation of Pma1 resulting in the acidification of the cytosol. Re-addition of glucose would result in the activation of the glycolysis pathway causing an increase in ATP levels resulting in a rise in the cytosolic pH.

A pH sensor would be able to sense changes in the intracellular or extracellular pH and convey those changes as a signal. Changes in external pH causes transcriptional changes in *S. cerevisiae* and these transcriptional responses have been studied. Rim101 pathway is required for responses to extracellular alkaline pH in yeast. Rim101 is a zinc-finger protein which gets activated by a C-terminal proteolytic cleavage simulated by extracellular alkaline pH. The C-terminal proteolytic cleavage of Rim101 removing an 8kd peptide from its C-terminal tail would make it active. Rim101 is active at neutral to alkaline pH (Lamb *et al*, 2001; Lamb & Mitchell, 2003). It has been suggested that alkalization of the extracellular medium resulting in a de-polarization of the membrane results in the activation of the signal transduction pathways in a Rim dependent manner. Rim101 and its processing pathways are essential for alkaline pH induced responses and the pathway is conserved (Serra-Cardona *et al*, 2015). Activation of Rim101 is vital for maintenance of internal pH homeostasis. Rim101 pathway is required for virulence in *C. albicans in vivo* (Mira *et al*, 2009). Since Rim101 could act as a pH sensor one could hypothesize that activation of Rim101 could be Mep2 dependent. Ammonium import during nitrogen starvation would create external alkalization of the cell which could in turn activate the Rim101 pathway. This pH responsive transcription factor is essential for the induction of pseudohyphal growth in yeast (Li & Mitchell, 1997). The role of Rim101 in the initiation of filamentous growth supports the idea that its activation could be governed by the

transport and signalling functions of Mep2. This could be tested by studying a shift in the size of Rim101 on a Western blot to see whether the transcription factor is activated in response to pH changes during low ammonia growth and whether the activation is Mep2 dependent. The pH model of Mep2 function fails to validate the role of Mep2 dependent pH in ammonium sensing. The next step would be to test the second model, which is the transceptor of Mep2 function.

6. Investigation of potential interaction partners of Mep2 to test the Transceptor model of Mep2 function

6.1. Introduction

During nitrogen limitation, diploid strains of *S. cerevisiae* undergo a dimorphic switch from a normal yeast form to a filamentous pseudohyphal form characterized by formation of filaments. This is thought to act as a scavenging mechanism for this non-motile species to search for nutrients under conditions of nutrient limitation. Pseudohyphal growth is characterised by a dramatic change in growth pattern, elongated cell morphology, unipolar budding pattern and an ability to invade growth substrate (Gimenzo *et al*, 1992; Kron *et al*, 1994). Filamentous growth is thus an important adaptive response in which a developmental transition in yeast is regulated by the presence or absence of nitrogen. *S. cerevisiae* does not undergo true hyphal growth, but a pseudohyphal growth instead, where cells are not multinucleate, but remain attached to each other producing a chain of cells. This dimorphic transition is an important adaptive response as it is vital for virulence in many fungal pathogens (Lorenz & Heitman, 1998) and thus demonstrates to be a novel target for antifungal drug design in medicine and agriculture. The dimorphic switch takes place when cells are grown under ammonium limiting conditions or in the presence of a non-preferred source of nitrogen. Catabolism of a non-preferred source of nitrogen leads to the export of ammonium into the extracellular environment, and hence ammonium remains the preferred nutrient that gets sensed (Boeckstaens *et al*, 2007).

Mep2 ammonium permease is essential for the induction of pseudohyphal growth in *S. cerevisiae* under nitrogen limiting conditions. Strains lacking Mep2 are able to obtain ammonium and grow at normal rates but are unable to undergo pseudohyphal differentiation. Among the three Mep proteins in *S. cerevisiae,* only Mep2 is essential for the induction of pseudohyphal growth. Mutations of the other two ammonium permeases Mep1 and Mep3 did not lead to any defects in pseudohyphal differentiation. This suggests that Mep2 functions an ammonium sensor mediating the signal transduction pathways to initiate filamentous growth (Lorenz & Heitman, 1998). Overexpression of Mep2 leads to an increase in the rate of pseudohyphal differentiation and even a modest increase in the expression level of the protein can trigger pseudohyphal growth even when grown in nitrogen rich medium.

The molecular mechanisms mediating ammonium sensing is still unclear. Among the two different hypotheses put forward to explain Mep2 function, the second model – the transceptor model (Rutherford *et al*, 2008) proposes that conformational changes of the transporter that gets triggered during ammonium transport enables the permease to interact with downstream signalling partners to initiate pseudohyphal growth. Thus Mep2 combines the functions of an active ammonium transporter and a nutrient sensor or receptor required for the induction of pseudohyphal growth, making it a 'transceptor'.

The two best characterized signalling pathways that play crucial roles in co-ordinating the induction of pseudohyphal growth and invasiveness are Mitogen Activated Protein Kinase (MAPK) cascade (Posas *et al*, 1998; Madhani & Fink, 1998) and cyclic AMP dependent Protein Kinase A (PKA) pathway (Robertson & Fink, 1998; D'souza & Heitman, 2001). *S. cerevisiae* has at least four different MAP Kinase cascades transducing an array of intracellular signals. They include the mating-pheromone pathway, the pseudohyphal growth pathway, the Protein Kinase C (PKC) pathway and the osmoregulatory pathway (Pasos *et al*, 1998). Even though the mating pheromone pathway and the pseudohyphal growth pathway have components in common, the two different pathways have their own unique elements and are activated in response to different external signals. Most of the components involved in these signal transduction pathways have been characterized. The nutrient sensing cAMP pathway functions in parallel to the MAP Kinase pathway to regulate filamentous growth. The small G-protein Ras2 plays a double role in the regulation of both MAPK and PKA pathways (Mosch *et al*, 1996; Roberts *et al*, 1997). Earlier studies have shown that both MAP Kinase and cAMP pathways which work in parallel to regulate pseudohyphal growth converge on the promoter of FLO11, a cell surface protein required for cell-cell adhesion (Rupp *et al*, 1999).

The sensing role of Mep2 in the signal transduction pathway initiating pseudohyphal growth still remains unclear and the precise mechanism by which the transporter interacts with any or either of the two signalling pathways during signalling needs to be elucidated. This could be through physical interaction with a downstream signalling partner. This chapter aims to identify potential interaction partners of Mep2 and to elucidate the sensing mechanism of Mep2 to initiate downstream signalling during pseudohyphal growth.

6.2. Global screen of protein-protein interactions using Protein fragment Complementation Assay (PCA) to identify potential interaction partners of Mep2

In order to identify potential interaction partners for Mep2, a Protein fragment Complementation Assay (PCA) was carried out to analyse in vivo protein interactions based on the enzyme dihydrofolate reductase (DHFR). Two potentially interacting proteins of interest are fused to complementary fragments of DHFR. If physical interaction of the proteins take place, then the complementary halves of the enzyme come together re-constituting enzyme activity detectable by the survival on selective methotrexate media (Remy *et al*, 2007). The yeast protein interactome was purchased from Open Biosystems.

(http://dharmacon.gelifesciences.com/cdnas-and-orfs/non-mammalian-cdnas-and-orfs/yeast/yeast-protein-interactome-collection/).

PCA identified a list of potential interaction partners for Mep2. From the list, we were only interested in only those proteins that had roles in the induction of pseudohyphal growth. Npr1 kinase, a serine/threonine protein kinase which fine tunes the activity of Mep2 via phosphorylation occupied position 196 in the list of Mep2 interacting proteins. Mep2 interaction with Npr1 kinase would be transient, hence this was set as a cut off point for Mep2 interacting proteins in the list to be analysed further. The proteins above the cut-off limit is included at the end as appendix and ordered according to the strength of interaction. Generic Gene Ontology (GO) Term Mapper was used to annotate the interaction partners based on their biological process i.e. their role in the induction of pseudohyphal growth.

The interaction partners for Mep2 involved in pseudohyphal growth are listed in the diagram below (Fig. 36). Among the interaction partners listed for Mep2, Bmh1, Bmh2 and Ste20 are part of the MAP Kinase pathway and Gpa2 is part of the PKA pathway inducing pseudohyphal growth. Whi3 regulates genes involved in cell cycle and Mep2 monomers have been shown to interact to form a trimeric complex (Rutherford *et al*, 2008). Moreover, Bmh1 and Bmh2 are known to associate with Ste20 in vivo which explains why Ste20 came up in the screen within the top hundred interaction partners of Mep2. Based on these results we hypothesise that Mep2 regulates the MAP Kinase cascade through physical interaction with Bmh1/2 to initiate pseudohyphal growth. In order to confirm this hypothesis, the next step would be to undertake immunoprecipitation studies to test for interactions between Mep2 and Bmh1/2, Gpa2.
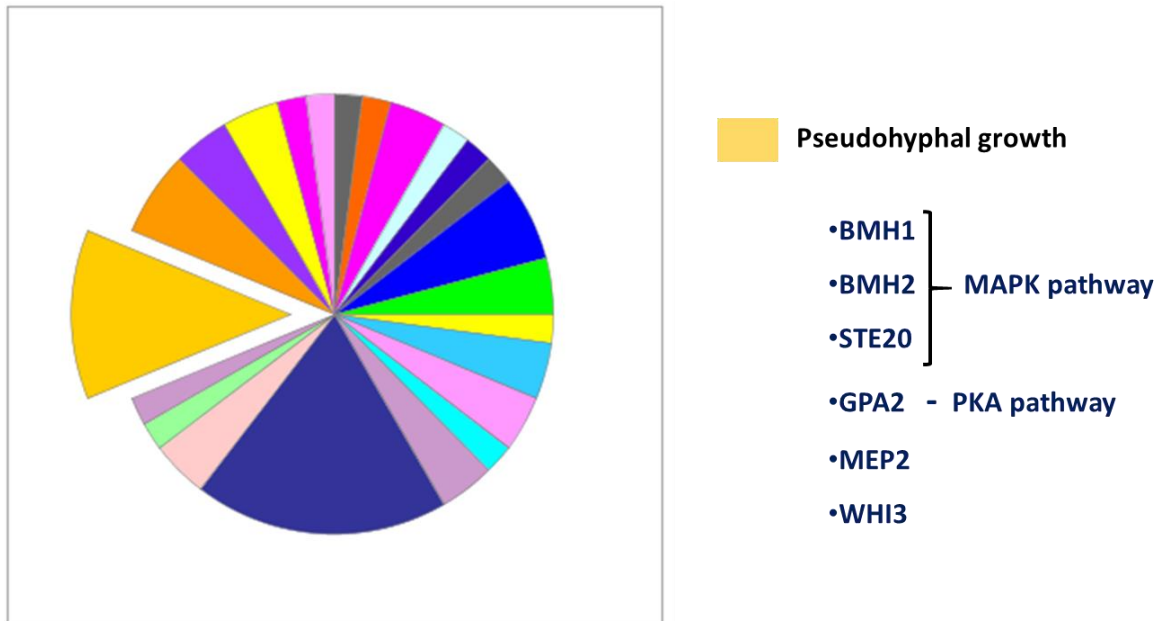
Figure 36: Pie chart representation of Mep2 interaction partners from PCA using Generic Gene Ontology (GO) Term Mapper for biological processes highlighting the genes involved in pseudohyphal growth in yellow. This forms 3.06% of GO term usage in the gene list (6 of 196 genes), and the highest proportion formed by transmembrane transporters (dark blue) with 10.2%. Figure adapted from http://pantherdb.org/

6.3. Immunoprecipitation studies to test for interactions between Mep2 and Gpa2, Bmh1

In order to test for physical interactions between Mep2 and Gpa2/Bmh1, Mep2 was FLAG tagged and Gpa2 and Bmh1 were Myc tagged. Mep2 plasmid carrying the FLAG tag was transformed into a *mep2/mep2Δ* background strain carrying the genomic Gpa2 or Bmh1-13Myc tag. The cells were grown in 0.1% proline media and co-immunoprecipitation followed by western immunoblotting was carried out. Results from the co-IP studies for a potential Mep2-Gpa2 interaction (Fig. 37) shows that upon immunoprecipitation of Mep2-FLAG, Gpa2-Myc gets co-immunoprecipitated in a non-specific manner. The control sample without Mep2-FLAG containing an empty vector showed non-specific bands indicating co-immunoprecipitation of Gpa2-Myc in the control. Co-IPs were repeated altering the protocol but the results remained the same. Hence we were unable to prove an interaction between Mep2 and Gpa2 through the course of this study.

Results from the co-IP studies for a potential interaction between Mep2 and Bmh1 (Fig. 38) shows that that upon immunoprecipitation of Mep2-FLAG, Bmh1-Myc does not get co-immunoprecipitated in the sample lanes.

Alterations were made to the Co-IP protocol with the addition of a cross-linker to the cell lysates before immunoprecipitation was carried out, and also by the inclusion of Anti-FLAG beads for immunoprecipitation. Furthermore, immunoprecipitation of Bmh1-13Myc was also carried out to ensure that the interaction was tested both ways. Results from the co-IP studies reveal the same pattern (Fig. 39) that upon immunoprecipitation of Mep2-FLAG in the presence of cross-linkers, Bmh1-Myc does not get co-immunoprecipitated in the sample lanes. Similar results were obtained upon immunoprecipitation of Bmh1-13Myc where Mep2-FLAG does not get co-immunoprecipitated in the sample lanes even in the presence of a cross-linker.

a)
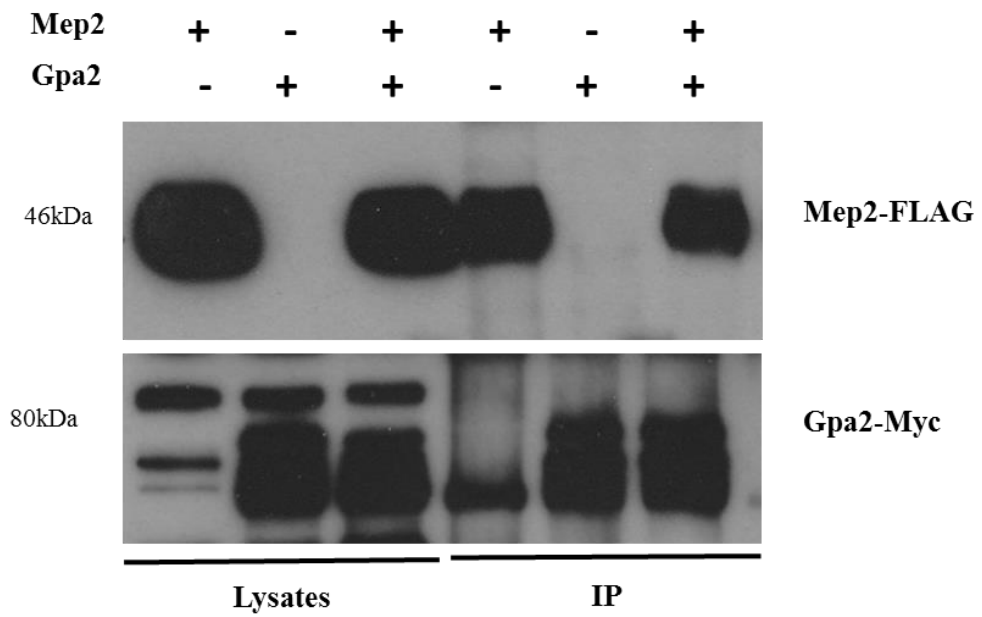
b)
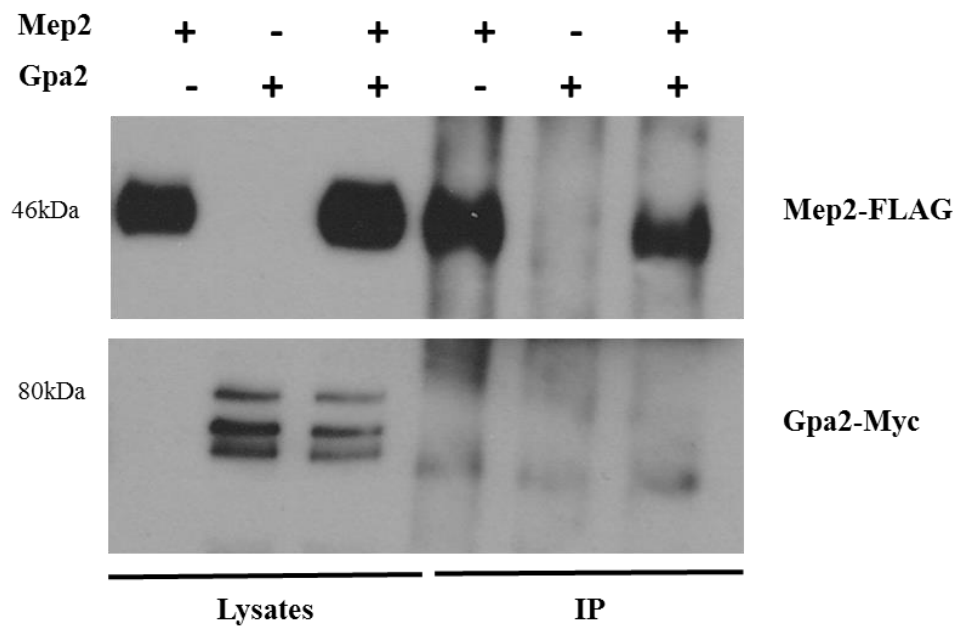
Figure 37: a) & b) Immunoprecipitation of Mep2-FLAG and detection of Gpa2-13Myc from cell lysates and immunoprecipitates using anti-FLAG and anti-Myc antibodies. Positive and negative controls alongside samples were grown in 0.1% proline media. Gpa2-13Myc was non-specifically immunoprecipitated from cells expressing a Mep2-FLAG plasmid.
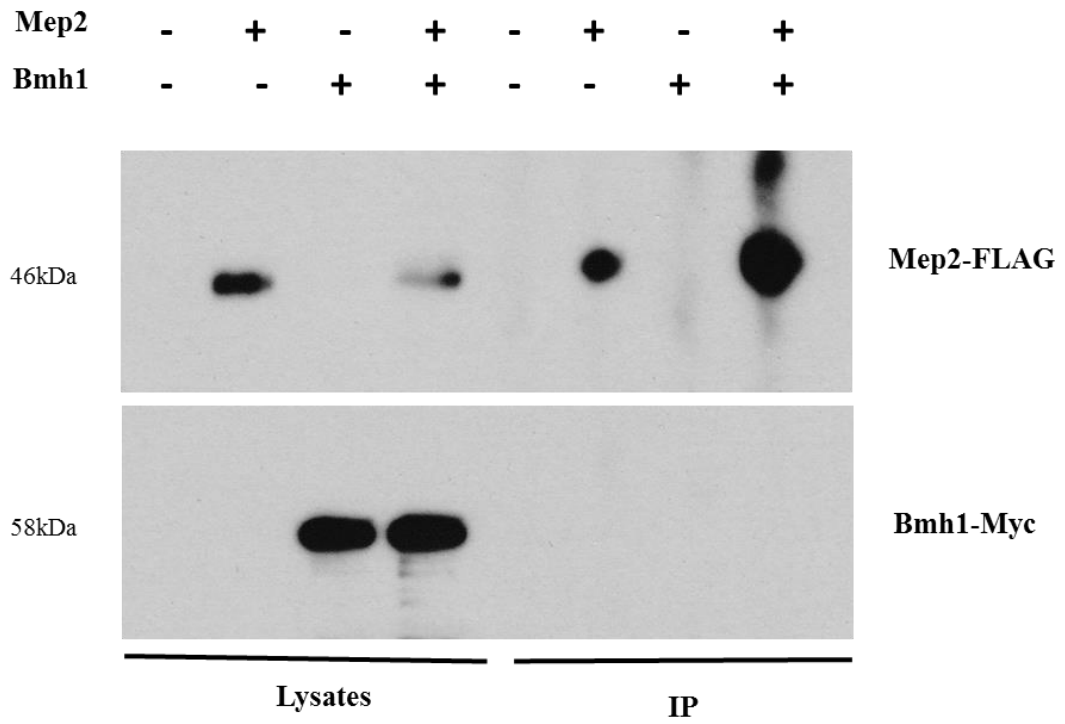
Figure 38: Immunoprecipitation of Mep2-FLAG and detection of Bmh1-13Myc from cell lysates and immunoprecipitates using anti-FLAG and anti-Myc antibodies. Positive and negative controls alongside samples were grown in 0.1% proline media. Bmh1-13Myc was not immunoprecipitated from cells expressing a Mep2-FLAG plasmid.
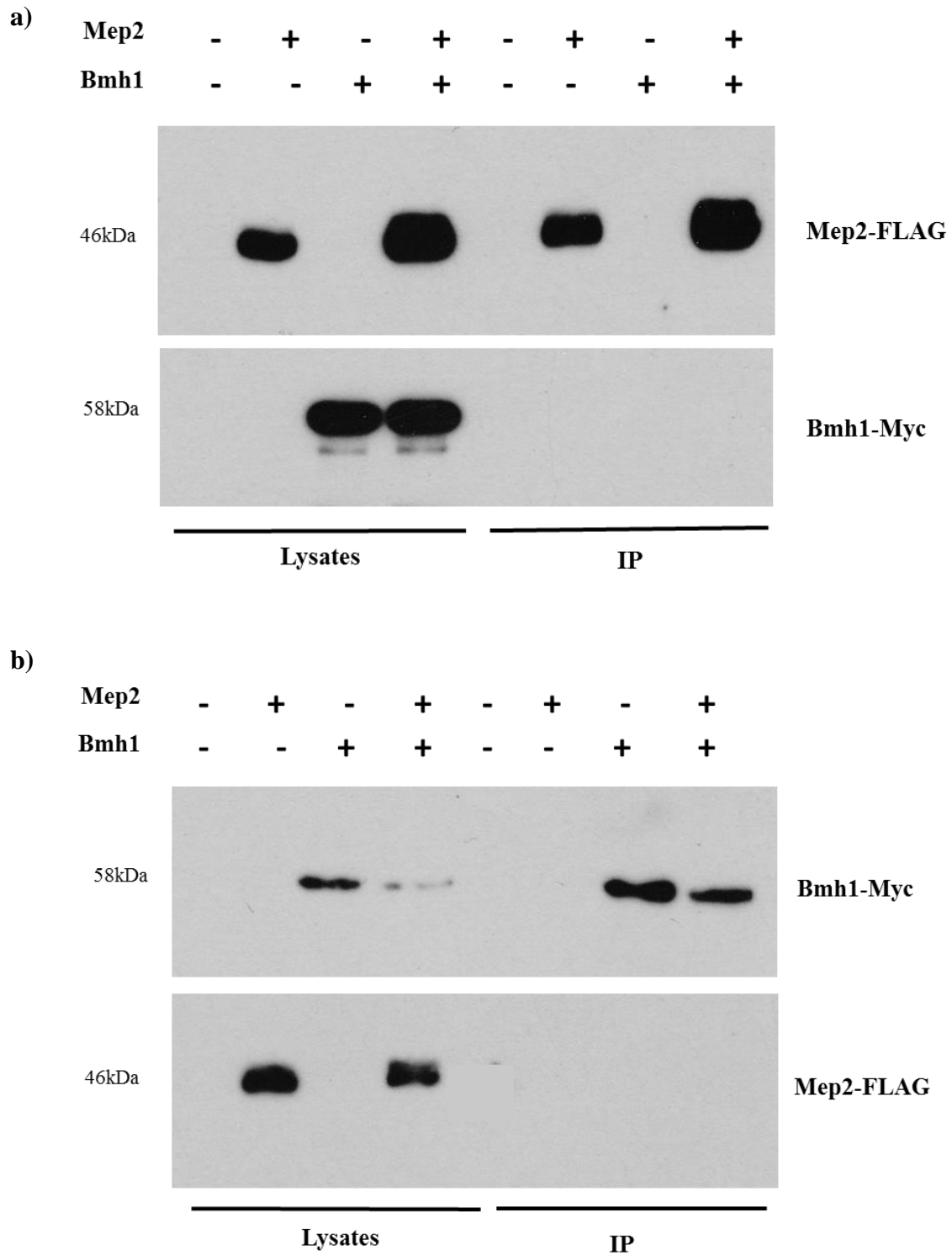
Figure 39: a) Immunoprecipitation of Mep2-FLAG and detection of Bmh1-13Myc or b) immunoprecipitation of Bmh1-13Myc and detection of Mep2-FLAG in the presence of a cross-linker from cell lysates and immunoprecipitates using anti-FLAG and anti-Myc antibodies. Positive and negative controls alongside samples were grown in 0.1% proline media. Neither Bmh1-13Myc nor Mep2-FLAG were not immunoprecipitated in their respective sample lanes in the presence of a cross-linker.

6.3.1. Mep2 interacts with Bmh1 and forms a complex at the plasma membrane

Membrane-enrichment of cell extracts grown in 0.1% proline media was carried out after being cross-linked and immunoblotted to test for interaction between Mep2 and Bmh1. The results from the cross-linking and membrane prep (Fig. 40) shows a Mep2 dependent enrichment of Bmh1 on the membrane compared to the sample where Mep2 is absent. This supports the notion that Mep2 interacts with Bmh1 and forms a complex at the plasma membrane.

The next step was to test for interactions between Bmh1 and signalling deficient Mep2 mutants. Mep2 plasmids carrying the point mutations and a FLAG tag were transformed into a *mep2/mep2Δ* background strain carrying the genomic Bmh1-13Myc tag. Mep2 separation of function mutants Mep2^{N246A}, Mep2^{H194E} and Mep2^{H348A} were also included in the interaction studies to test for loss of interaction in these mutants. The cells were grown in 0.1% proline media and cell lysates were prepared alongside membrane-enriched extracts for comparison between non cross-linked lysates and cross-linked membrane-enriched extracts. Results from the cross-linking and membrane prep of Mep2 mutants (Fig. 41) show that the levels of Bmh1 in the cell lysates were similar across all the samples. However, Mep2 dependent enrichment of Bmh1 was lost in the non-signalling Mep2 mutants and their Bmh1 levels were similar to the lane where Mep2 was absent.
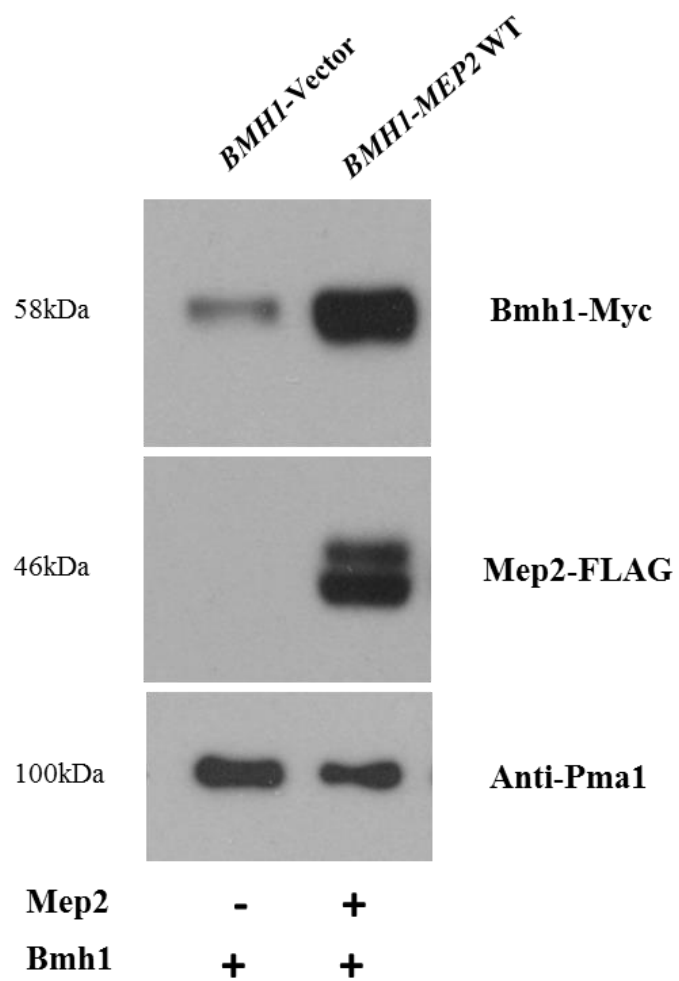
Figure 40: Cross-linking and membrane preparation of cell lysates grown in 0.1% proline media. The FLAG and Myc epitopes were detected by western immunoblotting. Levels of Pma1 was used as loading control.

a)

	BMH1-Vector	BMH1-MEP2 WT	BMH1-MEP2^{N246A}	BMH1-MEP2^{H348A}	
58kDa					**Bmh1-Myc**
46kDa					**Mep2-FLAG**
100kDa					**Pma1**
Mep2	−	+	+	+	
Bmh1	+	+	+	+	
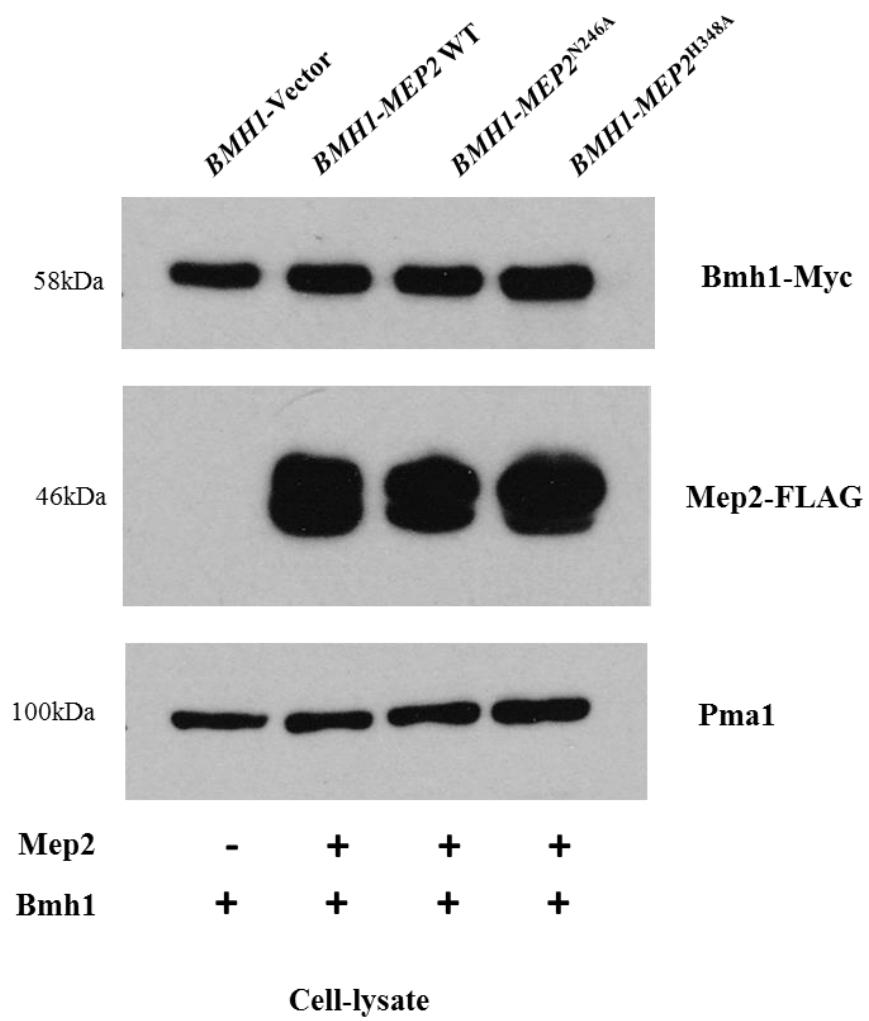
Cell-lysate

b)
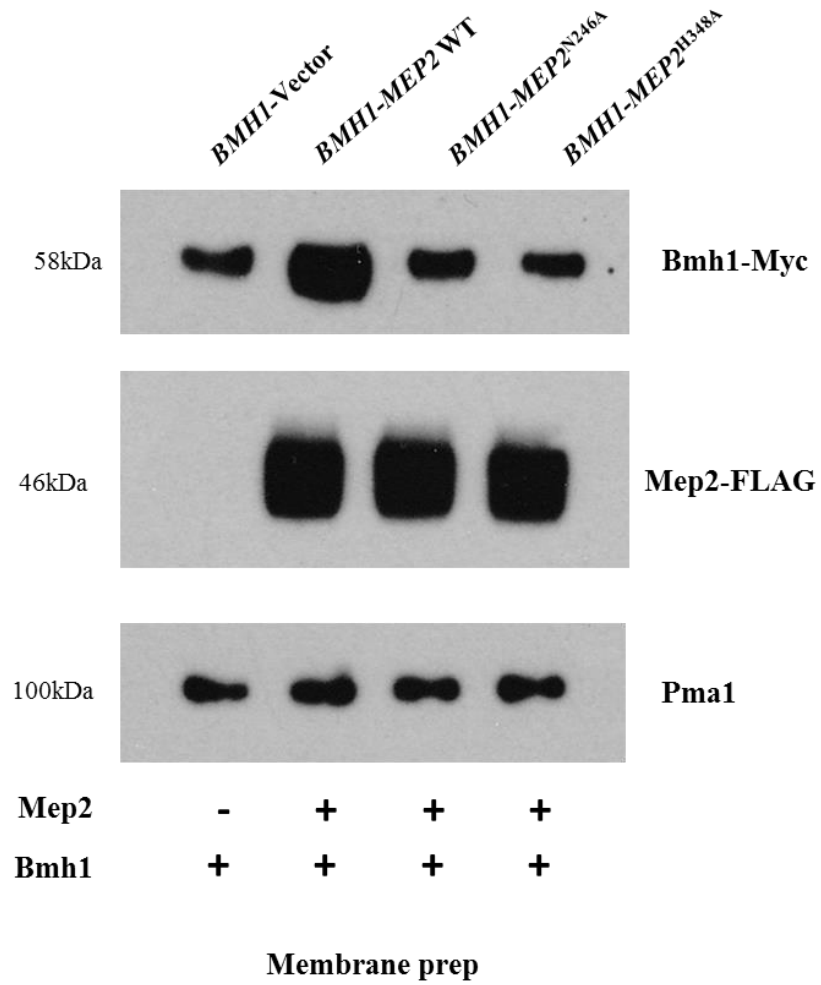
Figure 41: Preparation of samples of non-signalling Mep2 mutants and controls for comparison between a) non cross-linked cell lysates and b) cross-linked and membrane enriched extracts grown in 0.1% proline media. The FLAG and Myc epitopes were detected by western immunoblotting. Levels of Pma1 was used as loading control.

In order to test whether a hyperactive Mep2 mutant would show Mep2 dependent enrichment of Bmh1 as seen in the wild-type sample, Mep2^{G349C} mutant was also included in the interaction studies alongside the separation of function mutants. The cells were grown in 0.1% proline media and two sets of samples, one for cell lysates and the other for cross-linked and membrane enriched samples were prepared. The levels of Bmh1 were similar across all of the samples in the cell lysate (Fig. 42a). Results from the crosslinking-membrane prep samples (Fig. 42b) show that Mep2^{G349C} mutant shows a Mep2 dependent enrichment of Bmh1 similar to that of the wild-type sample. The signalling deficient mutants showed a reduction in the Mep2 dependent Bmh1 enrichment at the membrane.

a)
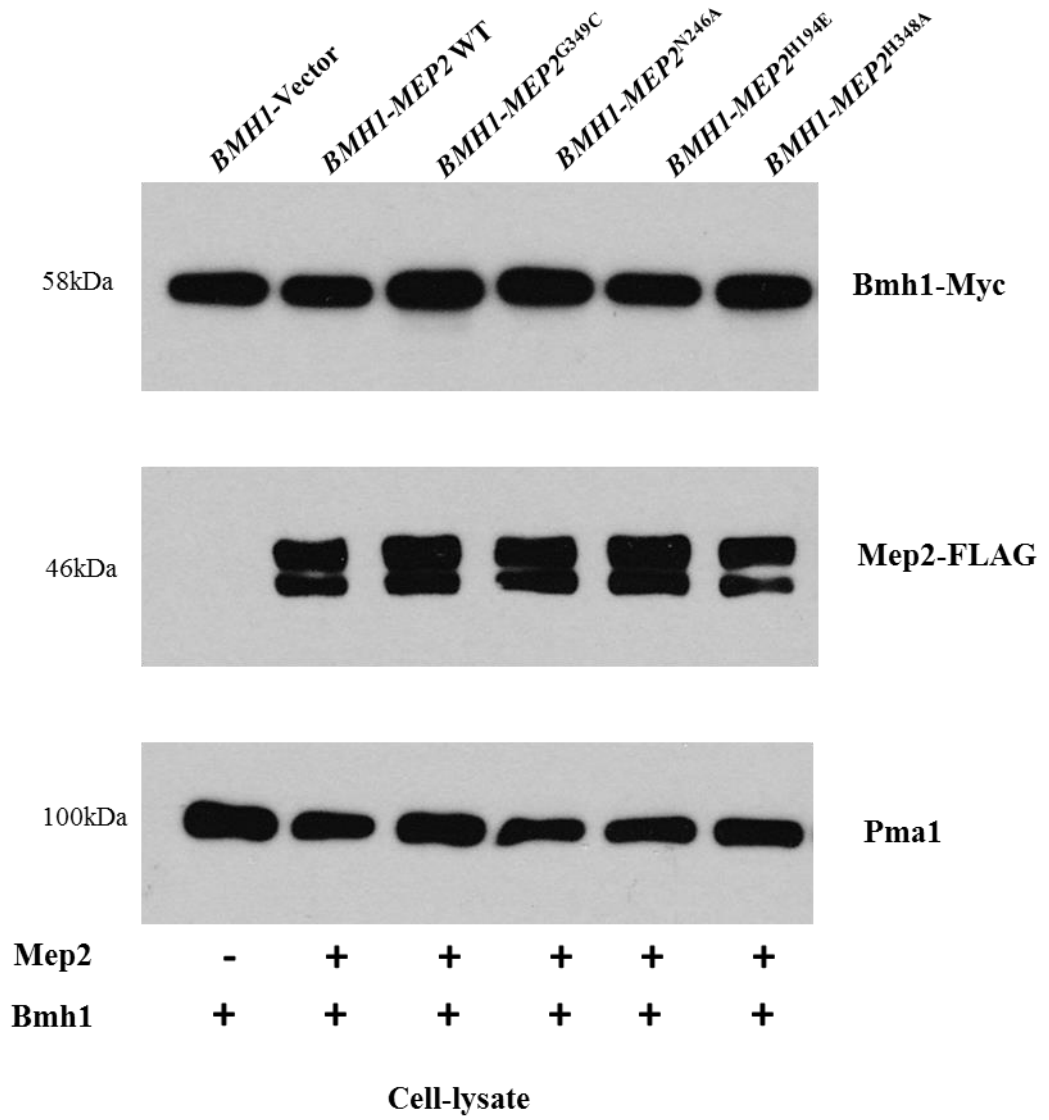
b)
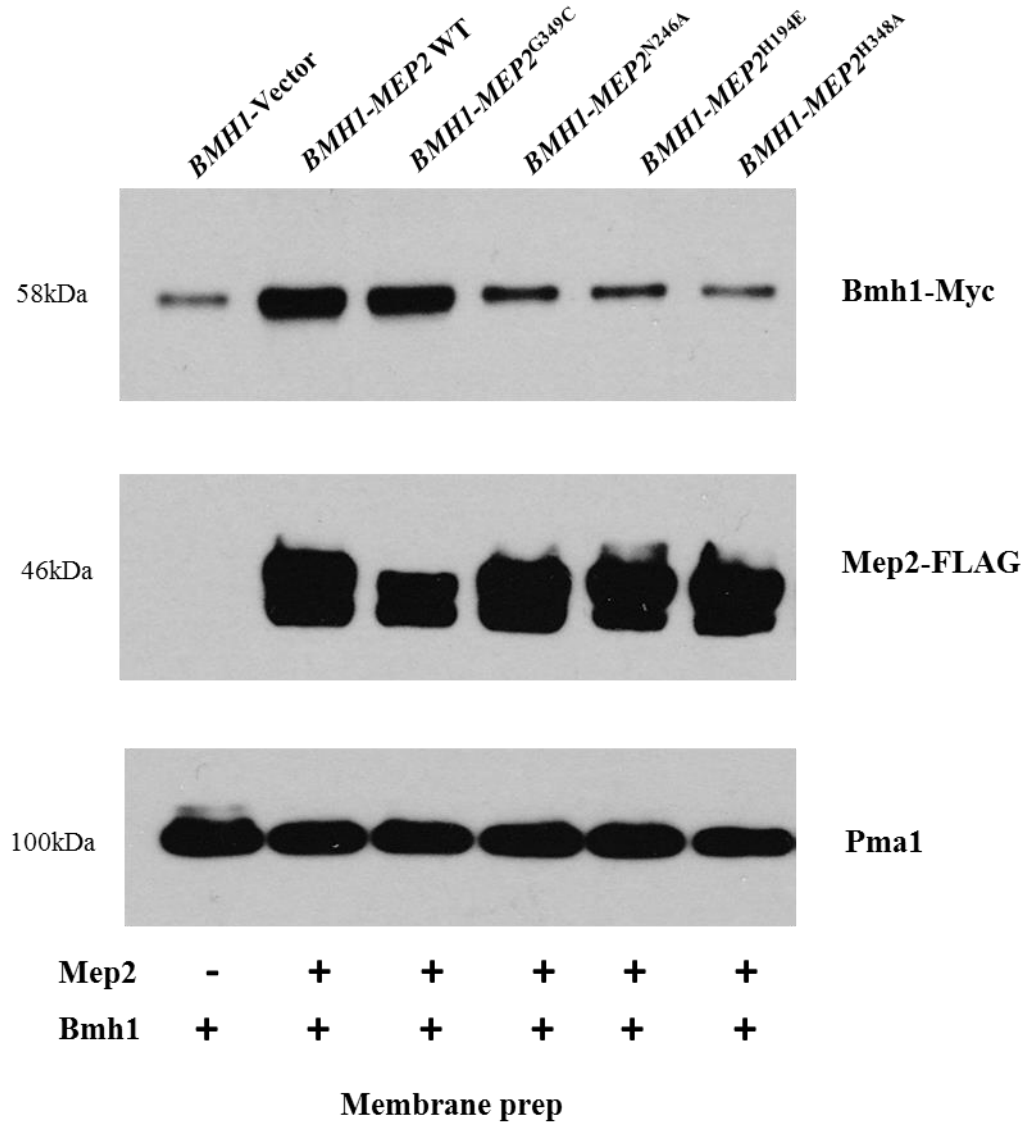
Figure 42: Non-signalling mutants and controls alongside a hyperactive Mep2 mutant for comparison between a) non cross-linked cell lysates and b) cross-linked and membrane enriched extracts grown in 0.1% proline media. The FLAG and Myc epitopes were detected by western immunoblotting. Levels of Pma1 was used as loading control.

6.3.2. Bmh1 binds Mep2 at the Threonine site at T459 as predicted by 14-3-3Pred

Bmh1/2 are 14-3-3 protein homologs, and a web-server 14-3-3Pred which predicts the 14-3-3 binding sites in proteins has predicted that Bmh1 binds Mep2 at the Threonine site at T459 of the C-terminal tail. In order to test this prediction, a loss of function Mep2^{T459A} mutant and a phosphomimmetic Mep2^{T459D} mutant were generated. Mep2 plasmids bearing these mutations were transformed into a *mep2/mep2Δ* background strain carrying the genomic Bmh1-13Myc tag. The cells were grown in 0.1% proline media and cell lysates were prepared alongside cross-linked membrane-enriched extracts to see whether mutation of the T459 residue to T459A would result in a loss in Mep2-Bmh1 interaction. Additionally, to test whether introduction of a negative residue at T459D would rescue the signalling defect caused by the T459A residue. Results from the cross-linking and membrane prep of Mep2 mutants (Fig. 43) show that introduction of Mep2^{T459A} mutation results in a reduction in the Mep2 dependent enrichment of Bmh1 which suggests that mutation of this residue at T459 affects binding of Bmh1 with Mep2. Moreover, introduction of Mep2^{T459D} mutation rescues the loss of interaction between Bmh1 and Mep2 as Mep2^{T459D} mutant shows enrichment of Bmh1 at the membrane. This confirms the hypothesis that the T459 residue is required for Mep2-Bmh1 interaction and Mep2 binds Bmh1 at the Threonine site at T459 of Mep2 C-terminal tail.

a)
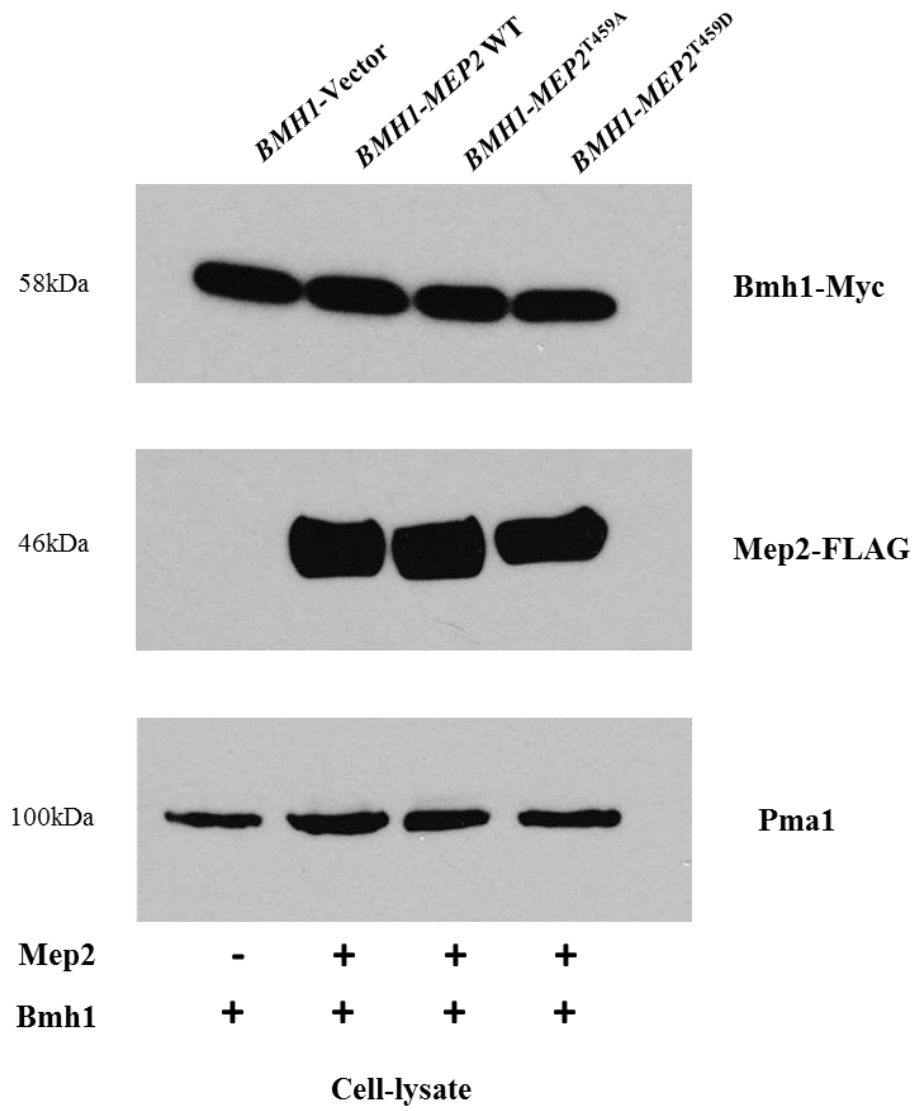
b)
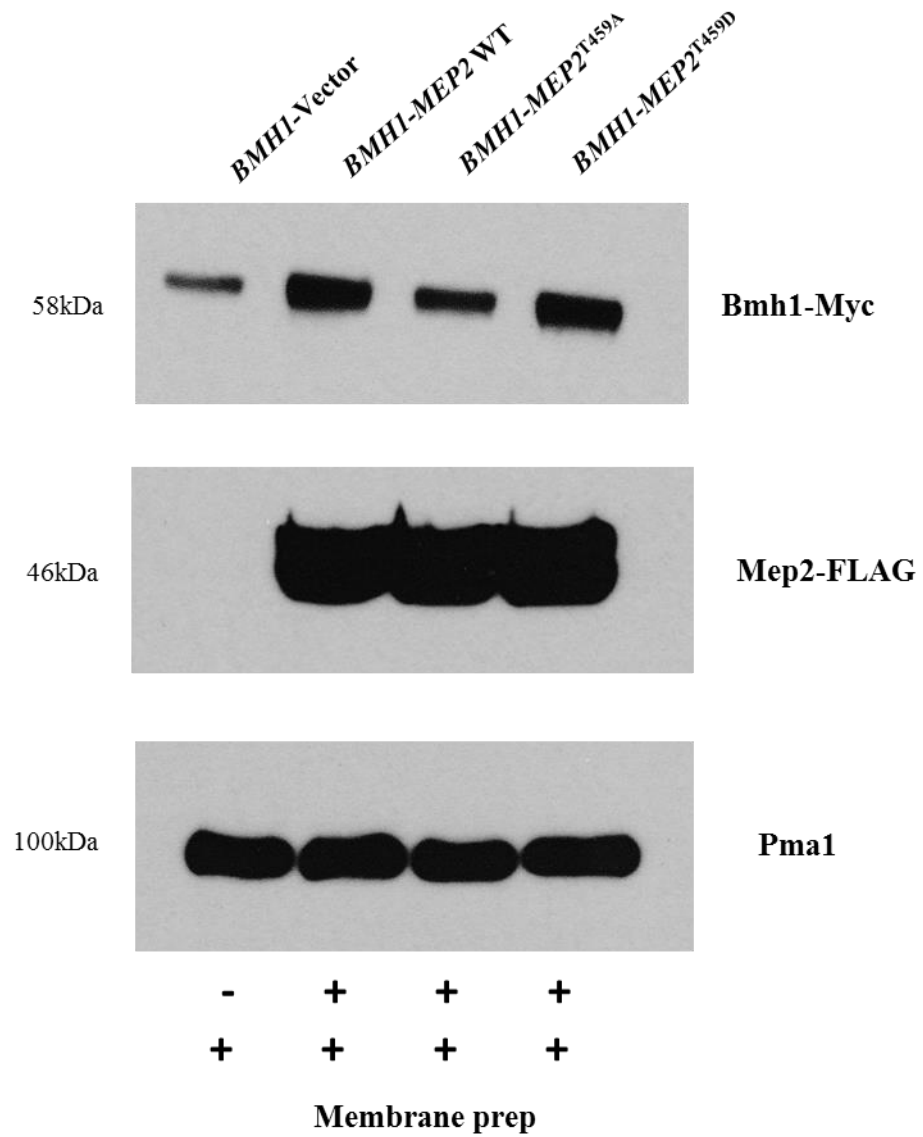
Figure 43: Mep2^{T459A} and Mep2^{T459D} mutants alongside controls for: a) non cross-linked cell lysates and b) cross-linked and membrane enriched extracts grown in 0.1% proline media. The FLAG and Myc epitopes were detected by western immunoblotting. Levels of Pma1 was used as loading control.

6.3.3. Mep2 and Bmh1 interaction levels correlate with the extent of pseudohyphal growth

In order to test whether Mep2^{T459A} and Mep2^{T459D} mutations affect Mep2 signalling, the ability of these mutants to induce pseudohyphal growth when grown under nitrogen limiting conditions were tested. Mep2^{T459A} and Mep2^{T459D} mutants alongside controls were transformed into *mep2/mep2Δ* strain and plated onto solid SLAD medium. The results from the pseudohyphal growth test (Fig. 44) shows that Mep2^{T459A} mutation has an effect on Mep2 signalling as this mutant showed marked reduction in its ability to undergo pseudohyphal growth. Mep2^{T459D} mutation however, was able to rescue the signalling defect imposed by the alanine substitution as this mutant showed pseudohyphal growth similar to wild-type levels. This demonstrates that phosphorylation of the T459 residue is essential for the signalling function of Mep2.

6.3.4. Alterations in Mep2 and Bmh1 interaction does not affect the transport function of Mep2

In order to find out whether alterations to the interactions between Mep2 and Bmh1 would affect the transporter function of Mep2, Mep2^{T459A} and Mep2^{T459D} mutants alongside controls were transformed into *mep123Δ* strain and growth tests were carried out. The strains were serially diluted and spotted on solid agar plates containing glutamate (0.1%) or ammonium sulphate (1mM) as nitrogen source and grown for 3 days at 30°C. Results from the growth assay (Fig. 45) show that Mep2^{T459A} and Mep2^{T459D} mutations does not affect the transporter function of Mep2 as those strains were able to complement the growth defects of *mep123Δ* strains on low ammonium medium indicating that the mutated versions of the protein has retained its transport function.

6.4. Mep2 regulates the MAP Kinase pathway for the induction of pseudohyphal growth

Taken together the results so far have allowed us to propose a model for the sensing function of Mep2. During low ammonium levels, Mep2 initiates filamentous growth by regulating MAP Kinase cascade via physical interaction with Bmh1/2 protein complex (Fig. 46).

a) Vector

b) WT – *MEP2*

c) *MEP2*^{T459A}

d) *MEP2*^{T459D}
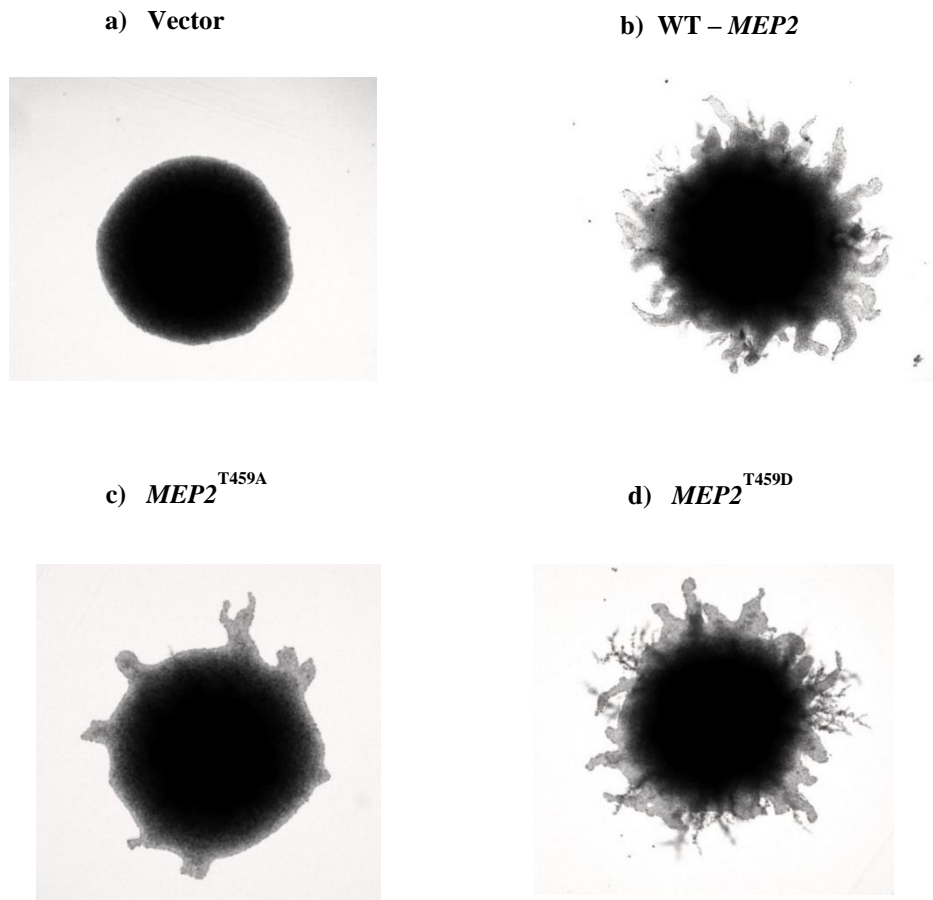
Figure 44: Pseudohyphal growth tests of Mep2 mutants and controls in *mep2/mep2Δ* background strain illustrated at 40X magnification. Cells were grown at 30°C for 6 days on SLAD plates containing 50µM ammonium sulphate as nitrogen source.
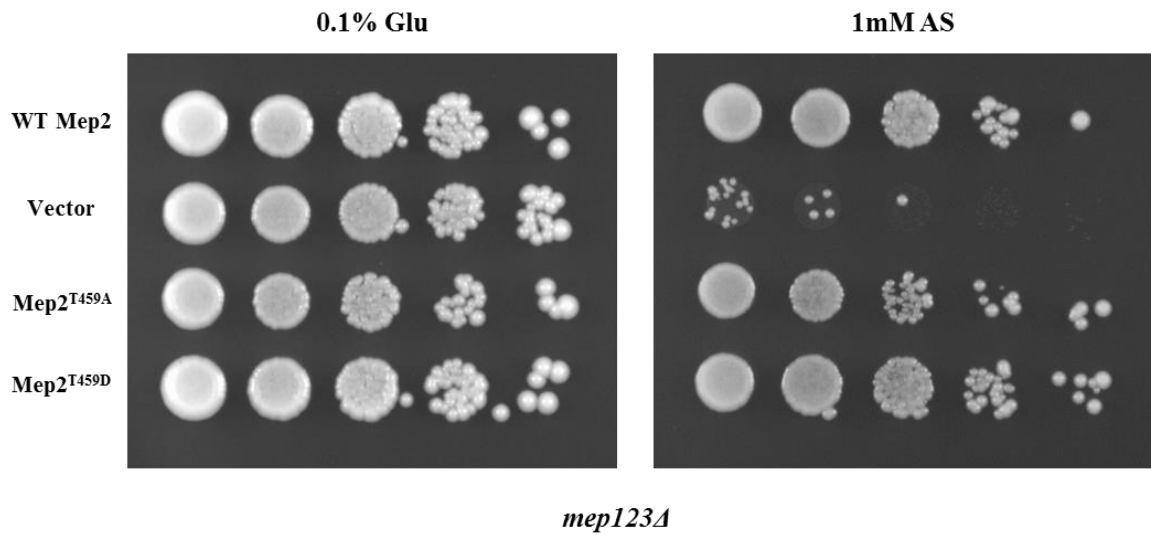
Figure 45: Growth of Mep2^{T459A} and Mep2^{T459D} mutants and controls in *mep123Δ* background strain serially diluted on solid agar medium containing 0.1% glutamate or 1mM ammonium sulphate as the sole nitrogen source at 30°C for 3 days.
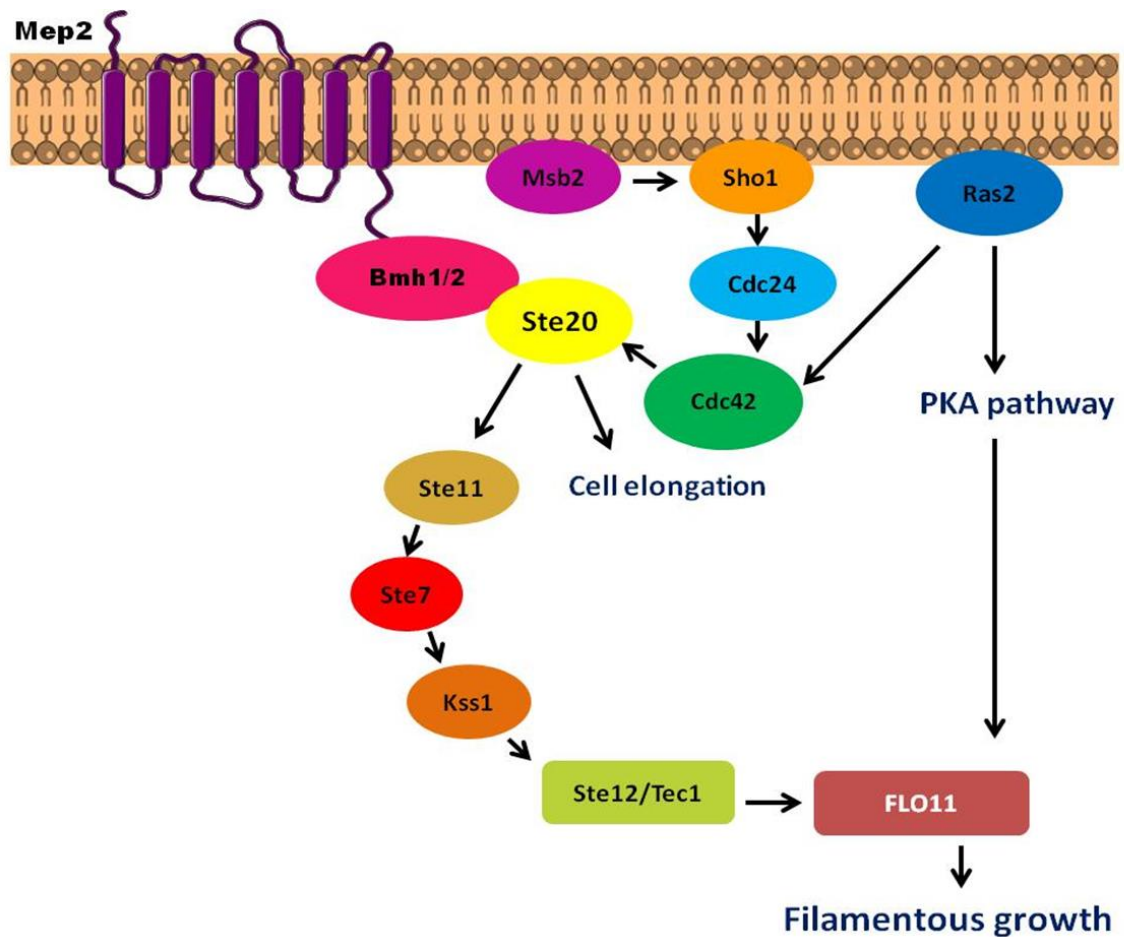
Figure 46: Model for Mep2 regulating MAP Kinase pathway to initiate pseudohyphal growth. During nitrogen limitation, Mep2 physically interacts with Bmh1/2-Ste20 protein complex to initiate pseudohyphal growth.

In order to confirm that Mep2 regulates the MAP kinase pathway to initiate pseudohyphal growth, a transcriptional reporter whose activity reflected the activation of the MAP Kinase pathway during pseudohyphal growth was used to test for Mep2 dependent activation of Ste12. ß-Galactosidase assays were used to measure the activity of Ste12 using a *lacZ* reporter plasmid which contains a Ste12 binding site. The *FG(TyA)-lacZ* reporter plasmid was co-transformed with Mep2 mutants and controls, and grown in synthetic minimal media without amino acids containing 0.1% proline as nitrogen source. Results from the ß-Galactosidase assay (Fig. 47) showed a Mep2 dependent activation of Ste12 in the wild-type strain verifying the model that Mep2 regulates the MAP Kinase pathway to initiate pseudohyphal growth. The *mep2/mep2Δ* strain showed a significant reduction in ß-Galactosidase activity compared to the wild-type strain as well as the the non-signalling mutants. Surprisingly, the hyperactive Mep2^{G349C} mutant showed a significant drop in ß-Galactosidase activity compared to the wild-type strain. The Mep2^{T459A} mutant showed a significant reduction in *lacZ* activity compared to the wild-type strain. The Mep2^{T459D} mutant was able to partially restore the activity of MAP Kinase compared to the Mep2^{T459A} mutant although they both showed a drop in their levels of ß-Galactosidase activity compared to the wild-type strain. Therefore, Mep2^{T459} residue is essential for the Mep2 dependent activation of the MAP Kinase pathway during pseudohyphal growth.
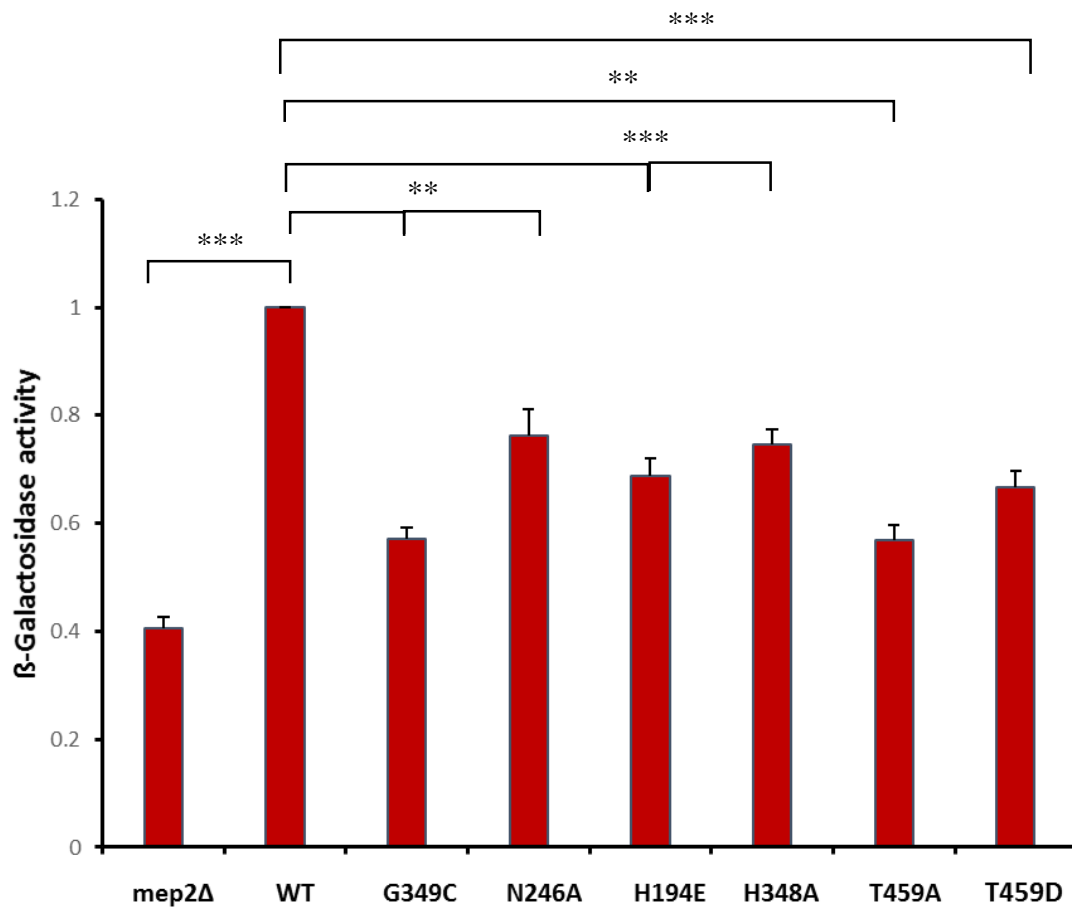
Figure 47: The *FG(TyA)-lacZ* reporter plasmid was co-transformed with Mep2 mutants and controls into a *mep2/mep2Δ* strain and grown in synthetic minimal media without amino acids containing 0.1% proline as nitrogen source. Error bars were calculated from standard deviations for triplicate repeats of each strain and the results were statistically examined using Student's t-test. Symbols ** and *** denote statistical differences at the p values of 0.01 and 0.001 respectively.

6.5. Split-ubiquitin based Yeast Two Hybrid (Y2H) screen to test for interactions between Mep2 and Bmh1

Another tool to test for interactions between Mep2 and Bmh1 would be Split-ubiquitin based Yeast Two Hybrid (Y2H) system for membrane proteins. In the membrane based Y2H system the C-terminal half of ubiquitin (Cub) is fused to the bait of interest and the N-terminal half (Nub) to the prey of interest. The C-terminal half of ubiquitin (Cub) is linked to an artificial transcription factor (TF), LexA-VP16 consisting of DNA-binding protein LexA from *E. coli* and the activation domain VP16 from Herpes Simplex Virus (HSV). Nubs contain a point mutation resulting in a low affinity for Cub to prevent spontaneous re-association and detection of false positives in the screen. Upon interaction between the bait and prey proteins, Cub and Nub re-associate leading to the re-constitution of a full length ubiquitin molecule, which is then recognized by endogenous cytosolic deubiquitinating enzymes (DUBs) resulting in the release of the TF. The TF is now free to enter the nucleus to activate the transcription of the His3 reporter gene allowing yeast strains to grow on a selective media lacking Histidine, indicative of prey and bait interaction.

A positive control was generated by fusing both halves of the ubiquitin with Mep2 and the plasmids were transformed into a reporter strain. The transformants were then spotted onto the surface of selective media plates and grown at 30°C for 2 to 3 days. Results from the Split-ubiquitin based Yeast Two Hybrid (Y2H) screen for the positive control (Fig. 48) Mep2 vs Mep2 shows that Mep2 forms a trimer and is capable of growing on selective media plates (SD+0.1%P+ade and SD-Trp-Leu-His) due to re-association of the ubiquitin molecule. In order to test for interactions between Mep2 and Bmh1, the C-terminal half of ubiquitin was fused to the bait of interest (Mep2) and the N-terminal half to the prey of interest (Bmh1) and transformed into the reporter strain. The transformants were grown overnight and serially diluted and spotted onto the surface of selective media plates and grown at 30°C for 2 to 3 days. Results from the Split-ubiquitin based Yeast Two Hybrid (Y2H) screen to test for interactions between Mep2 and Bmh1 (Fig. 49) indicate that Y2H assay is unable to demonstrate a positive interaction between the bait and prey of interest as there was growth in the control samples in selective media plates. This indicates non-specific association of the complementary halves of the ubiquitin molecule making the results from the assay unreliable.

a)

Mep2 vs Mep2

Cub Nub

- +

+ +

+ -
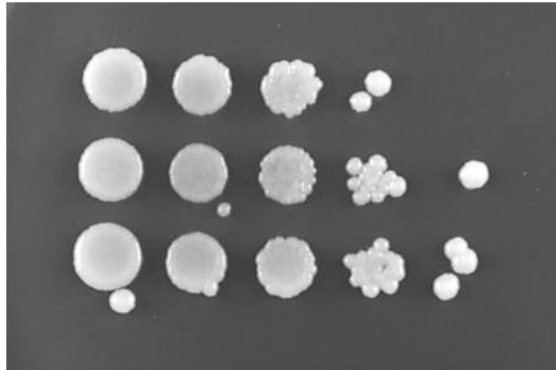
SD-Trp-Leu

b)

Mep2 vs Mep2

Cub Nub

- +

+ +

+ -

SD+0.1% P+ade

c)

Mep2 vs Mep2
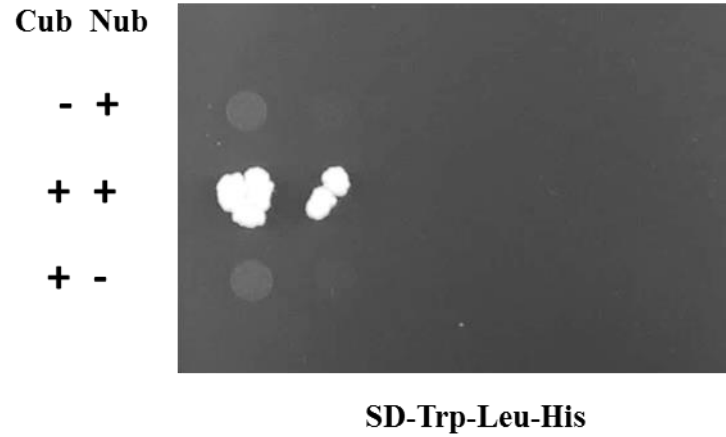
SD-Trp-Leu-His

Figure 48: Growth of C-terminal (Cub) and N-terminal (Nub) halves of ubiquitin fused to Mep2 and empty prey or bait constructs as controls. The strains were serially diluted and spotted on selective medium a) SD-Trp-Leu b) SD+0.1%P+ade c) SD-Trp-Leu-His plates and grown at 30°C for 3 days before photographing the plates.

a)

Mep2 vs Bmh1

Cub Nub

+ +

- +

+ -

+ + *
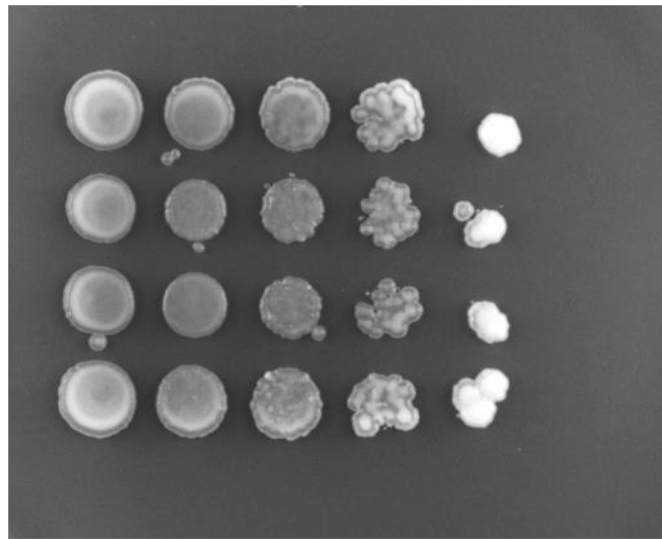
*** Mep2 vs Mep2**

SD-Trp-Leu

b)

Mep2 vs Bmh1

Cub Nub

+ +

- +

+ -

+ + *

*** Mep2 vs Mep2**

SD+0.1% P+ade

c)

Mep2 vs Bmh1

Cub	Nub	
+	+	
-	+	
+	-	
+	+	*

* Mep2 vs Mep2

SD-Trp-Leu-His
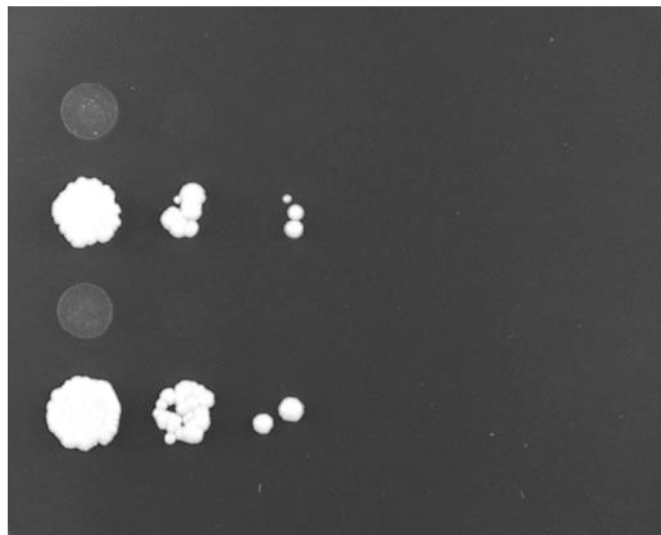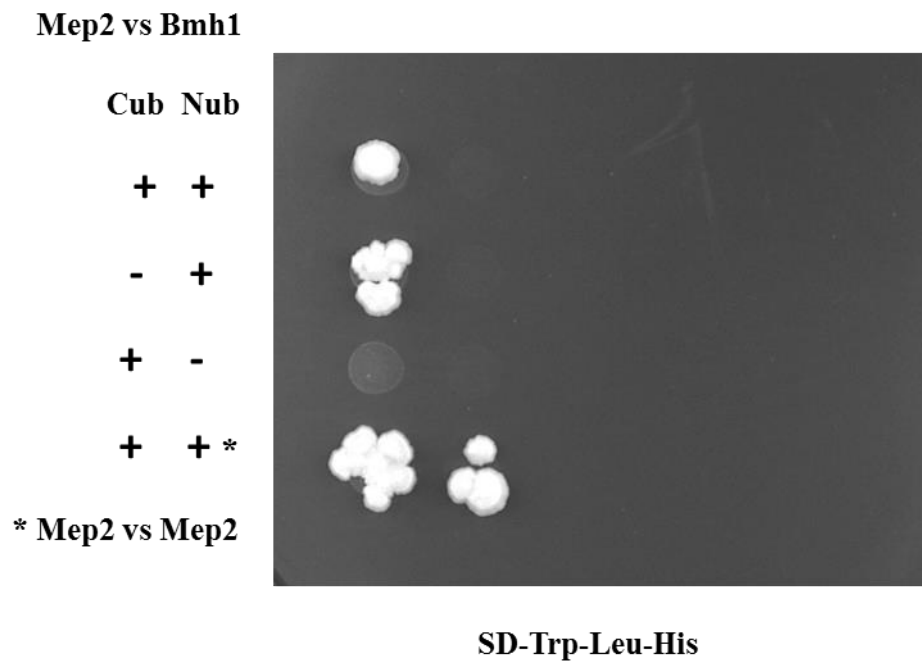
Figure 49: Growth of C-terminal half of ubiquitin fused to Mep2 (Cub) and N-terminal half to Bmh1 (Nub), and empty prey or bait constructs as controls. C-terminal and N-terminal halves of ubiquitin fused to Mep2 was used as a positive control. The strains were serially diluted and spotted on selective medium a) SD-Trp-Leu b) SD+0.1%P+ade c) SD-Trp-Leu-His plates and grown at 30°C for 3 days before photographing the plates.

6.6. Discussion

Among the two distinct models proposed to explain the sensing and signalling functions of Mep2, the second model, the transceptor model of Mep2 function proposes that the conformational changes of the transporter during substrate transport allows it to engage a downstream signalling pathway initiating pseudohyphal growth. In order to investigate the transceptor model of Mep2 function and to address the molecular mechanisms by which Mep2 senses ammonium during nitrogen limitation, PCA based on the enzyme DHFR was carried out to identify Mep2 interacting proteins *in vivo*. PCA is a powerful tool to detect protein-protein interactions as this technique allows the proteins to be expressed in their own locations at endogenous levels and undergo any post-translational modification or degradation as usual (Remy *et al*, 2007; Michnick *et al*, 2011). Among the list of potential interaction partners of Mep2 from the screen, Bmh1/2 were among the top five interaction partners and the G alpha protein Gpa2 was among the top 20 potential interaction partners of Mep2. Earlier work has shown that Bmh1/2 are 14-3-3 protein homologs essential for the induction of pseudohyphal growth and are part of the Ras/MAP Kinase pathway regulating pseudohyphal growth. Furthermore, they associate with Ste20 *in vivo* (Roberts *et al*, 1997) and this accounts for the fact that Ste20 made the list among the top 100 interacting proteins. The G alpha protein Gpa2 regulates the PKA pathway during pseudohyphal growth via interaction with the G-protein coupled receptor Gpr1 (Lorenz & Heitman, 1997).

Our PCA screen identified a list of proteins to be potential interaction partners of Mep2. The reason for this long list of interaction partners could be explained by pointing out that PCA occasionally identifies highly expressed proteins as false positives in the interaction (Tarassov *et al*, 2008). Moreover, some of these potential interaction partners of Mep2 might be physically close to Mep2 without physically interacting with the protein. But the physical proximity gets identified by PCA as an interaction resulting in the detection of false-positive interactions. In order to make sure the false-positives are not included in the analysis, GO Term Mapper was used to annotate these interaction partners based on their biological processes, and the potential interaction partners of Mep2 involved in the induction of pseudohyphal growth could be identified and these interactions could be tested further to identify physical interaction partners of Mep2.

Immunoprecipitation studies were undertaken to verify potential interactions between Mep2 and Gpa2/Bmh1 following the results from the PCA screen. We were unable to prove a Mep2-Gpa2 interaction using Co-IP assays as Gpa2 was immunoprecipitated in a non-specific manner. The wild-type Mep2 plasmid contains an N4Q mutation to avert N-glycosylation of

Mep2 to prevent high-molecular weight smearing during immunodetection. The absence of N-glycosylation, however has an influence on the ability of Mep2 to undergo pseudohyphal growth during nitrogen limitation as N4Q mutation perturbs filamentation to a limited extent (Marini & Andre, 2000). Similar negative results were obtained for immunoprecipitation studies to test for potential interactions between Mep2 and Bmh1. Even though specific bands were obtained for lysates, no bands were observed for the Co-IP samples. The inability of Co-IP assays to detect potential Mep2 and Gpa2/Bmh1 interactions might be due to the presence of N4Q mutation in the Mep2 plasmid. The lack of N-glycosylation might affect Mep2 signalling making the interactions more transient and difficult to capture using immunoprecipitation.

If the interaction between Mep2 and Bmh1 are transient and happens only briefly to initiate signalling during pseudohyphal growth, then those interactions should be captured when the protein makes the momentary contact with its interaction partner. Crosslinking agents could be used to capture or freeze the protein-protein interactions in place as they happen allowing even transient interactions to be detected. Cross-linking followed by preparation of membrane enriched extracts were carried out to test for potential interactions between Mep2 and Bmh1, and immunodetected using appropriate antibodies. A Mep2 dependent enrichment of Bmh1 on the membrane was evident for the wild-type compared to the sample where Mep2 was absent supporting the notion that Mep2 interacts with Bmh1 and forms a complex at the plasma membrane. The next step was to test for interactions between Bmh1 and the non-signalling separation of function Mep2 mutants. A hyperactive Mep2 mutant G349C was included as a positive control. Cell lysates which were not cross-linked were prepared alongside the membrane enriched extracts for comparison during Western blot. G349C mutant showed a Mep2 dependent enrichment of Bmh1 alongside the wild-type sample. All the signalling deficient mutants showed a reduction in the Bmh1 enrichment at the membrane similar to that of a Mep2 delete sample. The levels of Bmh1 were however similar across all the samples in the cell lysate. These results show that Bmh1 enrichment on the membrane is Mep2 dependent and the non-signalling Mep2 variants are unable to interact with Bmh1 resulting in an inability to initiate signalling during pseudohyphal growth. These results support the transceptor model of Mep2 function where transport of ammonium through the permease during ammonium limitation would prompt a conformational change of the protein involving the C-terminal tail which then allows Mep2 to physically engage signalling partners (Bmh1) thereby initiating pseudohyphal growth.

In order to test whether Bmh1 binds Mep2 at the Threonine site at T459 residue of the C-terminal tail of Mep2 following prediction using the web-server 14-3-3Pred which predicts the 14-3-3 binding sites in proteins, two mutants T459A which is a loss of function mutant and T459D, a phosphomimmetic mutant were generated. Crosslinking followed by preparation of membrane enriched extracts and cell lysates showed that a reduction in the Mep2 dependent enrichment of Bmh1 in T459A mutant and T459D mutant revealed that it was able to rescue the loss of interaction and demonstrated Bmh1 enrichment at the membrane similar to that of the wild-type sample. The results from the pseudohyphal growth test revealed that T459A mutation affected Mep2 signalling as this mutant showed striking reduction in its ability to undergo pseudohyphal growth. The T459A variant failed to give rise to colonies that produced pseudohyphae in most cases. Some superficial pseudohyphae grew on the surface of the agar for some colonies, but lacked the ability to undergo invasive pseudohyphal growth that is characteristic of wild-type pseudohyphal growth. The phosphomimmetic T459D mutant however, was able to rescue the signalling defect imposed by the alanine substitution in the T459A mutant and showed pseudohyphal growth levels similar to that of the wild-type strain. This shows that phosphorylation of the T459 residue is essential for the signalling function of Mep2 and, interaction levels of Mep2 and Bmh1 correlate with the extent of pseudohyphal growth. Furthermore, the Bmh1 binding site of Mep2 is located in the T459 residue of the C-terminal domain of the protein. These mutations nonetheless, did not seem to affect the ability of Mep2 to transport ammonium during nitrogen limitation as both mutants were transport proficient.

The results so far were in agreement with the proposed model for Mep2 regulating MAP Kinase pathway to initiate pseudohyphal growth through physical interaction with Bmh1. In order to prove that Mep2 regulates the MAP Kinase pathway to initiate pseudohyphal growth, a transcriptional reporter *FG(TyA)-lacZ* whose activity reflects the activation of the MAP Kinase pathway during pseudohyphal growth was used. In order to do that, Mep2 dependent activation of Ste12 using the *lacZ* reporter plasmid was tested using ß-Galactosidase assays. Results from the ß-Galactosidase assay showed a Mep2 dependent activation of Ste12 for the wild-type strain compared to the *mep2/mep2Δ* strain verifying the model that Mep2 regulates the MAP Kinase pathway to initiate pseudohyphal growth. All the non-sensing mutants showed a significant drop in ß-Galactosidase activity levels compared to the wild-type strain. This illustrates that the non-signalling Mep2 variants are unable to activate the MAP Kinase pathway to initiate pseudohyphal growth.

However, surprisingly, the hyperactive G349C and the phosphomimmetic T459D mutants showed a decline in their ß-Galactosidase activity levels. Similar results were observed by Roberts *et al* (1997) when *bmh1 bmh2* Δ strains displayed substantial reduction in the activity of the *FG(TyA)-lacZ* reporter compared to the wild-type strain, whereas overexpression of *BMH1* or *BMH2* did not result in a significant induction of this reporter. Overexpression of *BMH1* or *BMH2* however stimulated cell elongation and filament formation. Bmh1/2 have an additional function during pseudohyphal growth where they are involved in the formation of filaments and elongation of cells via physical interaction with Ste20. Roberts *et al* (1997) argue that the effect of Bmh1/2 activity on cell morphogenesis might be independent from their role in the regulation of the MAP Kinase cascade during pseudohyphal growth. This holds true for the results from this study as well since mutants showing lower levels of MAP Kinase activation exhibit hyperfilamentous pseudohyphal growth phenotype. Moreover, mutations to the conserved residues in Mep2 exhibit responses similar to mutations in Bmh1/2 supporting the interaction model. Another reason for the decline in their ß-Galactosidase activity levels could be explained by the hyperactivity of these mutants. Since they are hyperactive for filamentous growth, activation of Ste12 need not be at a higher level compared to the non-sensing mutants resulting in a negative-feedback loop. It might be possible to separate the reporter activity and filamentation responses under some conditions although this should be further tested. The putative phosphorylation site at the T459 residue of the Mep2 C-terminal domain is thus essential for Bmh1 binding to Mep2, regulation of MAP Kinase activity and pseudohyphal growth response in Mep2.

Since the transceptor model has been established, the next important question was to find out whether Mep2 and Bmh1 interaction is only to initiate pseudohyphal growth or are there any additional signalling roles for this complex. Since the T459A mutant was still able to partially undergo filamentous growth it is clear that Mep2-Bmh1 complex interacts to fulfil additional signalling function and Mep2 signals through additional pathways to fulfil its sensing role. Earlier studies have shown that Bmh1/2 associate with Ste20 *in vivo* and the association is not dependent on other MAP Kinase cascade components or Cdc42 binding domain of Ste20. Overexpression of Bmh1/2 had a positive impact on elongation of cells and formation of filaments which was dependent on the presence of Ste20. This highlights their role in appropriate cell elongation and filament formation induced by Ras2 and Cdc42 (Roberts *et al*, 1997). Ste20 has a significant role in cell morphogenesis independent of MAPK cascade and this could be achieved by a signalling junction where the signal bifurcates separating MAP Kinase signalling functions from the cell elongation functions of Ste20. Set20 includes one of

the main down-stream effectors of Cdc42. Mosch *et al* (1996) showed that Ras2 controls filamentous growth via the Cdc42/Set20 complex regulating cell morphology during filamentous growth and Cdc42/Set20 complex co-ordinates organization and position of the morphogenetic machinery. They show that under nitrogen starvation conditions, Ras2 activates Cdc42 which in turn activates Ste20 and/or Bmh1/2 proteins in order to activate the MAP Kinase pathway to initiate filamentous growth. Mep2-Bmh1 interaction during ammonium sensing could thus be for the polar extension of the hyphae during filamentous growth. Polar growth requires positional information and Mep2 might help with the positional signal as its membrane recruitment brings in nutrient substrate into the cell favouring growth in that direction. This in turn leads to recruitment of the morphogenetic machinery to that site which involves Bmh1/2-Ste20/ Cdc42-Set20 complex (Harris & Momany, 2004). Not all the components of the morphogenetic machinery involved in the formation and preservation of hyphal polarity have been discovered. Thus, Mep2-Bmh1 interaction might help the fungi to generate positional information for polarized growth during nitrogen limitation. This could even be the key function of the complex and initiating signals for pseudohyphal growth might be a secondary role. The 14-3-3 homologue Pdc1 in *U. maydis* was shown to have roles in controlling cell separation and establishment of cell polarity during filamentous growth (Pham *et al*, 2009).

The external stimuli for the dimorphic switch to pseudohyphal growth could be nutrient limitation, for instance depletion of a fermentable carbon source or nitrogen starvation. Pseudohyphal growth is also referred to as filamentous growth. The major changes during filamentous growth are increased cell adhesion, elongated morphology, highly polarised growth, alteration in budding pattern and an ability to invade growth substrate (Gimenzo *et al*, 1992; Kron *et al*, 1994). Filamentous growth has been inferred to as a foraging adaptation to enable yeast cells to explore the environment in order to find more favourable conditions during nutrient limitation. The dimorphic change to filamentous form is subtler in haploid *S. cerevisiae* when compared to its diploid form. In haploid cells the switch is characterised by partial morphological changes, formation of shorter filaments and increased cell-cell adhesion adopting an invasive growth phenotype (Roberts &Fink, 1994). The dimorphic switch takes place when cells are grown under ammonium limiting conditions or in the presence of a non-preferred source of nitrogen. Catabolism of a non-preferred source of nitrogen leads to the export of ammonium into the extracellular environment, and hence ammonium remains the preferred nutrient that gets sensed (Boeckstaens et al, 2007).

Even though dimorphism is not as prominent in *S. cerevisiae* compared to other yeasts, the accessibility to a wide range of tools to study this versatile eukaryote has made the budding yeast the organism of choice to study various factors involved in the filamentous transition during nutrient limitation. Moreover, lessons learnt from yeast about the regulation of this dimorphic switch have transpired to be the case with many fungal species (Madhani & Fink, 1998). Dissecting the exact mechanism behind ammonium sensing in fungi could us help to identify and characterise signalling pathways central for virulence in pathogenic fungi, and devise strategies to design novel antifungal drug targets.

Even though it is well known that nitrogen starvation acts as a trigger to initiate pseudohyphal differentiation, there exists uncertainty towards the exact mechanisms leading to the induction of this dimorphic switch. Four signalling pathways that play crucial roles by co-ordinating the induction of pseudohyphal growth and invasiveness have been well characterised. These includes the pheromone responsive MAP-Kinase (MAPK) pathway (Liu et al, 1993), the cAMP-PKA pathway (PKA) pathway (Robertson & Fink, 1998), Target of Rapamycin (TOR) pathway (Cullen & Sprague, 2000) and the Sucrose non-fermentable (SNF) pathway (Braus *et al*, 2003). In *S. cerevisiae*, the signalling pathways involved in the regulation of this morphogenetic switch are complex pathways working in parallel that feedback, crosstalk and interact with each other to co-ordinate filamentation response in yeast. Nonetheless, there isn't enough evidence to demonstrate that these pathways directly interact with the Mep2 to fulfil its ammonium sensing role (Lorenz & Heitman, 1998).

A crucial and shared element of these signalling pathways appears to be the GTP-binding protein Ras2 (Gimenzo *et al*, 1992). Earlier studies have shown that Gpa2, a heterotrimeric GTP protein α-subunit controls pseudohyphal growth by regulating cAMP levels and modulates a signal transduction pathway independent of the MAP Kinase cascade. Strains lacking Gpa2 show a defect in pseudohyphal differentiation and a dominant active allele of GPA2 initiates pseudohyphal differentiation even in nitrogen rich media, and filamentation defect of gpa2Δ strains were supressed by exogenous cAMP levels (Lorenz & Heitman, 1997). In their later studies Lorenz & Heitman (1998) showed that in a strain lacking Mep2, pseudohyphal growth could be restored by a dominantly active allele of GPA2 suggesting that Mep2 might be functioning upstream of Gpa2 in the signalling pathway to regulate pseudohyphal growth. Mep2 may directly interact with Gpa2 to initiate the signalling pathway which could be Gpa2 mediated. However, no evidence directly linking Mep2 and Gpa2 has been obtained till date. Van Nuland et al (2006) showed that Mep2 fulfils its transceptor function via cAMP-independent activation of the PKA pathway when starved cells were treated with ammonium,

and is not dependent on the metabolism of ammonium. However, this sensing function of Mep2 is not the same as permease function during initiation of pseudohyphal growth. A comparable transceptor function during induction of pseudohyphal growth is still uncertain.

Later studies have shown that overexpression of Mep2 induces pseudohyphal growth under normally repressing conditions and generates a transcriptional profile which is in agreement with the activation of the MAP Kinase pathway. Constitutively expressed Mep2 restored pseudohyphal growth in cAMP-PKA mutants. However, growth defects were not restored in mutants lacking MAP Kinase regulated transcription factor Ste12 suggesting that Ste12 is a down-stream effector of Mep2 and establishes the role of MAP Kinase pathway in pseudohyphal growth (Rutherford et al, 2008). The MAP Kinase cascade shares upstream components with the cAMP-PKA pathway and are shown to converge at a point which encodes for a cell surface flocculin gene FLO11 essential for pseudohyphal and invasive growth in both haploid and diploid cell types (Rupp et al, 1999).

14-3-3 proteins are a group of highly conserved abundant proteins whose precise function remains elusive. They are however known to interact with a lot of proteins and have roles in signal transduction, cell cycle regulation and apoptosis (Roberts *et al*, 1997; Hemert *et al*, 2001). 14-3-3 proteins were shown to be involved in actin cytoskeleton organization (Roth *et al*, 1999) and participates in the Ras signalling pathway in yeast (Gelperin *et al*, 1995). In *S. cerevisiae* strains lacking 14-3-3 proteins are sensitive to various environmental stress and mutants have a filamentation defect. Even though Bmh1/2 are essential for Ras/MAPK signalling cascade controlling pseudohyphal growth, they are dispensable for MAP Kinase signalling during mating (Roberts *et al*, 1997).

Taken together, this has allowed us to propose a model for the sensing function of Mep2. During low ammonium levels, Mep2 initiates filamentous growth by regulating MAP Kinase cascade via physical interaction with Bmh1/2 protein complex. This is in agreement with earlier work where over expression of Mep2 initiated a transcriptional profile which was in agreement with the activation of MAP Kinase pathway (Rutherford *et al*, 2008). Constitutively active Mep2 restored pseudohyphal growth in mutants lacking components of the Ras-PKA pathway. However, over expression of Mep2 did not compensate for the lack of Ste12 which is part of the MAP Kinase pathway, and did not induce filamentous growth in a Ste12 mutant. This strongly suggests that Mep2 and Ste12 are part of the same signalling pathway. Expression of alleles that are constitutively active for components of the PKA pathway (Ras2, Gpa2) or MAP Kinase pathways (Ste11) as well as overexpression of Ste12 were able to restore filamentous growth in strains lacking Mep2. This puts forward the theory that Mep2 may function upstream

of these components in the signalling cascade (Lorenz & Heitman, 1998). Overexpression of the components of the PKA pathway (Ras2) can compensate for the loss of the components of the MAP Kinase pathway including Ste12 and Tec1 transcription factors. Exogenous cyclic AMP restored filamentation defect in Ste12 or Tec1, or both Ste12 and Tec1 mutants (Lorenz & Heitman, 1997; Pan & Heitman, 1999). The fact that overexpression of Mep2 compensated for the loss of PKA signalling components Tpk2, Gpa2 and Ras2, and not the MAP Kinase component Ste12 points towards the fact that Mep2 initiates pseudohyphal growth through MAP Kinase pathway. In addition, the induction of Ste12 related and MAP Kinase pathway regulating genes as a result of Mep2 expression implies Mep2-dependent activation of the MAP Kinase pathway during filamentous growth. Results from the epistasis analysis imply that the position of Mep2 would be upstream of the MAP Kinase pathway which is in agreement with our PCA screen results that places MAP Kinase components involved in pseudohyphal growth as downstream effectors of the ammonium transporter Mep2.

In the fungal pathogen *Cryptococcus neoformans* mating in response to ammonium starvation relies on its high affinity ammonium transporter Amt2 which is essential for the induction of invasive growth (Rutherford *et al*, 2008b). This essentially implies that Amt2 initiates signals for invasive growth through MAP Kinase cascade. The molecular mechanistic aspects of signalling across Mep2 and its homologs might thus be conserved. The MAP Kinase and PKA pathways co-ordinate regulation of pseudohyphal growth and transmits signals to initiate filamentation in *C. albicans*. When effectors of the MAPK and PKA signalling pathways were deleted, filamentation defects were observed and significant reduction in virulence was detected suggesting that non-filamentous mutants were avirulent (Lo *et al*, 1997). Pseudohyphal differentiation in the plant pathogen *U. maydis* requires synchronisation between MAPK and cAMP-PKA pathways for the formation of filaments for colonisation and virulence. Nevertheless, cAMP pathway helps the pathogen to switch from the filamentous form to a normal yeast form as opposed to *S. cerevisiae*, and activation of PKA pathway represses formation of filaments suggesting that pseudohyphal growth in *U. maydis* is regulated by the MAP Kinase pathway (Kronstad et al, 1998; Durrenberger et al, 1998; Andrews et al, 2000).

The molecular mechanisms connecting Mep2 to pseudohyphal growth appears to be strongly conserved and could be studied across various evolutionarily distant homologues using *S. cerevisiae* as a model. Mep2 homologues from other fungal species were able to restore pseudohyphal growth when introduced into *S. cerevisiae* strains lacking endogenous Mep2. This suggests that the signalling roles of these high affinity ammonium permeases is evolutionarily conserved across homologues in various fungi. Filamentous growth signifies a

point of conjunction between several cellular pathways including the cell polarity, cell cycle and nutrition and is consequently a remarkable system to comprehend the association between various biological processes.

7. Final Discussion

7.1. Project summary

In order to respond to changing environmental conditions the yeast *Saccharomyces cerevisiae* must be capable of rapidly adapting to external changes and sense its environment. This is vital for its survival and many essential processes including growth, division, mating, response to stress and several other governing factors. One of the principal fluctuating elements in the environment is the availability of nutrients. Consequently, the ability to sense nutrients at the plasma membrane is a key step for survival, and microorganisms like yeast have developed a multitude of nutrient sensing plasma membrane proteins (Holsbeeks *et al*, 2004). These nutrient sensing membrane proteins detect the presence of particular nutrients and are induced in poor medium limiting for that nutrient in order to assist in the efficient uptake of the scarce nutrient. These nutrient transporters act as doorkeepers regulating essential nutrient-transport through the plasma membrane into the cell. Some of these transporters are capable of activating downstream signalling pathways permitting them to function as receptors, and hence often referred to as transceptors. One of these nutrient sensing pathways sustain high activity levels of the PKA in the presence of a fermentable carbon source and other nutrients critical for growth, making it the Fermentable Growth Medium (FGM) induced pathway (Schepers *et al*, 2012). Scarcity of an essential nutrient source alongside the occurrence of a fermentable carbon sources results in PKA downregulation and arrest growth. At the same time, re-addition of the starved substrate into the growth media results in the rapid activation the PKA targets resulting in the activation of trehalose even though the precise mechanism of signalling is still unclear (Thevelein & de Winde, 1999). The yeast ammonium transceptor Mep2 is involved in another distinct sensing mechanism whereby it induces pseudohyphal growth under conditions of nitrogen limitation. The ammonium sensing function of Mep2 is distinct from its signalling function during the rapid activation of the PKA pathway in cells starved for ammonium.

Two distinct models have been proposed to explain how Mep2 regulates this dimorphic switch during nitrogen limitation. The two models of Mep2 function were tested through the course of this study using separation of function mutants. Mutational analysis of previously published Mep2 mutants identified conserved residues that were able to uncouple the transport and signalling functions of Mep2. To our surprise, these separation of function mutants (N246A, H194E, H348A) mapped to the Mep2 conducting pore and were part of the ammonium

deprotonation (N246A, H194E) and reprotonation (H348A) sites during substrate transport. This highlights the essential role of ammonium deprotonation and reprotonation events in the downstream signalling function of Mep2. This data however, supports both pH model and transceptor model of Mep2 function. These mutations might alter the deprotonation or reprotonation events during ammonium import which could result in the proton either moving out to the periplasm (as opposed to getting co-transported into the cytosol) or following an incorrect path into the cytoplasm. Another possibility would be the ability of the mutants to bypass the deprotonation/reprotonation event conferred by these mutations, which could account for their improved abilities to transport ammonium. These mutations could render the protein in a different or unfavourable conformation than normal resulting in an inability to interact with downstream signalling partners or to initiate downstream signalling for pseudohyphal growth.

The results from this study following the testing of the first model, the pH model of ammonium sensing fails to support the model. Although there is evidence for the ammonium transport activity of Mep2 resulting in the acidification of the cytosol, the mutants caused acidification or alkalinization of the cytosol depending on their location within the Mep2 conducting pore. The mutants which were part of the ammonium deprotonation (N246A, H194E) site within the pore resulted in the acidification of the cytosol whereas the mutant part of the reprotonation (H348A) site caused alkalinization of the cytosol. It was interesting to note that a previously published hyperactive Mep2 mutant (G349C) which is located right next to the reprotonation (H348A) site mutant, and would therefore form part of the substrate reprotonation site resulted in the acidification of the cytosol. Thus, these results highlight the fact that Mep2 signalling is independent of intracellular pH changes. Our studies have examined the global variations in cytosolic pH and the localised pH changes brought about by Mep2 would be even higher towards the membrane.

The second model reveals the transceptor model of Mep2 function. Our structural studies have shown that Mep2 is closed on the intracellular side which suggests that it has to open to in order to import ammonium. In other words, the transporter has to undergo a conformational change during ammonium transport, and our studies have demonstrated that phosphorylation causes a conformation change in the C-terminal region of Mep2. Npr1 kinase phosphorylates Mep2 at the S457 residue of the C-terminal tail during ammonium limitation in order to activate the ammonium transporter for substrate import (Boeckstaens *et al*, 2014). This phosphorylation based regulation of the ammonium transporter results in a conformation change of the CTR

resulting in ammonium import. This conformational change might allow Mep2 to physically engage with a downstream signalling partner to initiate pseudohyphal growth.

Examination of the transceptor model of Mep2 function revealed that Mep physically interacts with the 14-3-3 protein Bmh1 and forms a complex at the plasma membrane. The genetic screen using PCA to determine potential interaction partners of Mep2 identified the 14-3-3 proteins Bmh1&2 as top hits. This interaction was confirmed using western analysis of membrane fractions and notably established that this interaction was lost when analysing the signalling deficient separation of function Mep2 mutants. Moreover, we have identified the 14-3-3 protein binding site in Mep2 to be the T459 residue of the Mep2 CTR, and that this interaction is essential for the Mep2 dependent activation of the MAP Kinase pathway. Separation of function Mep2 mutants that are unable to interact with Bmh1 fail to undergo pseudohyphal growth. Furthermore, T459A mutant had only partial interaction with Mep2 on the membrane surface and had very limited pseudohyphal growth abilities (with no invasive growth phenotype). This pseudohyphal growth defect and Mep2 interaction was however rescued in a phosphomimmetic T459D mutant which shows that phosphorylation of that residue is essential for the signalling function of Mep2. The transcriptional reporter for MAP Kinase activity *FG(TyA)::lacZ* (Mösch *et al*, 1996) confirmed that Mep2 activates the MAP Kinase pathway for the regulation of pseudohyphal growth and this is achieved via physical interaction with the 14-3-3 proteins. Although a clear Mep2 dependent activation of the MAP Kinase pathway was observed, which is consistent with the observations from an earlier study (Rutherford *et al*, 2008), the hyperactive G349C variant showed reduced levels MAP Kinase activation compared to the wild-type cells. Similar results were observed for the phosphomimmetic T459D mutant where there was only partial rescue of MAP Kinase activity compared to the T459A mutant. These results mirror the intricacy of the signalling system for which two possible explanations could be put forward. A reduction in the Mep2 dependent activation of the MAP Kinase pathway might not essentially correlate with a loss in pseudohyphal growth across the mutants. This might also point to the fact that the reporter system might not be the most accurate readout for MAP Kinase activation during pseudohyphal growth.

14-3-3 proteins Bmh1 and Bmh2 in *S. cerevisiae* are required for the activation of the Ras/MAP Kinase pathway for the regulation of pseudohyphal growth. Bmh1 and Bmh2 were found to have high levels of sequence identity between them (>90%). However, levels of Bmh1 was found to be more abundant and seemed to be at least 5-fold greater than that of Bmh2 in wild-type strains (Gelperin *et al*, 1995). Phosphorylation of the interacting proteins significantly increased the affinity of 14-3-3 binding even though prior phosphorylation of the target protein

was not found to be essential at all times. The binding sites of 14-3-3 proteins were found to have a consensus phospho-serine or phospho-threonine residue (Yaffe *et al*, 1997). Roberts *et al* (1997) demonstrated that although 14-3-3 proteins are essential for the regulation of the Ras/MAP Kinase pathway during pseudohyphal growth, they are not indispensable for the MAP Kinase activation and signalling during mating. They showed that Bmh1 and Bmh2 physically interact and form a complex with Ste20 *in vivo*, which is also a component of the MAP Kinase pathway regulating pseudohyphal growth. They showed that this interaction is independent of the other component in the pathway including Ste11, Ste5 or Ste12. They verified that *bmh1 bmh2* mutant strains displayed significant reduction in the activity of the transcriptional reporter *FG(TyA)::lacZ* which mirrors a precise defect in the Ras/MAP Kinase signalling pathway and an overall defect. They establish that alongside its role in the MAP Kinase pathway regulation during pseudohyphal growth, 14-3-3 proteins are also essential for cell elongation and formation of filaments, and are especially critical for the induction of cell elongation functions for Ras2 and Cdc42. Their exact involvement in the cell elongation function however, has not been fully identified. However, physical interaction and complex formation between the 14-3-3 proteins and Ste20 was found to be essential for this cell elongation function. Their mutational analysis suggested a role for 14-3-3 proteins in the signalling pathway downstream of Ras2 and Cdc42 and somewhere upstream of Ste11, at the level of Ste20 to regulate MAP Kinase pathway during filamentous growth and to govern certain unknown features of cell elongation. They demonstrated that Ste20 has a vital role in morphogenesis which is independent of its role in the regulation of the MAP Kinase pathway during pseudohyphal growth. Ste20, a member of the PAK (p21-Activated Kinase) protein kinase family is involved in the establishment of polarity. Set20 is essential for polarity changes happening during the growth cycle comprising emergence of bud and polarised growth, and during cell division, it phosphorylates Bni1 through Cdc42 for the initiation of polarisome complex formation (Goehring *et al*, 2003).

The next question would be whether similar 14-3-3 binding sites exist in other fungal species and whether these conserved in other fungal pathogens are conserved. In order to answer that question, alignment of putative 14-3-3 binding sites in *Saccharomyces cerevisiae*, *Ustilago maydis* and the human pathogens *Candida albicans* and *Cryptococcus neoformans* following the predictions from 14-3-3 Pred webserver (Fig. 50) showed that the 14-3-3 binding site in *C. albicans* and *C. neoformans* consists of threonine and serine residues respectively. The 14-3-3 binding site in *U. maydis* however, consists of an aspartate residue which is negatively charged. The alignment thus illustrates that the 14-3-3 binding sites are conserved and this mechanism

```
ScMep2   453-EPIRSK[T]SAQM-463
CaMep2   449-EPIRST[T]ISQP-459
CnAmt2   446-RLHRID[S]KPQF-456
UmUmp2   447-DFVRPE[D]GAEI-457
```

Figure 50: The 14-3-3 binding site in Mep2 is located in its C terminal domain. Alignment of putative 14-3-3 binding sites in *S. cerevisiae* ScMep2, *C. albicans* CaMep2, *C. neoformans* CnAmt2 and *U. maydis* UmUmp2 as predicted by the 14-3-3Pred webserver. Putative regulatory phosphorylation sites are highlighted in red in ScMep2, CaMep2 and CnAmt2 (T or S). The corresponding residue is occupied by a negatively charged aspartate in UmUmp2. Figure adapted from Chembath *et al* (in preparation).

of regulation of filamentous growth via Mep2-14-3-3 interaction might be conserved across pathogenic fungal homologues.

Even though our results did not agree with the pH model of ammonium sensing, it might very well be due to a loss of 14-3-3 protein interaction for the separation of function mutants. This interaction might be essential for an internal pH sensor to initiate signalling during pseudohyphal growth. Another possibility could be that the loss of 14-3-3 interaction might exert an antagonistic effect on the signalling function of Mep2. Another important question would be whether Mep2 also regulates PKA pathway via a potential interaction with Gpa2 during pseudohyphal growth. The PCA screen also identified the G alpha protein Gpa2 as a potential interaction partner for Mep2. However, our immunoprecipitation studies failed to establish an interaction between Mep2 and Gpa2.

Through the course of this study it has been shown that changes in intracellular pH does not influence ammonium sensing in Mep2. On the other hand, two major events are critical for the signalling function of Mep2. The first event is the deprotonation/proton relay/deprotonation of the substrate during ammonium transport. The separation of function mutants reveals that the deprotonation of NH_4^+ at the S2/deprotonation site involving the conserved residues N246 and H194; proton relay through the pore involving the conserved residues H194 and H348 and S4/reprotonation site involving the conserved H348 residue is indispensable for Mep2 signalling. Absence of any of these molecular events including deprotonation/proton relay/deprotonation of the substrate during ammonium import results in a loss of Bmh1 binding to Mep2. The second molecular event essential for the signalling function of Mep2 is the phosphorylation of the T459 residue followed by Bmh1 binding to Mep2. The absence of this phosphorylation event results in an inability of Bmh1 to bind to Mep2 as T459 is the Bmh1 binding site of Mep2. Loss of Mep2-Bmh1 interaction has two consequences, one of which is the inability to activate the MAP Kinase pathway for downstream signalling and the other is the inability to induce pseudohyphal growth during nitrogen imitating conditions.

7.2. Model for ammonium sensing and signalling function of Mep2

Our results so far have allowed to propose a model for the sensing and signalling function of Mep2 (Fig. 51). During ammonium limitation, phosphorylation of the S457 residue at the Mep2 C-terminal tail by Npr1 kinase activates the transporter for ammonium transport. The transporter undergoes a conformational change at the CTR, which is now in an open state and imports ammonia. The ammonium ion undergoes deprotonation at the H194 residue and NH_3 gas traverses down the pore. The proton gets relayed form the first conserved Histidine residue to the second, and gets reprotonated at the H348 residue and travels down into the cytoplasm as ammonium ion, which in turn results in the acidification of the cytosol. Nitrogen starvation results in an additional phosphorylation event possibly by TORC1 at the T459 residue, the 14-3-3 binding site at the Mep2 C-terminal domain. This results in a Mep2 dependent recruitment of the 14-3-3/Ste20 protein complex to the membrane. Mep2 physically interacts with Bmh1 and this has two consequences. One is the activation of the MAP Kinase pathway for the regulation of pseudohyphal growth. The other function is establishment of cell polarity and cell elongation. Our model is that 14-3-3 complex formation controls the Mep2 dependent localisation of Ste20 to the membrane to regulate the activation of the MAP Kinase pathway and for cell elongation during pseudohyphal growth. The establishment of cell polarity and cell elongation by the Ste20/14-3-3 complex happens at the part of the cell membrane where Mep2 is most active and imports ammonia, which would in turn allow the cells to grow towards a direction with plentiful source of ammonia.

7.3. Future work

The interaction between Mep2 and Bmh1 raises a number of interesting questions. Is Mep2-14-3-3 interaction conserved across homologues from other species? What is the significance of the potential phosphorylation site in the Mep2 C-terminal domain? Our alignment data of putative 14-3-3 binding sites in *S. cerevisiae* signalling homologues have shown that this 14-3-3 binding site is conserved across various pathogenic fungi. This, on the other hand raises further questions - How Mep2 homologues, which are structurally different to Mep2, able to initiate pseudohyphal growth when expressed in a yeast strain lacking endogenous Mep2? This suggests that the signalling roles of these high affinity ammonium permeases must be conserved across various evolutionarily distant homologues. Is that accomplished via a possible Mep2-14-3-3 interaction or pH regulation or through a combination of both? This could be an interesting avenue for further investigation.
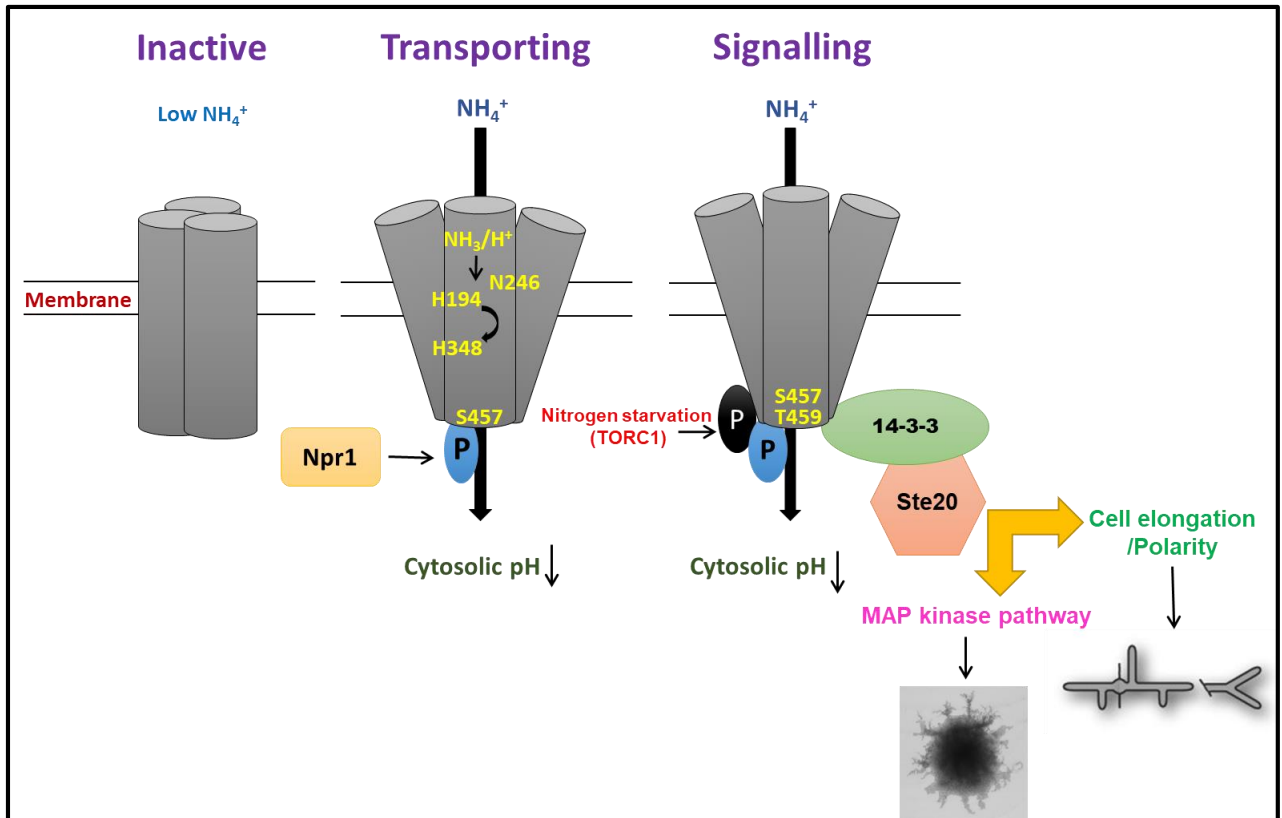
Figure 51: Model for ammonium sensing and signalling function of Mep2. Alongside regulating the MAPK pathway for the induction of pseudohyphal growth, 14-3-3 proteins control the Mep2 dependent membrane localisation of Ste20 to establish cell polarity at that point where Mep2 is most active. Figure adapted from Chembath *et al* (in preparation).

The localisation of Bmh1 and Ste20 to the membrane during nitrogen starvation could be tested to prove that their membrane localisation is Mep2 dependent. Another interesting experiment would be to test for Mep2/Bmh1 interactions using a non-transporting variant of Mep2, H194A. All of the previous studies have supported the notion that transport is necessary for signalling and interaction studies using this mutant would generate proof towards that hypothesis. It would also be interesting to test whether Bmh1 and Ste20 are membrane localised in the non-transporting Mep2 variant. It might very well be that even though Bmh1 and Ste20 are membrane localised in that mutant, the conformational changes of the transporter during substrate transport might be essential for the physical interaction between Mep2 and Bmh1 to initiate downstream signalling and activation of the MAP Kinase pathway. The cell morphology of the T459A and T459D mutants alongside wild-type strains during pseudohyphal growth could be examined to establish the role of the 14-3-3/Ste20 complex in the establishment of cell polarity and cell elongation.

Another interesting enquiry would be to understand how exactly Mep2 is able to distinguish between its transceptor function during pseudohyphal growth and PKA starvation response signalling? Re-supplementation of essential substrates such as ammonium, glucose or phosphate to starved cells resulted in the rapid activation of trehalase and PKA targets. This PKA starvation response must be conserved as it is observed across almost all transporting transceptors such as the amino acid transceptor Gap1, phosphate transceptor Pho84, ammonium transceptor Mep2 (Donaton *et al*, 2003; Schepers *et al*, 2012; Van Nuland *et al*, 2006). The exact mechanism by which Mep2 activates the PKA pathway in this starvation response is still unclear. However, the signalling pathways for the activation of the PKA targets must be different from the pseudohyphal growth pathway as the separation of function mutant (N246A) was able to activate trehalase and PKA targets as part of the starvation response but was unable to undergo pseudohyphal growth during nitrogen limitation.

This would then lead to the next question, to what extent is the nutrient transceptor signalling conserved? What is the implication of the Mep2-14-3-3 interaction for other transceptors? Even though Mep2 dependent activation of the MAP Kinase pathway has been shown through the course of this study, how exactly does Mep2 regulate Ste20 for the activation of the MAP Kinase pathway? Is it analogous to the role of Ste20 in the mating pathway as a downstream effector of the G-protein coupled receptor (GPCR) subunits? Thevelein & Voordeckers (2009) argue that receptors might have evolved from nutrient transporters via transitional transceptor stages, and demonstrates that transceptors might be an evolutionary functional link between transporters and receptors. Binding of a nutrient substrate or ligand to the transceptor induces

conformational changes resulting in the activation of a signalling pathway and GPCRs have nutrients as ligands.

Understanding the receptor function of these transceptors and precise mechanisms by which these nutrient transceptors are able to undergo signalling during nutrient limitation might have significant functional consequences. These findings could pave the way towards the development of specific anti-fungal agents or drug targets to efficiently manage fungal infections in plants and animals. Dissections of these signal transduction pathways could also benefit in the development of small molecules to shut down mechanisms involved in nitrogen sensing and downstream signalling in fungal pathogens.

8. References

Addinall S. G., Downey M., Yu M., Zubko M. K., Dewar J., Leake A., Hallinan J., Shaw O., James K., Wilkinson D. J., Wipat A., Durocher D., Lydall D. A genomewide suppressor and enhancer analysis of cdc13-1 reveals varied cellular processes influencing telomere capping in *Saccharomyces cerevisiae*. *Genetics*. 2008;180: 2251-2266.

Andrade S. L. A., Dickmanns A., Ficner R., Einsle O. Crystal structure of the archaeal ammonium transporter Amt-1 from *Archaeoglobus fulgidus*. *Proc. Natl. Acad. Sci.* 2005;102(42): 14994-14999.

Andrade S.L.A., Einsle O. The Amt/Mep/Rh Family of Ammonium Transport Proteins. *Molec. Memb. Biol.* 2007;24: 357-365.

André B. An overview of membrane transport proteins in *Saccharomyces cerevisiae. Yeast*. 1995; 11:1575–1611.

Andrews D.L., Egan J.D., Mayorga M.E., Gold S.E. The *Ustilago maydis ubc4* and*ubc5* genes encode members of a MAP kinase cascade required for filamentous growth. *Mol. Plant-Microbe. Interact.* 2000;13: 781–786.

Baday S., Orabi E. A., Wang S., Lamoureux G., Bernèche S. Mechanism of NH4$^+$ recruitment and NH3 transport in Rh proteins. *Structure*. 2015; 23: 1-8.

Baday S., Wang S., Lamoureux G., Bernèche S. Different hydration patterns in the pores of AmtB and RhCG could determine their transport mechanisms. *Biochem*. 2013; 52: 7091–7098.

Biswas K., Morschhauser J. The Mep2 ammonium permease controls nitrogen starvation-induced filamentous growth in *Candida albicans*. *Mol. Microbiol*. 2005; 56(3): 649-669.

Bizzarri R., Serresi M., Luin S., Beltram F. Green fluorescent protein based pH indicators for *in vivo* use: a review. *Anal. Bioanal. Chem.* 2009; 393 1107–112210.

Boeckstaens M., Andre B., Marini A. M. Distinct transport mechanisms in yeast ammonium transport /sensor proteins of the Mep/Amt/Rh family and impact on filamentation. *J. Biol. Chem.* 2008; 283(31): 21362-21370.

Boeckstaens M., Andre B., Marini A. M. The yeast ammonium transport protein Mep2 and its positive regulator, the Npr1 kinase, play an important role in normal and pseudohyphal growth on various nitrogen media through retrieval of excreted ammonium. *Mol. Microbiol*. 2007; 64: 534–546.

Boeckstaens M., Llinares E., Vooren P. V., Marini A. M. The TORC1 effector kinase Npr1 fine tunes the inherent activity of the Mep2 ammonium transport protein. *Nat. Commun*. 2014; 5: 3101.

Boeckstaens M., Merhi A., Llinares E., Van Vooren P., Springael J. Y., Wintjens R., Marini A. M. Identification of a Novel Regulatory Mechanism of Nutrient Transport Controlled by TORC1-Npr1-Amu1/Par32. *PLoS. Genet*. 2015; 11(7).

Bowman E. J., O'Neill F.J., Bowman B.J. Mutations of pma-1, the gene encoding the plasma membrane H+-ATPase of *Neurospora crassa*, suppress inhibition of growth by concanamycin A, a specific inhibitor of vacuolar ATPases. *J. Biol. Chem*. 1997; 272:14776-14786.

Brachmann C. B., Davies A., Cost G. J., Caputo E., Li J., Hieter P., Boeke, J. D. Designer deletion strains derived from *Saccharomyces cerevisiae* S288C: A useful set of strains and plasmids for PCR-mediated gene disruption and other applications. *Yeast*. 1998; 14: 115-132.

Braus G.H., Grundmann O., Brückner S., Mösch H.U. Amino acid starvation and Gcn4p regulate adhesive growth and *FLO11* gene expression in *Saccharomyces cerevisiae*. *Mol. Biol. Cell*. 2003; 14: 4272–4284.

Brett C. L., Tukaye D. N., Mukherjee S., Rao R. The yeast endosomal Na+ (K+)/H+ exchanger Nhx1 regulates cellular pH to control vesicle trafficking. *Mol. Biol. Cell*. 2005; 16: 1396–1405.

Carmelo V., Bogaerts P., Sá-Correia I. Activity of plasma membrane H+-ATPase and expression of PMA1 and PMA2 genes in *Saccharomyces cerevisiae* cells grown at optimal and low pH. *Arch. Microbiol*. 1996; 166: 315–320.

Causton H. C., Ren B., Koh S. S., Harbison C. T., Kanin E., Jennings E. G., Lee T.I., True H. L., Lander E. S., Young R. A. Remodeling of yeast genome expression in response to environmental changes. *Mol. Biol. Cell*. 2001; 12:323-337.

Colombo S., Ma P., Cauwenberg L., Winderickx J., Crauwels M., Teunissen A., Nauwelaers D., de Winde J. H., Gorwa M. F., Colavizza D., Thevelein J. M. Involvement of distinct G-

proteins, Gpa2 and Ras, in glucose- and intracellular acidification-induced cAMP signalling in the yeast Saccharomyces cerevisiae. *EMBO. J.* 1998; 17:3326-3341.

Conrad M., Schothorst J., Kankipati H. N., Van Zeebroeck G., Rubio-Texeira M., Thevelein, J. M. Nutrient sensing and signaling in the yeast *Saccharomyces cerevisiae. FEMS Microbiol. Rev.* 2014; 38, 254–299.

Conroy M. J., Durand A., Lupo D., Li X. D., Bullough P. A., Winkler F. K., Merrick M. The crystal structure of the *Escherichia coli* AmtB-GlnK complex reveals how GlnK regulates the ammonia channel. *Proc. Natl. Acad. Sci.* 2007; 104: 1213–1218.

Cook J.G., Bardwell L., Thorner J. Inhibitory and activating functions for MAPK Kss1 in the *S. cerevisiae* filamentous growth signalling pathway. *Nature*. 1997; 390:85–88.

Cooper T.G. Nitrogen metabolism in *Saccharomyces cerevisiae*. The Molecular Biology of the Yeast *Saccharomyces*: Metabolism and Gene Expression, (Strathern JN, Jones EW & Broach JR, eds) Cold Spring Harbor Laboratory Press, Cold Spring Harbor, NY. 1982; 39–99.

Coutts G., Thomas G., Blakey D., Merrick M. Membrane sequestration of the signal transduction protein GlnK by the ammonium transporter AmtB. *EMBO. J.* 2002; 21: 1–10.

Cullen P. J., Sprague G. F. Glucose depletion causes haploid invasive growth in yeast. *Proc. Natl. Acad. Sci.* 2000; 97: 13619–13624.

Cullen P. J., Sprague G. F., Pryciak P. The regulation of filamentous growth in yeast. *Genetics*. 2012; 190: 23-49.

Cutler N. S., Pan X., Heitman J., Cardenas M. E. The TOR signal transduction cascade controls cellular differentiation in response to nutrients. *Mol. Biol. Cell.* 2001; 12: 4103–4113.

D'Souza C. A., Heitman, J. Conserved cAMP signaling cascades regulate fungal development and virulence. *FEMS. Microbiol. Rev*. 2001; 25: 349-364.

Das M., Nuñez I., Rodriguez M., Wiley D. J., Rodriguez J., Sarkeshik A., Yates J. R., Buchwald P., Verde F. Phosphorylation-dependent inhibition of Cdc42 GEF Gef1 by 14-3-3 protein Rad24 spatially regulates Cdc42 GTPase activity and oscillatory dynamics during cell morphogenesis. *Mol. Biol. Cell*. 2015; 26:3520-3534.

De Craene J.O., Soetens O., Andre B. The Npr1 kinase controls biosynthetic and endocytic sorting of the yeast Gap1 permease. *J. Biol. Chem*. 2001; 276: 43939–43948.

Dechant R., Binda M., Lee S., Pelet S., Winderickx J., Peter M. Cytosolic pH is a second messenger for glucose and regulates the PKA pathway via V-ATPase. *EMBO. J*. 2010; 29: 2515–2526.

Dechant, R., Saad S., Ibáñez A. J., Peter M. Cytosolic pH regulates cell growth through distinct GTPases, Arf1 and Gtr1, to promote Ras/PKA and TORC1 activity. *Molecular. Cell*. 2014; 55(3): 409–21.

Delaunay A., Isnard A.D., Toledano M.B. H_2O_2 sensing through oxidation of the Yap1 transcription factor. *EMBO J*. 2000; 19: 5157–5166.

Deschuyteneer A., Boeckstaens M., DeMees C., VanVooren P., Wintjens R., Marini A. M. SNPs altering ammonium transport activity of human Rhesus factors characterized by a yeast-based functional assay. *PLoS. One*. 2013; 8: e71092.

Didion T., Regenberg B., Jørgensen M. U., Kielland-Brandt M. C., Andersen H. A. The permease homologue Ssy1p controls the expression of amino acid and peptide transporter genes in *Saccharomyces cerevisiae. Mol. Microbiol*. 1998; 27:643–650.

Donaton M.C., Holsbeeks I., Lagatie O., Van Zeebroeck G., Crauwels M., Winderickx J., Thevelein J.M. The Gap1 general amino acid permease acts as an amino acid sensor for activation of protein kinase A targets in the yeast *Saccharomyces cerevisiae. Mol Microbiol*. 2003; 50: 911–929.

Durnez P., Pernambuco M. B., Oris E., Arguelles J. C., Mergelsberg H., Thevelein, J. M. Activation of trehalase during growth induction by nitrogen sources in the yeast *Saccharomyces cerevisiae* depends on the free catalytic subunits of cAMP-dependent protein kinase, but not on functional ras proteins. *Yeast.* 1994; 10: 1049–1064.

Dürrenberger F., Wong K., Kronstad J.W. Identification of a cAMP-dependent protein kinase catalytic subunit required for virulence and morphogenesis in *Ustilago maydis*. *Proc. Natl Acad. Sci.* 1998; 95: 5684–5689.

Feller A., Boeckstaens M., Marini A.M., Dubois E. Transduction of the nitrogen signal activating Gln3-mediated transcription is independent of Npr1 kinase and Rsp5-Bul1/2 ubiquitin ligase in *Saccharomyces cerevisiae*. *J. Biol. Chem.* 2006; 281: 28546–28554.

Fong R. N., Kim K., Yoshihara C., Inwood W. B., Kustu S. The W148L substitution in the Escherichia coli ammonium channel AmtB increases flux and indicates flux and indicates that the substrate is an ion. *Proc. Natl. Acad. Sci.* 2007; 104(47): 18706-18711.

Forsberg H., Ljungdahl P. O. Genetic and biochemical analysis of the yeast plasma membrane Ssy1p–Ptr3p–Ssy5p sensor of extracellular amino acids. *Mol. Cell. Biol.* 2001; 21:814–826.

Fu H., Subramanian R. R., Masters S. C. 14-3-3 proteins: structure, function, and regulation. *Annu. Rev. Pharmacol. Toxicol.* 2000; 40:617-47.

Gancedo J. M. Control of pseudohyphae formation in *Saccharomyces cerevisiae*. *FEMS. Microbiol. Rev.* 2001; 25: 107–123.

Gander S., Bonenfant D., Altermatt P., Martin D.E., Hauri S., Moes S., Hall M.N., Jenoe P. Identification of the rapamycin-sensitive phosphorylation sites within the Ser/Thr-rich domain of the yeast Npr1 protein kinase. *Rapid. Commun. Mass. Spectrom.* 2008; 22: 3743–3753.

Gelperin D., Weigle J., Nelson K., Roseboom P., Irie K., Matsumoto K., Lemmon S. 14-3-3 proteins: potential roles in vesicular transport and Ras signalling in *Saccharomyces cerevisiae*. *Proc. Natl. Acad. Sci.* 1995; 92: 11539–11543.

Georis I., Feller A., Vierendeels F., Dubois E. The yeast GATA factor Gat1 occupies a central position in nitrogen catabolite repression-sensitive gene activation. *Mol. Cell. Biol.* 2009; 29: 3803–3815.

Gilstring C. F., Ljungdahl P. O. A method for determining the in vivo topology of yeast polytopic membrane proteins demonstrates that Gap1p fully integrates into the membrane independently of Shr3p. *J. Biol. Chem.* 2000; 275:31488–31495.

Gimeno C. J., Ljungdahl P. O., Styles C. A., Fink G. R. Unipolar cell divisions in the yeast *S. cerevisiae* lead to filamentous growth: regulation by starvation and RAS. *Cell.* 1992; 68: 1077-1090.

Giots F., Donaton M.C., Thevelein J.M. Inorganic phosphate is sensed by specific phosphate carriers and acts in concert with glucose as a nutrient signal for activation of the protein kinase A pathway in the yeast *Saccharomyces cerevisiae*. *Mol Microbiol*. 2003; 47: 1163–1181.

Goehring A.S., Mitchell D.A., Tong A.H., Keniry M.E., Boone C., Sprague G. F. Jr. Synthetic lethal analysis implicates Ste20p, a p21-activated potein kinase, in polarisome activation. *Mol. Biol. Cell.* 2003; 14:1501-1516.

Graff L., Obrdlik P., Yuan L., Loqué D., Frommer W.B., von Wirén N. N-terminal cysteines affect oligomer stability of the allosterically regulated ammonium transporter LeAMT1;1. *J. Exp. Bot.* 2011; 62: 1361–1373.

Grossmann G., Opekarova M., Malinsky J., Weig-Meckl I., Tanner W. Membrane potential governs lateral segregation of plasma membrane proteins and lipids in yeast. *EMBO. J.* 2007; 26: 1–8.

Gruswitz F., Chaudhary S., Ho J.D., Schlessinger A., Pezeshki B., Ho C.M., Sali A., Westhoff C.M., Stroud R.M. Function of human Rh based on structure of RhCG at 2.1 Å. *Proc. Natl. Acad. Sci.* 2010; 107: 9638-9643.

Harashima T., Heitman J. The Galpha protein Gpa2 controls yeast differentiation by interacting with kelch repeat proteins that mimic Gbeta subunits. *Mol. Cell.* 2002; 10:163–173.

Hemert M.J., Steensma H.Y., van Heusden G.P. 14-3-3 proteins: key regulators of cell division, signalling and apoptosis. *Bioessays*. 2001; 23: 936–946.

Hirimburegama K., Durnez P., Keleman J., Oris E., Vergauwen R., Mergelsberg H., Thevelein, J. M. Nutrient-induced activation of trehalase in nutrient-starved cells of the yeast *Saccharomyces cerevisiae*: cAMP is not involved as second messenger. *J. Gen. Microbiol.* 1992; 138: 2035-2043.

Höfken T., Schiebel E. A role for cell polarity proteins in mitotic exit. *EMBO. J.* 2002; 21:4851-4862.

Hofman-Bang J. Nitrogen catabolite repression in *Saccharomyces cerevisiae*. *Mol. Biotechnol*. 1999; 12(1): 35-71.

Holsbeeks I., Lagatie O., Van Nuland A., Van de Velde S., Thevelein J. M. The eukaryotic plasma membrane as a nutrient-sensing device. *Trends. Biochem. Sci*. 2004; 29:556-564.

Hurtado C. A., Rachubinski R.A. YlBMH1 encodes a 14-3-3 protein that promotes filamentous growth in the dimorphic yeast *Yarrowia lipolytica. Microbiology*. 2002; 148:3725-35.

Ishikita H., Knapp E. W. Protonation states of ammonia/ammonium in the hydrophobic pore of ammonia transporter protein AmtB. *J. Am. Chem. Soc*. 2007; 129: 1210–1215.

Javelle A., Lupo D., Ripoche P., Fulford T., Merrick M., Winkler F. K. Substrate binding, deprotonation, and selectivity at the periplasmic entrance of the Escherichia coli ammonia channel AmtB. *Proc. Natl. Acad. Sci*. 2008; 105(13): 5040-5045.

Javelle A., Lupo D., Zheng L., Li X. D., Winkler F. K., Merrick M. An unusual twin-His arrangement in the pore of ammonia channels is essential for substrate conductance. *J. Biol. Chem.* 2006; 281(51): 39492-39498.

Javelle A., Morel M., Rodríguez-Pastrana B. R., Botton B., André B., Marini A. M., Brun A., Chalot M. Molecular characterization, function and regulation of ammonium transporters (Amt) and ammonium-metabolizing enzymes (GS, NADP-GDH) in the ectomycorrhizal fungus *Hebeloma cylindrosporum. Mol. Microbiol*. 2003; 47:411-430.

Javelle A., Severi E., Thornton J., Merrick M. Ammonium sensing in *E. coli*: the role of the ammonium transporter AmtB and AmtB–GlnK complex formation. *J. Biol. Chem.* 2004; 279: 8530–8538.

Kankipati H.N., Rubio-Texeira M., Castermans D., Diallinas G., Thevelein J. M. Sul1 and Sul2 sulfate transceptors signal to protein kinase A upon exit of sulfur starvation. *J. Biol. Chem.* 2015; 290:10430-10446.

Khademi S., O'Connell J., Remis J., Robles-Colmenares Y., Miercke L. J., Stroud R. M. Mechanism of ammonia transport by Amt/MEP/Rh: structure of AmtB at 1.35 A. *Science.* 2004; 305: 1587–1594.

Khademi S., Stroud R. M. The Amt/MEP/Rh family: structure of AmtB and the mechanism of ammonia gas conduction. *Physiology* (Bethesda). 2006; 21419-429.

Kim J. H., Johnston M. Two glucose-sensing pathways converge on Rgt1 to regulate expression of glucose transcporter genes in *Saccharomyces cerevisiae*. *J. Biol. Chem*. 2006; 281: 26144–26149.

Klasson H., Fink G. R., Ljungdahl P.O. Ssy1p and Ptr3p are plasma membrane components of a yeast system that senses extracellular amino acids. *Mol. Cell. Biol*. 1999; 19: 5405-5416.

Kron S. J., Gow N. A. R. Budding yeast morphogenesis: signalling, cytoskeleton, and cell cycle. *Curr. Opin. Cell. Biol.* 1995; 7: 845-855.

Kron S.J., Styles C.A., Fink G.R. Symmetric cell division in pseudohyphae of the yeast *Saccharomyces cerevisiae*. *Mol. Biol. Cell*. 1994; 5: 1003-1022.

Kronstad J., De Maria A.D., Funnell D., Laidlaw R.D., Lee N., de Sá M.M., Ramesh M. Signaling via cAMP in fungi: interconnections with mitogen-activated protein kinase pathways. *Arch. Microbiol.* 1998; 170(6): 395-404.

Lamb T.M., Mitchell A.P. The transcription factor Rim101p governs ion tolerance and cell differentiation by direct repression of the regulatory genes NRG1 and SMP1 in *Saccharomyces cerevisiae. Mol. Cell. Biol*. 2003; 23: 677–686.

Lamb T.M., Xu W., Diamond A., Mitchell A.P. Alkaline response genes of *Saccharomyces cerevisiae* and their relationship to the RIM101 pathway. *J. Biol. Chem*. 2001; 276: 1850–1856.

Lamoureux G., Javelle A., Baday S., Wang S., Berneche S. Transport mechanisms in the ammonium transporter family. *Transfusion. Clin. Biol.* 2010; 17: 168–175.

Lande M.B., Donovan J.M., Zeidel M.L. The relationship between membrane fluidity and permeabilities to water, solute, ammonia and protons. *J. Gen. Physiol*. 1995; 106: 67-84.

Lanquar V., Frommer W. B. Adjusting ammonium uptake via phosphorylation. *Plant. Signaling. Behav.* 2010; 5:736–738.

Lanquar V., Loqué D., Hörmann F., Yuan L., Bohner A., Engelsberger W.R., Lalonde S., Schulze W.X., von Wirén N., Frommer W.B. Feedback inhibition of ammonium uptake by a phospho-dependent allosteric mechanism in *Arabidopsis*. *Plant. Cell*. 2009; 21: 3610–3622.

Lanz E., Slavik J., Kotyk A. 2′, 7′-bis-(2-carboxyethyl)-5(6)-carboxyfluorescein as a dual-emission fluorescent indicator of intracellular pH suitable for argon laser confocal microscopy. *Folia Microbiol (Praha).* 1999; 44: 429–434.

Lawless C., Wilkinson D., Young A., Addinall S., Lydall D. Colonyzer: automated quantification of micro-organism growth characteristics on solid agar. *BMC. Bioinfo.* 2010; 11: 287.

Li W., Mitchell A.P. Proteolytic activation of Rim1p, a positive regulator of yeast sporulation and invasive growth. *Genetics.* 1997; 145: 63-73.

Li X., Lupo D., Zheng L., Winkler F. Structural and functional insights into the AmtB/Mep/Rh protein family. *Transfus. Clin. Biol.* 2006; 13: 165–169.

Lin Y., Cao Z., Mo Y. Molecular dynamics simulations on the *Escherichia coli* ammonia channel protein AmtB: mechanism of ammonia/ ammonium transport. *J. Am. Chem. Soc.* 2006; 128, 10876–10884.

Liu H., Styles C.A., Fink G.R. Elements of the yeast pheromone response pathway required for filamentous growth of diploids. *Science.* 1993; 262: 1741–1744.

Lo H.J., Kohler J.R., DiDomenico B., Loebenberg D., Cacciapuoti A., Fink G.R. Nonfilamentous *C. albicans* mutants are avirulent. *Cell.* 1997; 90(5): 939-949.

Longtine M.S., McKenzie A., Demarini D. J., Shah N. G., Wach A., Brachat A., Philippsen P., Pringle J. R. Additional modules for versatile and economical PCR-based gene deletion and modification in *Saccharomyces cerevisiae. Yeast* 1998; 14:953-561.

Loque D., Lalonde S., Looger L. L., von Wire´ n N., Frommer W. B. A cytosolic trans-activation domain essential for ammonium uptake. *Nature.* 2007; 446: 195–198.

Lorenz M. C., Heitman J. Regulators of pseudohyphal differentiation in *Saccharomyces cerevisiae* identified through multicopy suppressor analysis in ammonium permease mutant strains. *Genetics.* 1998b; 150: 1443-1457.

Lorenz M. C., Heitman J. Yeast pseudohyphal growth is regulated by GPA2, a G protein alpha homolog. *EMBO. J.* 1997; 16:7008–7018.

Lorenz M.C., Heitman J. The MEP2 ammonium permease regulates pseudohyphal differentiation in *Saccharomyces cerevisiae*. *EMBO. J*. 1998a; 17: 1236–1247.

Lorenz M.C., Pan X., Harashima T., Cardenas M. E., Xue Y., Hirsch J. P., Heitman J. The G protein-coupled receptor Gpr1 is a nutrient sensor that regulates pseudohyphal differentiation in *Saccharomyces cerevisiae*. *Genetics*. 2000; 154:609-622.

Ludewig U., von Wirén N., Frommer W. B. Uniport of NH_4^+ by the root hair plasma membrane ammonium transporter LeAMT1;1. *J. Biol. Chem*. 2002; 277**:** 13548–13555.

Ludewig, U. Electroneutral ammonium transport by basolateral rhesus B glycoprotein. *J. Physiol.* 2004; 559, 751–759.

Ludewig, U. Ion transport versus gas conduction: function of AMT/Rh-type proteins. *Transfus. Clin. Biol.* 2006; 13, 111–116.

Lundh F., Mouillon J. M., Samyn D., Stadler K., Popova Y., Lagerstedt J. O., Thevelein J. M., Persson B. L. Molecular mechanisms controlling phosphate-induced downregulation of the yeast Pho84 phosphate transporter. *Biochemistry.* 2009; 48: 4497–4505.

Ma H., Kunes S., Schatz P. J., Botstein D. Plasmid construction by homologous recombination in yeast. *Gene*. 1987; 58:201-216.

MacDonald P. E., Joseph J. W., Rorsman P. Glucose-sensing mechanisms in pancreatic beta-cells. *Philos. Trans. R. Soc. Lond. Ser. B Biol. Sci.* 2005; 360: 2211–2225.

Madeira F., Tinti M., Murugesan G., Berrett E., Stafford M., Toth R., Cole C., MacKintosh C., Barton G. J. 14-3-3-Pred: improved methods to predict 14-3-3-binding phosphopeptides. *Bioinformatics.* 2015; 31:2276-2283.

Madhani H. D., Styles C. A., Fink G. R. MAP kinases with distinct inhibitory functions impart signaling specificity during yeast differentiation. *Cell*. 1997; 91:673–684.

Madhani H.D., Fink G.R. Combinatorial control required for the specificity of yeast MAPK signalling. *Science*. 1997; 275: 1314–1317.

Madhani H.D., Fink G.R. The control of filamentous differentiation and virulence in fungi. *Trends. Cell. Biol.* 1998; 8: 348– 53.

Madhani H.D. Interplay of intrinsic and extrinsic signals in yeast differentiation. *Proc. Natl. Acad. Sci.* 2000; 97: 13461-13463.

Magasanik B., Kaiser C.A. Nitrogen regulation in *Saccharomyces cerevisiae*. *Gene*. 2002; 290(1-2): 1-18.

Marini A. M., Boeckstaens M., Benjelloun F., Cherif-Zahar B., Andre B. Structural involvement in substrate recognition of an essential aspartate residue conserved in Mep/Amt and Rh-type ammonium transporters. *Curr. Genet*. 2006; 49: 364-374.

Marini A. M., Soussi-Boudekou S., Vissers S., Andre B. A family of ammonium transporters in *Saccharomyces cerevisiae*. *Mol. Cell. Biol.* 1997; 17(8): 4282-4293.

Marini A. M., Vissers S., Urrestarazu A., Andre B. Cloning and expression of the *MEP1* gene encoding an ammonium transporter in *Saccharomyces cerevisiae*. *EMBO J*. 1994; 13(15): 3456-3463.

Marini A.M., Andre, B. In vivo N-glycosylation of the mep2 high-affinity ammonium transporter of Saccharomyces cerevisiae reveals an extracytosolic N-terminus. *Mol. Microbiol.* 2000; 38:552–564.

Martínez-Espinoza AD., Ruiz-Herrera J., León-Ramírez C. G., Gold S. E. MAP kinase and cAMP signaling pathways modulate the pH-induced yeast-to-mycelium dimorphic transition in the corn smut fungus *Ustilago maydis*. *Curr. Microbiol*. 2004; 49:274-81.

Martínez-Munoz G.A., Kane, P. Vacuolar and plasma membrane proton pumps collaborate to achieve cytosolic pH homeostasis in yeast. *J. Biol. Chem*. 2008; 283(29): 20309-20319.

Mayer M., Dynowski M., Ludewig U. Ammonium ion transport by the AMT/Rh homolog LeAMT1. *Biochem. J.* 2006; 396: 431–437.

Merrell D. S., Camilli A. Acid tolerance of gastrointestinal pathogens. *Curr. Opin. Microbiol*. 2002; 5: 51–55.

Michnick S.W., Ear P.H., Landry C., Malleshaiah M.K., Messier V. Protein-fragment complementation assays for large-scale analysis, functional dissection and dynamic studies of protein-protein interactions in living cells. *Methods. Mol. Biol*. 2011; 756: 395-425.

Minc N., Chang F. Electrical control of cell polarization in the fission yeast *Schizosaccharomyces pombe*. *Curr. Biol*. 2010; 20:710-716.

Mira N. P., Lourenco A. B., Fernandes A. R., Becker J. D., Sá-Correia I. The RIM101 pathway has a role in *Saccharomyces cerevisiae* adaptive response and resistance to propionic acid and other weak acids. FEMS. Yeast. Res. 2009; 9: 202–216.

Mitsuzawa H. Ammonium transporter genes in the fission yeast *Schizosaccharomyces pombe*: role in ammonium uptake and a morphological transition. *Genes. Cells*. 2006; 11:1183-1195.

Morsomme P., Slayman C. W., Goffeau A. Mutagenic study of the structure, function and biogenesis of the yeast plasma membrane H^+-ATPase. *Biochim. Biophys. Acta*. 2000; 1469: 133–157.

Mosch H. U., Kubler E., Krappmann S., Fink G. R., Braus G. H. Crosstalk between the Ras2p-controlled mitogen-activated protein kinase and cAMP pathways during invasive growth of *Saccharomyces cerevisiae*. *Mol. Biol. Cell*. 1999; 10: 1325–1335.

Mösch H.U., Roberts R.L., Fink G.R. Ras2 signals via the Cdc42/Ste20/mitogen-activated protein kinase module to induce filamentous growth in *Saccharomyces cerevisiae*. *Proc. Natl. Acad. Sci. USA*. 1996; 93: 5352–5356.

Nakhoul N.L., Dejong H., Abdulnour-Nakhoul S. M., Boulpaep E. L., HeringSmith K., Hamm L.L. Characteristics of renal Rhbg as an NH4(+) transporter. *Am. J. Physiol. Renal Physiol*. 2005; 288, F170–F181.

Neuhäuser B., Dunkel N., Satheesh S. V., Morschhäuser, J. Role of the Npr1 Kinase in ammonium transport and signaling by the ammonium permease Mep2 in *Candida albicans. Eukaryot. Cell*. 2011; 10(3): 332–342.

Neuhauser B., Dynowski M., Ludewig U. Switching substrate specificity of AMT/MEP/ Rh proteins. *Channels 8.* 2014; 496–502.

Neuhauser B., Dynowski M., Mayer M., Ludewig U. Regulation of NH_4^+ transport by essential cross talk between AMT monomers through the carboxyl tails. *Plant. Physiol*. 2007; 143: 1651-1659.

Neuhauser B., Ludewig U. Uncoupling of ionic currents from substrate transport in the plant ammonium transporter AtAMT1;2. *J. Biol. Chem.* 2014; 289, 11650–11655.

Ninnemann O., Jauniaux J. C., Frommer W.B. Identification of a high affinity NH4+ transporter from plants. *EMBO. J*. 1994; 13: 3464- 3471.

Niranjan T., Guo X., Victor J., Lu A., Hirsch J. P. Kelch repeat protein interacts with the yeast Galpha subunit Gpa2p at a site that couples receptor binding to guanine nucleotide exchange. *J. Biol. Chem.* 2007; 282: 24231–24238.

Nishimura K., Igarashi K., Kakinuma Y. Proton gradient driven nickel uptake by vacuolar membrane vesicles of *Saccharomyces cerevisiae*. *J. Bacteriol*. 1998; 180: 1962–1964.

Orij R., Brul S., Smits G. J. Intracellular pH is a tightly controlled signal in yeast. *Biochim. Biophys. Acta.* 2011; 1810: 933–944.

Orij R., Postmus J., Ter Beek A., Brul S., Smits G.J. In vivo measurement of cytosolic and mitochondrial pH using a pH-sensitive GFP derivative in Saccharomyces cerevisiae reveals a relation between intracellular pH and growth. *Microbiol.* 2009; 155(1): 268–278.

Ortiz-Ramirez C., Mora S. I., Trejo J., Pantoja O. *Pv*AMT1;1, a highly selective ammonium transporter that functions as H^+/NH_4^+ symporter. *J. Biol. Chem.* 2011; 286, 31113–3112210.

Özcan S., Dover J., Johnston M. Glucose sensing and signalling by two glucose receptors in the yeast *Saccharomyces cerevisiae*. *EMBO. J.* 1998; 17: 2566–2573.

Özcan S., Leong T., Johnston M. Rgt1p of *Saccharomyces cerevisiae*, a key regulator of glucose-induced genes, is both an activator and a repressor of transcription. *Mol. Cell. Biol.* 1996; 16: 6419–6426.

Özcan S., Johnston M. Function and regulation of yeast hexose transporters. *Microbiol. Mol. Biol. Res.* 1999; 63: 554–569.

Palecek S. P., Parikh A. S., Kron S. J. Sensing, signalling and integrating physical processes during *Saccharomyces cerevisisae* invasive and filamentous growth. *Microbiology*. 2002; 148: 893-907.

Palmer G.E., Johnson K. J., Ghosh S., Sturtevant J. Mutant alleles of the essential 14-3-3 gene in *Candida albicans* distinguish between growth and filamentation. *Microbiology*. 2004; 150:1911-24.

Pan X., Heitman J. Cyclic AMP-dependent protein kinase regulates pseudohyphal differentiation in *Saccharomyces cerevisiae*. *Mol. Cell. Biol.* 1999; 19: 4874–4887.

Peeters T., Louwet W., Gelade R., Nauwelaers D., Thevelein J.M., Versele M. Kelch-repeat proteins interacting with the Galpha protein Gpa2 bypass adenylate cyclase for direct regulation of protein kinase A in yeast. *P. Natl. Acad. Sci.* 2006; 103: 13034–13039.

Pernambuco M. B., Winderickx J., Crauwels M., Griffioen G., Mager W. H., Thevelein J. M. Differential requirement for sugar phosphorylation in cells of the yeast *Saccharomyces cerevisiae* grown on glucose or grown on non-fermentable carbon sources for glucose-triggered signalling phenomena. *Microbiology*. 1996; 142: 1775-1782.

Pham C. D., Yu Z., Sandrock B., Bölker M., Gold S. E., Perlin M. H. *Ustilago maydis* Rho1 and 14-3-3 homologues participate in pathways controlling cell separation and cell polarity. *Eukaryot. Cell*. 2009; 8:977-989.

Pineda Rodó., Váchová L., Palková Z. In vivo determination of organellar pH using a universal wavelength-based confocal microscopy approach. *PLoS One*. 2012; 7:e33229.

Popova Y., Thayumanavan P., Lonati E., Agrochao M., Thevelein J. M. Transport and signalling through the phosphate-binding site of the yeast Pho84 phosphate transceptor. *P. Natl. Acad. Sci.* 2010; 107:2890–2895.

Posas F., Takekawa M., Saito H. Signal transduction by MAP kinase cascades in budding yeast. *Curr. Opin. Microbiol.* 1998; 1: 175–182.

Poulsen P., Gaber R. F., Kielland-Brandt M. C. Hyper- and hyporesponsive mutant forms of the *Saccharomyces cerevisiae* Ssy1 amino acid sensor. *Mol. Membr. Biol*. 2008; 25: 164-176.

Rawat S.R., Silim S. N., Kronzucker H. J., Siddiqi M. Y., Glass A. D. M. AtAMT1 gene expression and NH4+ uptake in roots of *Arabidopsis thaliana*: evidence for regulation by root glutamine levels. *Plant. J.* 1999; 19:143–152.

Remy I., Campbell-Valois F.X., Michnick,S.W. Detection of protein–protein interactions using a simple survival protein-fragment complementation assay based on the enzyme dihydrofolate reductase. *Nat. Protoc*. 2007; 2: 2120–2125.

Ripoche P., Bertrand O., Gane P., Birkenmeier C., Colin Y., Cartron J. P. P. Human rhesus-associated glycoprotein mediates facilitated transport of NH(3) into red blood cells. *Proc. Natl. Acad. Sci.* 2004; 101, 17222–17227.

Ritchie R.J., Gibson J. The permeabilities of ammonia, methylamine and ethylamine in the cyanobacterium, *Synechococcus* R-2 (*Anacystis nidulans*). *J. Memb. Biol*. 1987; 95: 131 - 142.

Roberts R.L., Fink G.R. Elements of a single MAP kinase cascade in *Saccharomyces cerevisiae* mediate two developmental programs in the same cell type: mating and invasive growth. *Genes. Dev.* 1994; 8: 2974-2985.

Roberts R.L., Mosch H.U., Fink G.R. 14-3-3 proteins are essential for RAS/MAPK cascade signalling during pseudohypal development in *S. cerevisiae*. *Cell*. 1997; 89: 1055–1065.

Robertson L. S., Fink G. R. The three yeast A kinases have specific signaling functions in pseudohyphal growth. *Proc. Natl. Acad. Sci*. 1998; 95: 13783–13787.

Robzyk K., Kassir Y. A simple and highly efficient procedure for rescuing autonomous plasmids from yeast. *Nuc Acids Res*. 1992; 20(14): 3790.

Rolland F., De Winde J. H., Lemaire K., Boles E., Thevelein J. M., Winderickx J. Glucose-induced cAMP signalling in yeast requires both a G protein-coupled receptor system for extracellular glucose detection and a separable hexose kinase-dependent sensing process. *Mol. Microbiol.* 2000; 38: 348–358.

Roosen J., Engelen K., Marchal K., Mathys J., Griffioen G., Cameroni E., Thevelein J. M., De Virgilio C., De Moor B., Winderickx J. PKA and Sch9 control a molecular switch important for the proper adaptation to nutrient availability. *Mol. Microbiol*. 2005; 55:862–880.

Rosado C.J., Mijaljica D., Hatzinisiriou I., Prescott M., Devenish, R.J. Rosella: a fluorescent pH-biosensor for reporting vacuolar turnover of cytosol and organelles in yeast. *Autophagy*. 2008; 4(2): 205-213.

Rubio-Texeira M., Kaiser C. A. Amino acids regulate retrieval of the yeast general amino acid permease from the vacuolar targeting pathway. *Mol Biol Cell.* 2006; 17: 3031–3050.

Rupp S., Summers E., Lo H.J., Madhani H., Fink G. MAP kinase and cAMP filamentation signalling pathways converge on the unusually large promoter of the yeast *FLO11*gene. *EMBO J*. 1999; 18: 1257–1269.

Rutherford J. C., Chua G., Hughes T., Cardenas M.E., Heitman, J. A Mep2-dependent transcriptional profile links permease function to gene expression during pseudohyphal growth in *Saccharomyces cerevisiae*. *Mol. Biol. Cell*. 2008a; 19: 3028-3039.

 Rutherford J.C., Lin X., Nielsen K., Heitman J. Amt2 permease is required to induce ammonium-responsive invasive growth and mating in *Cryptococcus neoformans*. *Eukaryot. Cell*. 2008b; 7: 237–246.

Saad S., Peter M., Dechant R. In scarcity and abundance: metabolic signals regulating cell growth. *Physiology* (Bethesda) 2013; 28: 298–309.

Sambrook J., Fritsch E. F., Maniatis T. Molecular Cloning: A Laboratory Manual, Cold Spring Harbor Laboratory, Cold Spring Harbor, NY. 1989.

Sanchez-Martinez C., Perez-Martin J. Dimorphism in fungal pathogens: *Candida albicans* and *Ustilago maydis* – similar inputs, different outputs. *Curr. Opin. Microbiol.* 2001; 4(2): 214-221.

Saville B.J., Donaldson M.E., Doyle C.E. Investigating host induced meiosis in a fungal plant pathogen. In Swan (Ed.) Meiosis - Molecular Mechanisms and Cytogenetic Diversity. 2013; 411-460.

Saville S. P., Lazzell A. L., Monteagudo C., Lopez-Ribot J. L. Engineered control of cell morphology in vivo reveals distinct roles for yeast and filamentous forms of *Candida albicans* during infection. *Eukaryotic. cell*. 2003; 2: 1053–1060.

Schepers W., Van Zeebroeck G., Pinkse M., Verhaert P., Thevelein J. M. *In vivo* phosphorylation of Ser21 and Ser83 during nutrient-induced activation of the yeast protein kinase A (PKA) target trehalase. *J. Biol. Chem*. 2012; 287:44130–44142.

Schiestl R. H., Gietz R. D. High efficiency transformation of intact yeast cells using single stranded nucleic acids as a carrier. *Curr. Genet*. 1989; 16: 339–346.

Schmidt A., Beck T., Koller A., Kunz J., Hall M.N. The TOR nutrient signalling pathway phosphorylates NPR1 and inhibits turnover of the tryptophan permease. *EMBO J.* 1998; 17: 6924–6931.

Schothorst J., Zeebroeck G. V., Thevelein J. M. Identification of Ftr1 and Zrt1 as iron and zinc micronutrient transceptors for activation of the PKA pathway in *Saccharomyces cerevisiae*. *Microb. Cell*. 2017; 4:74-89.

Sengupta S., Peterson T. R., Sabatini D. M. Regulation of the mTOR complex 1 pathway by nutrients, growth factors, and stress. *Mol. cell*. 2010; 40:310–322.

Serra-Cardona A., Canadell D., Ariño J. Coordinate responses to alkaline pH stress in budding yeast. *Microb. Cell*. 2015; 2: 182–196.

Seto-Young D., Perlin D. S. Effect of membrane voltage on the plasma membrane H+-ATPase of *Saccharomyces cerevisiae. J. Biol. Chem*. 1991; 266; 1383-1389.

Severi E., Javelle A., Merrick M. The conserved carboxy-terminal region of the ammonia channel AmtB plays a critical role in channel function. *Mol. Membr. Biol*. 2007; 24:161–171.

Shnaiderman C., Miyara I., Kobiler I., Sherman A., Prusky D. Differential activation of ammonium transporters during the accumulation of ammonia by *Colletotrichum gloeosporioides* and its effect on appressoria formation and pathogenicity. *Mol. Plant. Microbe. Interact*. 2013; 26:345-355.

Siegumfeldt H., Rechinger K. B. Jakobsen, M. Dynamic changes of intracellular pH in individual lactic acid bacterium cells in response to a rapid drop in extracellular pH. *Appl. Environ. Microbiol.* 2000; 66: 2330–2335.

Sikorski R. S., Hieter P. A system of shuttle vectors and yeast host strains designed for efficient manipulation of DNA in *Saccharomyces cerevisiae*. *Genetics*. 1989; 122: 19–27.

Smith D. G., Garcia-Pedrajas M. D., Gold S. E., Perlin, M. H. Isolation and characterization from pathogenic fungi of genes encoding ammonium permeases and their roles in dimorphism. *Mol. Microbiol*. 2003; 50: 259–275.

Sogaard R., Alsterfjord M., Macaulay N., Zeuthen T. Ammonium ion transport by the AMT/Rh homolog TaAMT1;1 is stimulated by acidic pH. *Pflügers. Arch. Eur. J. Physiol*. 2009; 458: 733–74310.

Soulard A., Cremonesi A., Moes S., Schütz F., Jenö P., Hall M. N. The rapamycin-sensitive phosphoproteome reveals that TOR controls protein kinase A toward some but not all substrates. *Mol. Biol. Cell.* 2010; 21:3475-3486.

Soupene, E., Ramirez R. M., Kustu S. Evidence that fungal MEP proteins mediate diffusion of the uncharged species NH3 across the cytoplasmic membrane. *Mol. Cell. Biol*. 2001; 21: 5733–5741.

Srivastava J., Barber D. L., Jacobson M. P. Intracellular pH sensors: design principles and functional significance. *Physiology* (Bethesda). 2007; 22:30–39.

Stanbrough M., Rowen D. W., Magasanik B. Role of the GATA factors Gln3p and Nil1p of *Saccharomyces cerevisiae* in the expression of nitrogen-regulated genes. *Proc. Natl. Acad. Sci.* 1995; 92: 9450–9454.

Strosser J., Ludke A., Schaffer S., Kramer R., Burkovski A. Regulation of GlnK activity: modification, membrane sequestration and proteolysis as regulatory principles in the network of nitrogen control in *Corynebacterium glutamicum*. *Mol. Microbiol.* 2004; (54): 132–147.

Tarassov K., Messier V., Landry C. R., Radinovic S., Serna Molina M. M., Shames I., Malitskaya Y., Vogel J., Bussey H., Michnick S. W. An in vivo map of the yeast protein interactome. *Science*. 2008; 320:1465-1470.

Teichert S., Rutherford J.C., Wottawa M., Heitman J., Tudzynski B. Impact of ammonium permeases mepA, mepB, and mepC on nitrogen-regulated secondary metabolism in *Fusarium fujikuroi*. *Eukaryot. Cell.* 2008; 7(2): 187-201.

Thevelein J. M. Signal transduction in yeast. Yeast. 1994; 10(13):1753-90.

Thevelein J. M., de Winde J. H. Novel sensing mechanisms and targets for the cAMP-protein kinase A pathway in the yeast *Saccharomyces cerevisiae*. *Mol. Microbiol*. 1999; 33:904–918.

Thevelein J. M., Voordeckers K. Functioning and evolutionary significance of nutrient transceptors. *Mol. Biol. Evol*. 2009; 26:2407-2414.

Thomas G. H., Mullins J. G., Merrick M. Membrane topology of the Mep/Amt family of ammonium transporters. *Mol. Microbiol*. 2000; 37: 331-344.

Ullmann R.T., Andrade S.L.A., Ullmann G.M. Thermodynamics of transport through the ammonium transporter Amt-1 investigated with free energy calculations. *J. Phys. Chem. B.* 2012; 116(32): 9690-9703.

van den Berg B., Chembath A., Jefferies D., Basle A., Khalid S., Rutherford J. C. Structural basis for Mep2 ammonium transceptor activation by phosphorylation. *Nat. Commun.* 2016; 7:11337.

Van Dijck P., Brown N. A., Goldman G. H., Rutherford J., Xue C., Van Zeebroeck G. Nutrient Sensing at the Plasma Membrane of Fungal Cells. *Microbiol. Spectr.* 2017; 5:2.

Van Nuland A., Vandormael P., Donaton M., Alenquer M., Lourenco A., Quintino E., Versele M., Thevelein J. M. Ammonium permease-based sensing mechanism for rapid ammonium activation of the protein kinase A pathway in yeast. *Mol. Microbiol.* 2006; 59: 1485-1505.

Van Zeebroeck G., Bonini B. M., Versele M., Thevelein J.M. Transport and signalling via the amino acid binding site of the yeast Gap1 amino acid transceptor. *Nat. Chem. Biol.* 2009; 5(1): 45-52.

Van Zeebroeck G., Kimpe M., Vandormael P., Thevelein J. M. A split-ubiquitin two-hybrid screen for proteins physically interacting with the yeast amino acid transceptor Gap1 and ammonium transceptor Mep2. *PLoS. One*. 2011; 6:e24275.

Van Zeebroeck G., Rubio-Texeira M., Schothorst J., Thevelein J. M. Specific analogues uncouple transport, signalling, oligo-ubiquitination and endocytosis in the yeast Gap1 amino acid transceptor. *Mol. Microbiol*. 2014; 93(2): 213-233.

Versele M., de Winde J. H., Thevelein J. M. A novel regulator of G protein signalling in yeast, Rgs2, downregulates glucose-activation of the cAMP pathway through direct inhibition of Gpa2. *EMBO. J.* 1999; 18:5577–5591.

Versele M., Lemaire K., Thevelein J. M. Sex and sugar in yeast: two distinct GPCR systems. *EMBO. Rep*. 2001; 2:574–579.

von Wiren N., Merrick M. Regulation and function of ammonium carriers in bacteria, fungi and plants. *Top. Curr. Genet*. 2004; 9: 95–120.

Vylkova S., Carman A. J., Danhof H. A., Collette J. R., Zhou H., Lorenz M. C. The fungal pathogen *Candida albicans* autoinduces hyphal morphogenesis by raising extracellular pH. *MBio*. 2011; 2:e00055-11.

Wacker T., Garcia-Celma J.J., Lewe P., Andrade S.L.A. Direct observation of electrogenic NH_4^+ transport in ammonium transport (Amt) proteins. *Proc Natl Acad Sci*. 2014; 111: 9995–10000.

Wang J., Fulford T., Shao Q., Javelle A., Yang H., Zhu W., Merrick M. Ammonium transport proteins with changes in one of the conserved pore Histidines have different performance in ammonia and methylamine conduction. *PLoS. ONE.* 2013; 8: e62745.

Wang S., Orabi E. A., Baday S., Bernèche S., Lamoureux G. Ammonium transporters achieve charge transfer by fragmenting their substrate. *J. Am. Chem. Soc.* 2012; 134: 10419–10427.

Winkler F.K. Amt/MEP/Rh proteins conduct ammonia. *Pflugers Arch*. 2006; 451: 701-707.

Wu B., Ottow K., Poulsen P., Gaber R. F., Albers E., Kielland-Brandt M. C. Competitive intra- and extracellular nutrient sensing by the transporter homologue Ssy1p. *J. Cell. Biol*. 2006; 173: 327-331.

Wykoff D. D., O'Shea E. K. Phosphate transport and sensing in *Saccharomyces cerevisiae*. Genetics. 2001; 159:1491–1499.

Xue Y., Batlle M., Hirsch J. P. *GPR1* encodes a putative G protein-coupled receptor that associates with the Gpa2p Galpha subunit and functions in a Ras-independent pathway. *EMBO J.* 1998; 17:1996–2007.

Yaffe M., Rittinger K., Volinia S., Caron P., Aitken A. The structural basis for 14-3-3: phosphopeptide binding specificity. *Cell*. 1997; 91: 961–971.

Yun C. W., Tamaki H., Nakayama R., Yamamoto K., Kumagai H. Gpr1p, a putative G-protein coupled receptor, regulates glucose-dependent cellular cAMP level in yeast *Saccharomyces cerevisiae. Biochem. Biophys. Res. Commun*. 1998; 252: 29–33.

Zaman S., Lippman S. I., Zhao X., Broach J. R. How *Saccharomyces* responds to nutrients. *Annu. Rev. Genet*. 2008; 42: 27–81.

Zheng L., Kostrewa D., Berneche S., Winkler F. K., Li X. D. The mechanism of ammonia transport based on the crystal structure of AmtB of *Escherichia coli*. *Proc. Natl. Acad. Sci*. 2004; 101 (49): 17090-17095.

Zidi-Yahiaoui N., Callebaut I., Genetet S., Van Kim C. L., Cartron J., Colin Y., Ripoche P., Mouro-Chanteloup I. Functional analysis of human RhCG: a comparison with *E. coli* ammonium transporter reveals similarities in the pore and differences in the vestibule. *Am. J. Physiol.* 2009; 297: C537-C547.

Zurita-Martinez S. A., Cardenas M. E. Tor and cyclic AMP-protein kinase A: two parallel pathways regulating expression of genes required for cell growth. *Eukaryot. Cell*. 2005; 4: 63–71.

Zurita-Martinez S. A., Puria R., Pan X., Boeke J. D., Cardenas M. E. Efficient Tor signalling requires a functional class C Vps protein complex in *Saccharomyces cerevisiae*. *Genetics*. 2007; 176:2139–2150.

9. Appendix 1

Results of PCA screen:

Gene	ORF	Mean colony size
TDH3	YGR192C	393406.516
BMH1	YER177W	332086.135
MRH1	YDR033W	315861.835
FMP45	YDL222C	293711.133
BMH2	YDR099W	282440.605
YBL029C-A	YBL029C-A	290082.74
MUP1	YGR055W	278016.458
TEF1	YPR080W	283169.668
FTR1	YER145C	282524.447
YDR089W	YDR089W	278794.924
HXT7	YDR342C	272798.517
GPM1	YKL152C	275150.209
YOP1	YPR028W	279373.733
MGA1	YGR249W	272284.988
SSA2	YLL024C	272661.346
CRP1	YHR146W	272462.728
GPA2	YER020W	271886.755
PDR12	YPL058C	274741.062
TPI1	YDR050C	259834.908
MEP2	YNL142W	268471.04
ENO2	YHR174W	263982.029
HXK2	YGL253W	252100.696
EIS1	YMR031C	261190.034
OST4	YDL232W	261031.906
TCB3	YML072C	262265.872
IST2	YBR086C	270657.117
MRPL11	YDL202W	270500.307
INA1	YLR413W	256229.038
PDC1	YLR044C	251060.481
YEF3	YLR249W	251677.601
AHP1	YLR109W	252709.107
ZUO1	YGR285C	258239.975
MYO5	YMR109W	249332.235
HXT3	YDR345C	250793.935
RTN1	YDR233C	250983.152

ARP4	YJL081C	247121.939
YGR130C	YGR130C	246231.354
GAP1	YKR039W	246119.055
VTC2	YFL004W	244881.771
GVP36	YIL041W	246641.631
TMA19	YKL056C	242373.672
FLC2	YAL053W	240134.723
CDC19	YAL038W	241190.948
TDH2	YJR009C	241613.584
MRPL39	YML009C	241122.453
MID2	YLR332W	237262.578
MTG1	YMR097C	236215.203
TSC13	YDL015C	240222.075
LAP2	YNL045W	231917.798
MET6	YER091C	226013.134
CSR1	YLR380W	234279.113
PFK1	YGR240C	229229.539
PMP1	YCR024C-A	228389.523
FLC1	YPL221W	231570.052
HNM1	YGL077C	229318.526
TPO3	YPR156C	231924.142
MSY1	YPL097W	230854.392
NUP53	YMR153W	222508.202
YGL108C	YGL108C	230417.398
GRH1	YDR517W	235567.428
PMP2	YEL017C-A	231814.838
TPO4	YOR273C	229785.569
YLR326W	YLR326W	224466.318
PET10	YKR046C	224982.013
THI7	YLR237W	227109.816
SKG1	YKR100C	221855.646
PMP3	YDR276C	228347.177
VMA2	YBR127C	226708.461
TIM10	YHR005C-A	231282.798
GND1	YHR183W	227681.026
URA7	YBL039C	223972.469
STE20	YHL007C	219949.185
SPF1	YEL031W	222129.113
RPP1B	YDL130W	220512.944
ASN1	YPR145W	223390.901
OST1	YJL002C	217149.607
PGK1	YCR012W	218385.853
KES1	YPL145C	216783.297
HXK1	YFR053C	217647.471

RNR1	YER070W	212466.065
RTK1	YDL025C	207674.381
SOD1	YJR104C	216703.553
MEP1	YGR121C	217080.495
RFS1	YBR052C	215672.493
CKA2	YOR061W	206920.466
PEX32	YBR168W	208574.228
SCS22	YBL091C-A	209882.069
SNQ2	YDR011W	212394.803
YLR407W	YLR407W	210200.424
TAZ1	YPR140W	211477.253
RNA1	YMR235C	213247.345
TPO1	YLL028W	211089.64
SIS2	YKR072C	209169.967
RPP1A	YDL081C	208877.087
AGP1	YCL025C	208989.399
SEC27	YGL137W	236677.268
SEC26	YDR238C	209512.357
LYS9	YNR050C	203107.255
RBD2	YPL246C	204222.525
SER33	YIL074C	202892.381
BOI1	YBL085W	215777.954
ATG15	YCR068W	197486.572
WHI3	YNL197C	203505.599
PFK2	YMR205C	204882.951
HSP82	YPL240C	202516.747
YJL016W	YJL016W	198896.453
TSC3	YBR058C-A	199670.564
HRK1	YOR267C	200457.448
MSC3	YLR219W	197568.068
UPC2	YDR213W	201063.754
PIL1	YGR086C	206340.001
ECM17	YJR137C	200853.774
PPZ1	YML016C	199598.569
RPP2A	YOL039W	195593.613
ABP1	YCR088W	195838.117
PDR16	YNL231C	196747.652
FMP27	YLR454W	197278.973
SNA3	YJL151C	193013.192
SHR3	YDL212W	196264.226
SSD1	YDR293C	195666.604
YIP3	YNL044W	197091.025
PYC2	YBR218C	196055.033
EDE1	YBL047C	195204.496

CAJ1	YER048C	193812.482
CDC21	YOR074C	201394.84
SRO7	YPR032W	188416.799
SYP1	YCR030C	195955.642
HSC82	YMR186W	189679.612
TIM9	YEL020W-A	191160.908
SVL3	YPL032C	191676.382
BEM1	YBR200W	192626.304
ADE17	YMR120C	189951.263
CAN1	YEL063C	186827.858
TIM18	YOR297C	189642.026
SSE1	YPL106C	178508.79
OPY2	YPR075C	192262.831
YMR010W	YMR010W	191050.139
SSB2	YNL209W	190622.996
NHA1	YLR138W	188853.557
HSL1	YKL101W	188572.197
SSE2	YBR169C	186465.302
MEP3	YPR138C	186209.279
TPO2	YGR138C	185418.409
SBP1	YHL034C	185167.036
CAP1	YKL007W	191371.627
POM33	YLL023C	184546.364
HSP104	YLL026W	189082.301
YOR1	YGR281W	183647.151
FPS1	YLL043W	186619.113
PTK2	YJR059W	194756.569
PHO84	YML123C	179672.109
CCT8	YJL008C	181770.545
ISF1	YMR081C	189522.069
YPR036W-A	YPR036W-A	185184.317
ALD6	YPL061W	184607.954
PST2	YDR032C	177912.088
FUI1	YBL042C	184166.224
DUR1	YBR208C	185631.488
TVP18	YMR071C	182954.783
MRP17	YKL003C	183898.227
DUR3	YHL016C	181044.471
NDI1	YML120C	177566.286
UIP4	YPL186C	179550.886
RPP2B	YDR382W	173844.292
REE1	YJL217W	181253.47
HSP30	YCR021C	175542.575
ISM1	YPL040C	180495.229

JSN1	YJR091C	179336.934
SEC63	YOR254C	175694.806
QDR3	YBR043C	178238.634
MAK16	YAL025C	171256.493
PIN2	YOR104W	179372.896
RSN1	YMR266W	177852.352
TSA1	YML028W	184464.718
GDI1	YER136W	179770.163
SVF1	YDR346C	171759.216
RTN2	YDL204W	178042.614
RPL16B	YNL069C	170824.852
SHM2	YLR058C	176622.002
ADE16	YLR028C	180076.394
VPS45	YGL095C	175205.512
MDG1	YNL173C	176911.791
QDR2	YIL121W	180012.417
CDC31	YOR257W	166584.127
RPS6B	YBR181C	180382.897
HXT2	YMR011W	180322.653
DDR48	YMR173W	170605.808
CCT2	YIL142W	174000.592
CAP2	YIL034C	173873.654
BUD4	YJR092W	178882.32
HXT1	YHR094C	176529.611
EMC5	YIL027C	174247.332
SUR7	YML052W	171484.408
GCS1	YDL226C	175179.832
TMA22	YJR014W	173611.179
TVP15	YDR100W	174916.466
NPR1	YNL183C	172175.02
SOP4	YJL192C	171681.89
KEX2	YNL238W	171876.561
SEC62	YPL094C	166902.894
ADK1	YDR226W	170478.612
TRR1	YDR353W	169284.198
TMC1	YOR052C	170959.918
HXT5	YHR096C	169884.146
CHS3	YBR023C	170572.211
RIC1	YLR039C	168094.389
ARO8	YGL202W	169879.247
PGM2	YMR105C	164754.449
MEF1	YLR069C	171331.126
YDR018C	YDR018C	166985.587
YDR034W-B	YDR034W-B	169466.036

PDR5	YOR153W	170846.367
PAR32	YDL173W	168548.975
ADE12	YNL220W	171731.009
YNK1	YKL067W	167694.909
CPA2	YJR109C	167629.948
PUF3	YLL013C	173380.389
SWH1	YAR042W	169482.219
MET17	YLR303W	163027.192
CUE5	YOR042W	167025.558
KEL1	YHR158C	164354.86
OLE1	YGL055W	164063.44
BBC1	YJL020C	165431.469
YGR026W	YGR026W	155596.688
ROT1	YMR200W	168368.509
RKM3	YBR030W	166695.883
GLN1	YPR035W	162905.214
VPS20	YMR077C	166922.285
OLA1	YBR025C	166343.203
ECM30	YLR436C	162770.75
GPX2	YBR244W	159115.272
MBF1	YOR298C-A	167128.736
AIM21	YIR003W	161763.465
CHS5	YLR330W	165173.189
RNH1	YMR234W	161820.159
PHO2	YDL106C	163060.636
YME2	YMR302C	164738.727
MSS4	YDR208W	167655.953
CDC33	YOL139C	164775.81
EMC2	YJR088C	167259.928
HUG1	YML058W-A	164285.922
RPS6A	YPL090C	165224.774
RIB4	YOL143C	164286.841
TPM2	YIL138C	159091.706
URA4	YLR420W	164944.605
IPP1	YBR011C	162764.507
INM2	YDR287W	158841.136
UGA1	YGR019W	166942.81
SHO1	YER118C	164155.174
SOL4	YGR248W	163413.985
HOS2	YGL194C	161284.356
FRD1	YEL047C	164773.717
HYR1	YIR037W	161849.136
BEM2	YER155C	163289.275
VMA9	YCL005W-A	163249.322

SLA1	YBL007C	162446.736
GND2	YGR256W	160038.727
CCT5	YJR064W	164390.707
CDS1	YBR029C	159222.541
ISC1	YER019W	166503.214
GNP1	YDR508C	169889.2
SED1	YDR077W	159725.076
ECM21	YBL101C	160440.054
SYG1	YIL047C	152932.226
SIM1	YIL123W	153579.888
RPL8A	YHL033C	153223.745
ASN2	YGR124W	160613.527
DIG2	YDR480W	154807.413
CDC11	YJR076C	157858.526
ATF2	YGR177C	160897.428
ARF2	YDL137W	153950.309
KEX1	YGL203C	135817.051
RPL34A	YER056C-A	160255.958
HSP12	YFL014W	158997.332
YDL218W	YDL218W	163361.889
TOS3	YGL179C	152445.638
ADE8	YDR408C	158649.185
HSP26	YBR072W	157435.388
TIP41	YPR040W	156892.397
YET1	YKL065C	157135.917
TMA20	YER007C-A	154159.366
CST26	YBR042C	162137.351
SSU1	YPL092W	149752.272
TEP1	YNL128W	151190.29
ADE1	YAR015W	154961.676
SSA4	YER103W	155713.977
RPL37A	YLR185W	155664.798
ETR1	YBR026C	157944.719
VIK1	YPL253C	143591.275
SPC105	YGL093W	156699.018
NUP1	YOR098C	156786.664
TGL2	YDR058C	150919.845
PIH1	YHR034C	152851.378
BUD2	YKL092C	153565.79
SEC9	YGR009C	154879.777
GIR2	YDR152W	152735.584
GLN3	YER040W	153983.928
ARC40	YBR234C	151607.179
ASC1	YMR116C	153397.96

SEL1	YML013W	153244.59
GRS1	YBR121C	158640.051
PLB1	YMR008C	154179.184
PCS60	YBR222C	151069.586
RTT101	YJL047C	154212.507
MTD1	YKR080W	151110.04
DSD1	YGL196W	151458.791
ECM34	YHL043W	153902.685
ATG14	YBR128C	150633.601
ERV15	YBR210W	152658.989
ARF1	YDL192W	152990.534
RUP1	YOR138C	153772.139
SYS1	YJL004C	150718.017
PSA1	YDL055C	151387.644
CAT8	YMR280C	151184.296
SBE2	YDR351W	149934.359
KRE5	YOR336W	147341.412
ZWF1	YNL241C	149625.811
RPL35A	YDL191W	148516.976
TRX2	YGR209C	148607.077
YHC1	YLR298C	150830.563
TIF2	YJL138C	154396.209
RAV1	YJR033C	143819.085
PMI40	YER003C	151494.589
TEM1	YML064C	150385.523
NEW1	YPL226W	149585.743
SEC28	YIL076W	148685.72
RPL43A	YPR043W	149530.184
HSP31	YDR533C	144046.822
CAB3	YKL088W	154353.893
CMK2	YOL016C	143616.209
RCK2	YLR248W	146147.26
ARP5	YNL059C	148789.878
NAP1	YKR048C	148711.404
UBP12	YJL197W	146239.152
PEX15	YOL044W	149375.179
ECM32	YER176W	147798.393
UBP1	YDL122W	148145.21
TPK2	YPL203W	148240.556
DOS2	YDR068W	148569.081
SKG3	YLR187W	147742.236
SIT4	YDL047W	148015.761
TIP1	YBR067C	164040.658
GPM2	YDL021W	136182.981

SBE22	YHR103W	147567.209
GET2	YER083C	147430.867
CCT6	YDR188W	150855.625
ERG11	YHR007C	147126.268
YSC84	YHR016C	145535.615
YCR043C	YCR043C	146102.214
RNR3	YIL066C	139207.688
RAD7	YJR052W	149771.644
SCD6	YPR129W	147394.273
VAS1	YGR094W	144287.07
AAT2	YLR027C	146285.144
PSR1	YLL010C	142408.357
SSH4	YKL124W	143400.165
MRP49	YKL167C	143073.959
TMA7	YLR262C-A	147599.001
VPS35	YJL154C	143454.874
SRV2	YNL138W	143957.639
RDI1	YDL135C	144228.504
YCK2	YNL154C	143288.163
COT1	YOR316C	145349.017
GUS1	YGL245W	144581.208
MSW1	YDR268W	145609.412
SFT2	YBL102W	143539.419
ILM1	YJR118C	142747.043
ENT4	YLL038C	144030.012
FAR8	YMR029C	144154.745
BFR1	YOR198C	142056.922
YBR056W	YBR056W	143192.498
YMR074C	YMR074C	148658.846
PTC5	YOR090C	146238.548
DIP5	YPL265W	144479.378
TSA2	YDR453C	142417.535
MRPL3	YMR024W	142336.198
TPK1	YJL164C	135202.51
TAO3	YIL129C	140005.486
CHS7	YHR142W	142586.535
NUM1	YDR150W	143537.294
PHO88	YBR106W	144497.517
HCH1	YNL281W	130849.133
TPK3	YKL166C	141823.152
KEG1	YFR042W	140938.684
SKG6	YHR149C	141558.52
SER1	YOR184W	140052.899
MRPL38	YKL170W	141666.959

FIT3	YOR383C	139669.103
RBL2	YOR265W	142554.762
RPL41A	YDL184C	141234.521
LRE1	YCL051W	147522.661
LRG1	YDL240W	141703.785
CYS4	YGR155W	142433.657
QCR9	YGR183C	141759.502
PUB1	YNL016W	140039.352
KTR7	YIL085C	135236.135
STM1	YLR150W	140829.867
MHP1	YJL042W	140693.123
PRP46	YPL151C	136346.964
TRK1	YJL129C	131417.271
TRM2	YKR056W	141883.376
MKS1	YNL076W	139342.44
RPB2	YOR151C	138447.012
PEP5	YMR231W	136867.204
PRP6	YBR055C	139301.196
GGA2	YHR108W	139200.394
MNN10	YDR245W	137021.139
MSH3	YCR092C	141398.077
PRM5	YIL117C	143568.641
RPS0A	YGR214W	133160.447
YJL049W	YJL049W	149318.342
PKH2	YOL100W	143500.052
YFL068W	YFL068W	140732.897
VTC3	YPL019C	139816.044
PAU2	YEL049W	144925.482
GCD1	YOR260W	138241.957
FPK1	YNR047W	134855.311
BNA3	YJL060W	138502.946
RPL21A	YBR191W	138482.006
YLR154W-B	YLR154W-B	142551.253
COG4	YPR105C	138668.486
GTS1	YGL181W	138027.746
BUD20	YLR074C	136458.219
RPE1	YJL121C	137099.05
ERG8	YMR220W	138932.335
LYP1	YNL268W	140043.02
KIN4	YOR233W	137192.726
ALD5	YER073W	133923.355
PWP2	YCR057C	136414.71
RVS167	YDR388W	138896.248
HOF1	YMR032W	138881.073

PYC1	YGL062W	139006.49
DSF2	YBR007C	135458.66
NET1	YJL076W	139163.887
SML1	YML058W	136225.097
VRP1	YLR337C	137393.254
SEC7	YDR170C	130677.524
YBL086C	YBL086C	141373.029
ATG3	YNR007C	136182.576
PRS3	YHL011C	136919.336
IRC22	YEL001C	137699.831
YKR045C	YKR045C	138791.099
ARF3	YOR094W	137378.065
OSW7	YFR039C	135740.833
ATG31	YDR022C	134962.254
SAP30	YMR263W	141041.993
SEC21	YNL287W	134865.808
SEC5	YDR166C	132890.522
PAU1	YJL223C	135782.164
PUS6	YGR169C	138335.142
SHU1	YHL006C	136309.759
CDC39	YCR093W	146274.383
RPS17A	YML024W	135074.439
PAM1	YDR251W	129828.316
SRB5	YGR104C	131814.012
MBR1	YKL093W	128371.784
SWC3	YAL011W	129924.321
HST4	YDR191W	133317.389
DNF1	YER166W	135344.085
MDH2	YOL126C	137698.248
RIB3	YDR487C	132164.24
SPR28	YDR218C	137144.517
SPR3	YGR059W	136516.192
NOP10	YHR072W-A	130036.55
YBL060W	YBL060W	134305.204
YDR182W-A	YDR182W-A	137533.387
COX14	YML129C	133257.556
MOB2	YFL034C-B	132240.674
ECM1	YAL059W	130545.337
RDS1	YCR106W	132181.171
RKI1	YOR095C	135212.908
PTC4	YBR125C	134376.906
SLY41	YOR307C	133455.037
SHS1	YDL225W	132592.579
TRP5	YGL026C	130636.622

YGR017W	YGR017W	129705.818
PXR1	YGR280C	131304.352
KIC1	YHR102W	135614.611
YKE2	YLR200W	141083.055
TPO5	YKL174C	136004.796
CLB3	YDL155W	140046.314
HIS5	YIL116W	130719.875
YGR021W	YGR021W	134252.534
AQR1	YNL065W	135294.714
YCT1	YLL055W	134189.449
PER33	YLR064W	134516.297
YGR266W	YGR266W	134861.789
PRP18	YGR006W	132198.487
PRY2	YKR013W	130470.549
POP8	YBL018C	134011.418
BUD14	YAR014C	132392.848
RTT102	YGR275W	135370.988
UBX7	YBR273C	131782.257
PDB1	YBR221C	133398.062
SFA1	YDL168W	132616.958
YBR056W-A	YBR056W-A	136316.837
TRS31	YDR472W	132997.253
CIS3	YJL158C	132055.692
KSS1	YGR040W	131838
YJL213W	YJL213W	132769.455
APD1	YBR151W	111325.604
VPS54	YDR027C	129918.523
RKM4	YDR257C	128019.57
XKS1	YGR194C	132880.483
CDC60	YPL160W	132553.055
STE5	YDR103W	132022.451
MLH1	YMR167W	131118.535
PCK1	YKR097W	130528.195
RNQ1	YCL028W	131633.378
NCA2	YPR155C	132538.588
YGR016W	YGR016W	131696.796
ARL1	YBR164C	131882.442
CTR1	YPR124W	131496.809
FAT3	YKL187C	128741.553
IML2	YJL082W	129773.451
ECM9	YKR004C	128390.678
INO1	YJL153C	125184.987
DLD3	YEL071W	132533.314
ADE5	YGL234W	131013.905

ESS1	YJR017C	132931.941
DOM34	YNL001W	132019.335
KEL2	YGR238C	132202.927
MRPS16	YPL013C	135043.012
ATG16	YMR159C	128163.899
WHI4	YDL224C	128971.886
SKM1	YOL113W	131127.474
PBP4	YDL053C	127684.115
RMD9	YGL107C	130847.303
TKL1	YPR074C	130030.96
IMG1	YCR046C	131126.698
GCD11	YER025W	132662.929
PRP11	YDL043C	131110.047
EDC2	YER035W	131164.53
POR1	YNL055C	130922.037
YIM1	YMR152W	132924.204
CLA4	YNL298W	130361.548
RCR1	YBR005W	130249.13
RIF1	YBR275C	131775.133
TIF5	YPR041W	135409.64
CAR1	YPL111W	128821.094
AXL2	YIL140W	131860.06
SAM1	YLR180W	129769.097
SHB17	YKR043C	130700.475
STE7	YDL159W	129706.538
PPS1	YBR276C	130122.378
NCS6	YGL211W	131058.855
ACP1	YKL192C	133257.413
RGA2	YDR379W	129237.873
SMK1	YPR054W	126060.608
WHI5	YOR083W	120281.227
SSK22	YCR073C	123103.685
ADE4	YMR300C	130092.294
VMA22	YHR060W	129824.64
RHB1	YCR027C	125408.86
AVO2	YMR068W	130542.042
PSP1	YDR505C	130091.851
TRS20	YBR254C	129080.453
CNB1	YKL190W	130125.563
VPS24	YKL041W	132741.723
FAA2	YER015W	127690.889
PAH1	YMR165C	130411.843
PTI1	YGR156W	126922.893
RGI1	YER067W	123934.91

YJR096W	YJR096W	127782.741
VID27	YNL212W	128234.852
SAM2	YDR502C	131283.04
INP52	YNL106C	122924.566
VPS60	YDR486C	128211.964
CDC26	YFR036W	127209.842
CSF1	YLR087C	128474.875
RRG9	YNL213C	130206.897
KTR5	YNL029C	127618.353
YFL067W	YFL067W	127517.787
RIM1	YCR028C-A	128156.312
RPL7B	YPL198W	121157.837
BRR6	YGL247W	126228.012
PEX27	YOR193W	128306.92
YJR061W	YJR061W	126955.877
HUR1	YGL168W	135331.599
RFU1	YLR073C	132535.6
ITR1	YDR497C	124910.592
CKA1	YIL035C	127654.666
IRC25	YLR021W	130884.401
EXO84	YBR102C	131771.132
LIA1	YJR070C	128463.025
CCH1	YGR217W	124019.733
MET2	YNL277W	129257.891
SNF1	YDR477W	144302.98
GPP1	YIL053W	126693.297
ZDS2	YML109W	128346.617
RPS0B	YLR048W	130186.05
DCS1	YLR270W	126328.782
CNA1	YLR433C	125397.849
GMC1	YDR506C	130006.303
UIP3	YAR027W	123110.605
SEC1	YDR164C	125006.429
JIP4	YDR475C	126938.933
MTC1	YJL123C	128689.103
BUB3	YOR026W	128389.986
BZZ1	YHR114W	122426.986
RPS4B	YHR203C	127592.563
STI1	YOR027W	127667.965
MEC3	YLR288C	128501.89
DCW1	YKL046C	125583.738
COX16	YJL003W	123944.482
SOV1	YMR066W	125394.864
YLR050C	YLR050C	126904.456

UTH1	YKR042W	126806.548
PEX6	YNL329C	128305.993
ECM8	YBR076W	126361.159
ZPR1	YGR211W	124254.874
UBI4	YLL039C	127134.309
SPL2	YHR136C	128155.881
SKI3	YPR189W	127241.17
IDP1	YDL066W	124189.023
SEC6	YIL068C	136611.49
PAC2	YER007W	126803.142
EFR3	YMR212C	126169.161
UBX5	YDR330W	123714.1
FLO5	YHR211W	132485.431
PUS5	YLR165C	123800.851
SST2	YLR452C	119072.616
NVJ1	YHR195W	125210.773
YER187W	YER187W	125286.312
RSB1	YOR049C	124105.872
DHH1	YDL160C	125128.311
ECM14	YHR132C	122523.909
FIG4	YNL325C	123535.054
FEN2	YCR028C	121766.614
SAE3	YHR079C-A	126035.983
RPS4A	YJR145C	124713.768
YLR257W	YLR257W	125044.285
MSK1	YNL073W	131454.511
RLI1	YDR091C	128718.192
DFG16	YOR030W	123270.782
DIA2	YOR080W	120592.918
HSV2	YGR223C	124715.746
YGR169C-A	YGR169C-A	123726.997
FSH2	YMR222C	125812.822
RGD1	YBR260C	123163.819
RMD8	YFR048W	121737.034
GIC2	YDR309C	156760.808
FET3	YMR058W	124720.652
MND2	YIR025W	124434.084
MRPL25	YGR076C	123128.71
TSL1	YML100W	124922.138
SUE1	YPR151C	121583.367
TMA17	YDL110C	124667.993
CCW12	YLR110C	117353.407
PRP39	YML046W	121354.897
YHR080C	YHR080C	96899.7364

FSH3	YOR280C	120567.183
YAR029W	YAR029W	119066.819
RAS2	YNL098C	123557.792
COX23	YHR116W	119868.486
HSP10	YOR020C	124485.02
MRPL22	YNL177C	124333.5
MDL2	YPL270W	124585.527
FUM1	YPL262W	125609.801
YML131W	YML131W	123926.132
RRP43	YCR035C	121605.959
MSS51	YLR203C	124690.635
SLY1	YDR189W	125434.663
GLC3	YEL011W	122665.238
GRX2	YDR513W	125531.938
HIS7	YBR248C	126597.201
RPL6A	YML073C	123868.696
DBP1	YPL119C	126535.708
STP4	YDL048C	122534.211
TKL2	YBR117C	117800.56
STE3	YKL178C	124979.65
AIM34	YMR003W	123960.858
DSK2	YMR276W	121550.162
PCL7	YIL050W	122490.794
URE2	YNL229C	126363.148
YLR030W	YLR030W	127873.846
CTT1	YGR088W	120866.385
YDL121C	YDL121C	124337.132
TAD3	YLR316C	120368.874
MRPL23	YOR150W	120669.568
AIM4	YBR194W	123369.64
RPB8	YOR224C	120579.355
RRP14	YKL082C	118727.9
TRS120	YDR407C	124175.954
ADO1	YJR105W	122711.758
SKN7	YHR206W	123136.284
DTD1	YDL219W	124640.396
PCC1	YKR095W-A	118902.095
PIS1	YPR113W	115729.318
YGL242C	YGL242C	122846.727
CWC25	YNL245C	119542.833
CMK1	YFR014C	123379.306
SLD5	YDR489W	125477.644
QNS1	YHR074W	117465.973
PIR1	YKL164C	122699.417

CMD1	YBR109C	120911.755
BOS1	YLR078C	120757.524
RAD17	YOR368W	122435.592
CDC50	YCR094W	117381.662
YER079W	YER079W	116681.79
SAM50	YNL026W	123725.909
PKH3	YDR466W	127830.967
KCC4	YCL024W	123519.837
SRP14	YDL092W	120830.275
CMS1	YLR003C	119178.848
HUL5	YGL141W	124872.793
YHR182W	YHR182W	121333.082
YBL113C	YBL113C	119871.602
SDO1	YLR022C	121935.712
SMF3	YLR034C	121690.595
UTR1	YJR049C	121625.073
YPK1	YKL126W	123080.052
SET6	YPL165C	120380.931
STB3	YDR169C	122034.273
SUP45	YBR143C	124458.946
YER175W-A	YER175W-A	124013.269
SLD2	YKL108W	119753.36
HIS1	YER055C	122604.085
RPC11	YDR045C	123591.265
LCB1	YMR296C	121871.141
YML082W	YML082W	120207.99
COX5A	YNL052W	120429.976
STE2	YFL026W	123592.198
CHK1	YBR274W	121300.752
VPS53	YJL029C	121747.95
TMN3	YER113C	124195.738
CRS5	YOR031W	123992.688
TMS1	YDR105C	121279.449
CSL4	YNL232W	116763.502
COF1	YLL050C	120133.677
EXG2	YDR261C	116876.547
MCM1	YMR043W	123393.174
NSE4	YDL105W	122063.1
LOT6	YLR011W	121272.665
CBP1	YJL209W	112740.743
CDC24	YAL041W	122136.679
PPM2	YOL141W	121621.598
NSG2	YNL156C	123348.288
RIO2	YNL207W	121805.398

RRP7	YCL031C	119782.457
YPT52	YKR014C	115305.593
CIN8	YEL061C	120502.007
MYO2	YOR326W	120542.072
SWC5	YBR231C	120045.53
AHC1	YOR023C	122476.797
NSR1	YGR159C	118875.491
THS1	YIL078W	114912.311
SLX1	YBR228W	119818.99
SDH2	YLL041C	120817.619
AFI1	YOR129C	119875.52
GPR1	YDL035C	119896.842
SPO12	YHR152W	120619.256
BIT2	YBR270C	121515.609
ECM25	YJL201W	120445.858
RAT1	YOR048C	120189.5
YPR078C	YPR078C	121719.698
FMP46	YKR049C	120008.408
FMP37	YGL080W	119850.914
LYS1	YIR034C	116904.974
GEP3	YOR205C	120182.347
STU1	YBL034C	119065.306
SPO20	YMR017W	120907.459
YML037C	YML037C	115852.364
XYL2	YLR070C	118881.919
IRA1	YBR140C	119150.015
IMD3	YLR432W	124650.847
YDR239C	YDR239C	119760.389
GRE1	YPL223C	125625.511
ERG13	YML126C	118559.563
SIS1	YNL007C	119723.532
HSP33	YOR391C	119436.595
YBL055C	YBL055C	119773.504
VPS34	YLR240W	112274.983
AIM26	YKL037W	122758.655
AGP2	YBR132C	117807.528
YBL039W-A	YBL039W-A	119670.459
NAT4	YMR069W	119102.415
FRE7	YOL152W	122459.952
ZDS1	YMR273C	119904.347
SAW1	YAL027W	119740.575
NSG1	YHR133C	119033.388
SDT1	YGL224C	117516.684
RPS1A	YLR441C	117501.232

SNO4	YMR322C	126897.682
APC5	YOR249C	119685.584
REH1	YLR387C	119254.098
EFM2	YBR271W	118822.417
TRS85	YDR108W	125729.534
NMD4	YLR363C	111512.725
HHF1	YBR009C	119481.057
NTC20	YBR188C	119508.405
SOL3	YHR163W	122277.412
PNG1	YPL096W	116915.226
LAG2	YOL025W	113740.548
ISD11	YER048W-A	119249.083
ATG26	YLR189C	115473.46
RPL29	YFR032C-A	120111.227
LTV1	YKL143W	111303.729
COQ8	YGL119W	115829.487
SFH1	YLR321C	118955.474
ECM27	YJR106W	119654.929
SMD1	YGR074W	117624.667
ALO1	YML086C	122639.231
ARP2	YDL029W	120091.861
MMT2	YPL224C	116852.491
MKT1	YNL085W	118757.864
APC11	YDL008W	115888.422
RPL19A	YBR084C-A	116639.656
ARE2	YNR019W	119362.976
UBP7	YIL156W	118994.248
RCL1	YOL010W	116500.153
MRM1	YOR201C	118322.029
PHO85	YPL031C	118813.145
YER156C	YER156C	118308.344
PEP1	YBL017C	120526.076
GSY1	YFR015C	119401.549
CWP2	YKL096W-A	116132.14
TOS2	YGR221C	117496.215
VPH1	YOR270C	114477.246
GEP4	YHR100C	118925.159
YBR071W	YBR071W	118458.043
PEX28	YHR150W	114342.796
PGA3	YML125C	119640.808
DOC1	YGL240W	121326.331
YJR149W	YJR149W	117203.956
NIS1	YNL078W	121946.915
NCE103	YNL036W	118621.846

PBA1	YLR199C	119184.781
TIP20	YGL145W	117806.242
ACH1	YBL015W	118318.275
LSG1	YGL099W	119786.348
FTH1	YBR207W	120726.379
YAL064W-B	YAL064W-B	118340.836
MKK1	YOR231W	113485.625
PSY4	YBL046W	117932.963
MIH1	YMR036C	118553.635
ZIM17	YNL310C	119732.216
CBR1	YIL043C	116938.214
COA4	YLR218C	117565.311
RPL12A	YEL054C	121336.565
SKI8	YGL213C	118847.744
YER188C-A	YER188C-A	120328.298
SEM1	YDR363W-A	116805.372
COG6	YNL041C	116066.495
UTP18	YJL069C	118801.993
DTR1	YBR180W	121779.034
SNX4	YJL036W	121005.256
MSO1	YNR049C	119384.051
SEC2	YNL272C	117215.833
GPG1	YGL121C	120455.237
RBA50	YDR527W	119214.886
RPS1B	YML063W	116572.731
FCY22	YER060W-A	115849.34
SRM1	YGL097W	117820.934
UBP9	YER098W	115521.416
DST1	YGL043W	121326.712
SOG2	YOR353C	117771.98
SSK2	YNR031C	117497.897
ATO2	YNR002C	115543.119
MSC7	YHR039C	117203.331
RPL8B	YLL045C	115446.064
EXG1	YLR300W	119056.539
RAD53	YPL153C	120898.713
YLR046C	YLR046C	116712.017
NTO1	YPR031W	117883.139
PIN3	YPR154W	117819.656
MIX17	YMR002W	119398.691
DUG1	YFR044C	116622.68
CDD1	YLR245C	116526.176
ARO80	YDR421W	116478.556
TMT1	YER175C	119071.6

AIM1	YAL046C	112337.53
CYT1	YOR065W	115970.609
BET5	YML077W	114728.127
CCM1	YGR150C	115325.372
RPL9A	YGL147C	106855.454
GDH2	YDL215C	117868.808
SMY1	YKL079W	114477.242
ADE2	YOR128C	113235.815
SRL1	YOR247W	127079.454
YKL100C	YKL100C	116366.655
HLR1	YDR528W	117916.944
SNZ1	YMR096W	115196.372
SLN1	YIL147C	116991.431
YJR079W	YJR079W	119493.377
YBL029W	YBL029W	117131.771
IMA4	YJL221C	116199.801
ERG29	YMR134W	117353.162
IMA5	YJL216C	120084.287
TRM5	YHR070W	115546.383
DCP2	YNL118C	115419.554
HOR7	YMR251W-A	120293.183
HOL1	YNR055C	117062.536
UBP11	YKR098C	118037.719
MSC2	YDR205W	114829.499
COX13	YGL191W	117450.668
MRPL28	YDR462W	119519.862
MFA2	YNL145W	115825.287
PCT1	YGR202C	117083.59
GFD1	YMR255W	115028.347
YPP1	YGR198W	123032.979
FMP24	YMR115W	117844.71
SEN54	YPL083C	111467.106
PHS1	YJL097W	117084.846
VHS3	YOR054C	116258.625
RLM1	YPL089C	115575.357
TIS11	YLR136C	109337.34
ARP6	YLR085C	115495.006
UTP11	YKL099C	117503.278
PTC2	YER089C	116614.271
YHR138C	YHR138C	114360.426
AIM24	YJR080C	115805.042
ATG32	YIL146C	110295.94
CLU1	YMR012W	112637.914
COQ5	YML110C	115920.533

SSA3	YBL075C	123257.89
YSY6	YBR162W-A	114143.468
TWF1	YGR080W	117397.205
VOA1	YGR106C	114234.04
YKR011C	YKR011C	113340.845
YAR023C	YAR023C	116597.23
SED4	YCR067C	109815.586
CDC16	YKL022C	113386.113
RPN5	YDL147W	115309.143
SEC16	YPL085W	116023.891
YAR064W	YAR064W	114328.795
FPR1	YNL135C	113640.238
GON7	YJL184W	118800.164
MCT1	YOR221C	116455.217
CYR1	YJL005W	115283.724
SHQ1	YIL104C	111999.82
HHF2	YNL030W	119601.599
NOP14	YDL148C	108692.571
LAP3	YNL239W	115542.308
FMP21	YBR269C	115259.144
YLL066C	YLL066C	115512.129
FMP25	YLR077W	114927.155
ECM4	YKR076W	115401.305
SNU23	YDL098C	115251.786
NIT2	YJL126W	117294.533
CPR8	YNR028W	112767.033
RPS13	YDR064W	113787.671
ADH6	YMR318C	114115.621
CRZ1	YNL027W	112665.566
HSE1	YHL002W	116114.559
YKL033W-A	YKL033W-A	112658.448
TAN1	YGL232W	115652.984
UBA3	YPR066W	115277.168
RPL18A	YOL120C	119590.606
TOS1	YBR162C	111275.915
ATG27	YJL178C	116896.227
SIP5	YMR140W	115180.15
HOM2	YDR158W	112574.859
MBA1	YBR185C	116782.179
IDH2	YOR136W	114773.197
GSF2	YML048W	113371.278
QRI5	YLR204W	110914.772
GLO2	YDR272W	115490.653
FRE6	YLL051C	114364.953

SMD3	YLR147C	114847.362
NEO1	YIL048W	116193.027
SGD1	YLR336C	114903.828
PUF4	YGL014W	114792.556
SUL2	YLR092W	114948.673
ICS2	YBR157C	114894.131
TIF34	YMR146C	115145.053
TOM6	YOR045W	116519.983
TRS130	YMR218C	115186.768
PHO81	YGR233C	114800.873
TAH11	YJR046W	115393.425
DAP1	YPL170W	113728.659
POG1	YIL122W	111899.619
UTP8	YGR128C	113441.189
COX9	YDL067C	111963.305
YML133C	YML133C	114872.321
YLL066W-B	YLL066W-B	116410.912
RPL16A	YIL133C	111418.058
YDR286C	YDR286C	114328.616
RLF2	YPR018W	122114.281
ATR1	YML116W	114418.548
SOF1	YLL011W	112967.869
QRI7	YDL104C	117304.383
NFU1	YKL040C	112854.425
HAP5	YOR358W	119428.747
BIM1	YER016W	112991.735
IZH1	YDR492W	113361.762
REX3	YLR107W	115049.416
CIR2	YOR356W	112655.313
FAU1	YER183C	114833.996
STP3	YLR375W	113243.79
RPB5	YBR154C	114711.222
SRS2	YJL092W	115176.219
TDA4	YJR116W	112871.317
YBR219C	YBR219C	115388.864
AEP1	YMR064W	113188.824
RPC10	YHR143W-A	114395.331
AAT1	YKL106W	112914.95
GAS3	YMR215W	114073.161
SOL2	YCR073W-A	114801.699
GCD6	YDR211W	113847.371